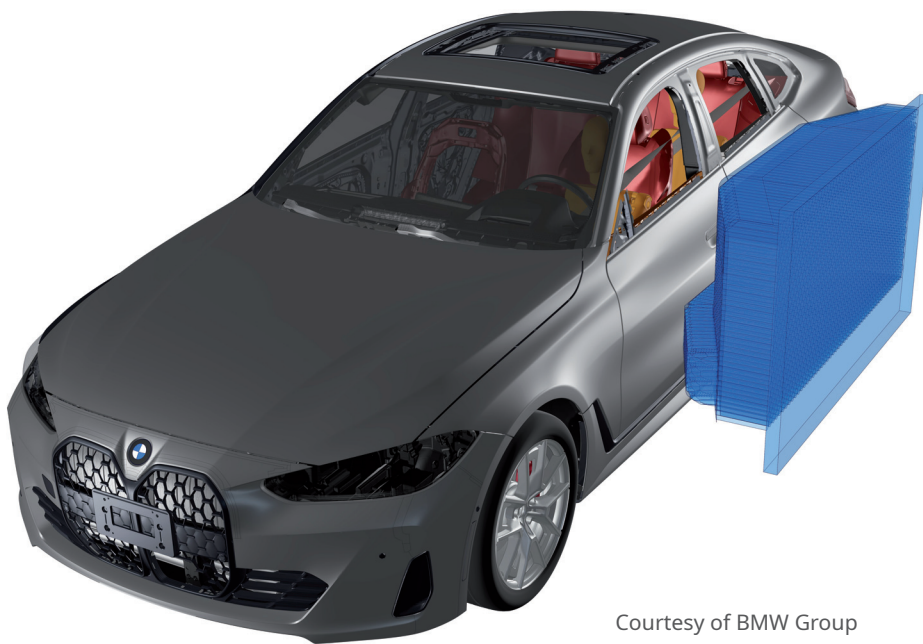


Book of Abstracts

16th LS-DYNA Forum 2022

11th - 12th October 2022 – Bamberg, Germany and online



Courtesy of BMW Group

Platinum Sponsors



Book of Abstracts

16th LS-DYNA Forum 2022

11 - 12 October 2022 – Bamberg, Germany

The conference is organized by



Copyright

Copyright © 2022 by DYNAmore GmbH. Permission to reproduce any papers contained herein is granted provided that credit is given to DYNAmore, the author, and his/her company. Authors retain their respective copyrights.

DYNAmore GmbH, Industriestr. 2, D-70565 Stuttgart, Germany
Tel. +49 (0)711 - 459600 – 0, E-Mail: info@dynamore.de, Web: www.dynamore.de

ISBN 978-3-9816215-8-7

Drive change safely

Achieve big evolutionary steps in your products, with low risk.

Contemporary industry demands short product evolution cycles. This requires new technologies that will accelerate engineering simulation, create new best practices, expand application fields, and unleash the benefits of collaboration. Deploy our software to broaden your simulation horizons, eliminate tedious tasks, speed up simulation processes, and empower collaborative decision making.

physics on screen

www.beta-cae.com

PLATINUM SPONSORS



GOLD SPONSORS



SILVER SPONSORS



SPONSORS

15 - 21

KEYNOTE PRESENTATIONS

Recent Developments in LS-DYNA, part I & II 22
Ansys/DYNAmore

Application Development with LS-DYNA & LS-OPT at BASF SE 22
Andreas Wüst (Simulation Engineering & Ultrasim® - BASF SE)

Advanced Modeling Approaches for fresh and aged Li-ion Batteries at different Levels of Detail in LS-DYNA 22
Christian Ellersdorfer (TU Graz)

Material Modeling for Engine Containment Studies. Is there a One-For-All-Metals Methodology? 22
Paul DuBois (Consultant)

CRASH I

A crash simulation methodology for Polypropylene foamed parts produced with core-back technology 23
M. Nutini (LyondellBasell)

Numerical validation of a sailplane fuselage crash test..... 24
C. Pohl, M. Hofmann, S. Schmauß, J. Löwe (TUM)

Prototyping and Virtual Testing of Sports and Work Helmets 27
C. Moos, M. Pfeiffer, Prof. S. Kolling (THM), K.-D. Klass (Senckenberg Gesellschaft)

PEDESTRIAN SAFETY

An enhanced modular approach for addressing the complexity of pedestrian analysis 29
N. Tsartsarakis (BETA CAE Systems)

Development of Mobile Security Barriers 32
M. Sebik (SVS FEM)

Simulation and Physical Testing of an Innovative ‘floating’ Shallow Mount Hostile Vehicle Barrier 34
J. Farley (Arup)

ELECTROMAGNETICS

Recent Developments of the EM-Module in LS-DYNA – A Discussion 35
L. Kielhorn, T. Rüberg, J. Zechner (TAILSIT)

Snapping magnets with LS-DYNA: Experimental Validations 36
I. Caldichoury, P. L’Eplattenier, T. Nguyen, S. Medikonda, M. Hernandez, C. South (Ansys)

Battery Management Systems (BMS) Analytics, Collaboration and Decision Making with support for Crash and Safety Test-Data using d3VIEW 39
S. Bala (d3VIEW)

POLYMERS

New material MAT_307: A viscoelastic-viscoplastic constitutive formulation to model adhesives during the complete manufacturing-crashworthiness process chain.....	40
T. Klöppel (DYNAmore)	
Material Characterization and Numerical Modeling of Monolithic Polycarbonate under Low and High Strain Rate Loadings.....	42
I. Colamartino, N. Ghavanini, L. Scampini, P. C. Astori, M. Anghileri, A. Perrier-Michon (Politecnico di Milano)	
Establishment of a robust methodology for modeling different types of failure behavior in thermoplastics materials.....	44
S. Mohapatra, S.Kamat (SABIC)	

BATTERY

Abuse characterization and simulation of battery cells and cell arrangements	54
M. Schwab, H. Pothukuchi, S. Riemelmoser (4a engineering)	
From Single Cell Abuse Experiments to Thermal Runaway in Electric Vehicle Crash Simulations	56
P. L'Eplattenier, I. Caldichoury, K. Kong, V. Challa, D. Bhalsod, S. Adya, M. Howard (Ansys)	
Nachhaltiger Leichtbau durch Monomaterialbauweise eines Batterischutzgehäuses	60
F. Huberth (Fraunhofer IWM), M. Hegde (KIT FAST)	
Electrochemical-Thermo-Mechanical Coupled Abuse Models for Lithium-ion Battery in LS-DYNA	61
K. Im, Z.-C. Zhang, G. Cook Jr. (Ansys)	
An anisotropic constitutive approach for analogous modeling of Li-ion cells	63
A. Trondl, F. Andrieux (Fraunhofer IWM)	

NUMERICAL METHODS

Instability and Mesh Dependence – Part 1: Analytical criteria	65
P. DuBois (Consultant), M. Feucht (Mercedes-Benz), F. Andrade, T. Graf, S. Conde, A. Haufe (DYNAmore)	
Instability and Mesh Dependence – Part 2: Numerical simulations.....	66
F. Andrade (DYNAmore), P. DuBois (Consultant), M. Feucht (Mercedes-Benz), T. Graf, S. Conde, A. Haufe (DYNAmore)	
Ansys LS-DYNA OneMPI Methodology.....	67
E. Day, J. Wang, F.-H. Rouet, B. Lucas (Ansys)	
Data-driven analysis of LS-DYNA's time step estimates and a machine learning based estimate.....	70
T. Willmann, M. Schilling, Prof. M. Bischoff (University of Stuttgart)	
Framework of conducting a reliability analysis using stochastic nonlinear FE models in LS-DYNA.....	72
C. Petrie, F. Oudah (Dalhousie University)	

FORMING I

Modeling variations in the virtual process chain of forming and joining.....	74
P. Brix (Mercedes-Benz)	
The Investigation of the Effect of Punch Velocity Increment on the Thickness of Plate Heat Exchanger (PHE) Layers	76
I. Şimşek (Bosch)	
A cost-effective Cold Roll-Forming FE model for industrial applications.....	78
L. Marconi (CRM Group)	
Forging simulation using the example of a knife.....	80
W. Rimkus, S. Zorniger (Hochschule Aalen)	
Ansys Forming – GUI for sheet metal forming simulation with LS-DYNA	81
V. Steininger (Tiwaquest)	

COMPOSITES

A closed multiscale simulation framework for the simulation of woven composite structures	82
M. Vinot, M. Holzapfel, N. Toso (DLR)	
Load Bearing Capacity Prediction of Non-Crimp Fabric Composites Using MAT54 and MAT58 Constitutive Models	85
A. Cherniaev (University of Windsor)	
Comparative Study of Impact Energy Absorption Performance of Cylindrical Honeycomb Structure Based on Origami Engineering	87
S. Tokura (TSR)	
Thermo-mechanical homogenization of laser-generated composite materials	89
S. Alameddin (University of Stuttgart)	

CRASH II

Automatic detection of similarities and exceptions in deformations and mesh functions over many crash simulation results.....	91
M. Pathare, Prof. J. Garcke, R. Iza-Teran, D. Steffes-lai (Fraunhofer SCAI)	
Development of a 2020 SUV vehicle FE model	93
R. Reichert (GMU)	
Electric Power Assisted Steering System In Vehicle Level CAE Simulation	95
G. Song (Ford Motor Company)	
Dynamic evaluation of vehicle roof systems under crash scenarios: An approach to early detection of potential concerns.....	97
D. Patil (Mercedes-Benz)	

HUMAN / MATERIAL MODELING

Advanced material modeling with user subroutines 106
 R. Abdusalamov, M. Hillgärtner, R. Chandrasekaran, K. Ngoc Vu, M. Itskov (RWTH Aachen)

Efficient gradient-enhancement of ductile damage for implicit time integration 108
 J. Friedlein, J. Mergheim, P. Steinmann (Friedrich-Alexander-Universität)

Method Development Characterization, Modeling and Simulation of Hygro-Thermo Effects in Thick Layer Adhesives 110
 F. Kötz, Prof. A Matzenmiller (Universität Kassel)

10 years human modeling at DYNAmore and future projects 112
 A. Gromer, D. Fressmann (DYNAmore)

FORMING II

Simulation of sheet metal forming and current developments 113
 M. Fleischer (BMW Group)

Analysis of Global Sensitivities for One-Step and Multi-step Deep-Drawing Simulations 117
 T. Lehrer, T. Daiminger, M. Wagner (OTH Regensburg), A. Kaps, Prof. F. Duddeck (TUM), I. Lепенies (SCALE)

3D-Shell Elements for Improved Prediction Quality in Sheet Metal Forming Simulations 119
 M. Schilling (University of Stuttgart)

Recent Developments in Dynaform 121
 J. Chen (eta)

MULTIPHYSICS

Oil Flow and Cooling Analysis using Incompressible SPH 122
 E. Yreux, S. Pathy (Ansys)

LS-DYNA Structured ALE: Recent Progress 123
 H. Chen (Ansys)

Recent Developments in WB LS-DYNA 125
 E. Plugge (Ansys)

CLOUD COMPUTING

Transitioning LS-DYNA workloads to the Cloud in the path to Digital Maturity 126
 I. Fernández (Gompute), D. Dorribo (Gridcore)

Enabling Performance Isolation for LS-DYNA in Multi-Tenant Supercomputing Platforms 130
 O. Maor, G. Shainer, Y. Qin, G. Cisneros-Stoianowski, D. Cho (HPC-AI Advisory Council)

DROP TEST

Drop Response Simulation of Balanced Armature Receivers for Hearing Aid and Professional Audio Applications	133
M. Javadzadeh Moghtader, M. Colloca (Sonion)	
Development of Fall Strength Design Method for Portable Products	135
J. Morimoto, Y. Hasebe (Toshiba Tec)	
Drop test simulation of short fiber composites with LS-DYNA in Ansys Workbench	137
F. Negri, S. Mendy, F. Pavia, S. Acharya, H. Mao, S. K. Meenakshisundaram (Ansys)	
Cumulative Loading on small home appliances during shipping.....	139
S. Chavan, S. V. Jagtap, N. Wankhede, A. Mandal, K. Kusupudi (Whirlpool)	

PROCESS

Parameteridentifikation zur Prozess-simulation des Hochgeschwindigkeits-Bolzensetzens.....	141
M. Gerkens	
Framework für die numerische Sensitivitätsanalyse von Prozessketten zur Herstellung komplexer Karosseriebauteile	144
S. Kriechenbauer, I. Lepenies (SCALE), S. Hensel (Fraunhofer IWU)	
A Deep Learning Approach to Predict the Deviation of Sheet Metal Parts in Deep Drawing Process	146
A. Farahani, J. Vitay, F. Hamker (TU Chemnitz)	
Connector Wear Modeling and Testing Validation of Server Hardware	148
A. Alfoqaha, E. Campbell, K. O'Connell, M. Hamid, S. Canfield, S. Khambati (IBM)	

WELDING AND HEAT TREATMENT

Simulation based distortion management for multiple stage assembly of welded structures	153
T. Loose (Dr. Loose GmbH)	
Change of material behavior due to Bake Hardening and its implementation in the simulation of the process chain	155
M. Hofmann (TU Dresden)	
Multi-Shape Modeling of Line Welds in Crash Models using ANSA.....	157
T. Fokylidis (BETA CAE Systems), N. Pasligh (Ford-Werke)	
Towards Faster 3D Simulations of CFRTP Induction Welding	160
M. Duhovic (TU Kaiserslautern)	

SDM

Automatic Outlier Detection for Crash Simulation Results 164
 C.-A. Thole, D. Borsotto, V. Krishnappa, K. Schreiner (SIDACT)

**Future Engineering Data Management: Datengesteuerte Produktentwicklung mit
 einem einzigen System für alle Engineering-Daten 166**
 C. Woll (GNS Systems)

**Introduction to Machine-Learning Capabilities in d3VIEW for Numerical,
 Categorical, and 2D Data Learn and Predictions for Data-Science and non-Data-
 Science Engineers 167**
 S. Bala (d3VIEW)

IGA

Towards the Isogeometric Aero-Engine 168
 M. Kober (BTU)

Isogeometric Analysis in ANSA, challenges and solutions 170
 L. Rorris (BETA CAE Systems)

**Isogeometric Shell Components in Full Vehicle Crash Simulations:
 Hybrid Modeling 172**
 L. Leidingner, S. Hartmann (DYNAmore), D. Benson, A. Nagy, L. Li, M. Pigazzini,
 L. Nguyen (Ansys), F. Bauer (BMW Group)

Analysis of 3D structures using IGA solids: Current status and future directions 174
 S. Hartmann, L. Leidingner (DYNAmore), M. Meßmer (TUM), D. Benson, A. Nagy, L. Li,
 M. Pigazzini, L. Nguyen (Ansys)

15 YEARS GISSMO

GISSMO 1: A short introduction to the basic options 176
 D. Koch (DYNAmore)

GISSMO 2: Application to metallic materials 177
 Prof. A. Haufe (DYNAmore)

GISSMO 3: Application to polymers 178
 S. Conde (DYNAmore)

Automated material model generation in VALIMAT - AUTOFIT & AUTOFITUREFIT 179
 B. Hirschmann, C. Schober, B. Jilka, H. Pothukuchi (4a engineering)

A Robust Method for Identifying GISSMO Regularization Behaviour 181
 N. B. Kulkarni, S. Jurendic (Novelis)

OCCUPANT SAFETY I

Development of component tests to reproduce the bending of seatbelt webbing under transverse load 183
 C. Meinel (BMW Group), O. Schoeneich (IAT)

A novel method for characterizing seatbelt webbing bending response under tension force 187
 S. Schilling, A. Soni, T.-M. Voigt, F. Manneck, S. Gathmann (Autoliv)

Occupant Safety prediction..... 190
 D. Drougkas, N. Tzolas Nikolaos (BETA CAE System)

Adaption and integration of CORA in the validation process of occupant safety simulations 192
 C. Meinel (BMW Group), O. Schoeneich (IAT), M. Pabst (BMW Group)

Automotive Occupant Protection pre and post ADAS event using a LS-DYNA/Carmaker Co-simulation Approach with Model Center Integrate 193
 A. Nair, Z. Zhang, S. Choudhary (Ansys)

OPTIMIZATION

LS-OPT Pro Status Update 194
 N. Stander, A. Basudhar (Ansys) K. Liebold (DYNAmore), C. Keisser (DYNAmore France), A. Svedin (DYNAmore Nordic); C. Neal-Sturgess (Univ. of Birmingham)

Graph and Heuristic based Topology Optimization of 3D crash structures - Presentation of all essential modules of the fully automatic process 196
 Prof. A. Schumacher, F. Beyer (University of Wuppertal)

Creation of 3D geometry from topology optimization results for thin-walled structures 198
 A. Kaloudis, A. Malotka (BETA CAE Systems)

Rapid Next Generation Material Calibration for LS-DYNA using Workflows for Metals, Elastomers, Polymers and Foams in d3VIEW in on-Premises and/or Cloud Platforms 200
 S. Bala (3DView), P. DuBois (Consultant)

Mode Tracking in the Presence of Shape and Mesh Changes 201
 A. Basudhar (Ansys)

CFD

Improvements of LS-DYNA ICFD's steady state solver 203
 I. Caldichoury, F. del Pin, R. Paz, P. Huang (Ansys)

New developments in LS-DYNA ICFD for the R14 release..... 204
 F. Del Pin, R. Paz, P. Huang, I. Caldichoury (Ansys)

Fluid-structure Interaction Simulation of a Patient-Specific Heart Model with Automated Segmentation Using Simpleware 207
 C.-J. Huang, F. Del Pin, C. Maurathm, T. Marchal (Ansys), G. Hyde-Linaker, C. Goddard, R. Bryan (Synopsys)

Overview of the dual-CESE solver in LS-DYNA and its applications	209
G. Cook, Z. Zhang, K. Im (Ansys)	
Development of a two-way flow Chinese-dome digester (TWF-CDD) for enhancing anaerobic digestion performance.....	216
E. Agbor-ambang (Soka University)	
LS-DYNA ENVIRONMENT	
DYNAmore ECO SYSTEM - News on DYNAmore's LS-DYNA-Tools.....	218
S. Mattern (DYNAmore)	
Recent Developments in Envyo.....	220
C. Liebold (DYNAmore)	
DYNAmore ECO SYSTEM: The artists formerly known as LS-DYNA Tools.....	221
T. Graf, M. Hübner (DYNAmore)	
LS-PrePost News.....	222
P. Ho (Ansys)	
OCCUPANT SAFETY II	
Positioning Human Body Models based on experimental data.....	223
M. Oikonomou, M. Athanasios (Aristotle University), J. Iraeus (Chalmers University), L. Rorris, A. Lioras (BETA CAE Systems)	
Biofidelic positioning, pre-processing and post-processing of Human Body Models with ANSA and META.....	225
L. Rorris, N. Tzolas, A. Lioras, A. Fokylidis (BETA CAE Systems)	
Virtual simulations of side sled tests	227
J. Prchal (CAE Engineer) A. Kafková (CAE Engineer)	
Robustness Analysis of Passenger Airbag Out-of-Position Deployment Using LS-DYNA and DIFFCRASH	234
T. Ishizuka, M. Okamura (JSOL), R. Taylor (Arup)	
IMPACT/BLAST	
Modeling terminal ballistics of 25x137 mm M791 APDS-T.....	236
M. C. Simsek, M. Büyük (NuroI Teknoloji)	
The use of blast load simulation to manage risks	238
A. S. Duvall (Nuclear Transport Solutions) J. Squire (Sellafield)	
Large-scale ALE and SALE LS-DYNA simulation methods exemplified by blast scenarios in a partially collapsed rock embedded facility.....	240
R. Heiniger, B. Hochholding, D. Schröder (DYNAmore Swiss), F. Ubertini (Dynamic Phenomena)	
Simulation of Shock Transient Analysis on Wabtec Diesel Engines for Naval Vessels.....	242
P. Selvaraj, D. Shea (Wabtec)	

NVH/FATIGUE

**Recent updates in linear solvers towards NVH and fatigue analysis
in Ansys - LS-DYNA 249**
Y. Huang, T. Littlewood, Z. Cui, U. Basu, F. Rouet, D. Benson (Ansys)

Acoustic simulation of RJ-45 connector assembly 251
S. Meenakshisundaram, S. Acharya, (Ansys)

CIVIL ENGINEERING

Numerical simulation of soil cutting using SPH and SPG approach 253
F. Farzaneh (Florida State University), H. Rokhy, A. Kabir (University of Technology)

**Investigation of various concrete material models to simulate seismic response of
reinforced concrete columns subjected to cyclic loading 255**
F. Farzaneh (Florida State University), H. Rokhy, A. Kabir (University of Technology)

Hydrogen Risk Analysis During Severe Accidents In A Nuclear Power Plant..... 257
J. Amponsah (MESA)



CORNELIS[™]
NETWORKS

Cornelis Networks is a technology leader delivering purpose-built high-performance fabrics for High Performance Computing (HPC), High Performance Data Analytics (HPDA), and Artificial Intelligence (AI) to leading commercial, scientific, academic, and government organizations.

OUR DEEP FABRIC HISTORY

At Cornelis, high-performance networks are in our DNA. We have built on our deep fabric roots going back to SilverStorm, PathScale, QLogic, Cray, and Intel to form Cornelis Networks. Our solutions combine and enhance the best attributes of existing fabric technologies, while supporting our customers' workloads and embracing open standards.

OUR CUSTOMERS

Cornelis supports over 500 global customer installations serving government, academic institutions, and commercial enterprises in our relentless pursuit of technological and scientific advancements. Our customer-centric philosophy is reflected in our products, professional services, and technical support offerings.

OUR TEAM

Cornelis is powered by visionary architects, world-class hardware and software engineers, seasoned marketing and support professionals, and veteran leadership, all focused on a single purpose: to deliver innovative solutions that advance the mission of our customers to solve the world's toughest problems.

<https://www.cornelisnetworks.com/>



Moving Forward for a Sustainable World

Fujitsu's purpose is to make the world more sustainable by building trust in society through innovation.

As the digital transformation partner of choice for customers in over 100 countries, our 124,000 employees work to resolve some of the greatest challenges facing humanity. Our range of services and solutions draw on five key technologies: Computing, Networks, AI, Data & Security, and Converging Technologies, which we bring together to deliver sustainability transformation.

A recent example is the supercomputer Fugaku that has been designed in co-creation with RIKEN. Fugaku remains one of the world's leading supercomputers and is used by scientists to solve many social problems.

Fujitsu Limited (TSE:6702) reported consolidated revenues of 3.6 trillion yen (US\$32 billion) for the fiscal year that ended on March 31, 2022 and remains the top digital services company in Japan by market share.

Find out more: www.fujitsu.com



Power at Scale with Intel® HPC Technologies

The Intel® comprehensive HPC technology portfolio helps customers achieve outstanding results for demanding workloads and the complex problems they solve.

Intel® HPC hardware is designed to scale from stand-alone workstations to supercomputers with thousands of nodes. Deep learning acceleration is built right into the chip, so Intel® processors are a great choice for innovative solutions that combine HPC and AI.

Intel also provides Intel® oneAPI cross-architecture software development tools for HPC. Intel's open software approach and collaboration with a wide range of partners worldwide support a broad ecosystem that helps developers realize more value from technology investments.

Learn more at: www.intel.com/hpc

ARUP

Arup is an independent firm of designers, planners, engineers, consultants, and technical specialists. Oasys Ltd is the software house of Arup and a distributor of the LS-DYNA software in the UK, USA, India, and China.

We have been working with the LS-DYNA software for over 30 years. Our in-depth knowledge of this powerful analysis solver has enabled us to create the Oasys Suite - a tailored suite of tools that give you the power to prepare models, interpret results and share solutions.

<https://www.oasys-software.com/dyna/>

Atos

science + computing, ein Unternehmen der Atos Gruppe, ist seit über 30 Jahren der kompetente Partner für den Aufbau und Betrieb großer und komplexer HPC-Umgebungen und bringt dabei langjährige Erfahrung in Konzeption, Implementierung, Betrieb und kontinuierlicher Optimierung und Automatisierung von HPC-Umgebungen für CAE-Anwendungen mit. Mit einem Team von mehr als 250 hocherfahrenen HPC-Experten konzentrieren wir uns auf die Entwicklung und Umsetzung von Lösungen für hochspezialisierte Anforderungen in den Abteilungen Forschung, Entwicklung und Konstruktion. Dabei legen wir besonderen Fokus auf:

- **Zuverlässigkeit und Agilität:** Die hochkomplexen Umgebungen und Workflows der verschiedenen R&D-Bereiche erfordern umfangreiches Industrie-Knowhow und ein ausgereiftes Betriebsmodell.
- **Betriebs- und Kosteneffizienz:** Die Nutzer sollen die Services als hoch performante Unterstützung erleben, damit sie sich vollkommen auf ihre eigene Aufgabe konzentrieren können. Unser Betrieb zeichnet sich dabei durch seinen hohen Grad an Automatisierungen und ein effizientes Shoring-Modell aus.
- **Stetige Innovation:** Durch kontinuierliche Verbesserungen, stetige Innovationen und frühzeitiges Erkennen von IT-Trends garantieren wir unseren Kunden einen zukunftsorientierten Service.
- **Berater & Partner.** science + computing ist für die Kunden ein langjähriger Vertrauenspartner, der sowohl auf technologischer als auch strategischer Ebene umfassend seine Expertise einbringt und einen Mehrwert liefert. Die umfangreiche Erfahrung und Best Practices helfen bei der Identifizierung und Umsetzung von Einsparungs- und Optimierungspotenzialen.
- **Klimaneutral:** Die Reduktion des CO₂-Fußabdrucks ist eine unverzichtbare Komponente unserer Lösungsarchitektur. Unsere Vorschläge und Empfehlungen setzen dabei an vielfältigen Stellen an und verfolgen sowohl inkrementelle als auch disruptive Ansätze. Darüber hinaus kann science + computing auch auf prozessualer Ebene unterstützen und Dekarbonisierungsmethoden und Net-Zero-Lösungen im Entwicklungsprozess verankern.

<https://atos.net/de/deutschland/sc>



BETA CAE Systems transformed CAE by introducing revolutionary automation software tools and practices into Simulation and Analysis processes almost 30 years ago.

Committed to our mission to enable engineers to deliver results of high value, we continue to offer state-of-the-art, high-performance software and best-in-class services. Our simulation solutions liberate low risk and high Return-On-Investment innovation.

The ground-breaking technology, the excellent services and our high standards of business ethics are the three pillars on which BETA was founded and grows since then.

Our passion for engineering, our drive for excellence, and our loyalty to customers and partners, are the key ingredients of our success. We first established our reputation in the Automotive sector and now we are proud of the deployment of our software also in the Aerospace, Defence, Biomechanics, Electronics, Energy, and other industries. Our solutions exceed their requirements in all the simulation disciplines, and allow for the development of the right product, for the right market, at the right time.

www.betacae.com



A Data-to-Decision Platform

d3VIEW, Inc. is head-quartered in Rochester Hills, Michigan, USA. Founded in 2003, the d3VIEW team is led by its Founder and Chief Executive Officer, Suri Bala, who with his decades of experience in the simulation industry and through continuous innovation, pioneered the data-to-decision platform with the mission of empowering engineers and scientists with knowledge and insights from their data to accelerate virtual product design, development and optimization.

Multiple interactive applications which are integrated seamlessly in one comprehensive platform not only make d3VIEW more appealing with its powerful features in the areas of data mining, storage, analysis, collaboration, visualization, prediction, material calibration, to name a few, but also extend the possibility of tremendous automation and tackling of complex engineering problems by anyone with minimal exposure or expertise. Originally designed and developed for addressing the pain points in Crashworthiness, d3VIEW is now widely used in a variety of other science and non-science areas including NVH, HVAC, Battery Management, Precision Medicine, Long Range Planning, etc.

For more information on how d3VIEW can help address your needs, please email info@d3view.com.



4a engineering GmbH is a technically oriented Research and Development company with a focus on plastics engineering and materials science. The core competence of 4a engineering GmbH resides in concept finding and optimization of product ideas based on the profound understanding and interpreting of physical and mechanical processes. 4a engineering GmbH works with a wide range of partially specially developed simulation software and analyzing methods. We are offering engineering and R&D services as well as our products **VALIMAT™**, **FIBERMAP™**, **MICROMECC™** and **IMPETUS™**.

IMPETUS™ sets new standards in the area of **dynamic material characterization**. The 4a-inhouse-developed testing system for the characterization of materials, especially plastics, is based on a pendulum working without additional actuation power. The testing system can be operated on a common office desk located in the Research & Development department.

VALIMAT™ is the software solution for managing material tests and for the generation of **validated material cards for plastics, composites, metals and foams**. The software automatically generates FE-Models for the relevant tests. The parameters for the material card are optimized by an automatic reverse engineering process. VALIMAT™ supports the most common FE-solvers and material cards. The functionality was proven by hundreds of projects.

www.4a-engineering.at / <http://impetus.4a.at>

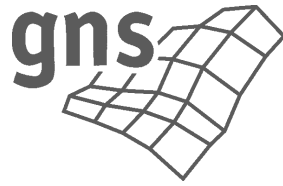


CASCATE GmbH was founded in June 2017 as a wholly-owned subsidiary of DYNAmore GmbH, based in Stuttgart. Motivated by the possibility of entering into a sales partnership with Siemens PLM Software, CASCATE GmbH offers software solutions in the area of simulation/CAE around the software packages:

- STAR-CCM+®
- Simcenter™
- Femap™

With a team of experienced engineers, we are happy to provide our customers with the appropriate support and services.

www.cascade.de



GNS has been active in the field of computer-aided simulation since 1994. The main business areas of the company include calculation services and the related software development.

The calculation services focus on crash simulation, numerical calculations for statics, strength and vibration behavior of structures as well as numerical simulation of forming and manufacturing processes.

GNS developed the software products Animator4, Generator4, OFSolv and OpenForm. With thousands of licenses sold worldwide, Animator4 is one of the most successful post-processors in the field of finite element structural simulation.

www.gns-mbh.com



Experts for smart CAx processes

Application | Automation | Tuning | Workflow

For more than 20 years GNS Systems optimizes IT processes around virtual product development. We are experts for CAx-applications, -automation, -tuning and -workflow. We bring our comprehensive engineering know-how to companies to help them achieve the best performance level for their simulation workloads.

www.gns-systems.de



SCALE GmbH is a subsidiary of DYNAmore Holding with headquarters in Ingolstadt and is specialized in technical development services for the automotive industry. In particular, the range of services includes software development for process and data management, as well as finite element method development and numerical optimization for functional design of vehicle components.

www.scale.eu

ANSYS

Engineering What's Ahead.

Simulation is a Superpower



Multiphysics simulation gives us the ability to explore and predict how products will work — or won't work — in the real world. *It's like being able to see the future, enabling you to innovate as never before.*

www.ansys.com

Recent Developments in LS-DYNA

Ansys/DYNAmore

Application Development with LS-DYNA & LS-OPT at BASF SE

Andreas Wüst (Simulation Engineering & Ultrasim® - BASF SE)

Advanced Modeling Approaches for fresh and aged Li-ion Batteries at different Levels of Detail in LS-DYNA

Christian Ellersdorfer (TU Graz)

Material Modeling for Engine Containment Studies. Is there a One-For-All-Metals Methodology?

Paul DuBois (Consultant)

A crash simulation methodology for Polypropylene foamed parts produced with core-back technology

Massimo Nutini, Markus Franzen, Mario Vitali

LyondellBasell Industries

1 Abstract

Light-weighting is not a new concept in the automotive industry, but it is now re-emerging as a fundamental strategy for a sustainable mobility as part of the trend towards circular economy. More rigorous targets in regards to reduced energy consumptions, emissions and pollutions are now the fundamental driving forces for the designers.

Polypropylene sandwich structures with foamed core have attracted much attention due to their advantage in terms of high strength-to-weight and high stiffness-to-weight ratio, low material usage and lightweight. Accordingly, the needs for numerical methodologies to predict their mechanical behavior is of paramount importance, since Finite Element (FE) analysis is recognized as an efficient tool for optimizing the use of material strength and to build structures with a minimal use of materials.

This paper proposes a simple numerical method to characterize and model the strain-rate dependent behavior of Polypropylene foamed parts produced with core-back technology. The method, based on a material three-layer model, is validated in a component test on industrial parts subjected to impact.

2 Numerical Method

The approach here presented was already proposed and applied to quasi static loading [1] and is now extended to dynamic/crash loading. It seems particularly suitable for parts produced with core-back foaming technology, which consist in: 1- injection of the melt polymer containing a Chemical Blowing Agent, during which a “skin” of compact solidified polymer forms in proximity of the mold surface, and 2- slight “opening” of the mold, during which the still melt “core” can expand into a foamed status.

The numerical procedure consist first of all in obtaining the Finite Element structural mesh from a modification of the unexpanded part mesh, by local modifications of the shell element total thickness as a function of the mutual orientation of the normal to the mesh element and the direction of the mold expansion. At the same time, a 3-layer (skin-core-skin) construction model is set for each element.

Skin layers are set to have an uniform thickness through the whole part, assumed in this case to be 0.45 mm, as from visual inspection of the exemplars used for validation. Skin material properties are set for the whole part as equal to those of the compact un-expanded material.

Core thickness is set for each element as the difference between the total thickness calculated in the first step and the thickness of the two skins, and is therefore different for each element in the mesh. Mechanical properties of the core are assumed to be derived from those of the unexpanded material through a scaling coefficient, which expresses a sort of a deterioration of the material properties due to the bubble generation in the core itself. Accordingly, such scaling coefficient is a function of the degree of expansion of the material and of the strain rate, and it is computed via FEM through reverse engineering, as the value which best reproduces bending tests carried out at various speeds on specimens with different expansion ratio.

In LS-DYNA simulations the MAT_024 law was chosen, with Gissmo criterion for damage and failure. The approach to damage was as in [3]. The bubble structure from foaming process was associated to a sort of pre-damage, computed based on elastic modulus variation vs. degree of expansion, obtained from tensile tests on samples with different expansion ratio. The damage threshold to rupture of the compact grade was then shifted based on such pre-damage for groups of elements having the same expansion ratio. Triaxiality dependence of fracture was taken from literature [4,5].

3 Experimental Validation

For the validation, an industrial part from automotive, for which the mold was available, with approximate dimensions of about 800 mm x 300 mm, with unexpanded thickness of 2.0 mm was used. The part was molded with core back technology and Chemical Blowing Agent, set to obtain exemplars with 3 different expansion ratios, with final thickness of 2.4 mm, 3.0 mm and 3.2 mm.

Parts were mounted and fixed on a support manufactured using 3D printing technology. High speed drop tower tests (2 m/s, 3 m/s and 4 m/s) with a spherical 65 mm diameter impactor and a mass of 20.7 kg were conducted at room temperature and then compared with the related simulations.

4 Results

The experimental force-displacement curves measured under the above mentioned experimental conditions of thickness and impact speed, were reasonably reproduced by the simulations. The overestimation of the force for high strains, observed in some cases, may be due to damage evolution with modalities different from those occurring under tensile loading, which the implemented model was based on. The good response of the model for low strains shows the validity of the three layer material model. The onset and propagation of fracture in the part are well captured by MAT_024/GISSMO. Examples are shown in the figures below.

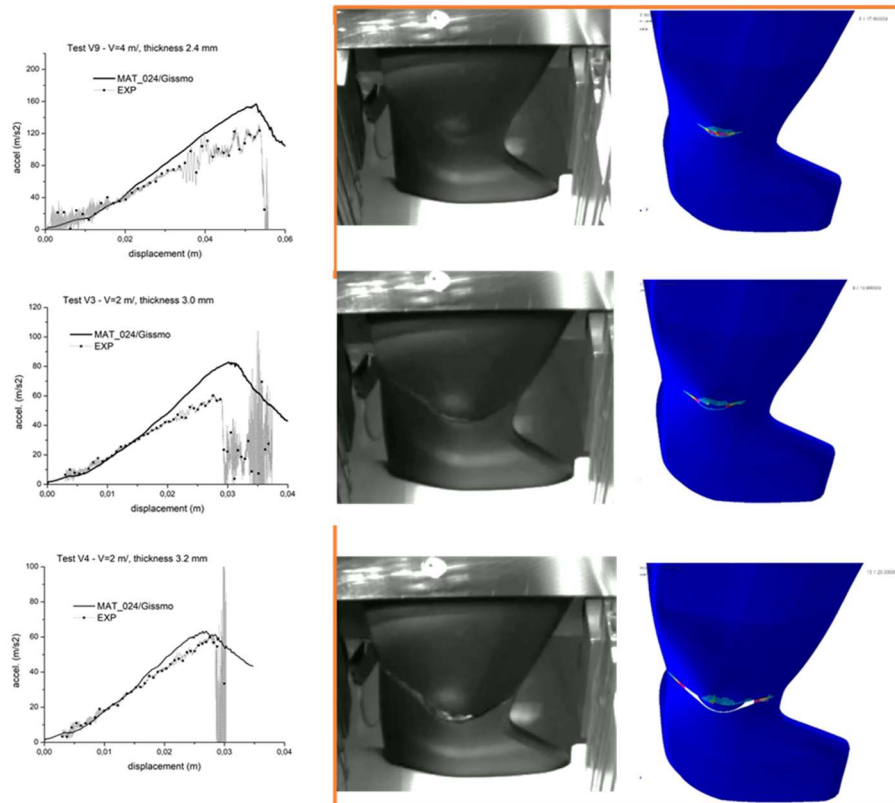


Fig.1: (Left) Force displacement measured under different test conditions and compared with MAT_024 results; (Right) From top to bottom: examples of images and plots at different time instants during the drop test at 2 m/s for a part expanded from 2.0 to 3.2 mm

5 Literature

- [1] M.Lecomte M, "Polypropylene: New Weight-Saving Opportunities", SFIP-Congress, 2011
- [2] Sadik T., Pillon C., Reglero Ruiz J.A., Billon N., "Polypropylene structural foams: Measurement of the core, skin and overall mechanical properties with evaluation of predictive models"; Journal of Cellular Plastics, Vol 53(1), 2017
- [3] Nutini M., Vitali M. " Characterization of Polyolefins for Design Under Impact: from True Stress/ Local Strain Measurements to the F.E. Simulation with LS-Dyna Mat. SAMP-1", 7th LS-DYNA German Forum, Bamberg, 2011
- [4] Lin. S., Xia Y., Lin C.H., Wang J., Gu G., "Stress State Dependent Failure loci of a Talc Filled Polypropylene material under Static Loading and Dynamic loading", 13th Int. Conference on Fracture, June 16-21, 2013
- [5] Dayan H., Andreassen E., Grytten F., Osnes H., Gaarder R.H., "Shear Testing of polypropylene materials analyzed by digital image correlation and numerical simulation", Experimental Mechanics, 2012

6 Acknowledgments

The authors and LyondellBasell thank the Company SMP Deutschland GmbH, Bötzingen for the collaboration, the molding of the parts and the experimental tests

Numerical Validation of a Sailplane Fuselage Crash Test

Christian Pohl¹, Marvin Hofmann¹, Simeon Schmauss², Joscha Loewe²

¹ Technical University of Munich, TUM School of Engineering and Design, Chair of Carbon Composites, Germany

² Akaflieg München e.V., Technical University of Munich, Germany

1 Outline

About 5 to 10 persons lose their lives in small engine plane and sailplane accidents throughout Germany every year. Static testing of sailplane fuselage structures is the state-of-the-art certification procedure following EASA CS 22.561 [1]. In order to increase the survival rate during hard landing or crash conditions, LuFo V-3 project CraCpit (Crash Cockpit) aims to investigate the crashworthiness of a redesigned sailplane fuselage. A full-scale crash test loadcase was defined with a velocity of 15 m/s, an angle of sideslip of 5° and an impact trajectory angle of 45° against a rigid barrier. The design process of the full-scale glider prototype was accompanied by several numerical model creations to fully exploit the design space regarding the passive safety concept.

2 Hardware Crash Test

The full-scale crash test was carried out successfully at the Flugwerft Schleißheim (see Fig. 1). Eight high-speed cameras were installed to document the crash test. A 3D Digital Image Correlation system was used for the analysis of the impact conditions and the crash behavior. Evaluation of possible injury risks under the resulting loads was based on sensor data of the H3 50 percentile dummy. Additional sensors such as acceleration sensors and strain gauges were integrated into the structure for further validation and monitoring of the failure mechanisms. The fuselage was tested non-destructively based on the principle of large area radiation scanning before and after the crash test to document non-visible damage of the structure. The mass distribution of the fuselage including dummy and test equipment was measured to be able to replicate it in the numerical model.

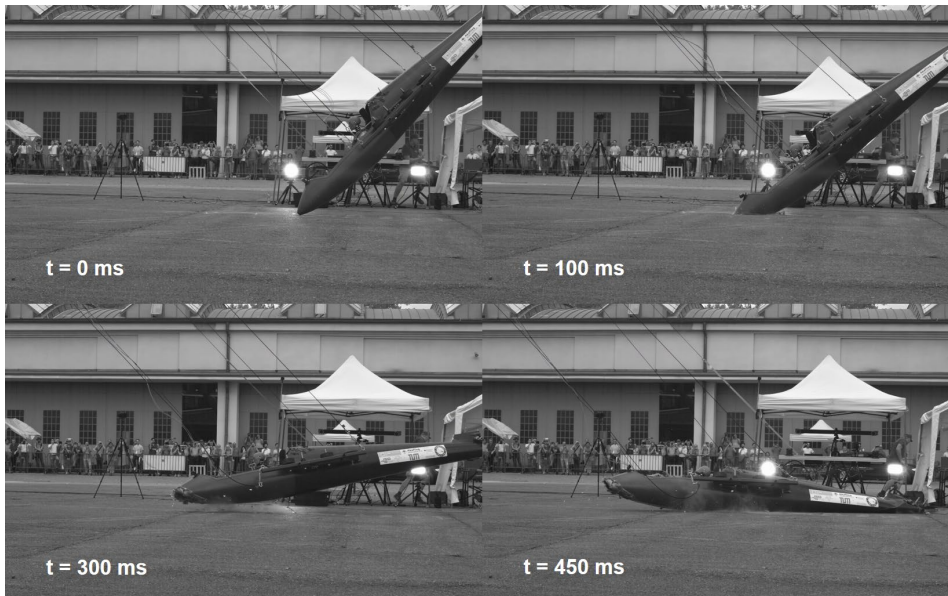


Fig. 1: Picture sequence of the first and second impact during the CraCpit crash test.

3 Numerical representation

One objective of the project is the predictability evaluation of fuselage crash simulations in LS-DYNA. Following the building block approach, material cards were defined based on quasi-static and dynamic properties of the integrated fiber-reinforced epoxy materials and adhesive.

***MAT_LAMINATED_COMPOSITE_FABRIC (*MAT_058)** was selected using the framework proposed by [2] to consider fracture toughness values and strain rate dependencies of the composite materials. To account for debonding failure, ***MAT_COHESIVE_MIXED_MODE_ELASTOPLASTIC_RATE (*MAT_240)** was utilized. The material cards were validated with omega-shaped generic subcomponent geometries in 3-point-bending experiments.

Inspired by preliminary works [3-6], the novel cockpit design was built up as a Finite-Element (FE) model based on the initial CAD data of Akaflieg München focusing onto the flight loads. The main structural adaptations were the introduction of massive reinforcement sandwich beams made of unidirectional CFRP and a foam core to ensure structural integrity. A layup optimization of the nose cone structure was conducted with LS-Opt to ensure the function of the crash concept in the fuselage [7]. This concept allows for controlled energy absorption in the nose cone section and reduction of the loads acting on the pilot by influencing the crash kinematics. Especially in the case of a crash against a soft barrier, the structure will be forced into a trajectory along the ground instead of punching the barrier. As for the hardware crash fuselage, tail unit and wings were represented by substitute masses. The FE model of the structure consists of 700,000 shell and 400,000 solid elements with a nominal mesh size of 6 mm. Cohesive elements were used to represent important structural adhesive connections inside the fuselage. A dummy model was positioned into the structure and the boundary conditions were taken over from the hardware crash test including a seat shell and belt system. This results in a calculation time of 30 hours for the first 150 ms of the crash using 28 Intel Xeon E5-2690 v3 cores providing a frequency of 2.6 GHz. The simulation facilitates a prognosis of the severity of the pilot's injuries and is a central element of the numerical model and crash concept validation.

4 Model Validation

The fuselage simulations show an accurate prognosis of the crash kinematics and damage behavior. Even small details of the failure in the simulation model are comparable to the hardware crash test. Passenger injury criteria of the simulation and the test show similar results, which proves the meaningfulness of the model. Head and neck injury criteria are non-critical for the pilot. The lumbar load criterion exceeds the critical value such that injuries of the spine could occur. During the crash test the substitute mass hit the ground. Due to the high stiffness of the structure, this has a significant effect on the evaluation of the second impact. Therefore, the mounting system carrying the substitute masses was modeled as well.

5 Summary

The presented results are a major step towards virtual certification in the aerospace sector. As a first step, virtual certification of smaller adaptations could be used to justify changes between the certified structure and future iterations. The validated simulation model should be utilized to calculate different load cases and conditions to enhance the understanding of various crash scenarios: a soft barrier could be modeled or the impact velocity could be increased. Crashworthiness of sailplanes and small engine planes still has potential for further optimization in future fuselage structures: a longer nose cone could help to absorb more energy in the early stage of a crash. Furthermore, the seat shell could be improved by integrating an energy absorbing structure below the pilot.

6 Literature

- [1] European Aviation Safety Agency: Certification Specifications for Sailplanes and Powered Sailplanes CS-22, Amendment 1, 24. September 2008.
- [2] Pohl C., Toenjes M., Liebold C., Ploeckl M., Koerber H., Avila Gray L., Colin D., Drechsler K.: Numerical prediction of composite damage behavior: A modeling approach including the strain-rate-dependent material response, Composite Structures, 115628, 292, 2022.
- [3] Lange Aviation GmbH, 01. September 2022, <https://www.lange-aviation.com/de/produkte/antares-21e/sicherheit/>.
- [4] Pottas, J.: A Numerical Investigation of the Crashworthiness of a Composite Glider Cockpit, Potchefstroom Campus of the North-West University, April 2015.
- [5] Schuster U., Wolf K.: Improvement of Sailplane Crashworthiness through Keel Beams with Silicone Cores, Technical Soaring Vol. 38, 28. April 2014, S. 16-26.
- [6] Sperber, M.: Untersuchung des Insassenschutzes bei Unfällen mit Segelflugzeugen und Motorseglern - Forschungsauftrag-Nr. L-2/93-50112/92, TÜV Rheinland GmbH - Institut für Verkehrssicherheit - Abteilung Luftfahrttechnik, Köln, 1998.
- [7] Jeberien, K.: Entwicklung und FEM-gestützte Optimierung eines Energieabsorberkonzepts für Segelflugzeuge zur Steigerung der Unfalltauglichkeit, Master's Thesis, TUM-LCC, 2021

Prototyping and Virtual Testing of Sports and Work Helmets

Christoph Moos¹, Marcus Pfeiffer¹, Stefan Kolling¹, Klaus-Dieter Klass², Urban Plangger³

¹Institute of Mechanics and Materials, Technische Hochschule Mittelhessen, Giessen

²Senckenberg Gesellschaft für Naturforschung Dresden, Dresden

³UVEX SPORTS GROUP GmbH & Co. KG

1 Motivation

Head protection is an important aspect not only for cyclists but also in the fields of work and sports. Systematic analysis of real-world accidents [1] as well as finite element (FE) simulations [2] point out the relevance of helmets for cyclists. In [3] the use of FE to predict the crash performance of different helmet designs for construction helmets is presented. These results show the necessity of helmet development as well as the capability of FE simulations to serve as a helpful tool within the process chain.

Aim of the present work is to determine the influence of different helmet structures, since structures on a body have a significant influence on its stiffness. Geometries of different complexity and their ability to absorb the energy of an impact and thus improve the damping properties were investigated. For this purpose, a basic geometry was designed, which was then virtually compared with different structures integrated into the outer shell. Biological templates of insect heads served as models for the structures. The optimized structures were manufactured using fused deposition modelling (FDM) and experimentally tested to verify the virtual optimization process.

2 Material Characterization

For the virtual analysis, material cards were generated for the materials Acrylonitrile Butadiene Styrene (ABS) and Expanded Polystyrene (EPS). Validation experiments were performed to verify the used material cards which were then used as a basis for the virtual structural optimization.

2.1 ABS

FDM may result in anisotropic material behaviour. Therefore, tensile and three-point-bending tests were carried out for 0°, 45° and 90° as well as 45° alternating material orientation to set up the material model. 45° and 90° tensile tests allow for linear elastic simplification until failure, see Fig.1(a). The mean elastic Poisson's ratio was 0.294 measured from tensile tests via digital image correlation. No significant strain rate dependency was observed in bending tests under different velocities, see Fig.1(b). As a simplified approach, alternating layer samples were used to fit the Young's modulus in ***MAT_ELASTIC** which was used together with ***MAT_ADD_EROSION** to represent the ABS material. FDM half-shell specimens were loaded in a compression test to validate the material card, see Fig.1(c).

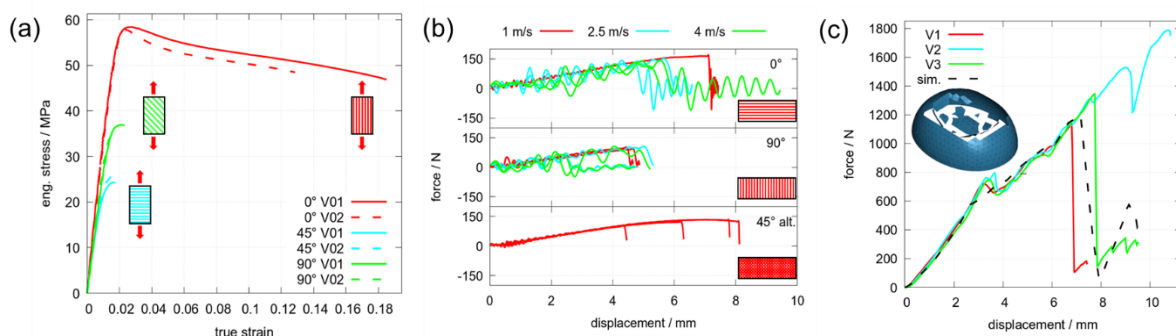


Fig. 1: (a) Results of the tensile tests; (b) Results of the dynamic three point bending tests; (c) validation of the material card ***MAT_ELASTIC** with ***MAT_ADD_EROSION**

2.2 EPS Foam

EPS was used as damping inlayer for the virtual examination. On the basis of quasi static tensile and dynamic compression tests, see Fig.2(a) and 2(b), ***MAT_SAMP-1** was calibrated to represent the

elastic-plastic material behaviour. Drop tower tests on damping structures of bicycle helmets were performed for validation, see Fig.2(c).

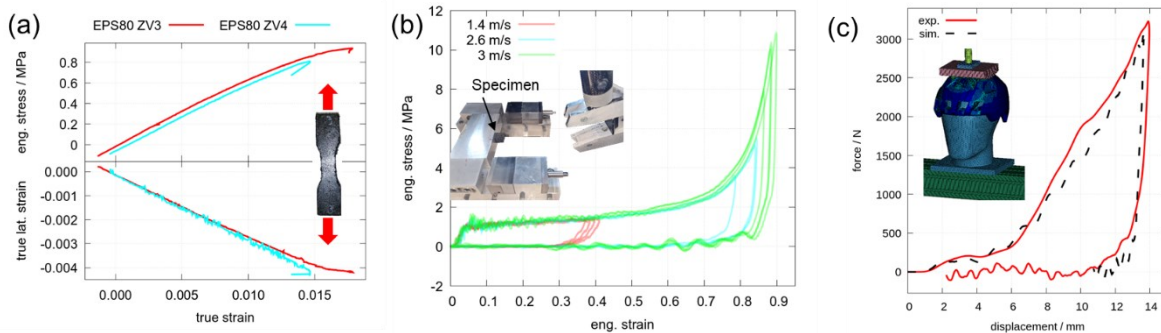


Fig.2: (a) Results of the quasi static tensile tests; (b) results of the dynamic compression tests; (c) validation of the material card `*MAT_SAMP-1`

3 Virtual Testing and Rapid Prototyping

A dummy head was modeled carrying a fixed EPS damping layer on which different helmet shells, based on biological models, were designed. They were crashed against a rigid wall at 5.4 m/s and the HIC (head injury criterion, see e.g. [4]) was computed to compare the designs, see Fig.3a. The most promising geometry (PA 5) was fabricated using FDM and tested in drop tower tests for validation against the reference geometry (smooth half shell PA 0), see Fig.3b.

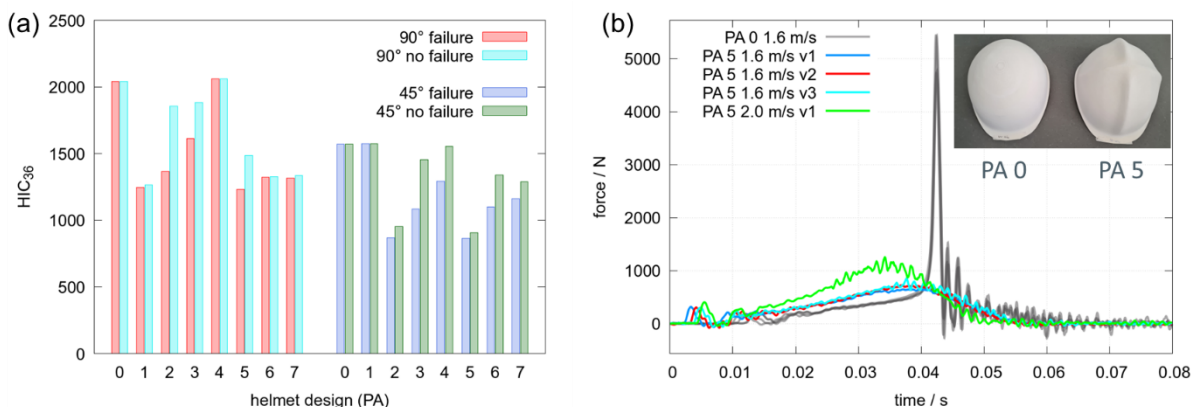


Fig.3: (a) Comparison of the virtually tested helmet structures using HIC_{36} ; (b) drop tower test results of the optimized geometry (PA 5) compared to the reference geometry (PA 0)

4 Summary

In the present work biological models were used to optimize the outer shell of helmets. Ridges in the head capsules of insects were transferred into the helmet structure and virtually tested. The characterization of relevant materials resulted in reliable FEM predictions for the rapid prototyping. A structurally improved helmet was produced via FDM and experimentally tested. In comparison to a smooth half shell helmet the structural improvements resulted in a significant reduction of the measured force in the conducted drop tower tests. The interaction of FEM and FDM allowed for fast development cycles to approach an optimized helmet structure.

5 Literature

- [1] Olivier, J. and Creighton, P.: "Bicycle injuries and helmet use: a systematic review and meta-analysis." *International Journal of Epidemiology* 46.1 (2017): 278-292.
- [2] Fahlstedt, M., Halldin, P. and Kleiven, P.: "The protective effect of a helmet in three bicycle accidents - A finite element study." *Accident Analysis and Prevention* 91 (2016): 135-143.
- [3] Long, J., Yang, J., Lei, Z. and Liang, D.: "Simulation-based assessment for construction helmets." *Computer Methods in Biomechanics and Biomedical Engineering* 18.1 (2015): 24-37.
- [4] Hess, R. L., Weber, K., Melvin, J. W.: "Review of literature and regulation relating to head impact tolerance and injury criteria" (1980)

An enhanced modular approach for addressing the complexity of pedestrian analysis

Nikolaos Tsartsarakis¹, Athanasios Lioras²

BETA CAE Systems SA

1 Introduction

Pedestrian analysis has been considered an important part of Safety standards for some time now. This specific CAE analysis differentiated itself from the start from other similar ones in the field through its large number of solver runs needed for each load case. Combining the latter with the modular approach of building models on one hand and the introduction of numerous new load cases on the other, provides a picture of the complexity involved. This presentation describes how the new modular run management approach of BETA CAE Systems for managing the mazy simulation model structure can be applied for the pedestrian analysis case.

2 Simulation Run Management approach of BETA Suite

The BETA Suite offers an integrated solution for comprehensive Simulation Run Management. The key characteristic of this approach is the flexibility and efficiency of modular model organization along with the robustness offered by the simulation run composition tools that guarantee the integrity of the run after every modification on module level.

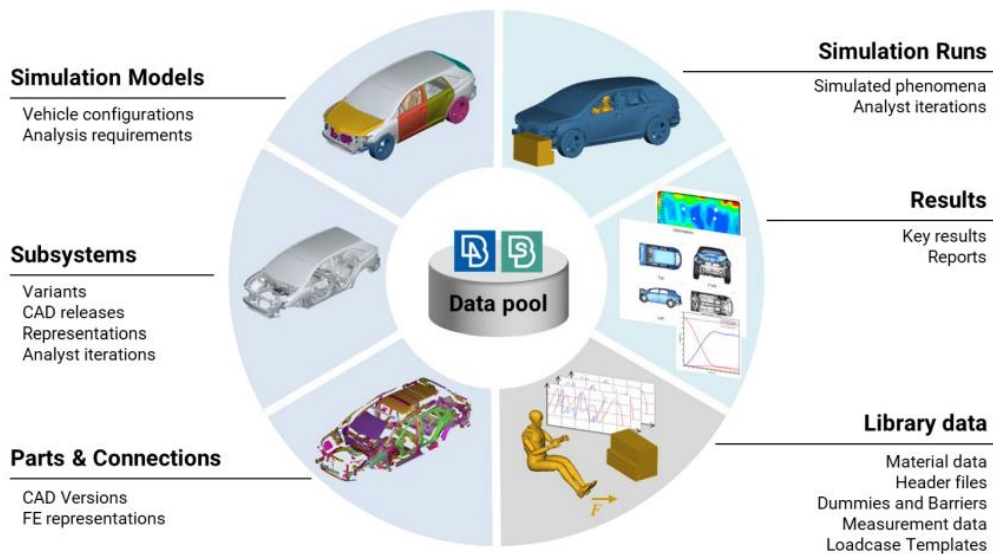


Fig.1: Main terms of Simulation Run Management approach of BETA Suite

This solution is compatible with both file-based and server-based data systems combining the latter with SPDRM back-end application of BETA Suite. Browsing and managing data can be accomplished through KOMVOS standalone front-end application as well as via ANSA and META, pre and post processor respectively.

	File-based DM	Server-based DM
Server	-	SPDRM Server
Client (desktop)	KOMVOS	
Client (embedded in BETA Suite Apps)	ANSA & META	

Fig.2: Summary table of Data Management solutions

3 Build Modular Pedestrian Loadcase in ANSA and solve in LS-DYNA

The uniquely close interaction between the data management system and the pre-processing pedestrian marking tool offers seamless generation of simulations.

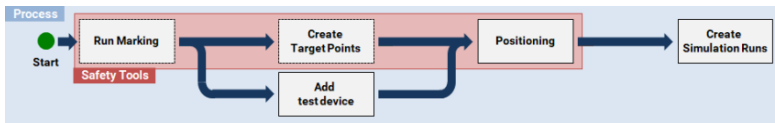


Fig.3: Workflow of building Modular Pedestrian Loadcase in ANSA

Through the Marking process, lines on the model and target points are generated according to the selected protocol. The test devices loaded from data system are positioned at each target point, through the positioning process. Runs are created massively, one for each target point and are stored in data system.

The runs are submitted in LS-DYNA solver, the output solver data are then stored in data system containing links with their respective runs.

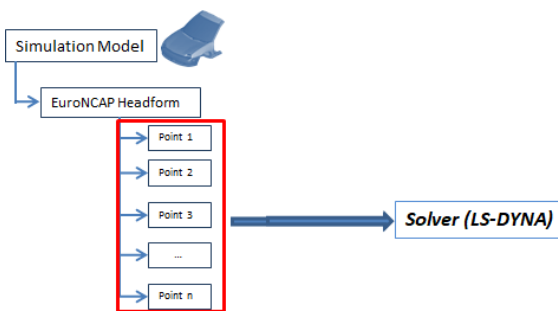


Fig.4: Graphical representation displaying the runs stored under Simulation Model and their submission to LS-DYNA Solver

4 Post-process Modular Pedestrian Loadcase

The dedicated pedestrian evaluation tool embedded in META post processor, facilitates the post processing of runs. Key performance indicators such as the Head injury criterion of the head impactor, Tibia and Femur moments curves of the leg impactor or section videos of the impact location of a single calculation are then stored individually in the data system through easy-to-use post-processing session files.

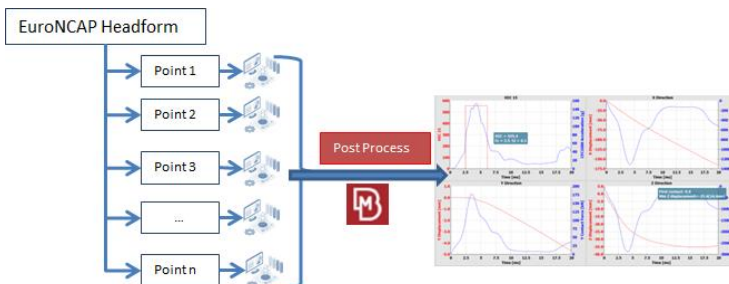


Fig.5: Apply post process actions on runs

The system can then collect upon demand all necessary key indicators from a series of runs and model versions so as to provide them to the post-processor pedestrian evaluation tool to achieve overview visualizations.

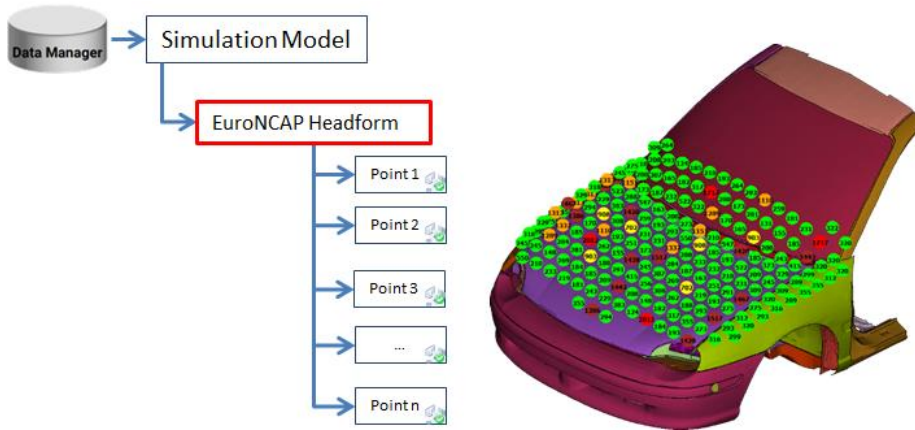


Fig.6: Achieve overview visualization of key results

The evaluation tool includes some unique functionality for the comparison of overview visualization and of individual key indicators between variants, whereby key results values still retain their link to their respective runs, models and subsystems in the data management system. Data related with the whole loadcase scenario such as summary reports of all the runs, spreadsheets required for specific protocols, images displaying an overview of all the key performance indicators are generated and then stored in the data system with references to the respective Loadcase.

5 Create Iterations

Runs that do not meet the performance criteria can be improved by applying modification on the model. This can be achieved by making a modification to one or more of model's contents and saving a new version of the model that contains references to the new modified contents. The variant runs can then be generated using the same Loadcase set it up for the baseline model. The runs are then created directly when the changes do not affect the exterior of the model. Otherwise, the marking and positioning process should be rerun in ANSA.

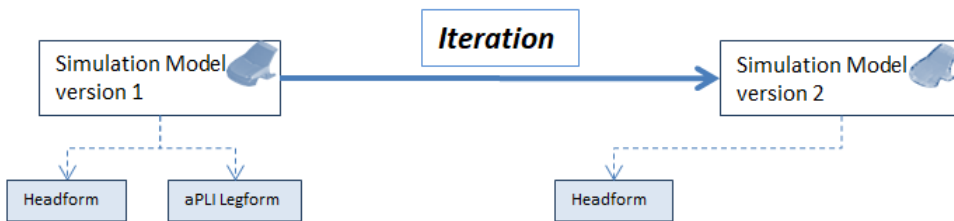


Fig.7: Create Simulation Model Iteration

The great benefit in this case is that changes are done only on the Subsystem level and then the Modular approach facilitates and streamlines assembling the new Simulation Model version (the main file for the model), combining it with the Loadcase needed and generating the new Simulation Runs (the simulations for submission).

6 Literature

- [1] ANSA User's Guide v23.0.0
- [2] META User's Guide v23.0.0

Development of Mobile Security Barriers

M. Šebík¹, M. Popovič¹, M. Drdlová²

¹SVS FEM s.r.o., Czech Republic

²Research Institute for Building Materials, Czech Republic

1 Introduction

Safety of the citizens should be a priority of all governments and municipalities in modern world. There are of course many threats that should be considered when dealing with public security. One of them is certainly a possible terrorist attack. The threat of the vehicle attack must be taken very seriously not only because of the possible effect of such attack but also mainly because of the accessibility of vehicles.

The security systems of cities these days usually contain (among other means of safety and preventive measures) fixed security barriers and mobile security barriers. Modern fixed security barriers like bollards, road blockers, gates, etc. can be in most cases implemented to the urban environment with no problem as they are already designed for this purpose. On the other hand for the temporary barriers, the authorities often choose mobile barriers designed for another purpose (traffic New Jersey barriers), police or firefighters' trucks or other objects like sand sacks etc. These measures cannot guarantee sufficient security of the area as they have not been designed nor tested for this purpose. There is also a group of mobile barriers that were developed in order to effectively stop the hostile vehicle but they do not satisfy an aesthetic function of the urban environment. These barriers often have steel structure with many spikes which makes them hazardous to be placed in the urban environment with many pedestrians passing by. To sum up, there is a missing piece among the mobile barriers. Barriers that would meet all the mentioned requirements and could be used by the municipalities to complement their anti-terrorist security system are still missing on the market.

This project is focused on the development of such barriers. To be more specific, this work is dealing with two levels of threat: a vehicle from N1 category (CWA 16221) – small van, 3,5 t, and N3 category (CWA 16221) – 8x8 truck, 30 t. All the virtual testing of the barrier was done in Ansys LS-DYNA explicit solver. Due to the fact that majority of the development of these barriers is done in the virtual world, it is possible to preview the results of the crash test simulations also in augmented reality.

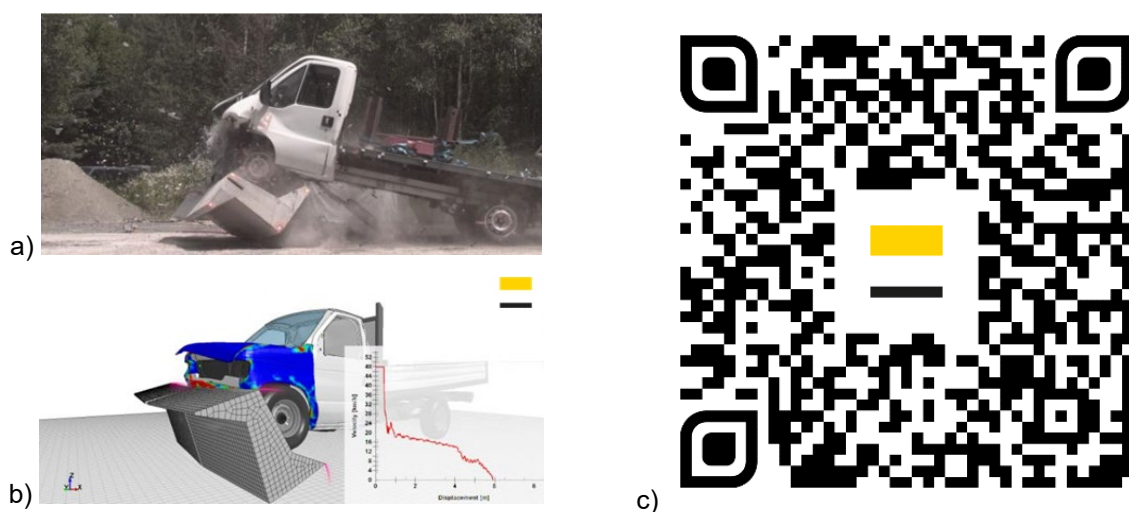


Fig. 1: N1 vehicle crash test: a) experiment, b) simulation, c) augmented reality

2 Model of barrier – ground contact

One of the crucial aspects when simulating mobile barrier crash tests is barrier- ground contact. Common approach utilizes automatic contact types like for example *CONTACT_AUTOMATIC_SURFACE_TO_SURFACE. This approach is, however, in cases of barriers with sharp edges and spikes which penetrate the surface of the ground often insufficient. This phenomenon cannot be well captured with common Coloumb friction model used in the contacts. Detailed model of this interaction that would capture well failure of the ground and penetration of the spikes would require extremely fine mesh which would cause extremely long runtimes.

Another approach was therefore presented in this work. A combination of DEM elements with Lagrangian elements that allows both Coloumb friction model on the surface and deeper penetration of sharp edges or spikes if necessary. In order to set up this model correctly it was necessary to corelate simulations with experimental results from ground surface indentation tests performed at various impact velocities and angles.

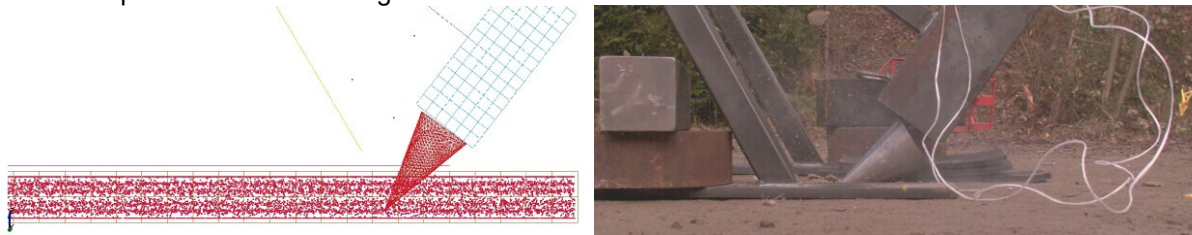


Fig.2: Ground surface indentation tests: simulation and experiment

3 Initial shape testing and full validation crash tests

In the initial phase, several cross sections of the barrier blocks were designed and virtually tested in various crash test scenarios. For this purpose, only reduced models of vehicles and barriers were used because this testing required several decades of simulations. The initial shape testing was performed for various settings of barrier – ground contact at 48 km/h, impact angle = 0°. Once the design was chosen based on the simulation results another set of simulations was performed for chosen barriers for N1 category and N3 category. These simulations were performed with full vehicle and barrier models to give more accurate prediction of the crash tests. In order to validate the results of simulations and prove the performance of individual barrier designs, a set of experimental crash tests took place. In case of N1 barriers there was a sufficient agreement between the simulations and the experiments. However, the experimental N3 test revealed a weak spot in the welds of the link between barrier blocks which was not predicted by the simulations. Next series of simulations was focused on this problem. Based on this analysis a new design of the link was introduced. Finally, the experimental crash test of N3 category with the new link between the barrier blocks proved performance of the new design.

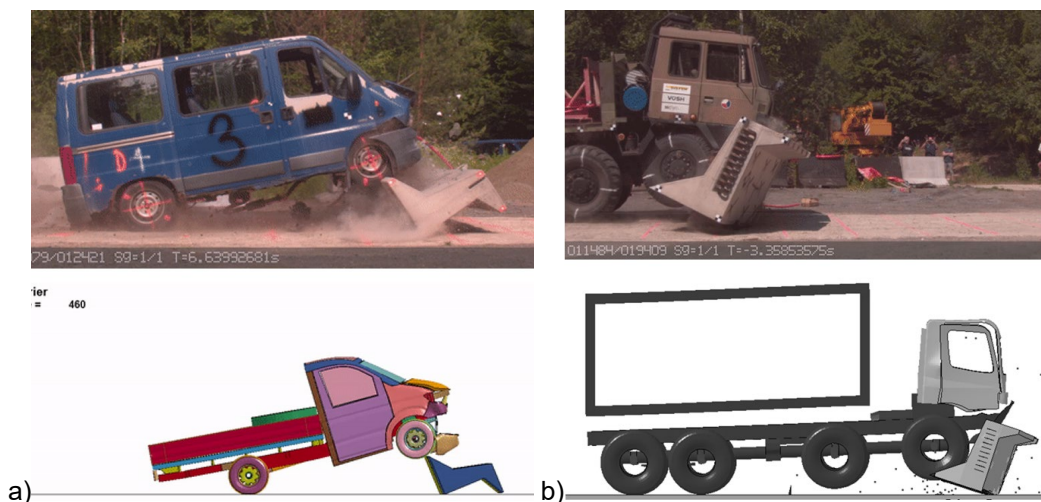


Fig.3: Experimental and virtual crash tests of a) N1 vehicle at 48 km/h and b) N3 vehicle at 48 km/h

The authors wish to express their gratitude and sincere appreciation to the authority of Ministry of the Interior of the Czech Republic, project PID: VI20192022129 for financial support.

Simulation and Physical Testing of an Innovative 'floating' Shallow Mount Hostile Vehicle Barrier

Jonathan Farley¹, Joel Smith², Daniel Aggromitto³, Luke Pasoe⁴

1,2,4 Arup, Australia
3 Arup, USA

1 ABSTRACT

Installation of hostile vehicle barriers into the streetscape of cities around the globe has increased significantly following several high-profile Vehicle as A Weapon (VAW) attacks in the last 10 years. Following the London Bridge attacks in 2017, congested bridge footpaths (adjacent to roadways) were identified as a potential risk to targeted vehicle ramming threats. An industry call was subsequently released to develop potential protection systems which could be installed on bridge structures which would provide protection and deterrence against such events.

The constraints generated for these sites are complicated including challenges such as very shallow available installation depths, limited capacity for additional dead-load, limited ability for positive fixivity to the substrate and the need to incorporate (sometimes multiple) movement joints. Conventional bollard systems typically require significant foundation depths (greater than 500mm depth) which would not be compatible with bridge structures. Even 'shallow mount' bollards (less than 500mm foundation depth) are rarely appropriate and can impart significant loads into the substrate on impact.

This paper summarises the work undertaken to successfully develop a floating (i.e.non-fixed) shallow mount bollard array designed to be installed where very little foundation depth is available. Using full vehicle crash models in Finite Element Analysis (FEA), an innovative new bollard array has been developed requiring only 100mm of depth. The design is intended to provide an option for protection of pedestrians on bridges where conventional bollards cannot be used, and temporary measures do not provide adequate protection.

Initial design development for the product was completed utilising CAD and FEA techniques to develop an optimised solution, minimising foundation depths and installation complexity. With the use of FEA, several different design iterations were investigated to enhance the product without the need for expensive and carbon costly trial and error physical testing.

The final design was then manufactured and physically tested to IWA14-1:2013, to prove compliance and performance and achieve an internationally recognised full rating. Following impact testing, the simulation was further refined against the test data and used to develop a gated system using the same core components. This gate was also tested and achieved the required vehicle barrier performance rating.

The work completed under the project outlines the value that advanced simulation can play when used as a development tool to reduce project timelines, costs, and material waste. The end products have achieved market leading protection performance and offer a solution for protection of the streetscape in very highly constrained site conditions.

Due to the sensitive nature of the work undertaken in this study, this paper will present an overview of the tasks. A redacted version of the presentation will be made available.

Keywords: Hostile Vehicle Mitigation, Vehicle Security Barrier, Crash, LS-DYNA, IWA14

Recent Developments of the EM-Module in LS-DYNA – A Discussion

Lars Kielhorn¹, Thomas Rüberg¹, Jürgen Zechner¹

¹TAILSIT GmbH, Graz, Austria

Since 2017 TAILSIT has maintained a close collaboration with Ansys/LST, formerly LSTC. Our partnership focuses mainly on the enhancement of LS-DYNA's electromagnetic (EM) solver module which is based on a coupling between Finite Elements (FEM) and Boundary Element Methods (BEM). This approach makes the EM solver highly suited for multiphysics problems. Prominent examples are, e.g., the simulation of parts moved by electromagnetic forces as well as processes like metal forming, welding, and induction heating.

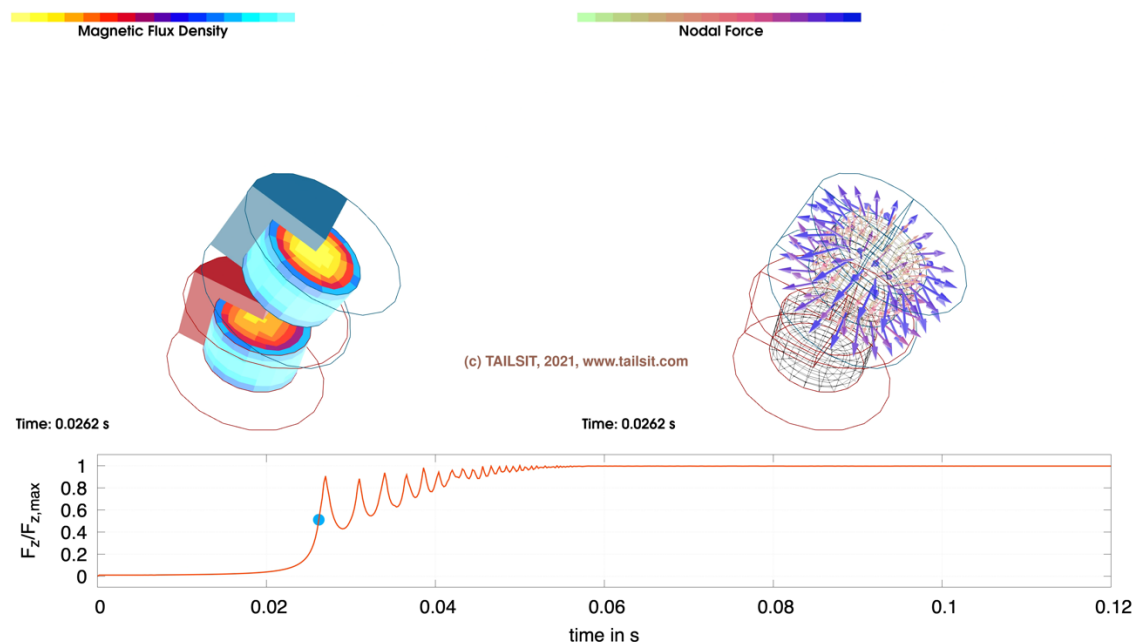
Amongst other things, TAILSIT has designed and implemented:

- A monolithic FEM/BEM solver,
- Support for ferromagnetic materials, permanent magnets and
- The calculation of EM forces

during these last four years. These new features considerably expand the range of applications in which LS-DYNA might be used nowadays.

One of TAILSIT's latest additions to the EM-solver module is the development of a robust and optimal scaling preconditioner for the system of equations that allows for the treatment of non-conducting regions in the FEM domain. In conjunction with LS-DYNA's mechanical capabilities, the preconditioner permits, e.g., the study of snapping and latching magnets (Fig. 1). Thanks to LS-DYNA's FEM/BEM coupling approach, the modeling of such phenomena can be done in an intriguingly simple fashion. This most recent development marks a vast improvement and truly represents a unique feature which is currently not available in any other commercial product.

In this talk we give a brief introduction to the theory and present some benchmark examples. We will address the capabilities and current restrictions of the EM module from our point of view and discuss some strategies on how to overcome them.



Two snapping magnets coated by non-magnetic material: magnetic flux density (left), nodal forces (right) and the total attracting force component (bottom)

Snapping magnets with LS-DYNA: Experimental Validations

Iñaki Çaldichoury, Micah Hernandez, Pierre L'Eplattenier, Sandeep Medikonda, Trang Nguyen, Chris South ¹

¹Ansys

1 Electromagnetic solver in LS-DYNA

The LS-DYNA EM module can be broadly divided into 2 categories: Eddy current solvers and Resistive solvers which gives it the necessary capabilities to perform a wide range of coupled mechanical/thermal/electromagnetic simulations [1]. This module makes it possible to introduce some source electrical currents into solid conductors, and to compute the associated magnetic field, electric field, as well as induced currents. These fields are computed by solving the Maxwell equations in the eddy-current approximation. The Maxwell equations are solved using a Finite Element Method (FEM) for the solid conductors coupled with a Boundary Element Method (BEM) for the surrounding air (or insulators). Both the FEM and the BEM are based on discrete differential forms (Nedelec-like elements).

Such novel implementation of the BEM-FEM numerical methods makes coupling with structural and thermal solvers quite straightforward and data transfer seamless. Which in turn makes LS-DYNA EM a powerful tool for all applications involving moving or deforming structures.

LS-DYNA R12 introduced a monolithic solver which allowed to simulate ferromagnets (See Figure 1) [2]. R13 expended the capabilities of the monolithic solver by introducing permanent magnet simulations [3]. With the R14 release, it is now possible to define non-conductor regions with non linear permeabilities (magnetostatics).

2 ANSYS Magnet snapping experiments

In order to validate LS-DYNA's FEM-BEM approach for magnet simulation and generate confidence in the numerical solution, Ansys DfR labs conducted an experimental validation study using N42 and N52 magnets. Tests include the measurement of static pull forces of magnets and, as a novelty, proposes a dynamic benchmark where magnets can move freely and snap together (See Figure 2). This allows to study in more details the multiphysics capabilities of LS-DYNA EM. Experimental procedure and results will be discussed in more details during the presentation (See Figure 3).

3 Future Outlook

Modern consumer electronic products are seeing a growing trend in the usage of simple permanent magnets in many high-tech devices such as phones, tablets, and laptops for connecting the many accessories such as protective covers, writing styluses, and keyboards. As a result of this, several new challenges are presented to an engineer while designing such products which include strong dependency on several factors such as number, location, and strength of magnets and their impact on the product performance such as snapping or latching.

The objective of the EM solver is to adress those Multiphysics challenges and advancing hand in hand with engineers when extending its capabilities as well as offering validation and correlation with experiments. Planned improvements include a better capture of magnetic forces when magnets are getting into very close contact to each other (BEM related numerical challenges).

4 Figures and Tables

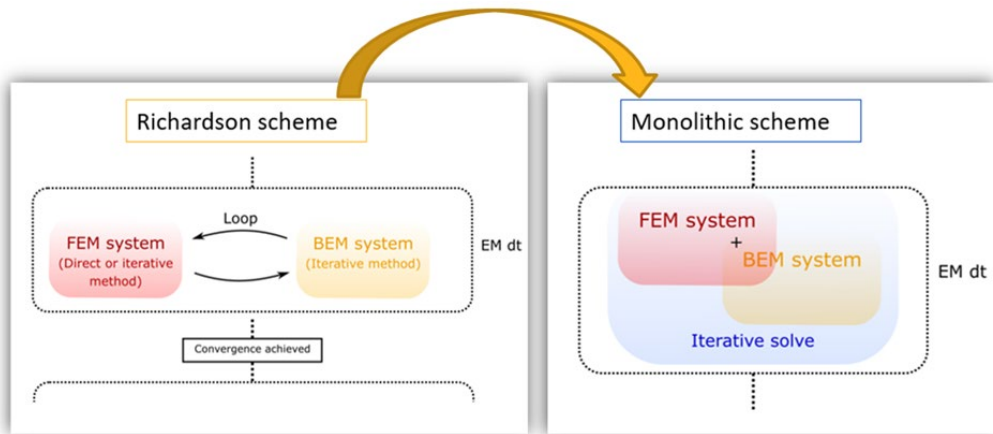


Fig.1: An illustrative comparison between the Classic Richardson and Newer Monolithic Scheme.

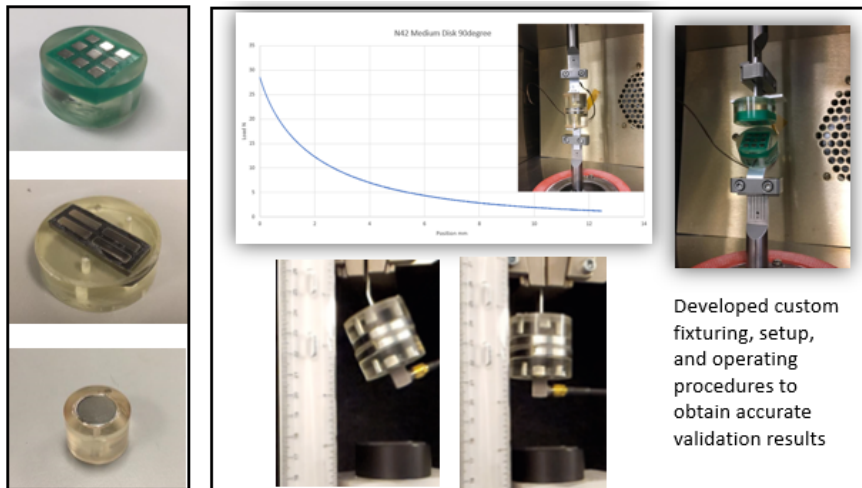


Fig.2: Ansys DfR labs experimental setup

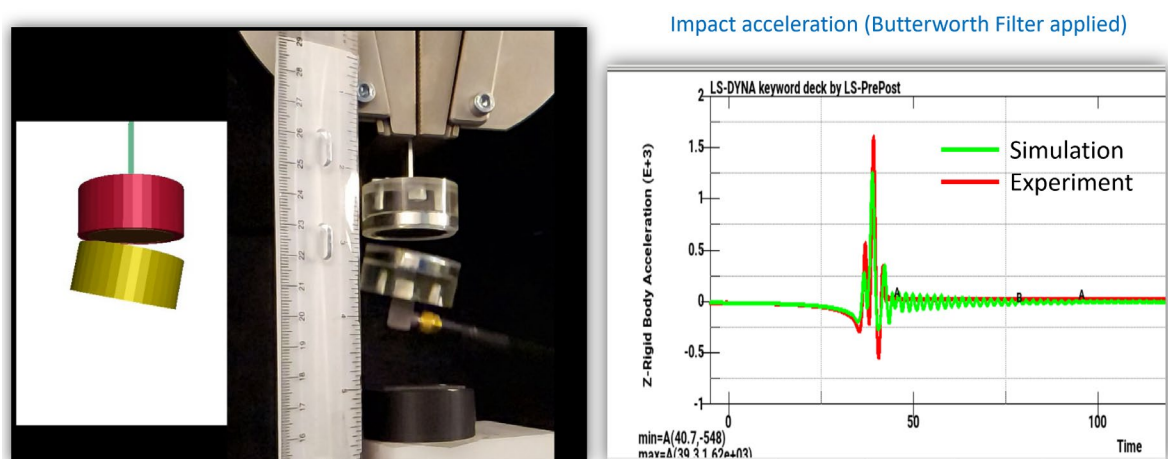


Fig.3: Qualitive and Quantitative validation for LS-DYNA EM technology

5 Literature

- [1] L'Eplattenier P. "A BEM Method For Electromagnetics In Complex 3D Geometries", WIT Transactions on Modelling and Simulation Volume 61, 2015, pages 311-326
- [2] Kielhorn L. " Robust FEM-BEM Coupling for LS-DYNA®'s EM module " 15th International Is-dyna conference, Detroit, June 2018
- [3] Kielhorn L. "Recent Developments of the EM module in Is-dyna" 13th European Is-dyna conference, Ulm, October 2022

Battery Management Systems (BMS) Analytics, Collaboration and Decision Making with support for Crash and Safety Test-Data using d3VIEW

Suri Bala¹, Weibing Li¹

¹d3VIEW Inc. + legal form

Abstract

Acquisition, storage and visualization of battery performance data presents several challenges due to its large data sizes, errors in acquisition and the required manual effort to validate the test. This paper will present solutions from d3VIEW to automate the import and visualization of the battery performance data. The paper will focus on technology to import, organize and classify incoming test data, and provide mechanisms to view standard plots that provides deep insights into battery performance. With built-in analytics, comparing different tests and battery-packs will be discussed that can accommodate millions of time-history points.

New material MAT_307: A viscoelastic-viscoplastic constitutive formulation to model adhesives during the complete manufacturing-crashworthiness process chain

Thomas Klöppel¹, André Haufe¹

¹DYNAmore GmbH, Stuttgart

1 Introduction

The new constitutive model *MAT_GENERALIZED_ADHESIVE_CURING / *MAT_307 in LS-DYNA is introduced in this contribution. It has been developed within the public funded joint research project “DigiBody” and is tailored to model adhesive materials throughout all steps of the manufacturing-crashworthiness process chain.

This implies that the material must be able to capture, on the one hand, important effects resulting from the manufacturing process such as the $\Delta\alpha$ -problem and viscous fingering and, on the other hand, the rather complex plasticity and damage behavior of fully or partially cured adhesives. Material *MAT_307 features a modular and flexible input format, which enables the user to freely combine different modelling approaches for the individual effects.

2 The constitutive modelling in *MAT_307

The new material formulation aims to model adhesives during the complete manufacturing-crashworthiness process chain. Existing material models in LS-DYNA mostly focus on single process steps. The temperature dependent model *MAT_277, for example, is tailored for manufacturing processes. It accounts for the evolution of the degree of cure, which affects the elastic and viscoelastic behavior [1]. In crashworthiness analyses, material *MAT_252 is often used for the adhesive part. It is based on the TAPO (Toughened Adhesive Polymer) model with a non-associated plasticity and an empirical damage formulation [2].

Material model *MAT_307 combines and extends the characteristics of *MAT_277 and *MAT_252. It makes use of a modular input structure that enables the user to combine different features. Moreover, it provides different options for most of these individual features.

To describe the evolution of the degree of cure, the user can choose from a list of different kinetic models. So far, different extensions and generalizations of the Kamal model are available. The degree of cure directly leads to a chemical expansion/shrinkage of the material, which can be addressed by different available approaches. The thermal expansion is also affected by the curing process.

The viscoelastic properties of the material are governed by experimentally determined master curves for shear and bulk moduli as functions of time. The Prony series expansions for those master curves are expected as input quantities. In most applications, the viscoelastic properties depend on temperature and degree of cure. In this material, these dependencies are realized with shifting functions acting on the moduli $G_i, G_\infty, K_i,$ and K_∞ (vertical shifting) and on the decay constants β_i (horizontal shifting). In contrast to MAT_277, both quantities, temperature and degree of cure, can be associated with both, vertical and horizontal, shifting operations.

The TAPO model implemented in *MAT_252 incorporates a non-associated $I_1 - J_2$ plasticity description with distortional hardening under plastic flow, which is also implemented in *MAT_307 as one option for the plastic behavior. An extension of the TAPO model with respect to temperature and curing effects has been proposed [3] for cohesive elements. The proposed effects, such as temperature dependent distortional hardening and a yield strength given as function of degree of cure and temperature, have also been implemented in the continuum model *MAT_307 as an option.

The new material offers different possibilities to model the material damage, which is represented by the evolution of a damage parameter D_1 . The isotropic empirical damage models used in *MAT_252 are available. In order to consider possible damage evolution during the manufacturing process, the effects of degree of cure and temperatures have to be considered. Material *MAT_307, thus, employs the proposed formulation in the extended TAPO model [3], for which the damage evolution is governed by the equivalent viscoplastic strain rate, the temperature, and the degree of cure.

In addition to this material damage, a second damage mechanism is considered in *MAT_307 estimating the effect of viscous fingering on the mechanical performance of the processed part. The basic idea is that the viscous fingering goes together with a reduction of the effective adhesive area between the joined parts and that this reduction can be interpreted as a structural damage expressed by a damage parameter D_2 . The material model estimates the area reduction based on the thickness stretch of the material using either an exponential approach or referring to a user-defined curve. It is further assumed, that area reduction is a reversible process in the liquid state of the material. As soon as the degree of cure reaches the gelation point the damage parameter D_2 remains constant.

3 Validation and parameter identification

Given the discussed modular input format it is possible to validate the implementation of the individual features separately for most cases. Different examples demonstrated that material *MAT_307 can reproduce the results of both *MAT_252 and *MAT_277 and, thus, validated the implementation of curing evolution, viscoelasticity, plasticity, and damage evolution.

The second damage algorithm representing the effect of viscous fingering has been validated by a relatively simple tensile test of the adhesive layer, the results of which are shown in Fig.1. If the damage algorithm is inactive, the mechanical answer of *MAT_307 agrees with the results of *MAT_252. Assuming a pre-damage by defining a constant D_2 of 20% reduces the stress response accordingly, while the shape of the curve remains unchanged. Last, the exponential damage evolution for D_2 has been artificially activated for the solid phase showing a rapid softening due to the thickness stretch applied.

After validation, the material has been calibrated to different experimental setups with different loading scenarios for a BETAMATE™ material provided by DuPont. Here, testing has been performed in a wide range of temperatures and with materials with different degrees of cure. The calibration was successful for the whole set of experiments.

4 Summary

The new material model *MAT_307 has been introduced, which is suitable to model the temperature and degree of cure dependent viscoelastic-viscoplastic behavior of adhesive materials within the manufacturing-crashworthiness process chain. Material damage evolution as well as an estimate for the softening due to viscous fingering are also considered.

The material could successfully be calibrated for different tensile and shear tests in a wide range of temperatures and for different degrees of cure.

5 Funding

This work was supported by the Federal Ministry for Economic Affairs and Climate Action of Germany for project "DigiBody" (Digital process chain for mapping and optimizing joining technologies in body-in-white constructions).

6 Literature

- [1] Klöppel, T.: "A new material model to simulate the thermo-viscoelastic behavior of adhesives within the curing process with LS-DYNA", automotive CAE Grand Challenge, Hanau, 2017
- [2] Burbulla, F., Matzenmiller, A.: "Materialmodell für Klebstoffe aus duktil modifizierten Epoxidharzen (TAPO-Modell)", Technischer Bericht zum Projekt P828, FOSTA, 2013
- [3] Matzenmiller, A., Kühlmeyer, P.: "Methodenentwicklung zur Simulation des thermo-mechanischen Verhaltens von Klebschichten in hybriden Fügeverbindungen während des Aushärtprozesses", Technischer Bericht zum Projekt P1087, FOSTA, 2018

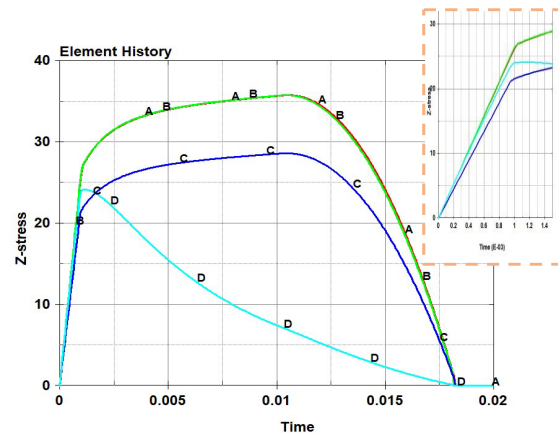


Fig.1: Response to tensile load of (A) *MAT_252, (B) *MAT_307, (C) pre-damaged *MAT_307, (D) *MAT_307 with estimated viscous-fingering.

On the implementation of MAT-SAMP for modelling of polycarbonate

N. Ghavanini¹, I. Colamartino², A. Perrier-Michon³, L. Scampini¹, P. C. Astori¹, M. Anghileri¹

¹LaST, Dpt. of Aerospace Science and Technology, Politecnico di Milano, Milan, Italy

²LaST, Dpt. of Mechanical Engineering, Politecnico di Milano, Milan, Italy

³École Nationale Supérieure de Mécanique et d'Aérotechnique, Poitiers, France

1. Introduction

Polymers are increasingly being used nowadays as lightweight solutions for many structural and mechanical applications, where safety and protection are of priority. As one of the most applicable polymers, Polycarbonate (PC) is a lightweight glassy thermoplastic that provides excellent optical transparency while offering significant impact-resistance behavior compared to traditional materials, such as laminated glass. Due to the PC's outstanding mechanical properties, specifically its high energy absorption capabilities, the mechanical deformation and failure under various loading conditions have been of interest to many engineers and researchers from both experimental and numerical standpoints. In many previous numerical implementations, conventional material models which are used for isotropic materials have also been proposed for PC. However, this material is strongly strain rate, temperature, and pressure-dependent. For this reason, suitable material models which are able to predict the PC's behavior at different loading rates must be implemented: amongst these models, SAMP-1, a Semi-Analytical Model for Polymers with C^{-1} differentiable yield surface is available in LS-DYNA, developed as an advanced material model for the simulation of thermoplastic polymers [2]. In this work, the tensile deformation behavior of polycarbonate in different strain rates was first characterized. Next, MAT_SAMP-1, MAT_JOHNSON_COOK and MAT_24 material cards were implemented. The differences in the deformation behavior are briefly outlined here.

2. Experimental campaign

In order to characterize the material and validate the models, a tensile test campaign at different strain rates was carried out to characterize the material in tension and provide the basis of the material cards calibration. The tensile tests were carried out following the related ASTM/ISO D638 [3]. Four specimens were tested in quasi-static conditions ($SR=0.001$ 1/s), five at moderate dynamic rates ($SR=0.1$ 1/s), and other five at high speed ($SR=3.33$ 1/s). Force and displacement were measured at the grips; true stress vs true strain curves at each strain rate are available in Fig. 1.

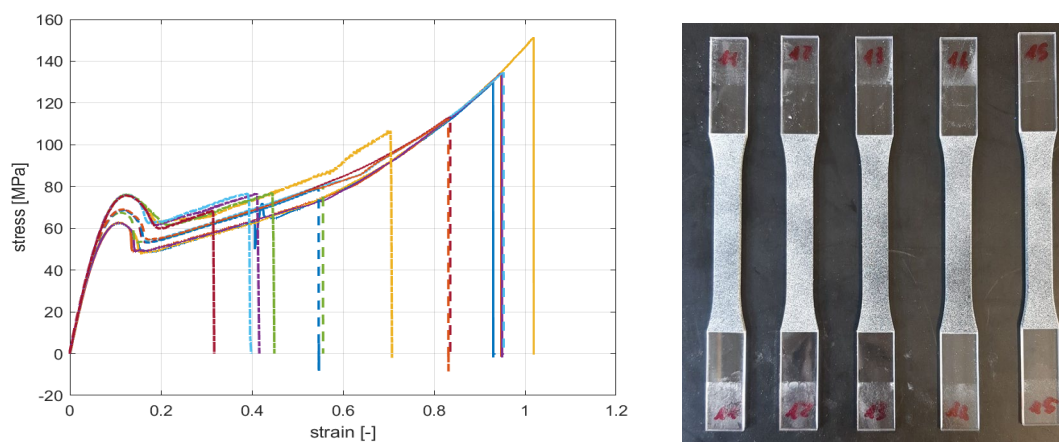


Fig. 1: Tensile tests results: quasi-static tests at $SR=0.001$ s⁻¹ (solid lines), low-dynamic tests at $SR=0.1$ s⁻¹ (dashed lines), high-dynamic tests at $SR=3.33$ s⁻¹ (dash-dotted lines). On the right, a picture of the specimens.

3. Numerical study

Dogbone models and tensile simulations were set up using solid hexadral elements with an element size of 1 mm in the gauge section. The simulations were performed using LS-DYNA R11. Compared

to tensile test results, a good correlation was noted in terms of plastic deformation and the overall stress-strain curve for each tensile loading speed. Besides the explicit method for the two dynamic tests, implicit simulations were also implemented to double-check the model's validity using both approaches and test the material card in quasi-static regime. The stress-strain correlation between experiments and numerical simulations for the dynamic case with a SR= 3.33 1/s is illustrated in Fig.2.

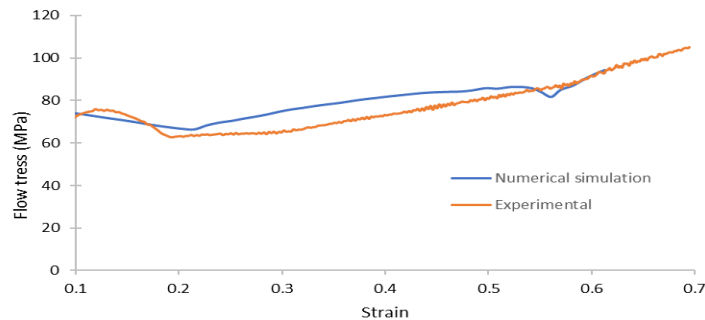


Fig 2. Post-yield true stress-strain curve correlation between numerical results and experiments

However, most notable result is found analysing the viscoplastic deformation behavior, as shown in different time steps using MAT_SAMP-1 and MAT_24 in Fig. 3. As can be noted in SAMP-1, the necking initiation and propagation throughout the model are captured, which is closer to the actual observations and physically more coherent. On the other hand, local necking captured with MAT_SAMP was not seen with traditional metal plasticity models, and the necking was localized at the center of the specimen.

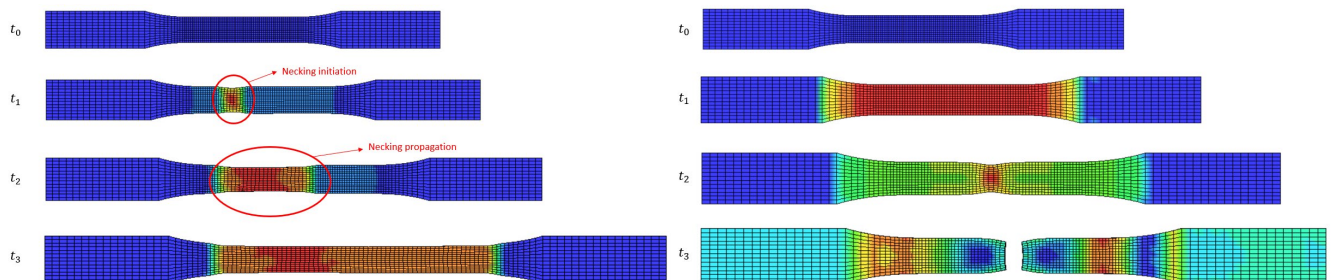


Fig 3. Viscoplastic deformation using SAMP-1 (left) and MAT_24 (right).

These results confirm the high accuracy of MAT_SAMP in predicting the actual viscoplastic flow behavior of PC.

4. Conclusions

Following the simulations and experimental tests, MAT_SAMP was found to be a better solution for the tensile simulation of polycarbonate. It can better predict the viscoplastic flow and different stages that an isotropic polymer goes through during the loading. As depicted in the stress-strain curve, using SAMP-1, the strain softening part was well captured, while with metal plasticity models such as MAT_24, the local necking and propagation were not observed.

5. Literature

- [1] Kolling, S. et al.: "SAMP-1: A Semi-Analytical Model for the Simulation of Polymers ". In: 4. LS-DYNA Anwenderforum, Bamberg, Germany (2005).
- [2] Modeling Guidelines Document. Version 12-1. LS-DYNA AerospaceWorking Group, 2012.
- [3] ASTM D638 - Standard Test Method for Tensile Properties of Plastics

Establishment of a Robust Methodology for Modeling Different Types of Failure Behavior in Thermoplastics Materials

Sindhu Kamat, Subhansu Mohapatra

SABIC Research and Technology Center, Bangalore, INDIA.

1 Abstract

Demand for engineering thermoplastics is in upward trend across industries due to its advantages such as lighter weight and part integration possibilities against traditional materials such as metals. To reduce design time and cost, industry employs numerical tools to keep prototyping and physical tests to a bare minimum. As a result, there is an ongoing need for simulation methods that can accurately predict the performance of plastics. Plastics have high sensitivity to factors such as temperature, loading conditions, and strain rate and hence it is important to understand and use right modeling techniques in numerical simulations. MAT-187 (Semi-Analytical Model for polymers) material model in LS-DYNA captures the detailed behavior of plastics such as strain-rate dependency, visco-plasticity, non-isochoric plastic deformation, pressure dependency of failure strain and loss in material stiffness due to damage. This paper deals with establishing a robust methodology for modeling different types of failure behavior (ductile/brittle) under different loading conditions in thermoplastics materials using a single MAT-187 material card. The materials studied in this paper are a group of unfilled amorphous resins from SABIC's ULTEM™ resins product family. The sensitivity of loading triaxiality to material failure was established through physical tests. A detailed triaxiality sensitivity curve was established from a combination of experimental measurements and empirical material behavior understanding. The material card using the generated triaxiality curve predicts the material behavior very well under a wide range of static and dynamic loading conditions covering ductile as well as brittle failures. This methodology has been validated for a range of unfilled polymers from ULTEM product family covering variables such as molecular weights and polymer blends.

2 Introduction

Thermoplastic materials have unique properties when compared to other materials and have greatly improved the quality of our daily lives. The usefulness of thermoplastics is attributed to the fact that they have a wide range of properties and can be transformed into end products using relatively simple and low-cost fabrication methods. It is critical to understand the composition and basic properties of these materials in order to fully utilize them.

Plastics are increasingly used in structural parts because they combine light weight, durability, and cost effectiveness with engineering features such as part integration, freedom to design intricate shapes, and high specific energy absorption capacity. An extensive understanding of properties and accurate implementation using FEA tools such as LS-DYNA® is required to predict the behavior of parts manufactured with plastics. In order to get reliable results from simulation, the FEA solver should support material models which predict the behavior of plastics accurately.

2.1 ULTEM Resin

The polymers studied in this paper belong to the ULTEM resin family of amorphous thermoplastic polyetherimide (PEI) materials from SABIC. ULTEM resins provide a unique combination of high heat resistance, stable dielectrics, strength, stiffness and dimensional stability and offers inherent

halogen-free FR, IR transparency, hydrolytic stability and chemical resistance. Owing to this, they are used in a wide variety of demanding applications.

2.2 ULTEM 1000 Resin

The basic methodology has been established on ULTEM 1000 resin and then validated on other resins of the ULTEM family. The unreinforced amorphous polyetherimide (PEI) resin ULTEM 1000 has a glass transition temperature (Tg) of 217°C. Excellent mechanical, electrical, and dimensional qualities at high temperatures are among its distinct features.

2.3 Material Models in LS-DYNA® software

LS-DYNA supports various material models for simulation of plastics. The materials model studied in this paper for modeling of the behavior of ULTEM polymers is MAT_SEMI-ANALYTICAL_MODEL_FOR_POLYMERS (*MAT_187). This model is chosen since all the necessary physics required for modeling unfilled polymers is available in the material model. This is described in Table 1.

Table 1 Comparison of material models in LS-DYNA® for modelling plastics

Material model	24	89	187	187-L	224	224_GYS	264	017
Material Models	Piecewise linear plasticity	Plasticity polymer	Semi - Analytical Model for	Semi - Analytical Model for	Tabulated Johnson Cook	Tabulated Johnson Cook GYS	Tabulated Johnson Cook Orthotropic	Oriented-crack
Viscoelastic								
Biaxial								
Shear								
Compression								
Damage								
Pressure								
Failure								
Strain Rate								
Triaxiality								
Post yield non								
Solid element								
Shell element								

2.3.1 MAT_SEMI-ANALYTICAL_MODEL_FOR_POLYMERS(*MAT_187)

MAT-187 is a semi-analytical polymer model with C1 continuity that envelops yield values in uniaxial and biaxial tension, uniaxial and biaxial compression, and shear [1]. It is a viscoplastic model, so it is appropriate for load cases where plastic strains are greater than elastic strains.

The yield criteria in the SAMP-1 model are based on an isotropic C-1 smooth yield surface, and the plastic flow rule is expressed using a non-associated potential function. The model accounts for pressure dependency by incorporating a yield function that incorporates pressure state, softening, and volumetric change by incorporating a parameter in the plastic potential function that is a function of plastic Poisson’s ratio.

2.4 Failure and damage modeling

LS-DYNA® software provides thermoplastic material models with damage failure modeling. These models include failure models incorporated within material models such as within *MAT_187 as

well as highly complex damage/failure models such as *MAT_ADD_GISSMO, which incorporates failure in relation to strain rate and Triaxiality [3, 9]. GISSMO (Generalized incremental stress-state dependent model) is a failure model that allows for an incremental description of damage accumulation, including softening and failure. The governing equation to determine the damage accumulation is given below

$$\Delta D = \frac{DMGEXP \times D^{(1-\frac{1}{DMGEXP})}}{\varepsilon_f} \Delta \varepsilon_p \quad (2.1)$$

Where D is the damage value ($0 < D < 1$). D is initialized to a value of 10^{-20} for all the damage types in the first-time steps.

ε_f is the equivalent plastic strain to failure

$\Delta \varepsilon_p$ is the equivalent plastic strain increment

DMGEXP is the damage exponent and is a material specific number.

A load curve defining critical plastic strain vs. triaxiality allows for a definition of triaxiality dependent material instability, which takes account of that instability and localization will occur depending on the actual load case. This offers the possibility to use a transformed Forming Limit Diagram as an input for the expected onset of softening and localization. Using this load curve, the instability measure F is accumulated using the following relation, which is similar to the accumulation of damage D except for the instability curve is used as an input:

$$\Delta F = \frac{DMGEXP}{\varepsilon_{p,loc}} F^{(1-\frac{1}{DMGEXP})} \Delta \varepsilon_p$$

With,

F Instability measure ($0 \leq F \leq 1$).

$\varepsilon_{p,loc}$ Equivalent plastic strain to instability, determined from ECRIT

$\Delta \varepsilon_p$ Equivalent plastic strain increment

As soon as the instability measure F reaches unity, the current value of damage D in the respective element is stored. Damage will from this point on be coupled to the flow stress using the relation described above.

2.5 Triaxiality

Triaxiality is defined as the ratio between the hydrostatic mean stress and the Von-Mises stress, and it helps to determine the state of stress. It is found to be the very important factor that influences the failure in polymers.

$$\text{Stress Triaxiality} = \frac{\sigma_m}{\sigma_{vm}}$$

3 Methodology

In order to carry out the analysis in LS-DYNA®, some form of material input data is required. For SAMP-1, these input data is generated by conducting experiments such as tensile tests at different rates, compression test and shear test at one strain rate. Standard experiments pertaining to plastics are selected and these experiments are carried out to generate Stress-Strain curves, which need to be further processed to convert into a format suitable for SAMP-1. In the following sections, a brief discussion on the experimental setup is mentioned, along with that of the associated FEA modelling to simulate these tests.

3.1 Stress-Strain curve generation

- The experiment data for tension, compression and shear were generated. This data was available as engineering stress-strain from equipment and were converted into true stress-plastic strain format.
- The multipoint data in *MAT_187 is defined as True stress vs Plastic strain curves. True strain is split into elastic and plastic strain to cater to this need.
- For all strain rates, the curves are extrapolated to the same end value of plastic strain. In the current study, the curves are extrapolated to the value of 0.56 which is the plastic strain of the

tension curve at lowest strain rate. The tension curves are defined in LCID-T and compression curve is defined in LCID-C of the *MAT_187 material card. A tabular input is given for tension curves in LCID-T where each row of the table defines a tension curve at its corresponding plastic strain rate.

4 Validation under dynatup test setups

The material model created based on the methodology described above has been validated against ASTM dynatup test in literature [2]. However, the same material parameters when used for ISO dynatup test simulation didn't yield good results. The material parameters need to be changed for good prediction against ISO dynatup test.

In ASTM D3763 dynatup test, a hemispherical steel impactor with a diameter of 12.7 mm impacts a clamped disc at an initial velocity of 3.3m/s. A 102 mm diameter specimen is used. For ISO 6603-2 dynatup test, a hemispherical steel impactor with a diameter of 20 mm impacts a square specimen of 60mm side length at an initial velocity of 4.4m/s. The impactor is in motion for both standards, causing the clamped stationary specimens to be impacted. Fig. 1 shows the impact test setup. Fig. 2 shows the impact test setup for ASTM-D3763 standard and Fig. 3 shows impact test setup for ISO-6603-2 standard. Due to a lower impactor to specimen diameter ratio and lower initial velocity in ASTM set-up, the failure tends to be more ductile than in ISO set-up where due to a higher diameter ratio and higher initial velocity, the failure tends to be brittle. However, it's desirable to have a single material card which can predict both types of failure.

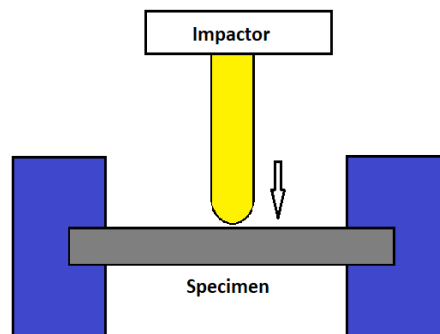


Figure 1: Dynatup impact test schematic model

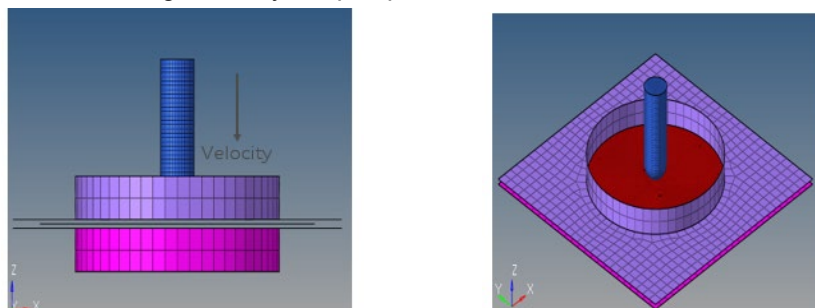


Figure 2: Dynatup FEA model- ASTM D3763

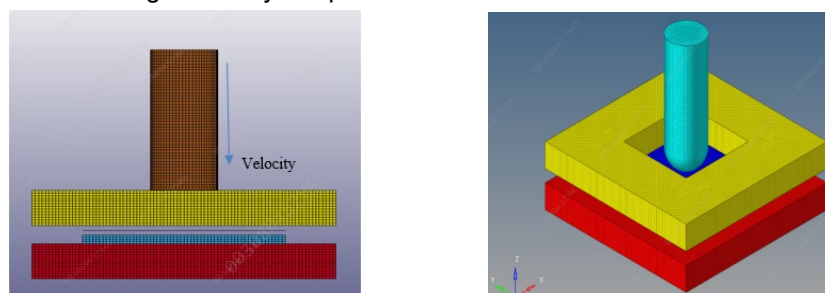


Figure 3: Dynatup FEA model- ISO-6603-2

4.1 Mesh sensitivity studies for modelling brittle failure

Since the failure is brittle in ISO set-up, at first a mesh sensitivity study was performed while using the same card that correlated well for ASTM test set-up. The mesh size was progressively refined to model the detailed high stress distribution. The results are shown in Fig. 4. It was found that at mesh size 0.3mm, the CAE curve correlated well with Dynatup test result as shown in Fig. 5.

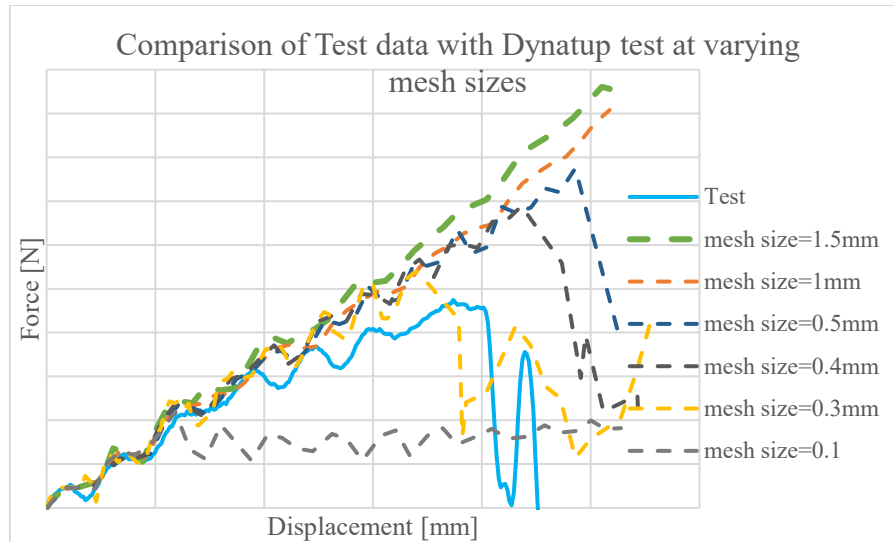


Fig 4. Comparison of test data with Dynatup test for ISO 6602-3 at varying mesh sizes.

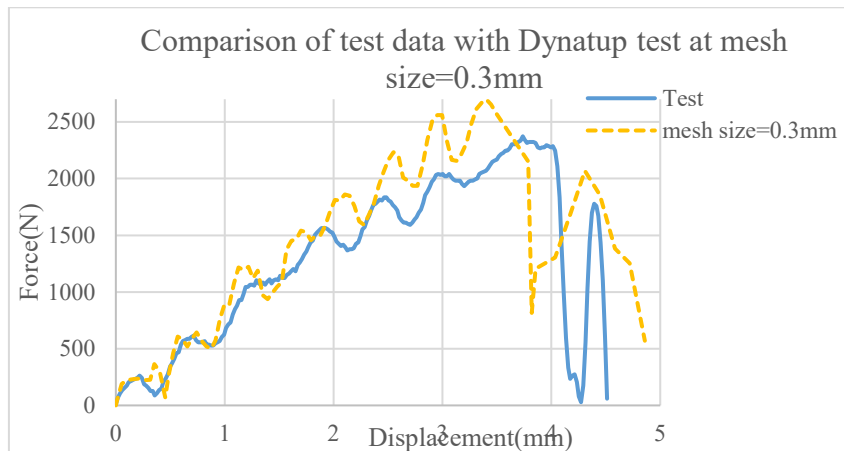


Fig 5. Comparison of test data with Dynatup test at 0.3 mm mesh size.

4.2 Mesh Regularization Study

- Mesh size 0.3mm is the finalized mesh size for the study. For real-time applications, mesh size between 1mm and 5mm is recommended. But 0.3mm mesh size is too fine. Hence, mesh regularization is needed to have a suitable computational cost.
- The simulation is performed for tensile specimen at three different strain rates of 1/s, 10/s and 100/s at mesh sizes varying from 0.3mm to 2mm.
- The plastic strain to failure value is scaled by a factor to match the results for all the mesh sizes.
- The investigation was also carried out for compression and shear specimen.
- For each test, a graph of mesh size vs. scale factor is plotted as shown in Fig. 6.
- The mesh regularization curve is generated using the data obtained from mesh sensitivity study. LCID_LC is the Load curve that specifies a factor that works multiplicatively on the value of EPFAIL depending on a characteristic element length, defined as the average length of spatial diagonals. The curve generated is implemented in *MAT_187 material card.

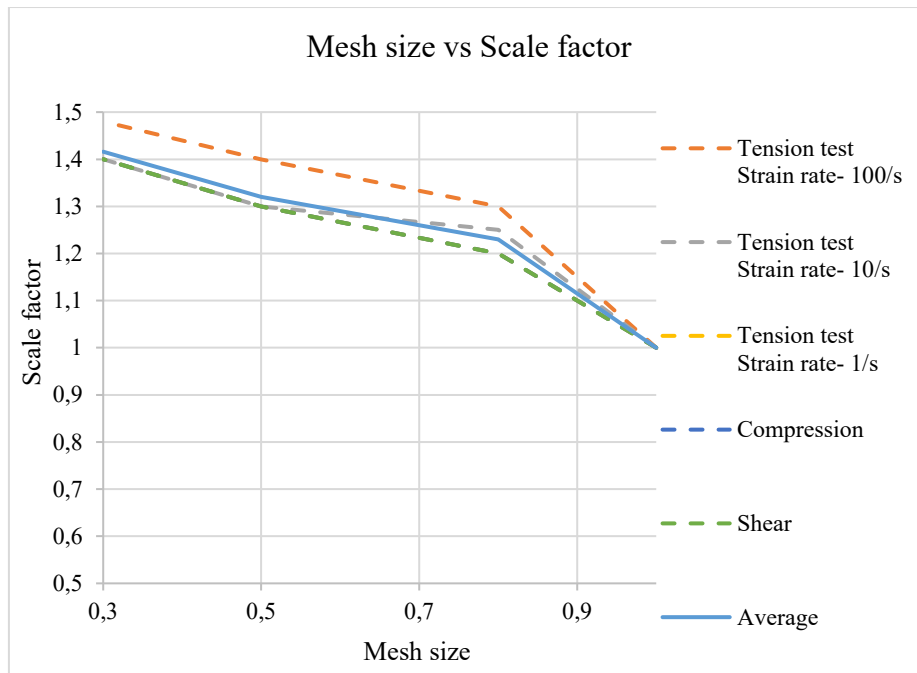


Fig. 6 Mesh size vs Scale factor

The mesh regularization curve is implemented in ISO-6602-2 Dynatup test model. However, it's found that the prediction using the mesh regularization curve is not accurate with a practical mesh size of 1mm.

5 Enhancement in Triaxiality based Failure Implementation

The specimen under ASTM dynatup loading is primarily under biaxial loading whereas it's under triaxial loading under ISO dynatup set-up owing to higher impactor to specimen diameter ratio and higher initial velocity. Since it is established in literature [3] that the failure in a highly notch sensitive material such as ULTEM resin is heavily dependent on the state of stress, one additional point on tri-axiality curve at tri-axiality of 1.0 was added. From the literature, the failure strain was considered lower than the failure strain at uniaxial loading condition.

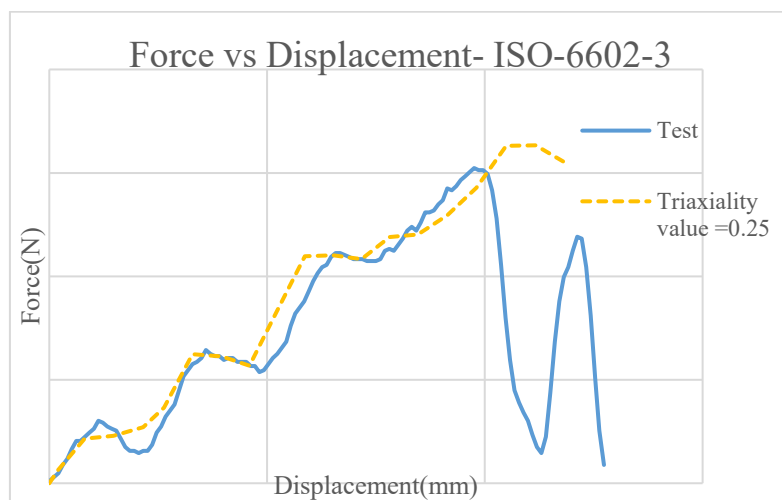


Fig. 7 Comparison of test data with Dynatup test at 1 mm mesh size

The results correlated well at 1mm mesh size with the failure strain value at tri-axiality of 1.0 set at 25% of uniaxial failure strain as indicated in Fig.7.

6 Robustness check of the methodology developed

The same material card considering the updated triaxiality value is updated in ASTM D3763 Dynatup test and the results correlated well for 1mm mesh size as shown in Fig 8. This ensures that the material model can predict both brittle as well as ductile failure since the failure in ISO dynatup test is brittle whereas that in ASTM dynatup test is ductile.

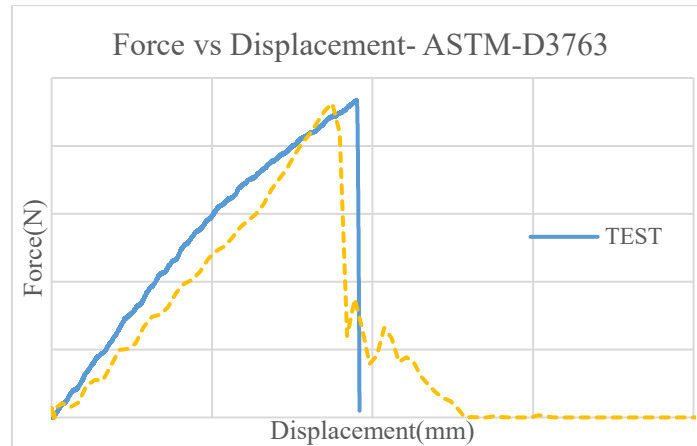


Fig. 8 Comparison of test data with Dynatup test-ASTM D3763 standard at 1 mm mesh size

The material model created was validated by implementing it in impact simulations for a range of unfilled polymers from ULTEM grades to ensure its robustness for use in real-time application development. Fig.9 shows the comparison between the Dynatup test results and simulation results for ULTEM 1010 material for ISO- 6603-2 standard. This material is very similar to ULTEM 1000 material except having a lower molecular weight and corresponding change in mechanical properties. The test result correlated reasonably well with the simulation result.

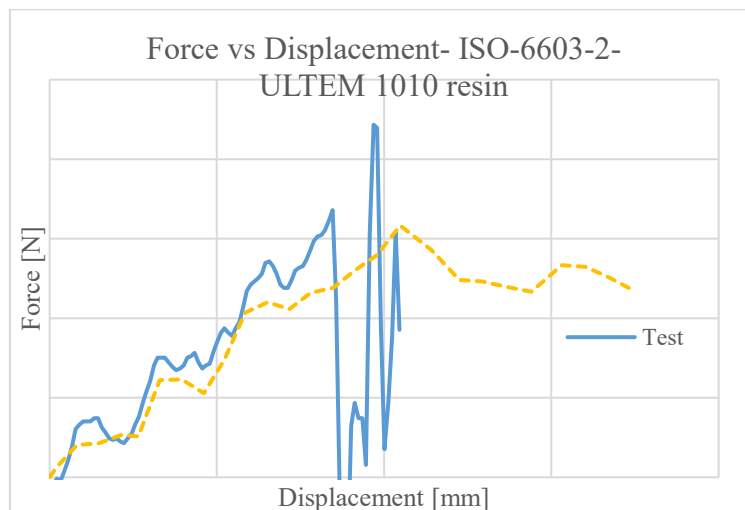


Fig. 9 Comparison of test data with Dynatup test-ISO-6603-2 standard for ULTEM 1010 resin

The same material modeling methodology was also used to create cards for ULTEM HU1000 and ULTEM HU1004 materials. These are healthcare grades of ULTEM family. HU1004 resin is a polymer blend with improved ductility. The results correlated well for ASTM-D3673 Dynatup test results for these materials for 1mm mesh size as shown in Fig 10 and Fig 11.

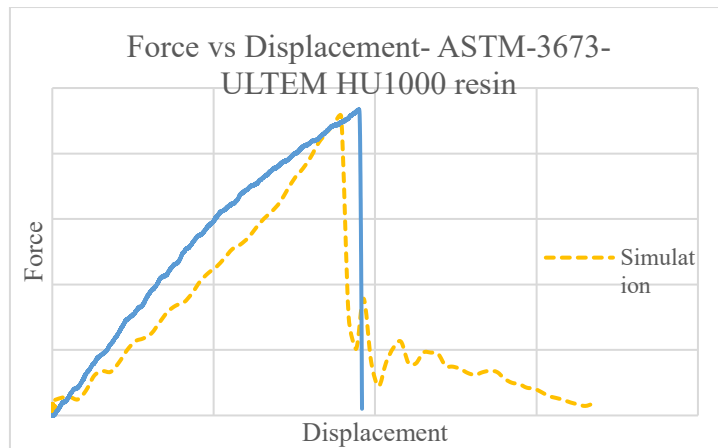


Fig. 10 Comparison of test data with Dynatup test-ASTM D3763 standard for ULTEM HU1000 resin

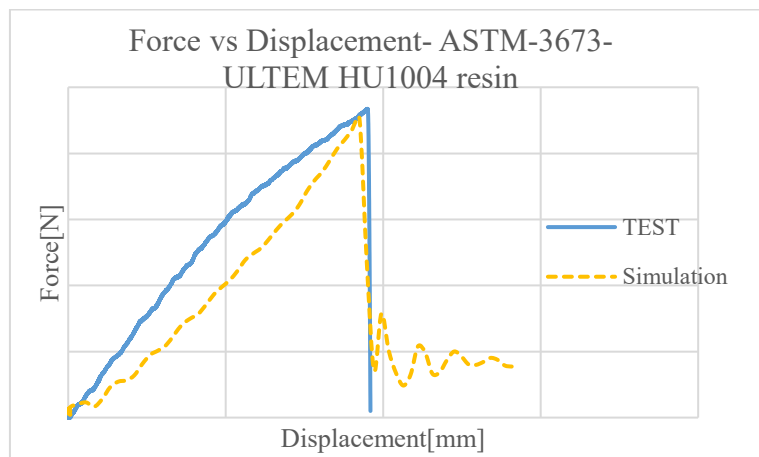


Fig. 11 Comparison of test data with Dynatup test-ASTM D3763 standard for ULTEM HU1004 resin

To further validate the material model under variety of possible test conditions, a static punch test was performed on a healthcare tray and corresponding simulation was carried out.

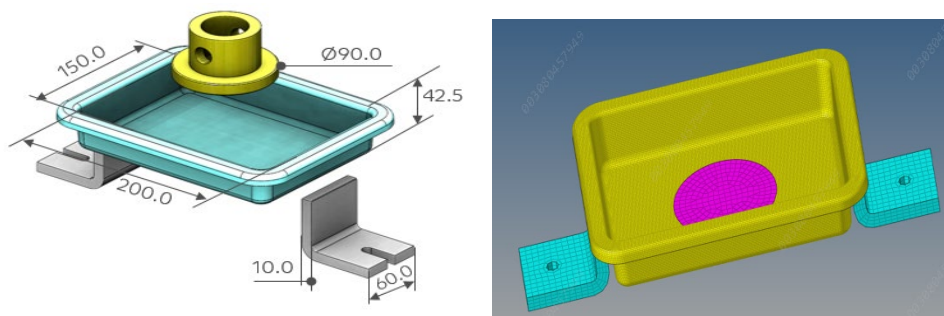


Fig. 12 (a) Part geometry (b) FEA model of the tray

The tray's geometry is depicted in the diagram. The tray's thickness is 2.5mm. The load was applied by progressively pushing a load pin against the tray while giving a vertical displacement until the part failed. The FEA model of the tray is shown in the figure, with the tray modeled using shell elements and the load delivered by a rigid loading pin pressing vertically downward against the tray. The output is shown against the experiment findings in the form of reaction force vs. displacement in figure 12.

Even under this static condition, the material card accurately predicts material behavior both quantitatively as well as regarding the failure mode. Fig. 13 (a) shows the validation of static tray test simulation results with the experimental curve and Fig. 13 (b) shows the failed tray in the static tray test simulation

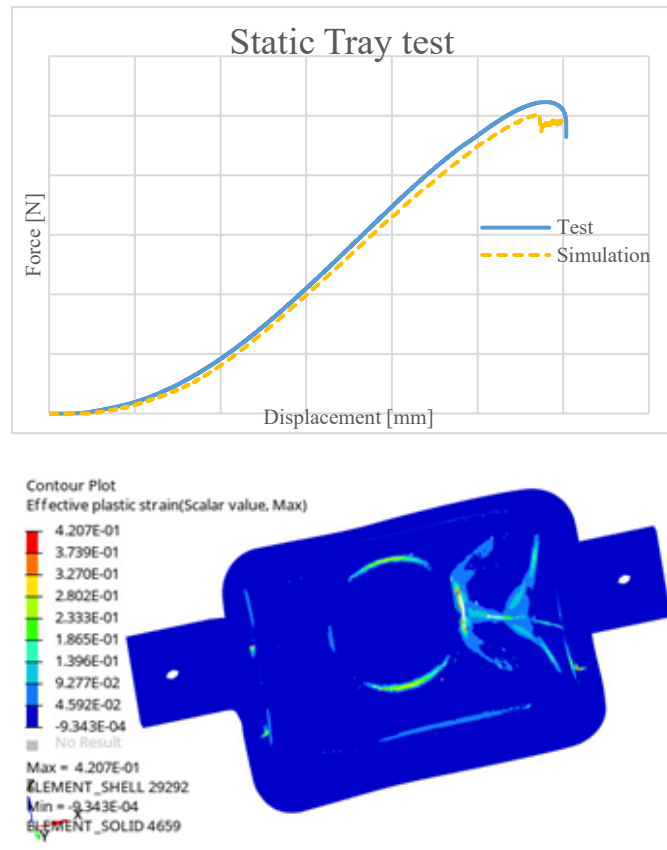


Fig. 13: (a) Correlation of tray test simulation results with experimental curve (b) Simulation results showing effective plastic strain in tray impact test

7 Conclusions

A detailed material modeling methodology for damage and failure of unfilled thermoplastics polymers have been established through this study. This material model is able to predict behavior of a variety of unfilled polymers from ULTEM family of polymers from SABIC accurately with varying molecular weight and blend composition under both static and dynamic loading as well as different geometry configurations. The use of accurate tri-axiality dependent failure parameters has been shown to be very important in predicting the damage and failure consistently across different materials, loading conditions and geometry configurations.

REFERENCES

1. S. Kolling, A. Haufe, M. Feucht, P. Du Bois. "SAMP-1: A Semi-Analytical Model for the Simulation of Polymers," in Proceedings of the 4th German Forum on LS-DYNA, Bamberg, Germany, 2005, A-II -27/52
2. Amrita U, Kottresh K and Subhransu Mohapatra "Determination of accurate material parameters using LS-OPT based optimization techniques", 13th European LS-DYNA Conference 2021, Germany.
3. Ronald P. Nimmer and Joseph T. Woods "An Investigation of Brittle Failure in Ductile, Notch-Sensitive Thermoplastics," POLYMER ENGINEERING AND SCIENCE, AUGUST 1992, Vol. 32, No. 16.
4. LS-DYNA KEYWORD USER'S MANUAL-VOLUME II – Material Models.
5. ULTEM resin, <https://www.rpstechnologies.co.uk/images/pdf/ultem-resin-1000.pdf>

Acknowledgements: SABIC and brands marked with TM are trademarks of SABIC or its subsidiaries or affiliates.

Abuse characterization and simulation of battery cells and cell arrangements

M. Schwab¹, H. Pothukuchi¹; S. Riemelmoser¹, R. Kießling¹

¹4a engineering GmbH

1 Background and Motivation

With respect to several standards and regulations, battery packs must pass certain tests related to their abuse behavior. Consequently, specific requirements have to be addressed and considered within the design process. Especially, the thermal propagation, induced by one cell and resulting in a catastrophic failure of the whole battery pack, must absolutely be mitigated or avoided. Hence, a deep understanding of the abuse behavior of the applied battery cells and their interaction in the battery pack are required for an efficient design and optimization of the battery system's overall safety behavior.

2 Methodology

In order to improve the battery pack's safety behavior in a time and cost efficient way, a multi-physical simulation model of a battery cell capable to resemble the cell's behavior during thermal runaway is required. Considering the course of events in an abuse scenario, a battery cell may first be mechanically loaded. Once a specific amount of deformation happened, an internal short circuit may arise. Due to the high currents associated with the short circuit, the cell starts to heat up. Finally, exothermic reactions of the cell components start to take place once the corresponding temperature levels have been exceeded and the thermal runaway is in full progress. Hence, a predictive simulation model needs to be capable to describe the interaction between mechanical, electromagnetic and thermal events.

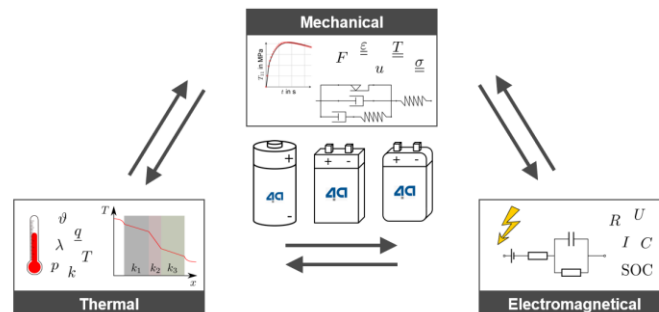


Fig. 1: Sketch of the multi-physical nature of battery cells. In order to describe a thermal runaway and its initiation, the interaction between mechanical, electromagnetic and thermal events needs to be modelled.

First, specific characterization tests have to be conducted at single cell level, which serve as a basis for the generation of a corresponding multi-physical simulation model of the battery cell. As the focus of this work is to study the thermal runaway event itself and its initiation via overheating, the mechanical interaction will not be further discussed. The electrical behavior of the battery cell can be well described with a so-called Randles's circuit. A Randles' circuit of first order features four parameters which need to be identified, the open circuit voltage (OCV), 2 ohmic resistances and 1 capacitance. Therefore, a test of slow charging phases with e.g. C/10 combined with short pulses of high current in charge and discharge direction is conducted. Additionally, the reversible heat generation, i.e. the entropic heat coefficient, which is the change of the cell's OCV with respect to temperature, is identified in a separate experiment. Together with the Joule heating term, the total heat generation of the cell can be described. Hence, these 2 experiments are sufficient to characterize the electro-thermal cell behavior during normal operation.

In order to characterize the thermal abuse behavior (i.e. thermal runaway behavior), an overheating experiment of the battery cell is performed. In this study, the cylindrical cell is heated up with constant

power at its bottom surface. Several thermocouples are applied on the heating element, the cell's surface, in the venting path above the cell and further away in the enclosed air volume to capture the evolution of temperature during the experiment. Also, the cell voltage is measured in order to identify the separator shutdown and the arise of an internal short circuit (ISC).

Considering the modelling part, a standardized and automatable model generation methodology is introduced and applied. LS-Dyna is used to solve the FEM Simulations, whereby the so-called batmac approach is used to model the cell's multi-physical behavior. The model features a first order Randle's circuit to describe the electrical behavior, Joule heating and reversible heat generation is considered and the electromagnetic solver is coupled with the thermal solver. The ISC is modelled using the *EM_RANDLES_SHORT keyword, wherein a custom function can be programmed to define the ISC initiation criterion and the associated short resistance. In this study, ISC initiation is modelled to take place once a corresponding initiation temperature is met. Finally, the exothermic reaction is modelled using the *EM_RANDLES_EXOTHERMIC_REACTION keyword. Again, a custom function can be programmed for defining the initiation criterion and the additional heat source. In this study, initiation is defined to take place once a specific temperature is exceeded. The heat generation is described by a generalized Arrhenius function and takes place until a specified maximum amount of heat has been generated.

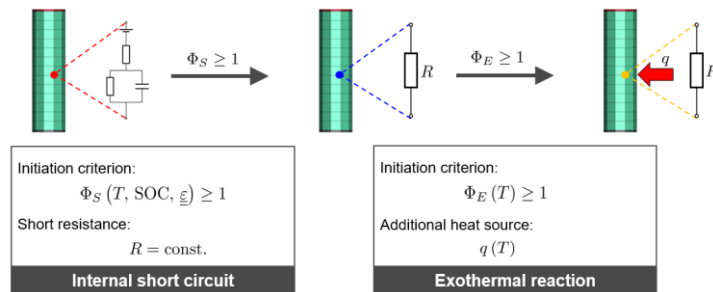


Fig.2: Modelling of the ISC and the exothermal reaction within the batmac approach in LS-Dyna.

3 Results and validation

To proof the practicality of the resulting models, some tests are exemplarily simulated and the arise of the thermal runaway is analyzed, whereby a good correlation between the experiment and the simulation has been found.

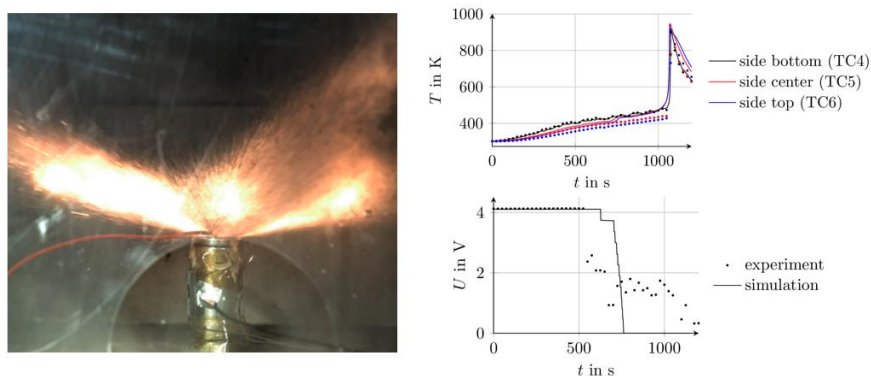


Fig.3: Left: Snapshot during single cell thermal runaway experiment. Right: Comparison between experimental measurements and simulation results showing a good correlation.

Finally, one of the investigated models is integrated in an abuse simulation of an arrangement of several cells. Exemplarily, the influence of design measures targeting the avoidance of the thermal propagation are studied and discussed. Additionally, the change of the current flow induced by the internal short circuit is analyzed.

From Single Cell Abuse Experiments to Thermal Runaway in Electric Vehicle Crash Simulations

Kevin Kong, [Pierre L'Eplattenier](#), Iñaki Caldichoury, Vidya Challa, Dilip Bhalsod, Srikanth Adya, Mike Howard

Ansys

1 Introduction

Safety is an important functional requirement in the development of large-format, energy-dense, lithium-ion (Li-ion) batteries used in electrified vehicles. Many automakers have dealt with this issue by enclosing the batteries into robust protective cases to prevent any penetration and deformation during car crashes. While this worked well for first-generation vehicles, consumers are increasingly interested in higher-range vehicles, which makes overengineered heavy protective cases detrimental for range. A more detailed understanding of battery behavior under abuse is, therefore, necessary to properly make design trade-offs.

Computer-aided engineering (CAE) tools that predict the response of a Li-ion battery pack to various abusive conditions can support analysis during the design phase and reduce the need for physical testing. In particular, simulations of the multi-physics response of external or internal short circuits can lead to optimized system designs for automotive crash scenarios. The physics under such simulations is quite complex, through coupling structural, thermal, electrical, and electrochemical. Moreover, it spans length scales with orders of magnitude differences between critical events such as internal shorts happening at the millimeter level, triggering catastrophic events like the thermal runaway of the full battery. The time scales also are quite different between the car crash happening in milliseconds and the discharge of the battery and temperature surge taking minutes to hours. A distributed Randles circuit model in Ansys LS-DYNA® can mimic the complex electrochemistry happening in the electrodes and separator of Li-ion batteries [1],[2],[3]. The Randles circuit model is also coupled with the mechanical solver of LS-DYNA where the deformations due to a battery crash allow the definition of criteria to initiate internal shorts.

In order to correlate mechanical deformations to the onset of internal shorting, subsequent appearance of thermal runaway, resulting gas emission, fire, and/or explosion, a series of crush experiments on automotive grade Li-ion pouch cells have been performed by Ansys. Benchmarks between experimental and numerical results from LS-DYNA allowed the tune up of cell dependent parameters. This paper will present the workflow from single cell experiments to obtaining the numerical parameters needed for a full electric vehicle crash modeling. The sequence of steps which are presented can be repeated for other electric or hybrid vehicles with different battery cells.

2 Numerical vs experimental benchmarks

Mechanical and thermal abuse experimental tests were performed on automotive grade Li-ion pouch cells. Parameter identifications in LS-DYNA simulations were then performed in order to get numerical results matching the experimental ones, so that these cells could be used in a full electric car crash simulation. The parameter identification was focused mostly on reproducing the experimental voltage drop due to internal shorts and consequent temperature elevation.

2.1 Characterization of the Randles circuit parameters of the cells

The electro-chemistry is represented in LS-DYNA by equivalent (Randles) circuits [1],[2],[3]. In order to characterize the parameters of these circuits, capacity as well as Hybrid Pulse Power Characterization (HPPC) tests were performed at different State of Charge (SOC), and temperatures. These are illustrated in Figure 1.

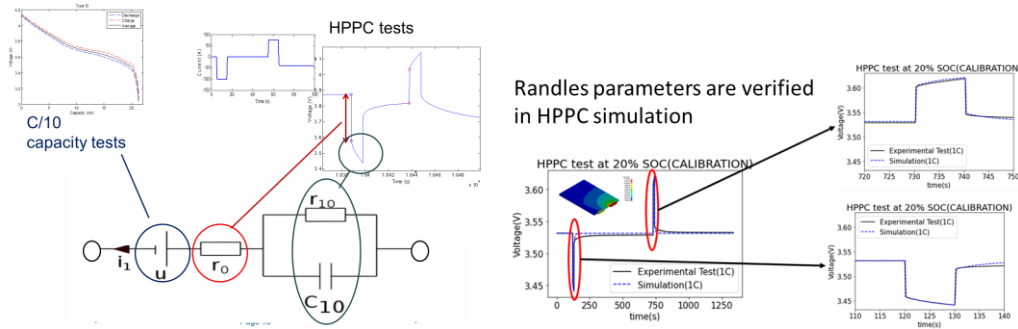


Fig. 1: Capacity and HPPC tests to characterize the cell

2.2 Mechanical abuse

Quasi-static compression and indentation tests with different indenter profiles were performed. The force, voltage, and temperature were measured as a function of the displacement of the indenter, as illustrated in Fig 2.

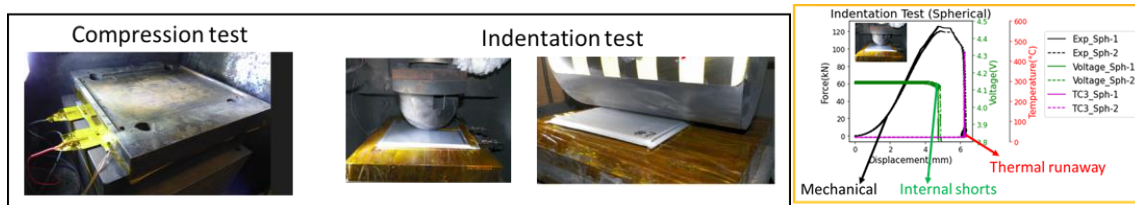


Fig. 2: Mechanical abuse: compression and indentation tests (left) along with typical experimental results (right)

The mechanical model of the cell (using ***MAT_CRUSHABLE_FOAM**) was optimized in order to match the measured force vs displacement in both compression and indentation tests. A criterion for the shorts was selected and short resistance in the simulation was then optimized in order to match the experimental voltage drop: A methodology has been developed to capture the experimental voltage drop of the cell during the internal shorts. Exothermal reaction models were added in order to match the temperature rise.

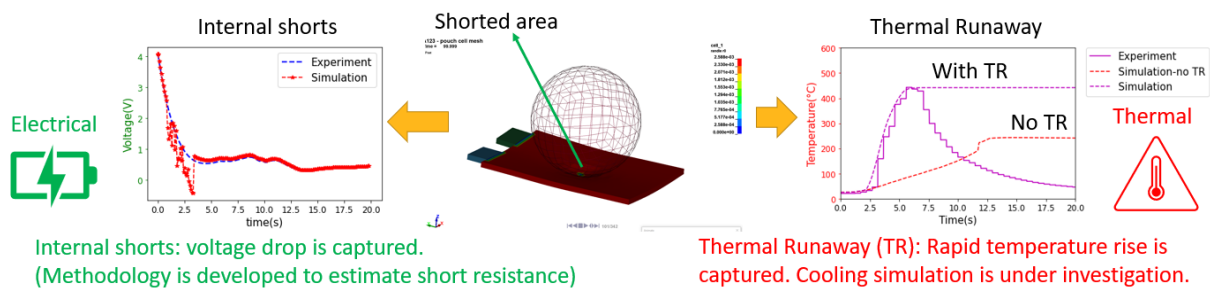


Fig. 3: Mechanical abuse: experimental vs numerical comparisons, first results

2.3 Thermal abuse

The same cells were placed in a pressure vessel, and a small heater was placed at the centre of the cell, on one side. The cell was locally heated, and the temperature was measured at different locations of the cell (other side as well as same side but at different locations than the heater). The voltage and temperature were also measured in order to characterize the internal shorts and the thermal runaway events.

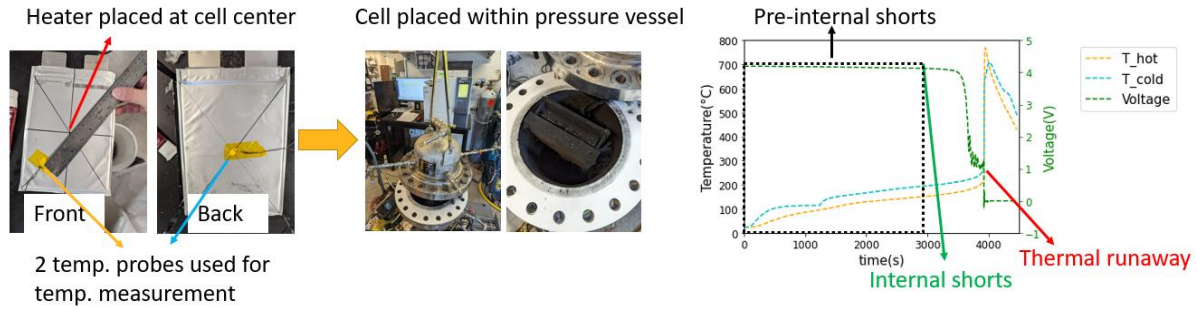


Fig.4: Thermal abuse: experimental setup and results

The numerical (highly anisotropic) thermal conductivity of the cell was tuned up in order to reproduce the correct temperature propagation before the short, both in plane and through thickness, as shown in Figure 5.

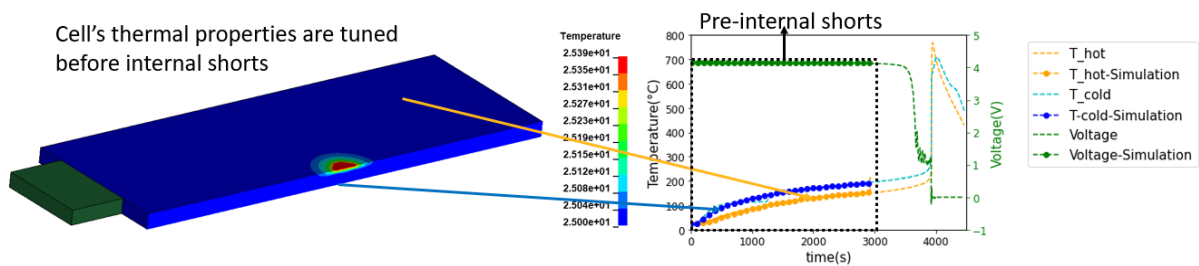


Fig.5: Thermal abuse: parameter identification of the thermal conductivity

The internal short onset and resistance were then optimized with the same methodology used in the mechanical abuse model to match the experimental results.

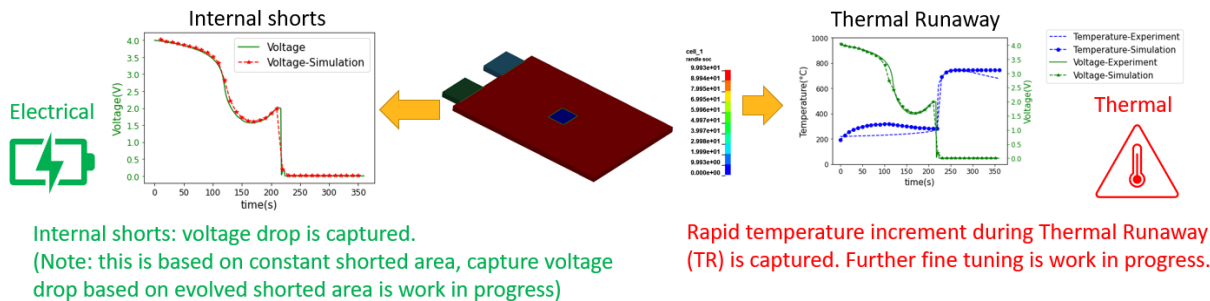


Fig.6: Thermal abuse: comparison between experimental and numerical results (voltage and temperatures)

3 Summary

Understanding the behaviour of cells during mechanical and thermal abuse is important, but the physics involved is quite complex. Hence Ansys decided to perform mechanical and thermal abuse tests on a typical automotive grade battery cell. The goal is to be able to get the needed parameters to be able to include such a cell in a full battery in an electric vehicle crash simulation. This work still is in progress, but this paper shows some first results and presents the sequence which could be reproduced for an automobile using another kind of cell.

4 Literature

[1] J. Deng, C. Bae, T. Miller, P. L'eplattenier and I. Caldichoury, "Multiphysics Battery Simulations Across Length Scales", Journal of the Electrochemical Society, 2019 166(14): A3119-A3121.

- [2] P. L'Eplattenier, I. Caldichoury, J. Marcicki, A. Bartlett, X. Yang, V. Mejia, M. Zhu, Y. Chen, "A distributed Randles circuit model for battery abuse simulations using LS-DYNA", Proceeding of the 14th International LS-DYNA User Conference, 2016.
- [3] P. L'Eplattenier, I. Caldichoury, "A Path Towards Including Batteries in Electric or Hybrid Car Crash Simulations with LS-DYNA", Proceeding of the 16th International LS-DYNA User Conference, 2020.

Nachhaltiger Leichtbau durch Monomaterialbauweise eines Batterischutzgehäuses

F. Huberth (Fraunhofer IWM), M. Hegde (KIT FAST)

Electrochemical-Thermo-Mechanical Coupled Abuse Models for Lithium-ion Battery in LS-DYNA

Kyoung-su Im¹, Zeng-Zan Zhang¹, and Grant Cook Jr.¹

¹ANSYS.Inc, Livermore, CA 94551, UST

1 Abstract

In this presentation, we report the status of electrochemical-thermal-mechanical (ECTM) coupled battery abuse models including i) aging model via solid-electrolyte-interface (SEI) formation and decomposition, ii) thermal heat flux model corresponding to SEI's reactions, iii) swelling model caused by intercalation/deintercalation of Lithium-ion among the electrodes, and iv) gas generation model due to Ethylene oxidation and Lithium hydration reactions on the electrode surfaces. Such models are intended to assist users in tackling problems ranging from the fundamental battery cell physics to the practical applications such as battery structure interaction. For the demonstration, we select the 10 cells problem of a lithium-ion battery stack, here, each cell consists of the anode current collector, anode, separator, cathode, and cathode current collector, respectively. The results demonstrate that after the ball impact the 10-cell stack, the mechanical deformation started and then, thermal runaway developed with a strong hot spot developed inside cell stack. As a result, temperature increased exponentially over the melting point of the lithium, 453K.

Parallel to ECTM demonstration, we will have a technical discussion about how we can further develop and validate the current multi-physics battery models to resolve our customers' problems.

2 Modeling

2.1 Aging model

The battery aging model developed in LS-DYNA is based on M. Safari, et. al [1] and Xiao-Guang Yang, et. al [2]. In these models, the evolution of the solid electrolyte interaction (SEI) is due to the main and side reactions. For the side reaction, it is required to solve Tafel-like type kinetics equation and need to be monitoring the rate of growth of the SEI layer.

2.1.1 SEI formation

The SEI reaction is given by $C_3H_4O_3 + Li^+ + e^- \rightarrow 0.5(CH_2OCO_2Li)_2 + 0.5C_2H_4$ and the corresponding heat flux is computed by

$$\dot{q}_{seif} = \sum_i k_{i,form} \cdot (\Delta H_i + zFV_{cell}), \quad k_{i,form} = A_i \prod_k c_k^{n_k} \cdot \exp\left(-\frac{\alpha F}{RT} \varphi\right)$$

2.1.2 SEI decomposition

The SEI decomposition is given by $(CH_2OCO_2Li)_2 \rightarrow Li_2CO_3 + C_2H_4 + CO_2 + 0.5O_2$ and its heat flux can be computed by

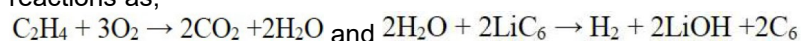
$$\dot{q}_{seid} = \sum_i k_{i,decom} \cdot \Delta H_i, \quad k_{i,decom} = A_i \sum_k c_{k,sei} \cdot \exp\left(-\frac{E_{ac}}{RT}\right)$$

2.2 Volume change

The volume change in the electrodes evaluates taking two steps: first, the porosity equation for the electrolyte is computed and then, by applying the summation rule of the volume fractions, the electrodes fraction is computed.

2.3 Gas generation

The gas generation can be evaluated by considering the ethylene oxidation and lithium hydration reactions as,



3 Results and discussion

Figure 1 shows the state variable and temperature changes by running 4 cycles with different times. The cycles consist of the discharging and charging modes.

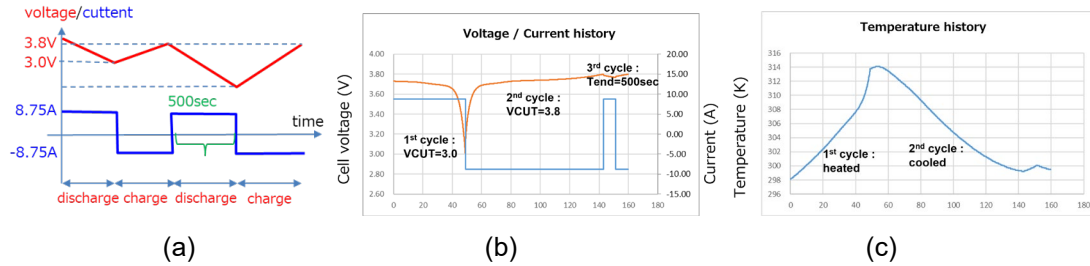


Figure 1 The state variables and thermal evaluation by running the 4 different cycles

Figure 2 shows the thermal analysis by impacting the rigid ball into the 10 cells of LIBS. Each cell has the negative current collector (10 μm), anode composite electrode (100 μm), separator (52 μm), cathode composite electrode (174 μm), and positive current collector (10 μm), respectively. During the deformation by impacting force, a cell's temperature increases due to both Joule heating and Peltier heating, which is mostly due to an exothermal reaction initiated by the entropy changes inside of the battery cell. Figure 2(a) shows the individual cell elements inside LIB stack to monitor the temperature changes as function of time and Figure 2(b) shows the temperature increasing of each cell elements. The rapid increasing of the temperature starts about 6s after the ball was in contact. After that point, temperatures in all elements increases exponentially to the thermal runaway. Although the present study is not modelling any chemical reaction mechanism, it is speculated that the chain reactions could be started after reaching the melting point of the lithium metal at 453 K.

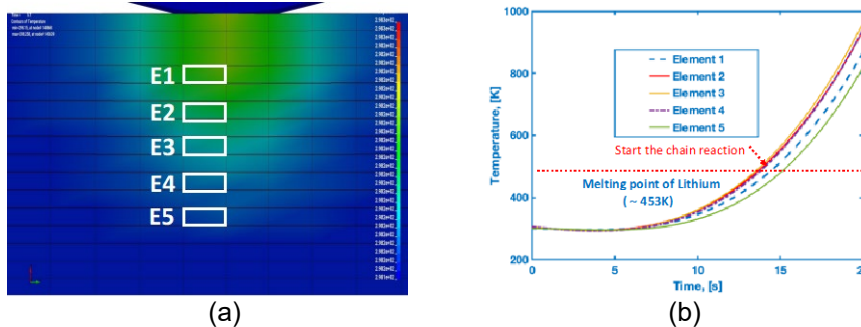


Figure 2 Analysis of the thermal runaways: a) individual cell elements inside battery cell stack, and (b) corresponding temperature increasing as function of time at each element.

4 Summary

In this study, we reported a new development of the electrochemical-thermal-mechanical coupling based on previously developed electrochemical LIB model in LS-DYNA. In 10 cells of a lithium ion battery stack, each cell consists of Graphite(LiC₆) anode/Separator/high performance layered LCO(LiCoO₂) cathode. With the present development of the battery-thermal-mechanical interaction, we strongly believe that users can apply this to more complex applications such as a cellular phone deformation and even EV battery deformation test in automotive industries.

5 Reference

[1] M. Safari, M. Morecrette, A. Teyssot, and C. Delacourt, *J. Electrochem. Soc.*, 156(3), A145-A153, 2009.
 [2] Xiao-Guang Yang, Yongjun Leng, Guangsheng Zhang, Shanhai Ge, and Chao-Yang Wang, *J. Power Sources*, 360, 28-40, 2017.

An anisotropic constitutive approach for analogous modeling of Li-ion cells

F. Andrieux ¹, A. Trondl ¹, S. Sommer ¹

¹ Fraunhofer Institute for Mechanics of Materials IWM, Woehlerstraße 11, 79108 Freiburg, Germany (Group: Crash Safety and Damage Mechanics, Business Unit: Component Safety and Lightweight Construction)

Battery Electric Vehicles (BEVs) play an important role to reduce CO₂ emissions for individual and public transportation, which are directly related to the predicted climate change. Therefore, a significant demand and further developments on BEVs are necessarily expected. To improve the crash safety of BEVs and the public acceptance of various safety aspects a thermal runaway (intrinsic failure and instabilities which can lead to explosions) of the commonly used Li-Ion cells should be avoided as far as possible or reduced to a tolerable minimum.

Improvements in engineering design concepts of BEVs are based strongly on simulations of the whole vehicle structure including Li-ion batteries. Due to computational performance reasons and the complexity of the intrinsic layered structure of Li-ion batteries simplified and homogenized analogous models are necessary [1,2]. Many approaches of analogous models of Li-ion cells to describe the deformation behavior often use the well proven (isotropic or anisotropic) compressible foam models [3, 1], which are originally developed for metallic or plastic foams as well as for highly repetitive cell-based structures such as honeycomb assemblies. The highly repetitive layered structure of Li-ion cells has principal similarities with the previous mentioned homogenized foams (e.g., high fraction of compacted active material) but differs also in terms of a composite structure (e.g., metallic foils/electrodes). Therefore, it is mostly not possible to describe the deformation states for all representative crash loadings (e.g., indentations, compressions, etc.) and different directions in a sufficient manner by using these well proven classical foam models. Due to these circumstances a transversal isotropic material model was suggested, which represents in principle a combination of a modified isotropic Deshpande-Fleck approach [4] by using a directional dependent weighted hydrostatic stress definition introduced by Benzerga and Besson [5]. This approach bases on an associated flow rule and a strain hardening depending on deviatoric and hydrostatic deformation. A motivation for the implementation of this model approach is the direct accessibility of all mechanical quantities which are needed for an electrical short circuit criterion. The validation and adjustment of the model parameters based on experimental investigations such as directional dependent indentations with different indenter-geometries as well as with constraint and non-constraint compaction tests at different spatial axes.

1 Modelling Approach

In comparison to “conventional” anisotropic plasticity models for metals like Aluminum, which bases in a simplified manner on different weight-factors of the stress-tensor components (Hill-type), the directional dependency for the presented approach is described by using a weighted hydrostatic stress portion, suggested by Deshpande-Fleck [4].

$$\sigma_h = h\sigma_{11} + h\sigma_{22} + (1-2h)\sigma_{33} \quad h \in [0,1] \quad (1)$$

In this approach the parameter h controls the transversal isotropic characteristic (if $h < 1/3$ direction 3 is more compressible and if $h > 1/3$ directions 1 and 2 are more compressible, $h = 1/3$ isotropic) of the model.

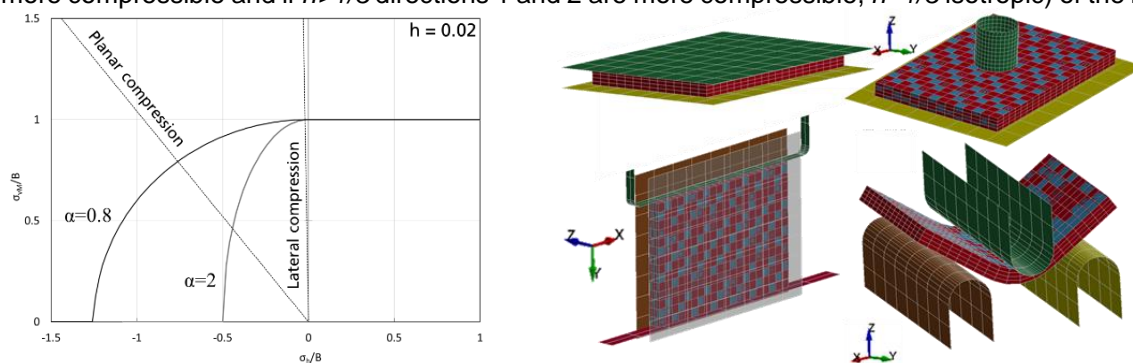


Fig. 1: Shape of yield surface in the (σ_h, σ_e) stress space (left); and investigated load cases (right).

Additionally, the conventional effective von Mises stress σ_e is used to formulate a generalized equivalent stress $\tilde{\sigma} = \sqrt{\sigma_e^2 + \alpha^2 \sigma_h^2}$ in the (σ_h, σ_e) stress space. The material parameter α is zero for tensional loadings and a constant value under compression, which results in a yield surface shown in Fig 1 (left). The evolution of the plastic strain tensor is formulated with an associated normality rule by using the asymmetrical yield function $\varphi := \tilde{\sigma} - B \leq 0$ depending on a linear combination of deviatoric hardening B_D and volumetric hardening B_V with $B := B_D(\varepsilon_D) + B_V(\varepsilon_V)$ and the effective von Mises strain ε_D as well as the volumetric strain ε_V , respectively. For the hardening behavior reasonable analytical (polynomial or exponential) approaches are used. Due to the compressibility of the homogenized layered system, the plastic strain tensor ε^p has to be splitted into a deviatoric and a volumetric portion $\varepsilon^p := \varepsilon_D^p + \varepsilon_V^p$, to formulate the associated plastic-flow in a complete manner with respect to volume changes.

2 Model implementation and calibration as well as comparison to experiments

A user defined material model `*MAT_USER_DEFINED_MATERIAL_MODELS` was implemented for testing the behavior of the developed approach. The simplified pouch cell model consists of the homogenized cell core using the implemented user defined model and the surrounding bag. 8-noded solid elements are used for the homogenized cell core. The bag is modeled with 4-node shell elements by using the same nodes on the outer faces of the cell core [1] and an elastic-plastic material behavior with `*MAT_PIECEWISE_LINEAR_PLASTICITY`. Indentation and compression tests in different directions and constraints are simulated (Fig. 1 right) to fit the parameters of the homogenized pouch cell model. To separate the different influences of deviatoric and volumetric strains, the presented adjustment of the model parameters use only the volumetric portion.

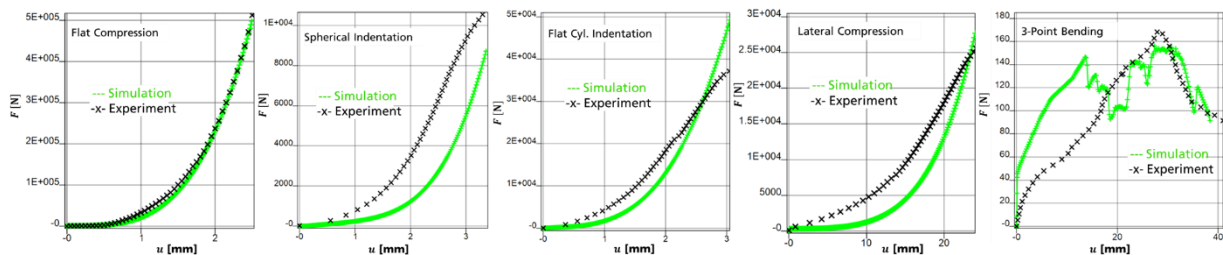


Fig.2: Comparison between experiments and homogenized model approach.

Further investigations related to pure deviatoric and a mixed approach are currently in working progress, as well as extensions for electrical damage and a short circuit criterion to trigger a thermal runaway by using appropriate Randle model approaches in LS-Dyna.

3 Summary

The suggested approach shows good agreements for all investigated load cases (Fig. 2). The parameter h controls the transversal isotropic behavior in a sufficient manner for the investigated representative loadings, which shows the global deformation characteristic of the lateral compression test. Further improvements of the model approach are currently tested and under development.

4 Literature

- [1] Trondl, A.; Sun, D.-Z.; Sommer, S.; "Simplified modeling of pouch cells under different loadings", 13th LS-DYNA European Conference and User's Meeting - Online and on-site. Book of abstracts: 5-7 October 2021, Ulm, Germany, ISBN: 978-3-9816215-7-0, pp. 164 (10 pages)
- [2] Schaufelberger, B.; Altes, A.; Matura, P.; "Modeling the Mechanical Behavior of a Li-Ion Pouch Cell under Three-Point Bending"; 13th LS-DYNA European Conference and User's Meeting - Online and on-site. Book of abstracts: 5-7 October 2021, Ulm, Germany, ISBN: 978-3-9816215-7-0
- [3] Elham, Sahraei; Hill, Rich; Wierzbicki, Tomasz.; "Calibration and finite element simulation of pouch lithium-ion batteries for mechanical integrity", Journal of Power Sources 201 (2012): 307-321
- [4] Deshpande, Vikram S.; Fleck, Norman A.; "Isotropic constitutive models for metallic foams", Journal of the Mechanics and Physics of Solids 48.6-7 (2000): 1253-1283
- [5] Benzerga A. A.; Besson J.; "Plastic potentials for anisotropic porous solids", European Journal of Mechanics - A/Solids, vol.20, issue.3, pp.397-434, 2001

Instability and mesh dependence – Part 1: Analytical criteria

P. DuBois¹, M. Feucht², F. Andrade³, S. Conde³, T. Graf³, A. Haufe³

¹Consulting Engineer, Alzenau, Germany

²Mercedes-Benz AG, Sindelfingen, Germany

³DYNAmore GmbH, Stuttgart, Germany

Abstract. Spurious mesh dependence is a known issue in finite element analysis whenever failure prediction is involved. This phenomenon is closely linked to the instability which takes place after a certain amount of plastic straining. For example, in the simulation of a typical tensile test, a homogeneous strain field along the geometry is firstly observed. At a certain point, diffuse necking takes place and both the strain and stress fields are no longer homogeneous. From that point on, spurious mesh dependence is also observed. For such a simple loading condition, the determination of the onset of mesh dependence is quite straightforward. However, this is not the case for arbitrary stress states. In this contribution, we consider a bifurcation analysis in order to determine the onset of plastic instability (in the sense of diffuse necking). The analysis is restricted to isotropic elasto-plastic constitutive models where in the present study we considered a J2-based plasticity model (*MAT_024), *MAT_SAMP-1 and also a Hill-based transverse isotropic model (*MAT_037). The bifurcation analysis has been carried out considering a Limit Point (LPBC) and General Bifurcation Criterion (GBC). Furthermore, the plastic instability theory proposed by Swift in 1952 has been extended to the three dimensional case and used as a criterion for determining the instability onset. A python program has been written which allows the three-dimensional visualization of the instability onset as a function of the plastic strain, the triaxiality and the Lode parameter. Therefore, an instability surface is obtained which in principle also corresponds to the onset of spurious mesh dependence in finite element analysis. We demonstrate how the instability surface looks like for a variety of materials and under which conditions the different instability criteria are different from each other. The predictions obtained here are then compared with simulation results presented in the second part of this contribution.

Keywords: Failure prediction, plastic instability, diffuse necking, mesh dependence, bifurcation analysis.

Instability and mesh dependence – Part 2: Numerical simulations

F. Andrade¹, M. Feucht², P. DuBois³, S. Conde¹, T. Graf¹, A. Haufe¹

¹DYNAmore GmbH, Stuttgart, Germany

²Mercedes-Benz AG, Sindelfingen, Germany

³Consulting Engineer, Alzenau, Germany

Abstract. The second part of this contribution is devoted to numerical simulations under specific boundary conditions aiming to detect instability. Firstly, a method had to be developed to keep any arbitrary stress state constant throughout deformation and the strain field homogenous until localization occurred. In the plane stress case (e.g., standard shell elements), determining the necessary boundary conditions which result in constant triaxiality can be analytically found by making some typical assumptions like negligible elastic strains, isochoric behavior, proportional loading and an isotropic J2-based plasticity model (*MAT_024). However, the three-dimensional case demanded the solution of the elasto-plastic problem beforehand in order to accurately determine the necessary boundary conditions (displacements) with the goal of keeping both the triaxiality and the Lode parameter constant throughout deformation. A series of blocks containing several elements with 1:1:1 aspect ratio has then been simulated under constant stress state and homogenous strain and stress fields for different materials. The onset of localization is observed whenever the homogenous field is lost and becomes heterogeneous. The plastic strain at which this occurs is taken as the begin of the instability (in the sense of diffuse necking). Comparing these simulation results with the predictions from the analytical bifurcation analysis from the first part of this contribution, we could observe that the Limit Point Bifurcation Criterion matches the simulations with great accuracy. The simulations also clearly show that using different element sizes in the calculation of the blocks leads to different (i.e., mesh dependent) solutions as soon as the heterogeneous strain field becomes apparent. In other words, the analytical prediction of instability directly leads to the prediction of when the finite element solution becomes spuriously mesh dependent. We can also show that, if the elastic properties are similar to those of metallic materials (i.e., $E \gg H$), all the three criteria adopted in this study give identical predictions regarding the onset of instability. A difference is only seen if the order of magnitude of the elastic regime is similar to the one of the plastic regime, a condition typically met for very soft materials. These findings are quite useful for industrial engineering problems involving large plastic deformations and ductile failure because it allows to determine from which point on a regularization strategy is necessary. A further application of the findings reported here is the regularization of failure models for any arbitrary combination of triaxiality and Lode parameter provided the underlying material model is isotropic and J2-based (like *MAT_024).

Keywords: Failure prediction, plastic instability, diffuse necking, mesh dependence, bifurcation analysis.

Ansys LS-DYNA OneMPI Methodology

Eric Day, Jason Wang, Francois-Henry Rouet, Bob Lucas

Ansys LST

1 Abstract

OneMPI was developed to reduce the number of LS-DYNA distributed-memory (“MPP”) executables. Historically, dozens of binaries are issued each LS-DYNA release. Contrast to other Ansys flagships, which issue just one or two executables. OneMPI minimizes the overabundance of MPP binaries by accommodating different flavors of MPI in a single binary. In setting a new environmental variable, LSTC_MPI, users can declare their preferred MPI: Intel, Platform, Open, or Microsoft. Supplement to OneMPI, LSTC_REDUCE will encourage identical decomposition and identical solutions from each MPI. OneMPI allows for a more flexible MPP binary, reduces QA tasks, and helps LS-DYNA align with other Ansys products.

2 Introduction

The current release system demands a multitude of LS-DYNA binaries to cover all platforms, compilers, architecture, parallel application, etc. The large quantity of binaries prolongs the QA process and burdens developers with debugging. OneMPI was developed to limit the number of MPP binaries by supporting multiple MPI in one. LSTC_REDUCE will greatly reduce inconsistencies from the OneMPI binary that would otherwise amount from using different MPI. The repeatability of OneMPI permits LST to thoroughly test with just one MPI; thus, reducing QA for LS-DYNA MPP nearly three-fold.

LS-DYNA OneMPI for Linux supports Intel, Platform and Open MPI. LS-DYNA OneMPI for Windows supports Intel and Microsoft MPI. Each ensuing LS-DYNA release with OneMPI will require approximately 26 MPP and hybrid binaries rather than 72. Future applications with similar functionality to OneMPI can further funnel down the number of LS-DYNA binaries. The transition will help LS-DYNA limit the complexity of release and better parallel other Ansys products.

Ansys Mechanical APDL, for instance, already has similar functionality to OneMPI. Their MPI wrapper library allows MAPDL to issue a single executable each release. MAPDL wraps all MPI functions into a common library, where MPI specific logic is detached to independent libraries. An MPI specific library is loaded at runtime based on the MPI defined in the library path environment. MAPDL supports Intel MPI, Open MPI, and Cray-MPICH on Linux, and Intel MPI and Microsoft MPI on Windows.

3 OneMPI Functionality

OneMPI is available in the master, DEV, version of the code. The base build of LS-DYNA OneMPI uses Intel MPI. Intel is the default MPI because many LS-DYNA customers use Intel chips and prefer the MPI support and software toolchain of Intel.

A new subroutine is implemented to read the LSTC_MPI environmental variable at runtime. The environment is set to either intelmpi, platformmpi, openmpi, or microsoftmpi. On execution, LS-DYNA initializes the MPI environment by querying the corresponding data structure defined in the MPI header file. In particular, LS-DYNA grabs the values of all the MPI constants that the Fortran bindings rely on, e.g. MPI_INTEGER, MPI_SUM, etc. The MPI constants are mapped to the LS-DYNA MPP constants, where LS-DYNA will then proceed as normal. OneMPI differs from traditional MPP binaries in that MPI constants are established at runtime rather than during compilation.

LS-DYNA is mostly written in Fortran but also uses C and C++, for example, our linear algebra package, SPOOLES, and linear constraint analysis package, LCPACK. When using the C bindings of MPI, the

Application Binary Interface (ABI) of different MPI implementations are largely incompatible. While MPI constants and types in Fortran are almost all integers, those in C, such as MPI communicators, requests, statuses, and handles are opaque types. The varied treatment of opaque data types across MPI leads to ABI incompatibility. Consequently, we chose to redirect MPI calls from LS-DYNA C code to the Fortran bindings using a compatibility layer. Redirecting to Fortran solves the data type differences, allowing OneMPI to be MPI agnostic.

MPI compatibility with OneMPI is determined by the constants defined in the MPI header file. LS-DYNA OneMPI is built with headers from Intel MPI 2018, Platform MPI, Open MPI 4.0.0, and Microsoft MPI 10.0. The MPI linked at runtime must share equal MPI constants to the LS-DYNA build MPI. The following are compatible with OneMPI: Intel MPI 20xx, all Platform MPI, Open MPI 4.x.x, Microsoft v10.0.

At run time, LS-DYNA will search for the dynamic libraries from the build MPI, Intel, regardless of the LSTC_MPI environment set. To use OneMPI with a different implementation of MPI, a common MPI runtime library must be created to link intel library file names to the corresponding Open and Platform MPI libraries.

4 Deployment – OneMPI Library

The OneMPI runtime library is generated by running a shell script, OneMPI_lib. The common library, OneMPI, will appear in the user's home directory. Soft links are used to point LS-DYNA to the correct dynamic MPI libraries installed on the machine.

The script assumes MPI is installed in /opt on Linux and C:\Program Files on Windows. Paths to Intel, Platform, Open, and Microsoft MPI can be edited at the top of the script. The MPI referenced must be compatible with OneMPI, as mentioned in the previous section. If a particular MPI development kit is not installed on the machine, then that MPI will be ignored when creating the OneMPI library. OneMPI will still function with the remaining MPI libraries.

5 Deployment – OneMPI Environment

The next step is to set your MPI environment. The following can be copy-pasted into your .cshrc file on Linux. Adjust for bash. Edit the MPI_ROOT paths for the MPI installed on your machine. LD_LIBRARY_PATH points to the OneMPI library and should not be edited.

The environment is similar on Windows. The Windows environment for Intel or Microsoft MPI is set by OneMPI_lib.bat. On Windows, LD_LIBRARY_PATH will instead appear under PATH.

```
#-----OneMPI-----
# intelmpi, platformmpi, or openmpi
setenv LSTC_MPI intelmpi

## Intel MPI
setenv MPI_ROOT /opt/intel/impi/2018.3.222/intel64
setenv PATH $MPI_ROOT/bin:$PATH
setenv LD_LIBRARY_PATH ~/OneMPI/intelmpi:$LD_LIBRARY_PATH

## Platform MPI
#setenv MPI_ROOT /opt/platform_mpi
#setenv PATH $MPI_ROOT/bin:$PATH
#setenv LD_LIBRARY_PATH ~/OneMPI/platformmpi:$LD_LIBRARY_PATH

## Open MPI
#setenv MPI_ROOT /opt/openmpi-4.0.0
#setenv PATH $MPI_ROOT/bin:$PATH
#setenv LD_LIBRARY_PATH ~/OpenMPI/openmpi:$LD_LIBRARY_PATH
#-----
```

Switch between MPI by setting LSTC_MPI to either intelmpi, platformmpi, openmpi, or microsoftmpi. Uncomment or replace the complementing MPI_ROOT, PATH, and LD_LIBRARY_PATH.

A result of Intel being the default build MPI is that the OneMPI binary can also be used as a normal LS-DYNA Intel MPI binary. Meaning that the LSTC_MPI environment and OneMPI common library are not necessary to run with Intel MPI. However, switching to Platform, Open, and Microsoft MPI is not possible without the new environment and library.

6 Deployment – LSTC_REDUCE

LSTC_REDUCE promotes equal and repeatable solutions when running MPP LS-DYNA. LSTC_REDUCE was developed years ago to fix the order of data summation within and across nodes [1]. By redirecting MPI_REDUCE to LST's own reduce routine, numerical variations accumulated from round-off error are limited, encouraging consistent and reproducible solutions from all MPI.

The trade-off with LSTC_REDUCE is that LS-DYNA can no longer exploit specialized MPI algorithms. This in turn means that LS-DYNA might run slower. Performance impact is most notable in implicit when paired with hundreds of MPI ranks. For example, LS-DYNA's multifrontal code (used for Implicit Mechanics and Multiphysics) opportunistically uses asynchronous MPI communication to assemble frontal matrices that are shared amongst multiple processors. A consequence of disabling asynchronous MPI communication with LSTC_REDUCE is that LS-DYNA cannot utilize the highest performing factorization kernels.

LSTC_REDUCE is disabled by default. Enabling LSTC_REDUCE is at the discretion of the user. If repeatability is important, LSTC_REDUCE should be used. If performance is the main priority, LSTC_REDUCE should remain disabled.

LSTC_REDUCE is enabled with one of the following methods.

1. Add keyword ***CONTROL_MPP_IO_LSTC_REDUCE** to your input deck.
2. Use a text editor to create *pfile*. Add the following: `general { lstc_reduce }`
Add `p=pfile` to your LS-DYNA command line.

7 Summary

OneMPI is a leap towards reducing the number of LS-DYNA binaries. A single MPP binary will function with all LS-DYNA supported MPI implementations, which fundamentally benefits developers, LST QA, and customers. Convolutions surrounding MPP binary selection are lessened. Copious efforts to debug and test many MPP binaries are reduced. Time once spent on the lengthy LS-DYNA release process can now be spent on new feature development and increased validation.

8 Literature

- [1] Hallquist, J: Recent Developments in LS-DYNA, 2009, p. 55

Data-driven analysis of LS-DYNA's time step estimates and a machine learning based estimate

Tobias Willmann¹, Maximilian Schilling¹, Manfred Bischoff¹

¹ Institute for Structural Mechanics, University of Stuttgart
Pfaffenwaldring 7, 70550 Stuttgart, Germany
{willmann;schilling;bischoff}@ibb.uni-stuttgart.de

1 Abstract

In explicit simulations, an estimation of the critical time step is necessary to ensure a stable computation. LS-DYNA calculates the critical time step for an element by dividing a characteristic element length by the speed of sound of the respective material. To obtain the characteristic length, simple formulas are used, e.g. for shell elements, the area of the element divided by its longest edge or divided by its longest diagonal [1]. According to the Encyclopedia of Computational Mechanics [2], these estimates can be considered state of the art in explicit dynamics. Unfortunately, these estimates are not conservative, which is why the safety factor "tssf" has to be used in `*CONTROL_TIMESTEP`.

In this presentation, we analyze the performance of the estimates for shell elements mentioned above based on a data-driven approach. From this insight, we derive conservative versions of the time step estimates. Furthermore, we present a new approach for time step estimation based on neural networks, which achieves significantly better results than the current estimates with only little extra cost.

2 Introduction

LS-DYNA provides several options for the timestep estimation of shell elements. With the definitions

$$l_e^{LSE} = \frac{A}{l_{max}} \quad l_e^{LDE} = \frac{A}{d_{max}}$$

where l_{max} is the longest side and d_{max} is the longest diagonal, the user can select one of the following options by changing the value "isdo" in `*CONTROL_TIMESTEP`:

- isdo = 0: the maximum of l_e^{LSE} and l_e^{LDE} is chosen as the characteristic length
- isdo = l_e^{LDE} is chosen as the characteristic length

isdo = 2 and 3 are not considered here due to warnings and unavailability, see [3]. The critical time step size is calculated by dividing the characteristic length by the speed of sound c . The exact solution for the critical time step size on element level can be found by solving the eigenvalue problem

$$(\mathbf{K} - \omega_i^2 \mathbf{M}) \mathbf{v}_i = \mathbf{0}$$

where \mathbf{K} is the element stiffness matrix and \mathbf{M} is the element mass matrix. The critical time step can be calculated as $\Delta t_{crit} = \frac{2}{\omega_{max}}$. This equation can be reformulated to obtain the exact characteristic length

$$l_e^{exact} = \frac{2c}{\omega_{max}}$$

The critical time step of an element with its size being uniformly scaled by a factor α , i.e. each side length is multiplied with α , is α times the critical time step of the unscaled element. This relation holds for both the estimates for the characteristic length and the exact value. The relative estimation error

$$e = \frac{|l_e^{estimation} - l_e^{exact}|}{l_e^{exact}}$$

is the same for the scaled and the unscaled element. Therefore, we focus on the dependency of the estimation error on the element *shape*, regardless of its size, and define the dimensionless quantities

$$\frac{1}{\omega^{LSE}} = \frac{l_e^{LSE}}{\sqrt{A}} = \frac{\sqrt{A}}{l_{max}} \quad \frac{1}{\omega^{LDE}} = \frac{l_e^{LDE}}{\sqrt{A}} = \frac{\sqrt{A}}{d_{max}} \quad \frac{1}{\omega^{exact}} = \frac{l_e^{exact}}{\sqrt{A}} = \frac{2c}{\sqrt{A} \omega_{max}}$$

by dividing the estimates and the exact characteristic length by the square root of the element area.

3 Results

Figure 1 shows scatter plots of 153,697 blue dots, each of them representing the estimated critical time step plotted versus the exact critical timestep for a shell element with a specific shape. Each of these elements has the following properties:

- The length of the shortest edge is at least 0.1 times the length of the longest edge.
- Every angle is between 20° and 160°.

The horizontal axis shows the exact solution and the vertical axis shows the estimation for the estimates indicated in the caption. For dots on the red line, the estimation and the exact solution coincide, i.e. the closer a blue dot is to the red line, the better the estimate is for the corresponding element. Dots below the red line indicate conservative estimates.

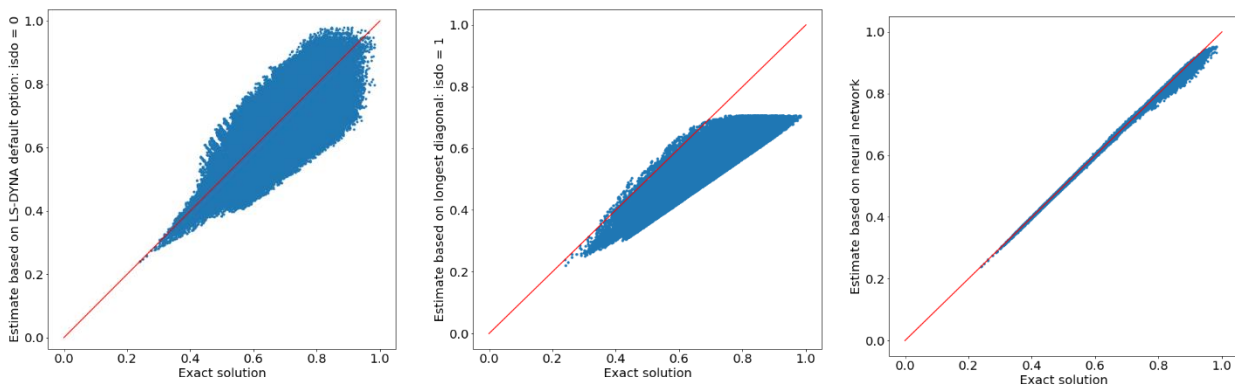


Fig. 1: Estimation results of 153,697 elements for different estimation methods: *isdo=0* (left), *isdo=1* (center), estimation calculated by a neural network (right)

The estimation based on *isdo = 0* has a maximum error of 42.2% and an average error of 10.3%. For *isdo = 1*, these values are 41.4% (maximum) and 27.35% (average). Although the average error is higher, this estimate has the advantage that it is conservative for the vast majority of the elements.

The rightmost plot in Figure 1 shows an improved estimate. A neural network was used to estimate the characteristic length. It is a feed-forward neural network with only one hidden layer (50 neurons in the hidden layer), trained with data obtained from exact computations of the characteristic length as outlined above. For this estimate, the maximum error is only 7.1% and an average error of 0.23% is obtained.

Due to the limited length of this extended abstract, we omit technical details regarding the derivation of the dimensionless quantities for comparing the estimate quality, the creation of the element dataset, and technical details regarding the time step estimation using a neural network. For further details, we refer to a paper in preparation [4].

4 Acknowledgements

Support for this research was provided by the EFB - European Research Association for Sheet Metal Working under Grant AiF 21466N / EFB 06/219. Within the scope of the Programme for Industrial Collective Research (Industrielle Gemeinschaftsforschung, IGF) it was funded by the German Ministry of Economic Affairs and Energy via the German Federation of Industrial Research Associations -- AiF (Arbeitsgemeinschaft industrieller Forschungsvereinigungen e.V.) based on a decision of the German Bundestag. This support is gratefully acknowledged.

5 Literature

- [1] Livermore Software Technology Corporation (LSTC) – LS-DYNA® Theory Manual, 2019
- [2] Benson, D.J., “Explicit Finite Element Methods for Large Deformation Problems in Solid Mechanics”, In: Encyclopedia of Computational Mechanics Second Edition, 2017
- [3] Livermore Software Technology Corporation (LSTC) – LS-DYNA® Keyword User’s Manual Volume I, r:14186, 2021
- [4] Willmann, T., Schilling, M., Bischoff, M., “Data-integrated timestep estimation using neural networks”, Manuscript in preparation

Framework of conducting reliability analysis of concrete beams using stochastic nonlinear FE models in LS-DYNA

Connor Petrie¹, Fadi Oudah¹

¹Department of Civil and Resource Engineering, Dalhousie University, Canada

1 Introduction

Reliability analysis is a powerful tool that allows engineers to approximate the safety (probability of failure) of a certain component, through probabilistic evaluation of the performance under specific conditions (Nowak and Collins 2010). Non-linear finite element (FE) analysis can be used to approximate the response of structural components (beams, columns), and capture the response in the non-linear region, without extensive experimental testing. Stochastic FE refers to modeling the spatial variability in the structural response using random fields. The advantage of stochastic FE over conventional FE is the ability to represent certain parameters as a 3-dimensional random field of correlated values, rather than using mean values. In the case of a reinforced concrete (RC) beam, the random field can be generated to capture the spatial variability of the concrete strength. The two major issue of conducting reliability analysis using stochastic FE models generated in LS-DYNA is (Petrie 2022): i) discretizing the secondary stochastic mesh onto the original FE model to generate a stochastic FE model; and ii) the need to run many simulations in order to evaluate the safety probabilistically through reliability analysis. In the present work, a framework to conduct reliability analysis using stochastic non-linear FE models of a strengthened concrete beam using LS-DYNA, is presented.

2 Methodology

A LS-DYNA-Python-MATLAB interface has been developed to link and automate the creation of the stochastic and elements-based FE mesh, run several simulations in parallel, and extract the response of the component for conducting the reliability analysis. Figure 1 shows the flowchart of the automated computer code developed using the proposed interface.

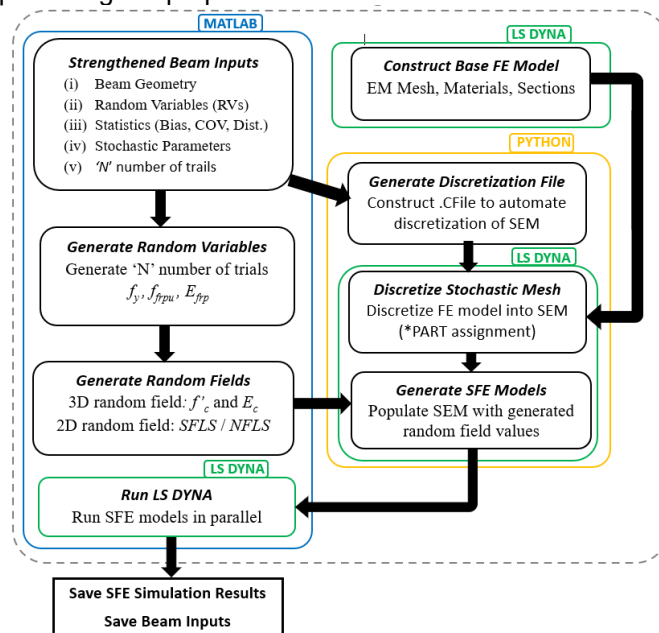


Fig. 1: Flowchart of LS-DYNA-Python-MATLAB interface to generate stochastic FE model in LS-DYNA.

The main MATLAB script is to generate the random field using the EOLE method (Li and Der-Kiureghian 1993) and to discretize the stochastic mesh. A Python script is used to call and manipulate the SFE files in LS-DYNA. An open-source Python code package was used to call and manipulate the input file (.k file) (Diez, 2018). This package was used as a base to develop a script in Python to be called by

MATLAB to populate the stochastic mesh with the generated random field values. The running of stochastic FE simulations in LS-DYNA SMP solver has been automated through MATLAB and has been optimized to run several simulations in parallel. In this work a total of 9 simulations were run in parallel to improve computation time. All analysis were run on the structural assessment and retrofit (SAR) research group server: a windows-based server with dual Intel Xeon Gold 5220R 2.20GHz processors (48 cores), a NVIDIA Quadro P620 graphics card, and 128 Gb of available RAM. The parallelization of the LS-DYNA solver mean that the efficiency of the reliability analysis will only be limited by the available computational power.

3 Discretization of Stochastic Mesh in LS-DYNA

To conduct stochastic FE, the user must take a typical LS-DYNA FE element mesh and overlay a secondary stochastic mesh and assign the random field values. For simplicity of application, it is typical that the FE mesh be a subset of the stochastic mesh (Sudret and Der-Kiureghian 2000). This is to ease the burden of discretization the stochastic mesh in LS-DYNA. FE mesh elements can be grouped together through special definition of groups within the FE software. In LS-DYNA, the stochastic mesh can be included through the assignments of numerous ***PART** to represent each element of the discretized random field, which can be assigned the unique value. The discretization of the stochastic mesh through assignment of unique ***PART** in LS-DYNA is tedious and needs to be done for each new configuration of beam and mesh density. Command files (.Cfile) can be used to automate the discretization process. A Cfile is a command file read by LS-DYNA that can execute a series of commands within the program to build, or modify, an FE model. An automated computer code has been developed in MATLAB to take the base FE model generated and discretize the model to include a secondary stochastic element mesh using Cfile assignment. The Cfile is generated based on the chosen density of stochastic mesh and will generate unique ***PART**, ***MAT**, ***SEGMENT**, and ***CONTACT** to represent each stochastic element in the stochastic mesh. Figure 2 shows a sample image of the same generated 3D strengthened beam model in LS-DYNA, showing both the FE mesh (left) and stochastic mesh (right). Each 3D stochastic mesh element is made of 4 FE mesh elements in each direction (x, y, z), making the dimensions of a single FE mesh and stochastic mesh equal to 12.5x12.5x10 mm and 50x50x40 mm, respectively.

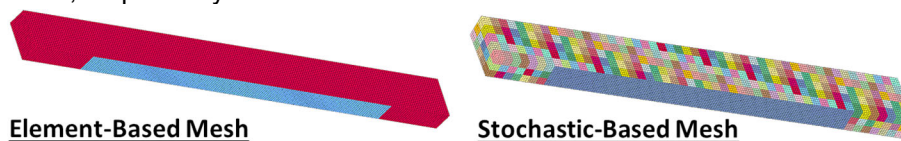


Fig.2: Representation of the spatial variation of concrete strength through an RC beam.

4 Summary

Results show that the proposed framework is capable of generating stochastic FE models with varying FE element and stochastic mesh sizes. The stochastic FE models are shown to be capable of capturing the spatial variation in the material strength of the concrete beam. Moreover, this automated framework allows the user to evaluate multiple simulation in parallel to increase the efficiency of the reliability analysis. Applications of the automated LS-DYNA-Python-MATLAB interface are possible on many other FE models where the use of mean values for material parameters does not capture the response of the member under load. Future research is aimed at generalizing the interface to be used to discretize the stochastic mesh of any FE model in LS-DYNA to represent chosen material parameter as random fields.

5 Literature

- [1] Nowak, A., and Collins, K. (2000). "Reliability of Structures". The McGraw-Hill Companies.
- [2] Sudret, B., and Der-Kiureghian, A. Der. (2000). "Stochastic Finite Elements and Reliability - A state-of-the-art report". Univ. of California, Berkeley, CA: Dept. of Civil and Environmental Engineering.
- [3] Li, C., and Der-Kiureghian, A. (1993). "Optimal discretization of random fields." *ASCE-ASME Journal of Mechanical Engineering*, 119(6), 1136–1154.
- [4] Diez, C. (2018). "Build your own LD-DYNA Tools Quickly in Python," In the proceedings of the *15th international LS-DYNA Users Conference 2018*.
- [5] Petrie, C. (2022). "Reliability analysis of externally bonded FRP strengthened beams considering existing conditions: Application of stochastic FE and conditional probability". Master's thesis, Dalhousie University, Canada.

Modeling of variations in the virtual process chain of forming and joining of sheet metal parts

Patrick Brix¹, Mathias Liewald², Markus Kuenzel¹

¹Mercedes-Benz AG, 71509 Sindelfingen, Germany

²Institute for Metal Forming Technology, Holzgartenstraße 17, 70174 Stuttgart, Germany

1 Introduction

The increasing demand for high quality products combined with a shortened time-to-market poses major challenges for the automotive industry, particularly with regard to the manufacturing processes of sheet metal assemblies for the body-in-white. Virtual process chain simulation, which is based on non-linear finite-element-method (FEM) and links sheet metal forming and manufacturing joining simulation, is therefore performed early in the virtual design stage of a car-body [1]. Here, one of the main objectives is to predict the dimensional accuracy of the single sheet metal parts as well as of the joined sheet metal assemblies. However, the sheet metal forming process is subject to process-related variations that can adversely influence the springback behavior of the sheet metal parts [2]. The different springback states of the single sheet metal parts in turn can influence the sheet metal assembly's dimensional accuracy [3]. Hence, accounting for these variations in the virtual process chain simulation can help in identifying the sheet metal parts and the process-related variation parameters with the highest influence on the dimensional accuracy of the sheet metal assembly. As a result, the tolerances for non-critical sheet metal parts and parameters can be extended in the virtual design stage and the generated process understanding can be used to derive robust manufacturing processes. However, integrating variations in the virtual process chain simulation comes with high simulation effort regarding the amount of simulations to be performed.

One approach to reduce the simulation effort is to represent the virtual process chain using the method of metamodeling, like presented in this contribution. Based on the type of metamodel and the number of variation parameters, a minimum number of virtual process chain simulations has to be performed in order to be able to make predictions for any combination of the variation parameters with the metamodel. For example, linear polynomial metamodels require a lower number of virtual process chain simulations to be performed to build the metamodel. However, they do not consider potential non-linear effects of the manufacturing processes. Quadratic polynomial metamodels, on the other hand, take into account non-linear effects, but require a higher number of virtual process chain simulations to be performed to build the metamodels.

High predictive quality of the metamodels is required in order to perform a metamodel-based Monte-Carlo (MC) simulation and thus a tolerance analysis of the process chain that considers the influences of the manufacturing processes and its variation parameters. The application of this method can then lead to more robust manufacturing processes and extended tolerances for sheet metal parts and therefore to time and cost savings in the ramp-up phase of a car-body.

In this contribution, polynomial linear and quadratic types of metamodels were investigated for representing variations in the virtual process chain of sheet metal forming and joining of a two-part principle sheet metal assembly. For this purpose, 12 variation parameters were sampled and the metamodels were trained with the computed springback results of the sheet metal parts and the sheet metal assembly by the FEM.

2 Simulation method

The virtual process chain simulation consisting of sheet metal forming and manufacturing joining simulation was performed with the FE code LS-Dyna. The sampling of the variation parameters and the construction of the metamodels was done with LS-Opt. The simulation process including the two-part principle sheet metal assembly is shown in figure 1. The sheet metal forming simulations of the two sheet metal parts (Al6014, Al5182) included gravity calculation of the blanks, closing of the tools, sheet metal forming, part trimming and springback of the final sheet metal part with a 3-2-1 locating scheme. The sheet metal assembly simulations were started with positioning of the two sheet metal parts along two locating pins in the sheet metal assembly fixture. In the next step, the sheet metal parts were fixed in their nominal position with clamps located on the frame and on the flange of the outer sheet metal part. Four clinching points between the flanges connected the sheet metal parts to produce the sheet metal assembly. Finally, a springback simulation of the sheet metal assembly was

performed with a 3-2-1 locating scheme. The entire process chain was simulated with *MAT133/*MAT_BARLAT_YLD2000 and Coulomb's law of friction.

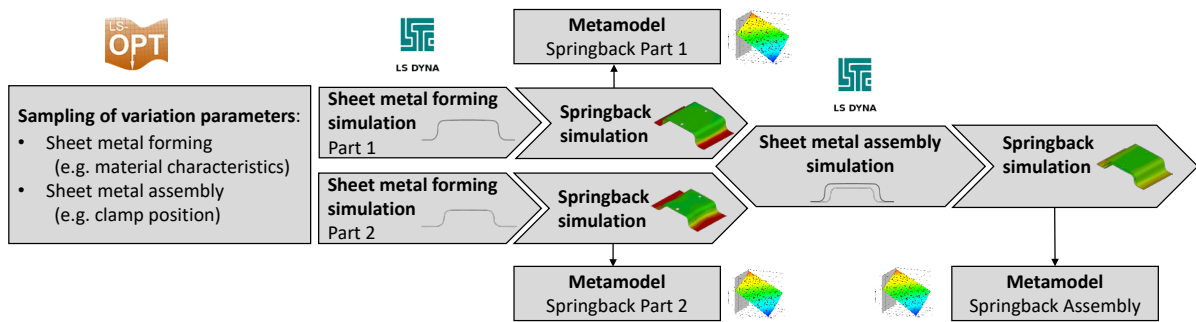


Fig.1: Visualization of the simulation process and the two-part sheet metal assembly

2.1 Variation parameter

The process parameters blankholder force and friction coefficient of the sheet metal forming processes and the material characteristics Young's modulus, yield strength, tensile strength and thickness of the blanks were used as variation parameters (n). The D-optimal experimental design was used for sampling the parameters.

2.2 Linear and quadratic metamodeling approach

The minimum required number of simulations for the D-optimal experimental design was $\text{int}(1.5(n+1))$ for the linear approach and $\text{int}(0.75(n+1)(n+2)+1)$ for the quadratic approach [4]. Using the 12 variation parameters mentioned above, 20 virtual process chain simulations for the linear approach and 138 virtual process chain simulations for the quadratic approach were performed to compute the springback and use the results to train the metamodels.

3 Metamodel accuracy

Table 1 summarizes the metamodel accuracy in terms of the multiple coefficient of determination (R^2) and the normalized (mean) root mean squared error (nRMSE) of the investigated metamodels for springback prediction. The results are shown for the example of the same node on the flange of part 1 after sheet metal forming and after sheet metal assembly in dependence of the number of virtual process chain simulations performed.

Metamodel	Sheet metal forming flange of part 1		Sheet metal assembly flange of part 1	
	20 Simulations	138 Simulations	20 Simulations	138 Simulations
Linear polynomial	0.986 / 1.94 %	0.974 / 2.44 %	0.831 / 11.2 %	0.563 / 15.9 %
Quadratic polynomial	- / -	0.996 / 0.95 %	- / -	0.921 / 6.76 %

Table 1: Metamodel accuracy for springback prediction (R^2 /RMSE)

4 Conclusion

The quadratic approach showed the best results in metamodel accuracy for springback prediction after sheet metal forming with nRMSE of 0.95 % and after sheet metal assembly with nRMSE of 6.76 %, indicating non-linear effects in the manufacturing processes. However, in terms of the effort-benefit-ratio with respect to the number of simulations to be performed, the linear approach also showed notable results.

5 Literature

- [1] Kästle, C: "Simulationsmethode zur Beurteilung der Maßhaltigkeit von rollgefalzten Karosseriebaugruppen im Zusammenbau", Universität Stuttgart, Dissertation, 2016
- [2] Zheng, H: "A meta-model based approach to implement variation simulation for sheet metal parts using mesh morphing method", 13th European LS-DYNA Conference, 2021
- [3] Brix, P: "Predicting springback variation and process-reliable tolerance limits of outer car-body panels by stochastic sheet metal forming simulation", IDDRG, 2021
- [4] Stander, N: "LS-OPT User's Manual, Version 7.0", 2020, p. 186

The Investigation of the Effect of Punch Velocity Increment on the Thickness Reduction of PHE Plates

İbrahim Şimşek¹, Yiğit Gürlü¹, Prof. Alper Taşdemirci²

¹Bosch Thermotechnology
²Izmir Institute of Technology

1 Introduction

Sheet metal forming is one of the most widely used production technique in heating and cooling applications especially in plate heat exchangers. PHE enables two fluids with different temperatures to transfer heat between each other, and is preferred in many areas of the industry owing to the high heat transfer efficiency. On the other hand, it can also be used as a secondary heat exchanger in combi heaters, and it provides heat transfer between the hot water in the burners and domestic water in the combi while preventing the mix of each other. In order to increase the cost efficiency in PHE production, the decrease in the production times is generally sought by increasing the punch velocity in the press machine. However, this increase in the punch velocity is well limited with the strain rate sensitivity of the sheet material used. Since the strain rate sensitivity determines new values of both failure strain and stress levels attained in the structure. In this study a 316L stainless steel PHE was investigated. Stainless steel is known of its high strain rate sensitivity[1], thus this effect needs to be taken into account both in the manufacturing process and its numerical simulation. In the sheet metal forming simulations, ***MAT133_BARLAT_YLD2000**[2] material model was selected due to allow of both strain rate dependency and anisotropic constitutive behavior definition. A static and dynamic mechanical characterization study was carried out in order to determine the material model constants and the numerical model of the sheet metal forming was prepared accordingly. The thickness of the numerically deformed plate was compared with that of experimentally manufactured. A good agreement was noted between the experimental and numerical results. Having a validated numerical model allowed us to re-run the simulation for different punch velocities and determine the limits of thickness reduction without causing any failure attained in the sheet metal. Thus it became possible to determine the optimum punch velocity domain in order to save manufacturing time.

2 Numerical Modelling

Modeling activities started with the simplification of the CAD shown in Fig.1. Material parameters obtained from static and dynamic test data are defined with ***MAT133_BARLAT_YLD2000**. Tool and blank elements were defined as shells. For the 0.3mm blank was modeled with fully integrated shell formulation **ELFORM 16**. Contacts between punch, die, and blank were defined by ***CONTACT_FORMING_SURFACE_TO_SURFACE**. [2] As for some of the boundary and initial conditions, the production facility was carefully examined and investigated using the high speed camera in order to measure some of the parameters including the punch velocity profile. It is defined by ***BOUNDARY_PRESCRIBED_MOTION_RIGID**.

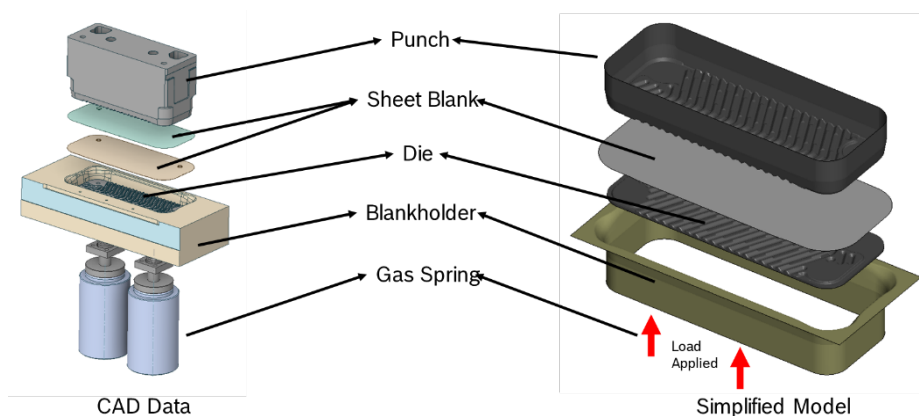


Fig.1: Plate forming elements (left) and its numerical model (right)

3 Results

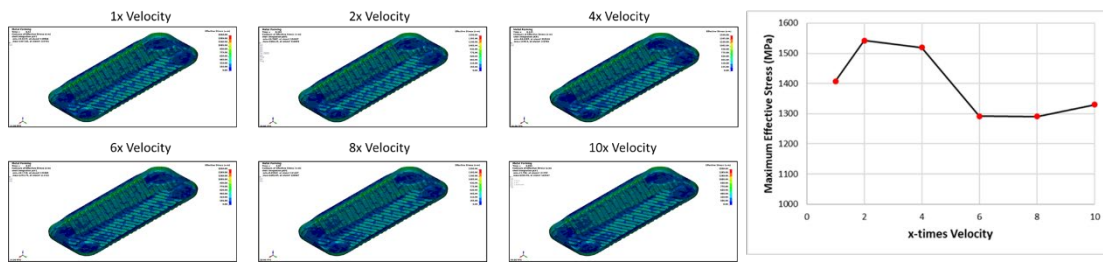


Fig.2: Effective stresses under different velocity for plate

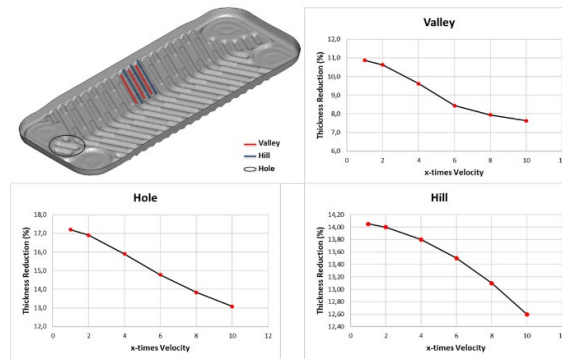


Fig.3: Thickness reduction (%) under different velocity for 3 different region in plate, (Valley, Hole, Hill)

Percent thickness reductions at different velocities were compared for 3 different regions. (Fig.3). The correlation between velocity and region was the same in all regions. As a result of this study, although the punch velocity increased, the increase in material strength affected the formability performance. Thickness reduction decreased. When the plate is examined from the cross-section, it is possible to observe quality problems in shaping as the speed increases. It is seen in the graph in Fig.4.

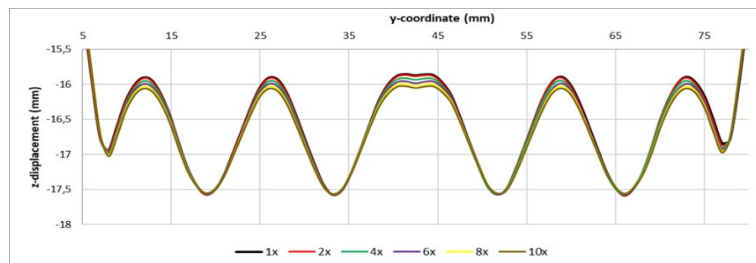


Fig.4: Cross-section comparison of the plate along the y-axis

4 Summary

As a result, the capability of the machine and the simulation results were evaluated together. As a result of this evaluation, it is thought that there will be no problems with 2x speed increase. For 4x velocity, the results are at the level of 1-1.5 percent difference with the current situation in terms of thickness reduction. Starting from these levels, a value between 2-4 x velocity increase can be selected by evaluating it on the production side. In addition to this, optimizing gas spring forces should be considered in future studies. As the strength of the material increases as high speeds are increased, the gas spring force, which is kept constant, affects the formability performance. For forming process optimization, process parameters should be evaluated as a whole, not alone.

5 Literature

- [1] Tasdemirci, Alper, et al. "Crushing and energy absorption characteristics of combined geometry shells at quasi-static and dynamic strain rates: Experimental and numerical study." *Thin-Walled Structures* 86 (2015): 83-93.
- [2] LS-DYNA Keyword User's Manual, LSTC, December 2018

A cost-effective Cold Roll-Forming FE model for industrial applications

Leonardo Marconi¹, Timothy Senart¹, Claudia Cofano¹

¹Dept. INNOVATIVE DESIGNS & ASSEMBLY SOLUTIONS, CRM Group, Liège, Belgium

1 Introduction

Cold Roll Forming (CRF) is one of the most productive processes for manufacturing thin-walled products with constant cross section. It consists of a continuous bending operation, where a long metal sheet is gradually formed through pairs of rotating rolls (called stations). The CRF process is widely used in aerospace, construction, automotive and industries with large production volumes [1]. It gained high interest in the industry to form Ultra-High Strength Steels (UHSS), due to limitations of these steel grades when formed through traditional stamping processes [2]. UHSS grades permit to pursue advanced structural optimization and to achieve lighter design solutions.

CRF is a complex process affected by multiple problems, such as wave, torsion, twist or bow defects and elastic spring back. Finite Element Analysis (FEA) is employed at the industrial level as an efficient tool to examine the process, in order to predict defects and optimize productivity.

The objective of this research is to develop a time-effective numerical methodology using the commercial Finite Element (FE) software LS-DYNA to simulate the cold roll-forming process. The forming process of a U-shaped profile is simulated and validated experimentally. In a future step, the outcome from this simulation will be used to better understand the effects of the manufacturing process on the performance of the final product.

2 FE Methodology

The FE model is expected to help designing the process, by predicting unbalanced springback and excessive longitudinal strain, a key quality indicator in designing a CRF line [3]. The resulting strain field can be used to initialize FEA accounting for the impact of manufacturing on final product performances. The simulation of the full steady-state process of the sheet uncoiling and passing through the rolls would require a great amount of computational power and time. To decrease the analysis time, a portion of the sheet is modelled. The continuity of the process is ensured by guiding the ending nodes of the blank (see fig. 1). In the model, rolls slide across the sheet without rolling, thus a small portion of the tools is modelled. Since the U-profile is symmetric, only half of it is simulated. Guiding boundary conditions are defined for each ending node of the simulated portion of the sheet. A script automates the creation of the thousands of equations needed, making the preprocessing fast, versatile and user-friendly. The guiding method is a kinematic approximation, thus it is not sufficient to ensure the continuity of the simulated sheet. The strip should be long enough so that the boundaries do not obstruct the results, which are computed in middle of the sheet. Steady-state properties typical of CRF processes, for which state variables are time-independent for a given position [4] must be ensured in the central section.

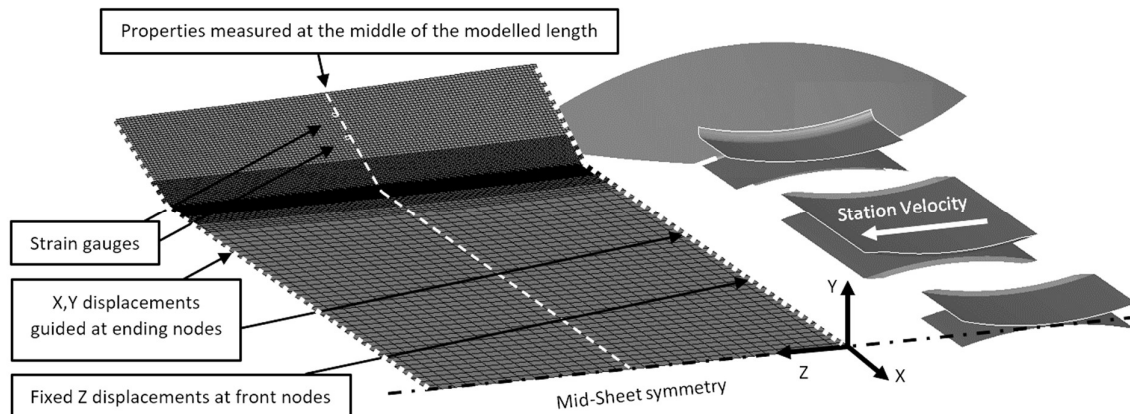


Fig. 1: Roll-forming model schematics and mesh

The FE model using the implicit method is constructed. The sheet is discretized through fully integrated shell elements which are chosen as a tradeoff between computational cost and accuracy for non-severe bending scenarios and small sheet thickness. The material law of the S350GD grade sheet is obtained through tensile tests and implemented as `*MAT_PIECEWISE_LINEAR_PLASTICITY`. Mesh size, material law and the use of shell elements are validated numerically and experimentally through 90° 3-point bending tests on specimens from the same sheet. Rolls are modelled as rigid. Outputs and assumptions of the CRF methodology are validated through an experimental cold roll-forming campaign.

3 Experimental validations

Numerical results and model assumptions are validated against two experiments on 2000x360x0.63 mm sheets of S350GD grade steel. The roll-forming line consists of 9 stations placed at a regular distance of 250 mm. The blank is formed into an U-shaped profile with 30 mm flanges. Strain gauges and 3D scan are employed to study strain and kinematics of the process. The flange longitudinal strain, and the final cross-section at the mid-length of the sheet are used for the validation. The model assumptions are verified during the test. Blank misalignment, roll eccentricity, roll axis deformation and influence of blank free edges on gauges signal are checked to be negligible. The final product cross-section shows a deviation from the forming flower geometry due to a design issue of the last two stations.

4 Summary

The aim of the project is to create a FE methodology able to give fast and reliable results about the mechanical variables throughout the cold roll-forming process. To meet the requirements of the industry, the model is designed to be efficiently set-up and computed in a short time. A script makes the procedure of pre-processing fast and versatile, based on the roll-forming flower of the line. The methodology is evaluated thoroughly and validated against strain gauges and 3D scan data from the roll-forming experimental campaign. The final cross-section is found dependent on the forming flower used to create the guiding, thus design flaws of the last two stations cause a discrepancy between FEM and experiment. The analysis results show a good correlation within a competitive lead time for industrial applications. High sensitivity is found to material yield stress and gauge placement angle. The uncertainty range of the numerical solution is individuated as a result of a sensitivity analysis (see fig. 1). The analysis runs in less than 24 hours on 18 CPU (Intel(R) Xeon(R)W-2195 2.30GHz). As future work, a semi-rigid rolls model is implemented by modelling the tools stiffness through discrete springs and beams. It aims to investigate the effects of friction and interference force between rolls and sheet.

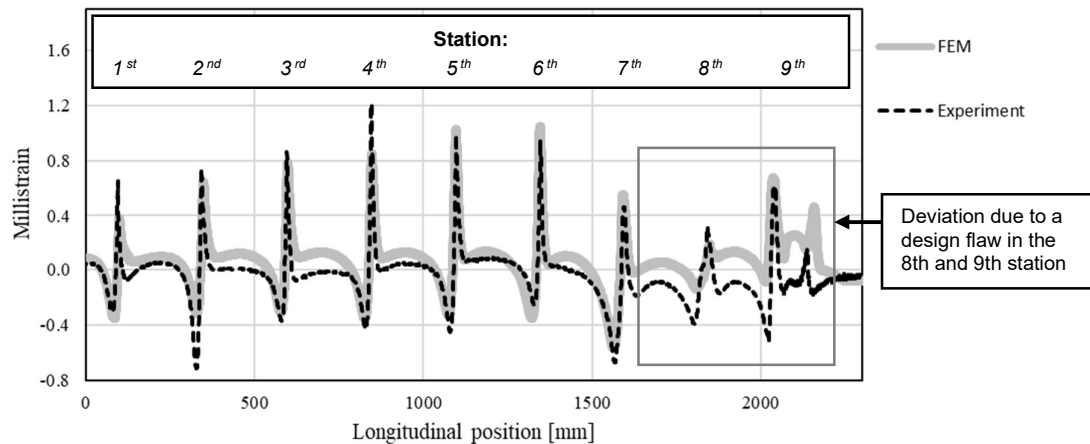


Fig.2: Experimental and numerical longitudinal strain comparison on the flange.

5 Literature

- [1] Liu, H., Liu, Z., and Zou, Z.: "FEM Simulation of Cold Roll Forming in the Car's Anti-Collision Beam" *Journal of Computational and Theoretical Nanoscience* 9.9, 2012, 1472-1476
- [2] Tsang, K. S., et al.: "Industrial validation of strain in cold roll forming of UHSS", *Procedia Manufacturing* 15, 2018, 788-795
- [3] Liu, C.F., et al.: "A new mathematical model for determining the longitudinal strain in cold roll forming process", *The International Journal of Advanced Manufacturing Technology* 79.5, 2015, 1055-1061
- [4] Mahajan, P., Abrass, A., and Groche, P.: "FE simulation of roll forming of a complex profile with the aid of steady state properties", *steel research international* 89.5, 2018, 1700350

Forging simulation using the example of a knife

W. Rimkus, S. Zorniger (Hochschule Aalen)

Ansys Forming – GUI for sheet metal forming simulation with LS-DYNA

V. Steininger (Tiwaquest)

A closed multiscale simulation framework for the simulation of woven composite structures

Mathieu Vinot¹, Martin Holzapfel¹, Nathalie Toso¹

¹ Institute of Structures and Design, German Aerospace Center, Stuttgart, Germany

1 Abstract

Keywords: woven composites, virtual testing, multiscale simulation

The rapid evolution of climate change in the last decade rises the requirements on aeronautics and automotive transportation systems in the field of sustainability. Composite materials have been widely used for their high specific properties compared to metallic materials. On the downside, they are particularly relying on oil-derived raw materials and can only be recycled to a lesser extent. Furthermore, composites require high experimental effort for the mechanical characterization compared to their metallic counterparts. To accelerate the development and manufacturing of new sustainable alternatives (oil-free or bio-derived materials), new solutions are being developed on the numerical level. In particular, multiscale simulations are benefiting from the recent advances in the computational field and the improvement of hardware. In the present work, a closed multiscale simulation framework is developed on the microscale, mesoscale and macroscale. The prerequisites for the multiscale chain are discussed and some key steps towards the model generation are detailed. After generating and computing the finite-element models, the material properties are transmitted between the different scales upstream without any user intervention up to the macroscopic scale. In this paper, we illustrate the potential of the developed methodology at the example of a glass-fibre reinforced woven structure under a generic loading. In particular, key remaining issues in the field of the multiscale simulation are raised.

2 Modelling approach

A key aspect of multiscale simulation is the realistic geometrical representation of the composite constituents, particularly at lower scales where their material behaviour is simpler than at higher scales. The model generation bases on the works documented in [1] and [2] for the microscopic and mesoscopic scales. On the microscale, random clusters of fibres can be generated for a given fibre volume content up to 70 % and a user-defined fibre waviness, often resulting from the manufacturing process. On the mesoscale, the woven textile is modelled by randomly shifting the layers of woven material and compacting them to reach the final fibre volume content. The realistic three-dimensional models of the composite material are generated (Fig. 1) and simulated with period boundary conditions via the command `*CONSTRAINED_MULTIPLE_GLOBAL`.

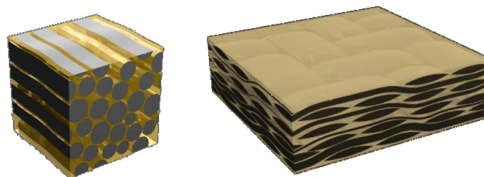


Fig.1: Generated microscopic (left) and mesoscopic (right) models

As one of the main constituents of composites, the resin material and its plastic behaviour play a large role in fracture patterns. An accurate prediction of composite failure can therefore only be reached with an adequate material model. The present work focuses on the `*MAT_187_SAMP-1` coupled to an `*MAT_ADD_DAMAGE_DIEM` card to depict accurately the load-dependent material plasticization and the triaxiality-dependent plastic strain at failure. Material tests have been performed under tension, compression and shear to obtain the required stress-strain relationship.

The single fibres are modelled with a simple orthotropic material model `*MAT_054_ENHANCED_COMPOSITE_DAMAGE` in which failure is driven with a maximal strength criterion under tension loading only. At the mesoscale, the material model for the infiltrated yarns must consider their various failure patterns. To this aim, a `*MAT_262_LAMINATED_FRACTURE_DAIMLER_CAMANHO` is automatically generated by postprocessing the results from the microscale. By extracting material data

from the mesoscale, a material card for the `*MAT_054_ENHANCED_COMPOSITE_DAMAGE` is characterised.

3 Results

The simulated stress vs. strain relationships for different load cases are illustrated in Fig. 2 for several unit cells at the microscopic and mesoscopic scales respectively. The simulation approach allows for the characterisation of the scatter in the material properties and of the post-failure material behaviour. The later is particularly necessary for the determination of the SLIM values in some composite material cards within LS-DYNA. Fig. 3 presents the structural damage in the composite part on the macroscopic scale under a generic tool drop load case.

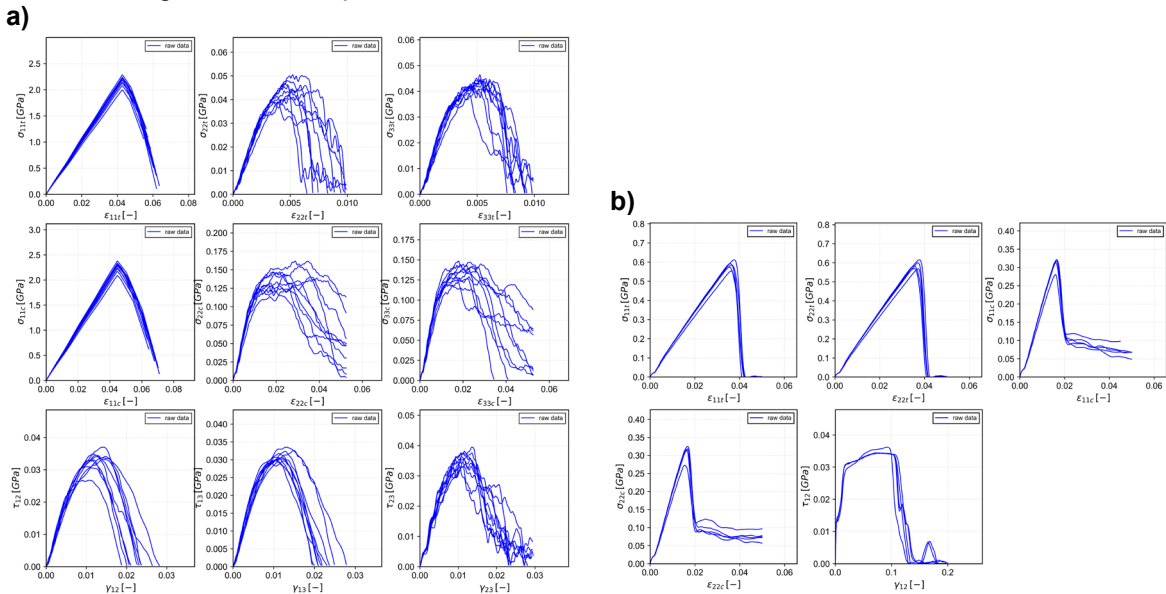


Fig.2: Stress vs. strain curves for the microscopic (left) and the mesoscopic (right) models under in-plane and out-of-plane loadings

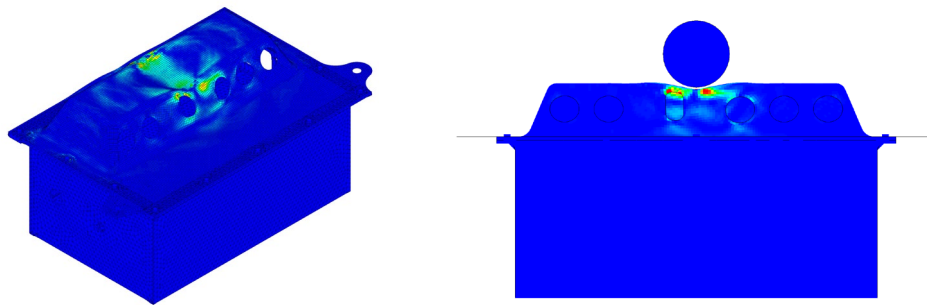


Fig.3: Structural damage in the woven composite part under generic tool drop scenario

4 Summary and outlook

The present paper illustrated the potential of multiscale simulation in the sizing of structures. With the experimental characterisation of the resin material only and considering typical values for the fibre's properties, it was possible to determine the necessary material properties of the woven composite for a structural simulation. The currently available material models in LS-DYNA are sufficient for an accurate representation of the composite behaviour at every scale. The present approach will be extended for the calculation of fracture toughness's at every scale, which generally require extensive experimental work and is of importance for crash applications and energy absorbing structures.

5 Literature

[1] M. Vinot, M. Holzapfel and N. Toso, (2019) Towards virtual material characterization of unidirectional composites with microscopic simulations. 1st European Conference on Crashworthiness of Composite Structures - ECCCS-1, 19.-21. Nov. 2019, Belfast, Ireland.

[2] J. Dittmann, M. Vinot, P. Middendorf, Peter, N. Toso, and H. Voggenreiter, (2021) Simulation supported manufacturing of profiled composite parts using the braiding technique. In: Stuttgart Conference on Automotive Production (SCAP2020) Advances in Automotive Production Technology – Theory and Application. Springer Berlin Heidelberg. doi: [10.1007/978-3-662-62962-8](https://doi.org/10.1007/978-3-662-62962-8). ISBN 978-3-662-62961-1.

6 Acknowledgements

This research and development project was performed within the research campus ARENA2036 in the project “Digitaler Fingerabdruck” and is funded by the Federal Ministry of Education and Research (BMBF), Germany under the supervision of Project Management Agency (PTKA) in Karlsruhe. The author is responsible for the contents of this presentation.



FORSCHUNGS
CAMPUS

öffentlich-private Partnerschaft
für Innovationen

Load Bearing Capacity Prediction of Non-Crimp Fabric Composites Using MAT54 and MAT58 Constitutive Models

Milad Kazemian¹, [Aleksandr Cherniaev](#)¹

¹ Department of Mechanical, Automotive and Materials Engineering, University of Windsor, 401 Sunset Ave., Windsor, Ontario, Canada N9B 3P4

1 Introduction

Non-crimp fabrics (NCFs) are increasingly used in the industry to manufacture composite structures due to a combination of high mechanical properties and excellent manufacturability. As with other composites, in-service damage can be a cause for a severe reduction in the load-carrying capacity of NCF-reinforced plastics. In this experimental and numerical study, two constitutive material models previously used only for damage prediction in unidirectional (UD) tape and woven fabric-reinforced materials (LS-DYNA's *MAT_ENHANCED_COMPOSITE_DAMAGE – MAT54 and *MAT_LAMINATED_COMPOSITE_FABRIC – MAT58) were evaluated for simulating transverse crushing of composite parts processed from non-crimp carbon fabric. For this purpose, UD NCF components of tubular shape were subjected to transverse crushing through a controlled indentation of a metallic cylinder. The experiment results were compared with numerical modeling. Verification metrics included the observed and the predicted patterns of interlaminar damage, the extent of delamination, as well as the ability of the models to replicate the force-displacement response exhibited by the tested specimens.

2 Numerical model

A numerical model that replicates the tubular component crushing test was developed in LS-DYNA. Its major features are depicted in Fig. 1. In the model, the composite layup was represented using stacked TSHIELD elements, each representing one “physical” ply of the NCF material. A uniform element size of 0.7 mm was used. The support and the loading cylinder were represented as rigid bodies.

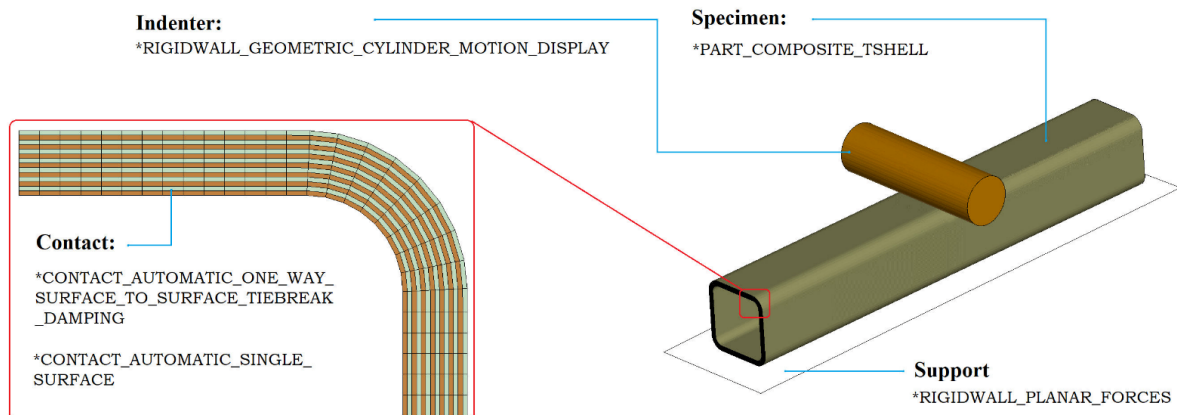
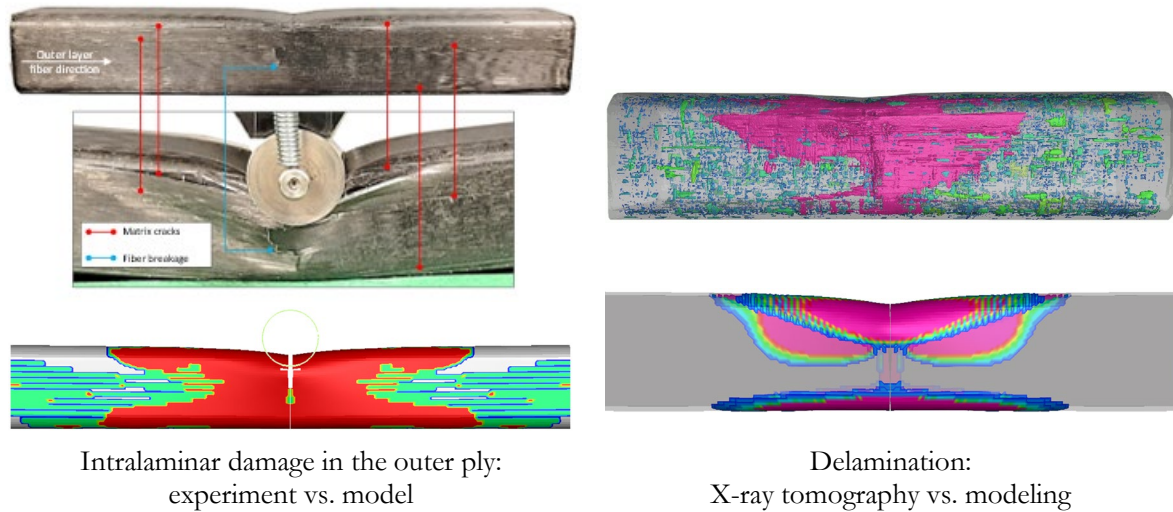


Fig. 1: Developed LS-DYNA numerical model

MAT 54 and MAT 58 were used to represent interlaminar behavior. To represent delamination (intralaminar behavior), the contact interfaces between the 14 TSHIELD layers were added using *CONTACT_AUTOMATIC_ONE_WAY_SURFACE_TO_SURFACE_TIEBREAK with OPTION 9.

3 Results

Metrics to evaluate the numerical predictions specific to the crushing phase included comparison of the damage in the outer layer of the specimen (visual vs. predicted), extent of delamination (CT-scan vs. models), and the force-displacement diagrams (recorded in experiments vs. produced by LS-DYNA). Some results are illustrated in Fig. 2.



Intralaminar damage in the outer ply:
experiment vs. model

Delamination:
X-ray tomography vs. modeling

Fig.2: Damage induced by indentation to the NCF part: experiment vs. modeling

The force-displacement diagram corresponding to the crushing phase of the specimen with $[0_4, 90_3]_S$ layup is shown in Fig. 3, comparing the experimental results and the modeling predictions. As can be deduced from the figure, both MAT54 and MAT58 models equally adequate predict the force-displacement response of the specimen during this phase.

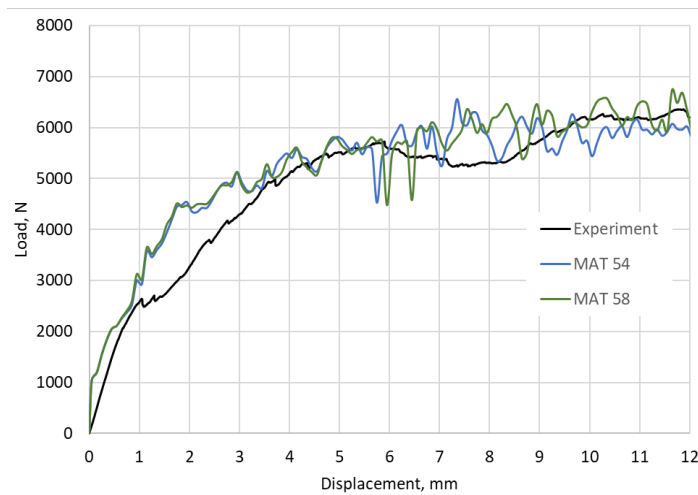


Fig.3: Force-displacement diagrams: experiment vs. numerical modeling

4 Summary

This numerical and experimental study was conducted to investigate the applicability of two constitutive material models previously used only for UD tape and woven fabric-reinforced materials to modeling of damage in composite parts processed from non-crimp carbon fabric. Despite differences in their formulations (strength criteria-based MAT54 vs. CDM-based MAT58), both material models were found to be robust and reasonably well predict damage induced by transverse crushing in UD NCF parts. This included the representation of qualitative patterns of interlaminar damage, the extent of intralaminar damage (delamination), as well as the prediction of force-displacement response exhibited by the tested tubular components. Future work must be focused on investigating the applicability of MAT54 and MAT58 for the prediction of the residual load-bearing capacity of damaged NCF parts under transverse loading, as well as consideration of other loading scenarios, such as axial crushing.

Comparative Study of Impact Energy Absorption Performance of Cylindrical Honeycomb Structure Based on “Origami Engineering”

Sunao Tokura¹

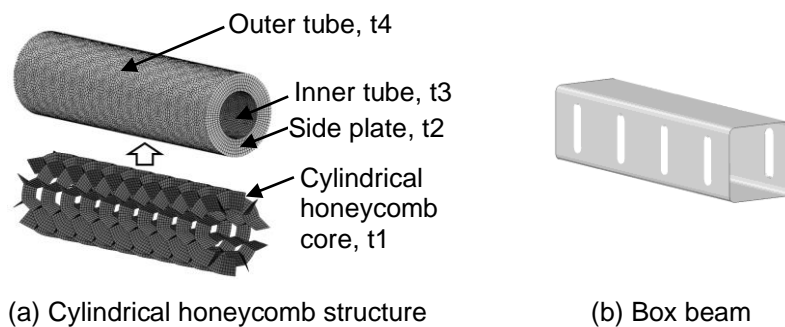
¹Tokura Simulation Research Corporation

1 Introduction

With the progress of shift to electric vehicle, improvement of "electricity cost" has become a highly important issue. In order to improve electricity costs of EV, it is necessary to reduce the weight of the vehicle body, but in BEV, the weight of the battery itself occupies a large proportion, so it is necessary to further reduce the weight of the other vehicle body components. On the other hand, the role of the box beam for absorbing impact energy is very important for the crashworthiness of automobiles, but the ratio of the box beam to the weight of the vehicle body is relatively large. Therefore, research and development of impact energy absorbing members using composite materials are underway. However, when the composite material is destroyed, a large number of debris such as microplastic is scattered and causes a great environmental load. Therefore, the impact energy absorbing member needs to be manufactured of metal materials that can be easily recycled. For this reason, the application of a crash beam with a lightweight cylindrical honeycomb structure proposed by “Origami Engineering” is being considered. In this paper, we discuss the applicability of a lightweight cylindrical honeycomb structure material that has the equivalent or higher performance as the impact energy absorption performance of a conventional box beam through the crash simulation using Ansys LS-DYNA[1].

2 Cylindrical Honeycomb structure

Ishida[2] has proposed the cylindrical honeycomb structure as a lightweight and high strength material together with a practical manufacturing method. In this paper, the FEM model shown in Fig. 1(a) was created based on her research. When actually incorporating it into the vehicle body, it is necessary to fix it by welding or bolting, so the outer plate, inner plate, and side plate are attached so as to cover the honeycomb core, and it consists of four parts together with the core. The core size (length of one side) is 30 mm, and a flat honeycomb with a height of 30 mm with top and bottom plates is rolled into a cylinder with an outer diameter of 140 mm. The length of the cylinder is 507.86 mm, which is the size of 10 cores arranged vertically. The thickness of each part (t1-t4 in Fig.1(a)) is 1 mm as a baseline model. For comparison, a box beam model is also prepared as shown in Fig.1(b). The box beam has a shape close to the actual members used in many automotive bodies today, with a length of 500 mm



and a cross-sectional dimension of 125 mm × 125 mm, which is almost the same as the cross-sectional area of a cylindrical honeycomb. Beads with a width of 20 mm, length of 85 mm, and depth of 10 mm are provided at four locations on the left and right sides. The corner has a fillet of R10 mm and the plate thickness is 2.5 mm.

Fig. 1: FEM model geometries

3 Material properties

The material of the structure is steel, which is modeled as an isotropic elastic-plastic material *MAT_024 in LS-DYNA. Young's modulus is 205 GPa, Poisson's ratio is 0.3, yield stress is 300 MPa, and mass density is 7.87×10^{-9} ton/mm³. The masses of cylindrical honeycomb and box beam are 4.76 kg and 4.90 kg, respectively. An actual steel material fails at a plastic strain of about 0.3. But if this is

applied to the elements of 4-5 mm length, the fracture judgment becomes too strict. So, we defined the failure strain as 0.9 considering the ratio of the element size and the local failure region size.

4 Analysis conditions and optimization

A rigid wall with a mass of $m = 400$ kg impacted at a velocity of $v = 50$ km/h. So, the initial kinetic energy is 38580 J. *CONTACT_AUTOMATIC_SURFACE_TO_SURFACE is defined between the member and the rigid wall. *CONTACT_AUTOMATIC_SINGLE_SURFACE is defined on the member. In addition, optimization of the cylindrical honeycomb structure was attempted. The objectives are to minimize the mass and the initial peak force of impact force. The design variables t1-t4 were optimized in the range of 0.1 mm to 1.0 mm.

5 Results and discussion

Figure 2 shows the final deformed shape of each model. The box beam shows large period buckling at the bead intervals. The cylindrical honeycomb shows finer period buckling mode. This means that the cylindrical honeycomb can absorb the energy constantly in wider region. Figure 3 shows the impact force history. And the summary of the results are also shown in Table 1. In particular, reduction of the initial peak force in the impact force history is important to reduce the occupant injury criteria. The optimized cylindrical honeycomb model is 46.5% lighter in mass, 85% more absorbed energy per unit volume, and 63.7% lower in initial peak force than the conventional box beam.

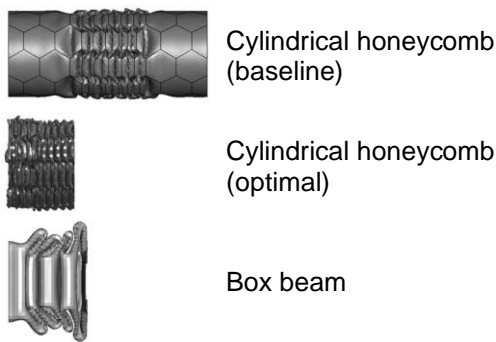


Fig.2: Deformed shapes

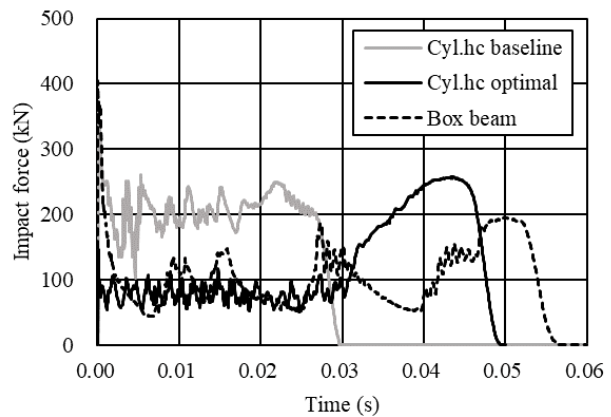


Fig.3: Impact force history

Table 1: Result summary

Model	Mass (kg)	Absorbed energy (J)	Absorbed energy/mass (J/kg)	Initial peak force (kN)
Cylindrical honeycomb (baseline)	4.759	38292.6	8046.3	357.547
Cylindrical honeycomb (optimal)	2.622	37667.7	14365.4	146.491
Box beam	4.899	38037.8	7764.6	403.953

6 Conclusions

It was shown that the cylindrical honeycomb structure devised by origami engineering has light weight, excellent energy absorption performance and impact safety performance compared to conventional impact energy absorbing members. A wide range of applications as an impact energy absorbing component is expected in the future.

7 References

- [1] Ansys 2021 R2 LS-DYNA User's Guide, Ansys Inc., 2021
- [2] Sachiko Ishida, Design of cylindrical honeycomb cores – Geometric consideration –, Mec. Eng. J., Vol.5, No.4, 2018

Thermo-mechanical homogenization of laser-generated composite materials

Shadi Alameddin, Renan Pereira Alessio, Felix Fritzen

Data Analytics in Engineering, Institute of Applied Mechanics, University of Stuttgart

This work presents a multiscale simulation framework that will be used for the simulation and experimental validation of eigenstresses in composite materials generated via laser melt injection. The composite material is obtained by adding tungsten carbide particles into the melt pool of a metallic substrate to generate surface coatings. These coatings are used to boost wear-resistance, more precisely to protect metallic surfaces against abrasion and erosion. The coating significantly extends the part's lifetime due to the outstanding material characteristics of the locally produced metal matrix composite (MMC). Eigenstresses, which are the residual stresses left in the MMC material after the coating process, shall be investigated and predicted within the framework of this project and their effect on the lifetime shall be estimated.

Computational homogenization is employed to predict the thermo-mechanical response of heterogeneous structures. In such schemes, the constitutive response of every material point in the macro scale is obtained by solving a microscopic boundary value problem on a representative volume element (RVE) with boundary conditions from the corresponding macroscopic point. Direct numerical simulations (DNS) of RVE response, e.g., in FE² context, are computationally demanding. In contrast, reduced order models (ROM) and data-driven surrogate models provide an appealing and efficient alternative to DNS. Hence, our goal is to use reduced order models and machine learning to tackle the challenging multi-scale thermo-mechanical problem during the laser melt injection process.

Therefore, an interface to LS-DYNA was developed to allow for the direct integration of surrogate models written in Python and C++ [1]. Then various data-driven models to predict the effective behavior on the microscale were investigated [2]. Experimental thermocycles and neutron diffraction measurements of residual stresses are used to validate simple direct numerical simulations. After that and to make two-scale simulations feasible, the established isothermal nonuniform transformation field analysis (NTFA) from [3,4] is extended toward anisothermal settings with strongly temperature-dependent material parameters.

The proposed method is based on computational homogenization paired with ROM. It allows for full temperature dependence of the material parameters in all phases. In addition, the method is considered nonintrusive, i.e. it does not require any modification or update to the DNS software. DNSs are queried at few temperatures to provide the building blocks to construct an energy minimization problem that outputs an optimal basis for any other intermediate temperature. This reduced problem is solvable in real-time. Different from other homogenization approaches, not only effective quantities are predicted but also full field solutions. The accuracy and efficiency of the algorithm are demonstrated on various RVEs over a wide temperature range, from 300K to 1300K. An open-source implementation and further details will be available via [5].

Acknowledgment

The IGF-Project with the IGF-No.: 21079 N / DVS-No.: 06.3341 of the “Forschungsvereinigung Schweißen und verwandte Verfahren e. V.” of the German Welding Society (DVS), Aachener Str. 172, 40223 Düsseldorf was funded by the Federal Ministry for Economic Affairs and Climate Action (BMWK) via the German Federation of Industrial Research Associations (AiF) in accordance with the policy to support the Industrial Collective Research (IGF) on the basis of a decision by the German Bundestag. Furthermore, the authors gratefully acknowledge the collaboration with the members of the project affiliated committee regarding the support of knowledge, material and equipment over the course of the research.

Contributions by Felix Fritzen are partially funded by Deutsche Forschungsgemeinschaft (DFG, German Research Foundation) under Germany's Excellence Strategy - EXC 2075 – 390740016. Felix Fritzen is funded by Deutsche Forschungsgemeinschaft (DFG, German Research Foundation) within the Heisenberg program DFG-FR2702/8 - 406068690.

The authors acknowledge the support by the Stuttgart Center for Simulation Science (SimTech).

Literature

- [1] S. Alameddin, F. Fritzen: Thermo-mechanical homogenization of composite materials. 13th European LS-DYNA Conference, 2021.
- [2] J. Herb: Machine Learned Prediction of the Response of Uncertain Micro-structures. B. Sc. thesis, University of Stuttgart, 2021.
- [3] F. Fritzen, T. Böhlke: Nonuniform transformation field analysis of materials with morphological anisotropy. Composites Science and Technology 71:4, p. 433-442, 2011.
- [4] F. Fritzen: Microstructural modeling and computational homogenization of the physically linear and nonlinear constitutive behavior of micro-heterogeneous materials. KIT Scientific Publishing, 2011.
- [5] <https://github.com/DataAnalyticsEngineering/AdaptiveThermoMechROM>

Automatic detection of similarities and exceptions in deformations and mesh functions over many crash simulation results

Prof. J. Garcke¹, R. Iza-Teran¹, M. Pathare¹, D. Steffes-lai¹

¹Fraunhofer SCAI, Schloss Birlinghoven 1, 53757 Sankt Augustin

1 Abstract

The growing complexity of FEM models together with increasing requirements and regulations for crash safety lead to large development trees in the CAE crashworthiness development process. That is, during the virtual product development, numerous design changes are applied and analysed until the final model satisfies given design criteria. The leading challenge is how to compare several simulation results automatically to detect global events, for example unexpected deformation behavior or distribution of mesh functions. We observe a lack of simple to use procedures to automatically categorize design measures together with their impact on simulation results.

To address these challenges, we have developed a tool SimExplore to easily analyse the impact of design variations as an important step in the overall simulation data analysis workflow. SimExplore enables an overview over many simulations pointing out their similarities and exceptions in deformations and mesh functions automatically. It provides the CAE engineer with an browsable overview of all the simulations analysed in terms of clusters and outliers due to deformations and mesh functions. The simulations within a cluster show similar deformation behavior, that is, the cluster representatives reflect the different deformation modi. Moreover, outliers are detected, which show different, and most often unwanted, behavior. All these deformation modi and outliers are identified, documented and visualized within SimExplore using a structured data representation allowing a smooth integration in any simulation process data management tool for documentation and further analysis. A combination with the results of ModelCompare is also possible, where ModelCompare identifies differences between two models by comparing two similarly discretized finite element models.

The capabilities of SimExplore are demonstrated on an academic submodel car crash, where the wall thicknesses of several selected components have been varied. SimExplore detects several deformation modes as well as identifies several outliers showing unexpected folding behavior of the identified parts.

2 Detailed Workflow

The first step of the framework deals with a comparison of two input configurations for a numerical simulation by ModelCompare. Thus, it consists of the identification of the design measures realized through model adaptation. The identification of design measures is based on parts and their discretization (mesh), and thus independent of the parts meta data, such as their identifier or name. Examples of design measures (groups) are changes in geometry, multiparts, that is several parts are merged into one part, changes in spotwelds and rigid body elements, material ID and thickness changes. All the identified design measures are stored in a structured format, namely in JSON files.

The second step of the overall approach deals with the comparison of two simulation results based on the design measures applied by SimCompare, using the full output data, namely displacement and functions on meshes. The approach analyses functions on meshes rather than scalar data or sensor / curve data. More precisely, the impact of design changes can be analysed in terms of data functions either on the nodes (such as displacements or nodal mass) or elements (such as plastic strains, stresses, or failed elements) depending on the analysis objective. Thereby, detailed insight in local influences can be evaluated with respect to a certain design change. The comparison results, that is the local events found, are stored partwise in structured JSON files supporting further post processing. In particular, for each part selected, the part-ID, part-name, metricvalue, as well as minimum and maximum deviation in the part is stored.

The determination of the most affected parts over all the two-sided comparisons using SimCompare are collected. Depending on a threshold specified by the user, affected parts between all simulations are determined.

For the third step a series of geometry-driven features (so-called geometric Fourier spectra) representing the displacements or mesh functions from the selected parts as selected by SimCompare for all time steps are computed. From the obtained geometric features per part for all parts and time steps, an optimization algorithm will select three coefficients for all simulations that shows the best overall separation into clusters. In addition at each time step a clustering score is computed that also selects the time steps which, from the point of view of clustering, shows increased separation. Clustering and outlier identification finalizes this part of the workflow.

Using the information computed in the previous steps, an interactive part allows the user to seamlessly analyze different parts or part combinations. The visual representation of the simulations and parts is based on a 3D representation of the geometric features. Each point in this representation provides an intuitive overview of the similarities and exceptions in the simulations with respect to the chosen functions, allowing an easy-to-use exploration of the results of the simulations. Clustering and outlier detection are visualized in such a representation.

3 Figures

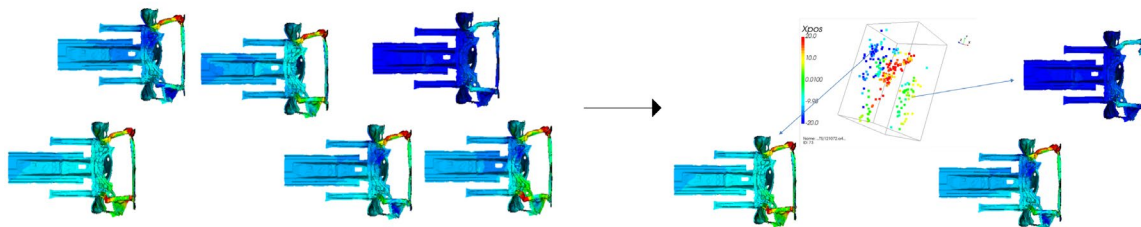


Fig.1: Various simulations are arranged based on our geometry-driven features. Simulations forming clusters and outliers can be easily explored.

4 Summary

The framework is aimed for an automatic event detection in crashworthiness analysis results that provides a comparison of FE simulation results based on arbitrary node or element data functions. The parts with the largest differences are automatically highlighted. We consider the presented framework as an important step towards automatic design and event detection in an overall simulation data analysis workflow. In particular, it allows to systematically analyse a design development tree to detect interesting deviations in the crash behaviour caused by design changes. The employed structured data representation highly simplifies the documentation for example in simulation data management tools, as well as the further analysis of the observations found by for example artificial intelligence approaches. Additionally, it builds the basis for automatic pdf report generation, which allows the creation of human readable documentation of the changes and results.

5 Literature

- [GPP17] J. Garcke, M. Pathare, and N. Prabakaran. ModelCompare. In Scientific Computing and Algorithms in Industrial Simulations: Projects and Products of Fraunhofer SCAI, pages 199–205. Springer International Publishing, Cham, 2017
- [ITG19] R. Iza-Teran and J. Garcke. A geometrical method for low-dimensional representations of simulations. SIAM/ASA Journal on Uncertainty Quantification, 7(2):472–496, 2019.

Development of a 2020 SUV vehicle FE model

Rudolf Reichert, Umashankar Mahadevaiah, Cing-Dao (Steve) Kan, Lukas Fuchs

Center for Collision Safety and Analysis, George Mason University, USA

1 Objective

Finite element (FE) vehicle models allow researchers to conduct diverse simulation studies. Members of the Center for Collision Safety and Analysis (CCSA) at the George Mason University (GMU), that also built the core team of the formerly known National Crash Analysis Center (NCAC), have been developing a fleet of publicly available FE vehicle models [1] over the past 25 years. This paper describes the latest model, representing a 2020 Nissan Rogue SUV vehicle, shown in Figure 1. Note that the vehicle has been named as the Nissan X-Trail in all countries it is sold, except for the United States and Canada, where it called Nissan Rogue.

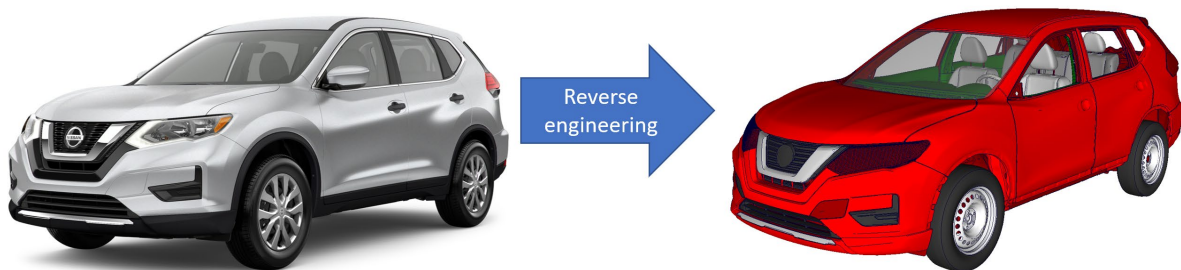


Fig.1: 2020 Nissan Rogue (a) physical vehicle and (b) developed FE model

2 Methods

State-of-the-art modeling techniques were used to develop a detailed SUV vehicle model. A reverse engineering process, which included geometry generation, vehicle tear down, meshing, connection modelling, and material characterization, was used. Data from available and conducted full-scale crash tests allowed to validate the FE model for multiple impact configurations. Side impact load cases included the Moving Deformable Barrier (MDB), pole, and static door crush configurations. The NCAP rigid barrier and NHTSA's frontal oblique impact scenarios were used for validating performance in frontal impact conditions. Furthermore, pedestrian safety characteristics were validated using the adult head form, child head form, upper leg, and lower leg impactors according to respective EuroNCAP test data [2].

3 Results

The developed detailed FE model of a crossover SUV consists of about 1300 parts and 3 million elements representing geometry, connections, and material characteristics of relevant structural and interior components. A uniform mesh with an average element size of 8 mm and a timestep of 0.9 microsecond was used. The developed FE model showed good correlation when compared to respective frontal and side impact test results, based on Correlation and Analysis (CORA) [3] and ISO 18571 [4]. Maximum absolute velocity, measured at the middle of the B-Pillar was 6.8m/s and 7.1m/s in simulation and test (NHTSA #8546), respectively. Maximum exterior crush in the oblique pole side impact configuration was 398mm and 390mm in simulation and test (NHTSA #9780), respectively. The 2020 Nissan Rogue FE model showed good correlation with available test results at most impact locations when evaluating pedestrian safety, as illustrated in Figure 2.

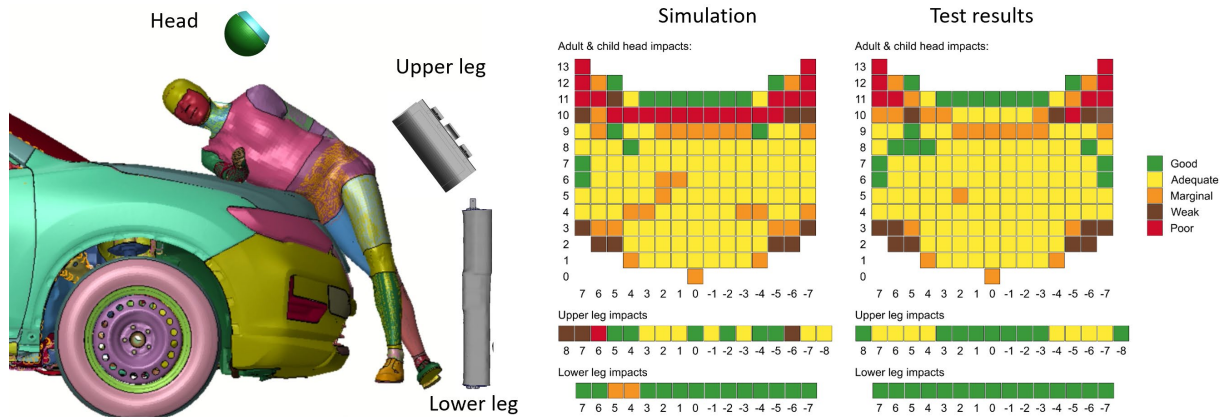


Fig.2: Simulation versus test correlation for pedestrian safety impact configurations.

4 Discussion and Limitations

The FE model represents relevant exterior and interior parts, including body in white, wheels, axles, suspension, seats, door trims, pedals, steering wheel, and instrument panel. Correlation of structural deformation and kinematics for frontal and side impact configurations is considered good. Adding non-structural components allowed to achieve overall good correlation with respect to pedestrian safety. Detailed head lights and windshield wipers are not modeled in the latest FE model version, which explains the potential for improvement for respective pedestrian safety configurations in these areas.

5 Conclusion

A detailed FE model representing a 2020 Nissan Rogue SUV vehicle has been developed using a reverse engineering process. It showed good correlation with existing crash test data for frontal, side, and pedestrian safety impact configurations.

6 Acknowledgement

This research was mainly funded by the National Highway Safety Administration. We thank our colleagues, Daniel Brown, Kevin Arellano-Moya, Doug Wang, Dhafer Marzougui, and Christopher Story for their significant contributions. Pedestrian impactor FE models were obtained from Ansys LST and “ATD Models GmbH”. The pedestrian GHBM FE model was obtained from Elemance.

7 Literature

- [1] <https://www.ccsa.gmu.edu/models>
- [2] Euro NCAP. Official Nissan X Trail 2014 safety rating results. Euro NCAP. 2014 <https://www.euroncap.com/en/results/nissan/x-trail/7883>
- [3] Thunert, C: “CORApplus User’s Manual, Version 4.0.4.” Partnership for Dummy Technology and Biomechanics, 2017
- [4] Barbat, S. et. al.: “Objective rating metric for dynamic systems (Paper Number 13-0448)”, 23rd Enhanced Safety of Vehicles Conference, Seoul, Republic of Korea, 2013

Electric Power Assisted Steering System In Vehicle Level CAE Simulation

Gavin Song, Jason S. Wou, Chris Rolls, Michael Vlademar

Ford Motor Company

Abstract

The steering system is to provide the driver with the possibility of lateral vehicle guidance, i.e. to influence the lateral dynamics of the vehicle; moreover, it is crucial to promptly translate the steering input to have the vehicle in high-quality directional stability. An electrical power assisted steering (EPAS) system is the sophisticated variant to meet higher requirements for vehicle safety, ride comfort, and driver-assist. This research is to investigate if a CAE methodology could be innovated to better simulate the durability of a steering system under various working scenarios; figure out the critical features of the modeling; conduct a correct analysis procedure for validating the modeling and collecting data for evaluation. With step by step in modeling and analysis, a well-established example of CAE model of EPAS is enabled to highlight the novelty of steering vehicle level CAE methodology and therefore achieve the research goal.

Vehicle Level Steering System Compliance Modeling

The loads on a vehicle level steering system are composed of four major inputs - body structure support, chassis structure support, road response input through a tire, driver torque input on the steering wheel. The critical mechanisms on the steering system are translational and universal joints of the intermediate shaft, a torsion bar between the intermediate and lower shaft, rack and pinion at the bottom end of the lower shaft, ball screw for a connection between the rack and the right tie rod. Fig. 1 describes the above-mentioned vehicle level steering system compliance modeling.

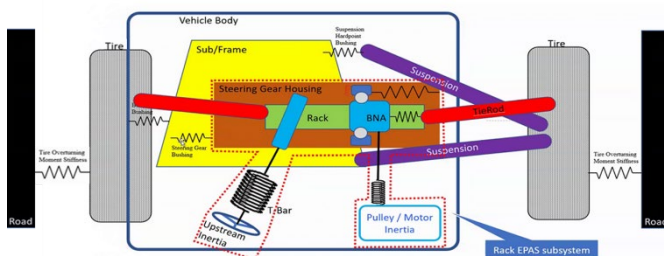


Figure 1. Vehicle level steering system compliance modeling

Electric Power Assisted Steering Modeling

To characterize the movement of the shaft and rack so that fully represent the steering system, five critical mechanisms are modeled – ball screw and pinion gear on the rack, and torsional bar, two universal joints and translational joint on steering shaft.

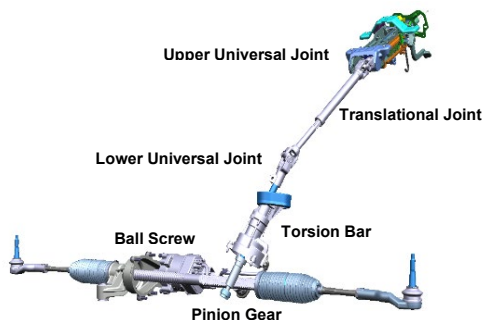


Figure 2. Six critical mechanisms to characterize the steering system

Summary

The goal of the research to explore the novelty of vehicle level steering CAE methodology has been achieved, through a transient explicit dynamic methodology.

- All the critical mechanisms are well modelled, including universal and translational joints, torsion bar, rack and pinion gear, and ball-screw.
- Contact surfaces between any two components are defined to precisely simulate kinematic compliance and reaction load transfer.
- It uses body and chassis structure as boundary condition to directly involve the compliance of body and chassis under rack load, instead of boundary condition with assumption at the component level.
- It applies the external load directly on the steering system, instead of applying the reaction force on components that are derived from force-induced frequency response analysis on the steering system with an assumption of boundary condition.

The innovation on EPAS simulation created great benefit compared with the existing CAE methods.

- Comprehensive modeling of steering gear and its boundaries provides a much more accurate simulation of how every component is reacting to the external forces to a greater extent.
- Achieve a better understanding of the motion of the steering components during a high loading event.
- Make a better estimation of movable range and component tolerances at every design milestone.
- Timely pinpoint the issues of a component over stress, Fatigue, and NVH.
- Applicable for advanced steering systems and ADAS features with the high-level compliance modeling ready.

Literature

- [1] Gillespie, Thomas D., "Fundamentals of Vehicle Dynamics", ISBN-13: 978-1560911999, SAE International
- [2] Harrer, M., Pfeffer, P., "Steering Handbook", ISBN 978-3-319-05448-3, DOI: 10.1007/978-3-319-05449-0
- [3] Timothy A. Drotar, Richard R. Lundstrom, "Advanced Vehicle Dynamics for Passenger Cars & Light Trucks", SAE Seminar C0415
- [4] Diglio, P., Falbo, G., Bai, J., and Gu, J., "A Test-Based Procedure for the Identification of Rack and Pinion Steering System Parameters for Use In CAE Ride-Comfort Simulations," SAE Technical Paper 2009-01-2090, 2009, <https://doi.org/10.4271/2009-01-2090>.
- [5] Rahmani, Ali, Rao, P.V.M., Saha, Subir., "Kinematic and sensitivity analysis and optimization of planar rack-and-pinion steering linkages", Mechanism and Machine Theory, 2009
- [6] Kamble, Naresh, Saha, S.K., "Developing a Virtual Prototype of a Rack and Pinion Steering System", Int. J. Vehicle Systems Modeling and Testing, Vol. 2, No. 1, 2007
- [7] Lee, Junho, Chang, Hyuk-Jun, "Multi-parametric Model Predictive Control for Autonomous Steering Using an Electric Power Steering System", Journal of Automotive Engineering, 2019, Vol. 233(13)3391-3402
- [8] Leishman, R. and Chase, K., "A New Tool for Design and Analysis of Optimized Rack and Pinion Steering Mechanisms," SAE Technical Paper 2009-01-1675, 2009, <https://doi.org/10.4271/2009-01-1675>. Vehicle Steering Characteristics with Changing Ratio Rack and Pinion Transmission", Advances in Mechanical Engineering, 2015, <https://doi.org/10.1177/1687814015619279>
- [9] Zarak, C. E., and Townsend, M. A. (June 1, 1983). "Optimal Design of Rack-and-Pinion Steering Linkages." ASME. J. Mech., Trans., and Automation. June 1983; 105(2): 220–226. <https://doi.org/10.1115/1.3258512>
- [10] <https://www.mathworks.com/matlabcentral/>

Dynamic Evaluation of Vehicle Roof Systems under Crash Scenarios:

An approach to early detection of potential concerns

Dhanaji Patil¹, Anand Malipatil¹, Rajesh Reddy¹, Naresh Kulkarni¹,
Roopesh Chodankar¹, Sunil Raveendran¹

¹Mercedes-Benz Research and Development, India Pvt Ltd, Bengaluru, India.

1 Abstract

Vehicle development is an intricate process where numerous sub-systems and parts are developed and integrated to form the final product. Though performance of each vehicle sub-system could be meeting the requirements in isolation, it is critical to adhere to the requirements as a system in a complete form. Eventually, any non-fulfilment of meeting regulatory or consumer metric requirements would potentially lead to design changes in the final stages of development, resulting in delays in realizing the product and increased cost. Therefore, it is essential to have a sub-system development process, which replicates the full vehicle performance testing conditions, during the initial phases of vehicle development. Moving towards the era of battery electric vehicles (BEV), amongst the many challenging crash scenarios, side pole crash is one of the severe load case considering the safety of floor mounted HV batteries, including structural integrity of the body in white (BiW) and other sub-systems. In this quest, structural integrity of roof sub-system and its connection with BiW, as damage and separation of sunroof system could hamper the occupant safety, which is of utmost importance. The current work proposes a digital sub-system level test, developed to evaluate performance of sunroof in side pole impact scenario derived from requirements specified by regulatory authorities and rating agencies such as FMVSS214, ECE R135, US & Euro NCAP. The proposed loadcase would help evaluate standalone roof behavior during early phases of development, when the BiW design is not yet finalized. This alternative digital setup helps to gauge roof design performance and optimize for crash functionality in the early phase of product development. This, in turn, helps in developing a robust roof system. The methodology considers the performance measure parameters such as internal energy, intrusion, velocities, deformation patterns and force characteristics. The developed sub-system load case outcome closely resemble the roof sub-system behavior in full vehicle under side pole impact.

Keywords: *Passive safety, Side pole impact, Roof sub-system, CAE, Crashworthiness, Dynamic sub-system, BiW*

2 Introduction

Car development is a mammoth task consisting of numerous activities for the development of different sub-assemblies. The development of sub-assemblies is done separately and its consensus with the BiW during the full vehicle integration is a major challenge, especially fulfilling the regulations from different regions (ECE, FMVSS). One such challenge is side load case. Fig.1 represents a side pole load case setup for FMVSS214 [12].

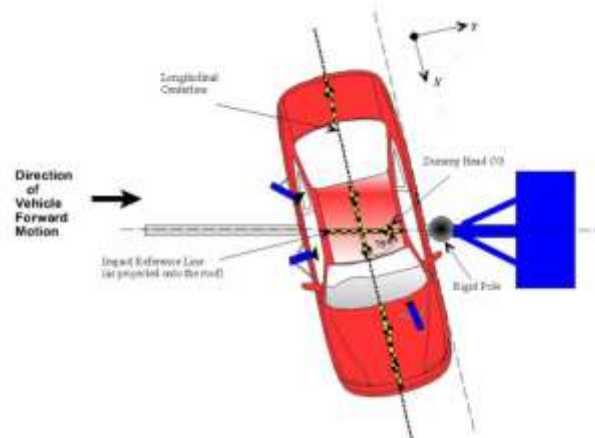


Fig. 1: FMVSS 214 [12]

The side impact statistically falls at number 2 position to be severe for occupant injuries after frontal impacts, it accounts for about 27 percent of the 23,437 people killed in passenger vehicles in 2009 [1]. Out of the side barrier and side pole impacts, the side pole is considered to be more fatal among the two, considering the safety of the occupant and damage to the Car structure, since the pole is narrow and imparts large force over small surface area unlike side barrier [2]. Due to the significant intrusion of the pole into the car, roof sub-system is a module, which is significantly affected in the side pole crash scenario. Often it is observed that, the roof sub-system is detached completely, which is a drastic loss of structural integrity. This could put the passenger and the vicinity of the vehicle in danger.

Extensive research has led into developing countermeasures on BiW structures [3] and understanding the response of occupants during side impacts [4,5]. In addition, many investigations has also been conducted on use of composite materials [6] and design optimizations for structures[7]. Moreover, there are studies involving the sub-system side impact tests developed and discussed in literature with focus on occupant safety and the behavior of door modules [8][9][10][11]. Hence, there is a requirement to develop a sub-system level test, which provides a fair comparison of roof behavior in side pole impact.

The goal of this paper is to present a methodology for developing a sub-system level load case for the vehicle roof, whose behavior is comparable to that of the roof system in full vehicle side pole crash. Further, this test would help to identify the influencing parameters and their limits, which then, can be provided as input to the teams developing the roof system.

The development of this methodology was carried out through finite element based crash simulations with dynamic loading of roof structure. In addition, a load case setup of fixtures to digitally conduct the dynamic loading scenarios is proposed, which would eventually be a benchmark for the roof development team to carry out the test.

3 Methodology

The challenge is approached with a dynamic analysis to develop the generalized sub-system setup, which is flexible and scalable to accommodate roof system from different carlines. It is necessary to ensure the digital fixture on which the roof sub-system is mounted to transfer the impact load to the roof in the manner as in full vehicle impact.

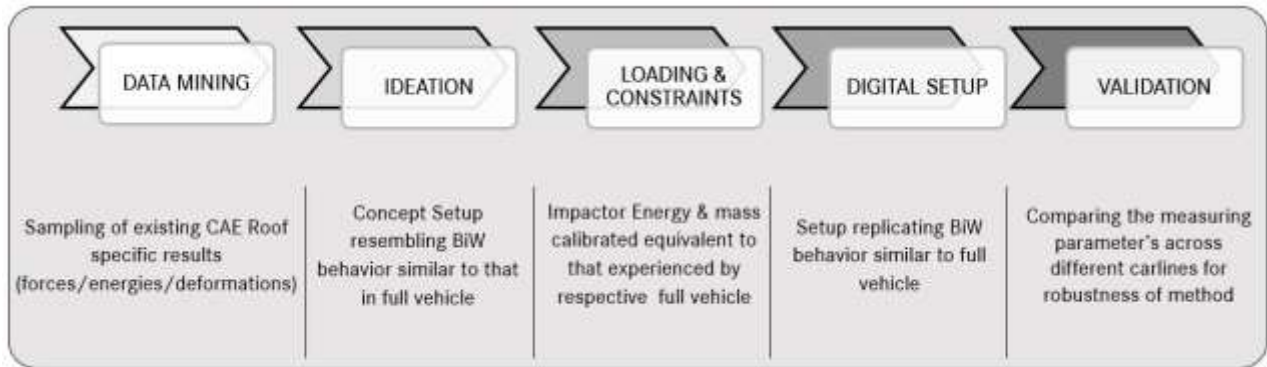


Fig. 3: Process flow

Initially data is collected from previous scenarios relating to Force levels passing through the principal cross members, energies experienced by roof sub-system parts and deformation patterns, so as to get a fair idea about behavior of roof sub-system in full vehicle.

Followed by reducing the model to only primary load carrying members resembling A-pillar, B-pillar, C-pillar, front and rear roof header. Multiple concepts were ideated to come to a version explained in detailed in section 4.

Loadings and constraints to match the energy sent to the roof sub-system are implemented inform of telescopic rectangular tube and hinges to replicate the translation and rotational behavior of struck side during impact. This lead to a generalized setup replicating the behavior similar to full vehicle.

In order to reinforce the confidence over developed method, this approach is evaluated over five different vehicle categories considering different vehicle weights, structures, construction (small, mid, large) and types (BEV, ICE) .

Below are the categories taken under investigation:

1. Hatchback.
2. Sedan.
3. SUV
4. Mid-size SUV electric
5. SUV electric

Fig. 5.1.1. and Fig. 5.1.2. compare forces on principal members extracted at locations F1 and F2 from full vehicle and sub-system simulation. These is discussed in detail in section 5.1.

Lastly, a relative comparison of force, energy absorbed and deformations by the roof parts in full vehicle and sub-system simulations are explained.

Simulations were carried out with the LS-DYNA [13] explicit solver and the comparison of sub-system behavior was made with that of full vehicle.

4 Dynamic Digital Test Set-up

4.1 Load case environment

This paper proposes a load case setup as shown in Fig. 4.1.1. It includes the impact side and the non-impact side support pillars. These pillar's resemble A, B and C pillar of the car respectively. These pillars are bound together by impact and non-impact side Roof rail on the left and right sides respectively, in addition front header and rear header are modelled as simplified structures. These represent the front most and the rear most regions of the BiW cross members, on which the Roof is mounted.

The impact and non-impact side support pillars are modelled with material of very high strength to ensure proper load transfer to the roof sub-system. The material and thickness of the roof rails, front

header and rear header are calibrated so as to replicate the stiffness in the full vehicle BiW structure, and have comparable deformations as in full vehicle simulations.

In the event of side pole crash, the sill and the door act as initial load absorbing and energy transferring members, due to vehicle inertia and high stiffness at the bottom of vehicle, the vehicle tends to rotate about sill and Pole comes in contact with roof rails, loading the roof system. The Roof system has translation motion in the Global Y direction at the impact side due to pole intrusion, and rotation of impact side support pillars about the X-axis.

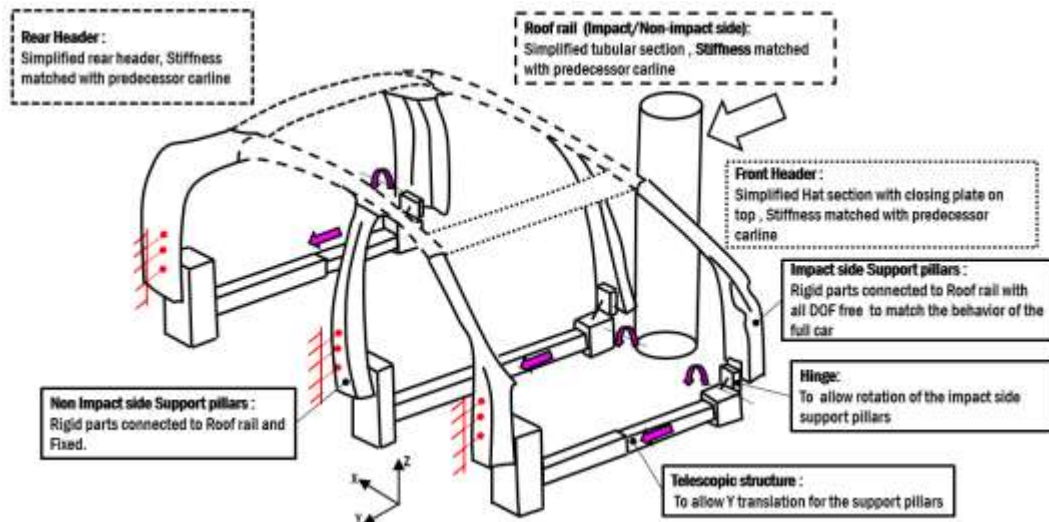


Fig. 4.1.1: Proposed Sub-system level test setup

To achieve a similar intrusion of the Roof system in Y translation, a telescopic arrangement is provided between the impact side and non-impact side support pillars at the bottom region. In addition, it is observed in full vehicle, there is negligible Y translation of the A, B and C pillar in the unstruck side. Hence, all degrees of freedom are fixed on the non-impact side support pillars. Rotational behaviors of the Pillar on the impact side about the X-axis is provided through a hinge placed at the base of each impact side support pillars. The impactor used in the test setup is a cylindrical rigid pole with a diameter of 254mm. The mass “M” and velocity “V” of the impactor is varied based on the energy taken by the roof system alone as measured in full vehicle side pole impact digital simulation. Differences in the energy imparted to the roof across in different categories of vehicles are captured by varying the mass and velocity of the pole. Such an arrangement makes it possible to replicate the behavior of roof system observed in the full vehicle side pole impact.

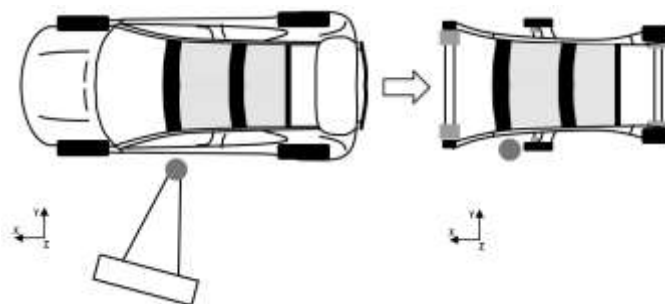


Fig. 4.1.2: Comparison between Roof sub-system mounted on full vehicle and on reduced environment

4.2 Loading and Constraints

Fig. 4.2 shows the orientation and impact direction of the rigid pole to the Roof system. A rigid pole inclined at 75deg, represents the side impact scenario for roof sub-system development. Multiple pole positions along the length of roof rail are evaluated to check the performance of developed roof sub-

system. The boundary constraints, loading conditions and respective pole positions are considered based on Regulations and NCAP protocols for full vehicle side impact.

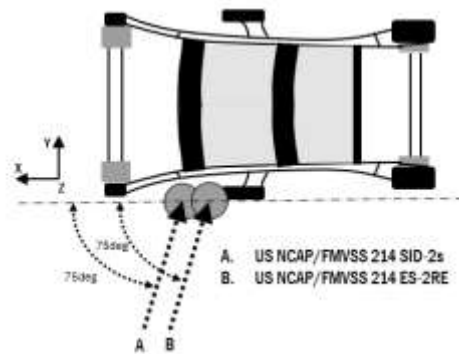


Fig. 4.2: Loading directions for proposed dynamic sub-system test

In this approach velocity, “V” is applied to the Pole of mass “M”, which can be measured as the kinetic energy being applied to the system. Although the amount of energy applied to the full vehicle is very high, this energy is absorbed by a large number of vehicle sub-systems, such as Doors, Roof, Sill, energy absorbers in Sill, etc. Therefore, only that part of the energy, which is associated with the Roof sub-system, needs to be taken into account for our sub-system level evaluation. The value of this kinetic energy is obtained by averaging the energy absorbed by the Roof sub-system parts in the full vehicle simulations in different loading scenarios.

4.3 Evaluation Parameters

Performance of sub-system against that of the full vehicle is validated by considering two different types of parameters.

Objective parameters:

1. Energy absorbed by the roof parts.
2. Force on principal roof cross-members.

Subjective parameter:

1. Overall deformation of the roof system.

Forces on principal roof members are measured at different locations such as frontal Roof structural member [F1 (section A-A)] and middle Roof structural member [F2 (section B-B)] Fig.4.3.1.

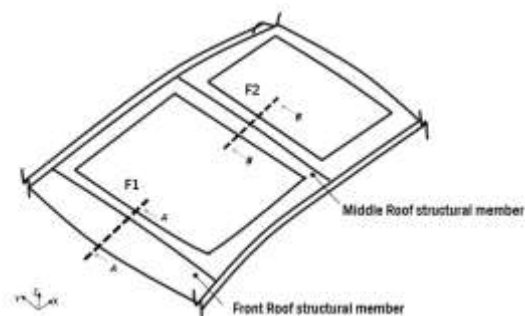


Fig. 4.3.1: Cross-sectional force measuring locations (F1 & F2) for Roof system

Fig.4.3.2. shows a typical example of overall deformation of the roof system, which consists of mainly three focus areas such as buckling/bending of principal roof members, roof parts separation (separation

of upper half from lower half of the roof system) and global deformation of the roof system due to side pole impact crash loads.

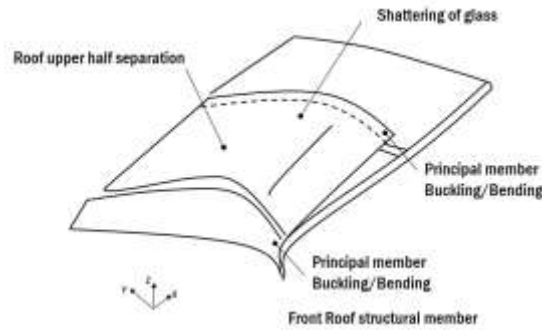


Fig. 4.3.2: Overall deformation of the Roof system under crash loads

4.4 Tolerance for force value comparison

Due to the generalization of the sub-system to accommodate roof from different platform and the assumptions made in the simulation model, the outcomes from simulation are assumed to have deviation of +/- 20% of the base value, which is derived from maximum force experienced in full vehicle. The deviation limit helps for result comparison and gives confidence on the sub-system setup, which is indicative of the degree of closeness of its behavior in comparison to the full vehicle side pole impact.

5 Results

5.1 Force comparison

Fig. 5.1.1 and Fig. 5.1.2 is a comparison plot between full vehicle and sub-system values of maximum cross section force measured at the location as shown in Fig.4.3.1. F1 and F2 respectively of the roof sub-system across different carlines under investigation. As discussed in section 4.4, the limit of +/-20 % of full vehicle values are considered acceptable deviation for comparison.

As clearly observed, the sub-system analysis values are comparable with the values obtained in the full vehicle side pole impact simulation.

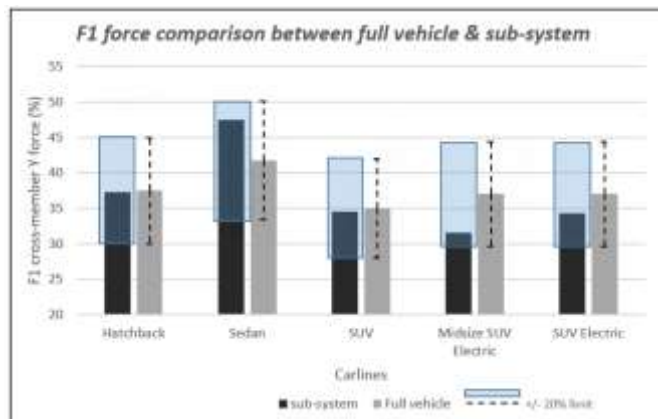


Fig. 5.1.1: F1 cross-member force comparison between sub-system & full vehicle across different carline

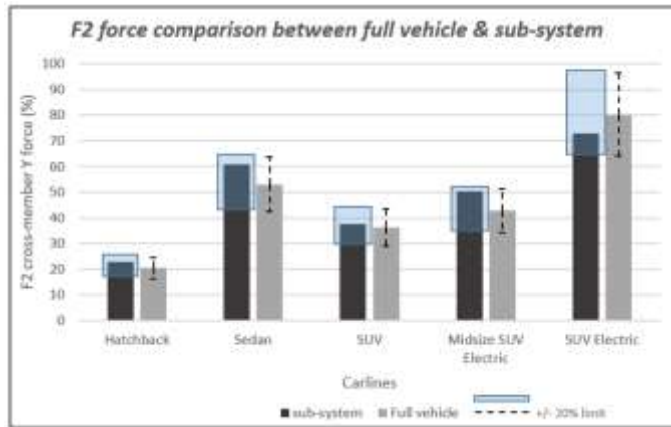


Fig. 5.1.2: F2 cross-member force comparison between sub-system & full vehicle across different carline

5.2 Deformation comparison

Two different carlines sampled from the present work under investigation are showcased in this section. Refer Fig. 5.2.1 and Fig.5.2.2.

Deformations observed of the roof sub-system is comparable to those obtained from the dynamic full vehicle side pole impact simulations.

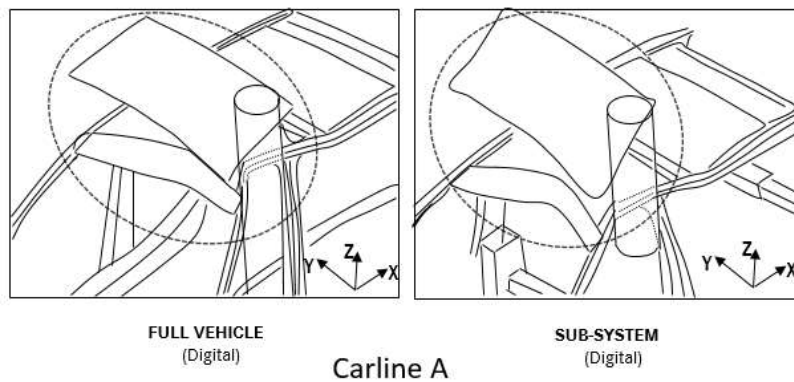


Fig. 5.2.1: "Carline A" Deformation comparison

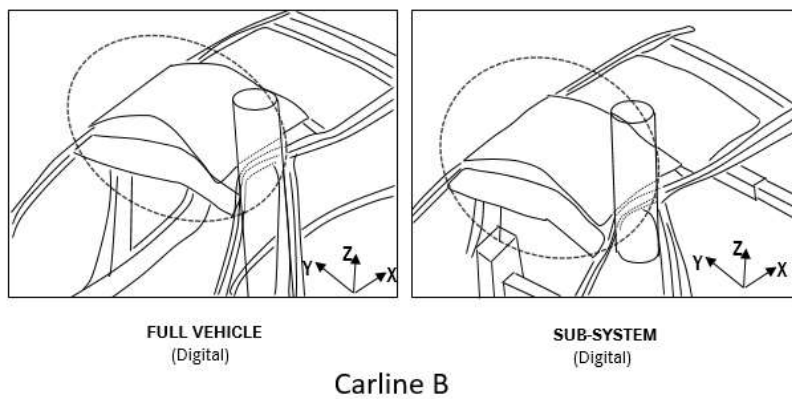


Fig. 5.2.2: "Carline B" Deformation comparison

5.3 Internal energy comparison

Fig. 5.3 shows the Internal energy of Roof system at maximum intrusion. It is observed that the values of sub-system are similar to those obtained from the full vehicle side pole impact simulations. It can be concluded that in terms of Internal energy absorbed by the Roof structure under investigation, the sub-system loading arrangement is aligned closely to full vehicle side pole impact simulations.

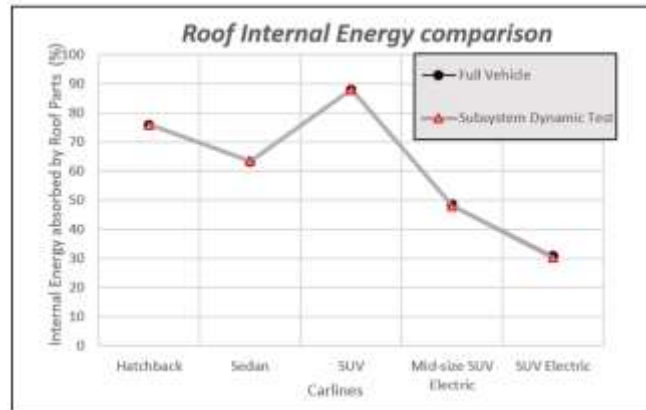


Fig. 5.3: Roof Internal Energy comparison between sub-system and full vehicle simulation

6 Conclusion

The proposed sub-system load case addresses the challenges faced during later stages of vehicle testing and certification, failing which, leads to redevelopment of roof structures causing delays and increased cost to the program.

The energies, forces in principal members and deformations are found to be comparable with the full vehicle digital simulations.

Hence, the proposed digital methodology allows us to predict behavior and provide inputs during the early phases of development. There by saving cost and delays in development time.

The proposed digital method needs to be experimentally validated to improve the reliability of this methodology, this is seen as the future scope of the present work.

7 Acknowledgement

The authors gratefully acknowledge the support provided by Mercedes-Benz Research and Development India (MBRDI) and Mercedes-AG, for the research work leading to this paper. Authors would like to express their gratitude to Mr. Prasanna Gonuguntla, Head- RD, MBRDI and Mr. Naresh Kulkarni, HOD- Passive Safety & CFD- RD, MBRDI who rendered their valuable support during the research period.

8 Literature

- [1] Teoh, E.R. and Lund, A.K.: "IIHS side crash test ratings and occupant death risk in real-world crashes", J. Traffic injury prevention, 12(5), 2011, 500-507.
- [2] Wang, D., Dong, G., Zhang, J. and Huang, S.: " Car side structure crashworthiness in pole and moving deformable barrier side impacts ", J.Tsinghua Science & Technology, 11(6), 2006, 725-730.
- [3] Strother, C.E., Kent, R.W. and Warner, C.Y.: " Estimating vehicle deformation energy for vehicles struck in the side ", J. SAE transactions, 107(6), 1998, 306-322
- [4] Ruan, J.S., Khalil, T. and King, A.I.: " Human head dynamic response to side impact by finite element modeling ", J. Biomechanical Engineering, 113(3), 1991, 276-83
- [5] Farmer, C.M., Braver, E.R. and Mitter, E.L.: " Two-vehicle side impact crashes: the relationship of vehicle and crash characteristics to injury severity ", 29(3), 1997, 399-406

- [6] Patberg, L., Philipps, M., Dittmann, R. and Adam, H.: " Application of Fibre-Reinforced Composites in the Car Side Structure", SAE Technical Paper 980746, 1998, 7
- [7] Nelson, D. and Sparke, L.: " Improved Side Impact Protection: Design Optimisation for Minimum Harm ", SAE Technical Paper 2002-01-0167, 2002, 12
- [8] Stein, Douglas J.: "Apparatus and Method for Side Impact Testing." SAE Transactions, vol. 106, 1997, pp. 945-51.
- [9] Hopton, J. R., and A. R. Payne.: "Comparison study of EuroSID, USSID, BioSID performance using MIRA's new M-SIS side impact simulation technique." SAE PUBLICATION SP-1174. TECHNOLOGIES FOR OCCUPANT PROTECTION ASSESSMENT: PAPERS PRESENTED AT THE INTERNATIONAL CONGRESS & EXPOSITION, FEBRUARY 26-29, 1996, DETROIT, MICHIGAN, USA (SAE TECHNICAL PAPER 960103), 1996, p. 53-9
- [10] Miller, P. Michael, and Hai Gu.: "Sled testing procedure for side impact airbag development.", SAE transactions, 1997, 937-944
- [11] Vaidyaraman, Srimi.: "Modeling and simulation of sled and barrier test for side impact applications.", PROCEEDINGS OF THE FIFTH INTERNATIONAL MADYMO USERS'MEETING, NOVEMBER 3 AND 4, 1994, p. 75-84
- [12] National Highway Traffic Safety Administration.: "FMVSS No. 214 Amending side impact dynamic test adding oblique pole test.", Final Regulatory Impact Analysis, 2007
- [13] Manual, LS-DYNA Keyword User'S., and I. Volume.: "Version 971." Livermore Software Technology Corporation 7374", 2007, 354

Advanced material modeling with user subroutines

Rasul Abdusalamov¹, Markus Hillgärtner¹, Rajesh Chandrasekaran¹, Khiem Ngoc Vu¹, Mikhail Itskov¹

¹ Department of Continuum Mechanics, RWTH Aachen University, Aachen, Germany

1 Introduction

Due to rapid advances in materials science, new material models are increasingly needed. A variety of standard models exists which are motivated either by a phenomenological or mechanistic point of view. Even if the provided experimental data shows all relevant mechanical effects, the quality of the fit strongly depends on the material model. Thus, implementation of new constitutive models matching all necessary phenomena often becomes indispensable.

In this contribution, we present new approaches to develop material models and implement them into commercial FE-software like LS-DYNA by means of user subroutines. When dealing with elastomers or polymers experimental data from uniaxial, equibiaxial and pure shear tests should be obtained first. Often, temperature as well as rate dependent effects are also considered. We will introduce recent research approaches strongly focused on data-driven models, such as neural networks [1] or symbolic regression [2,3].

2 Continuum Mechanical Framework

By creating a continuum mechanical framework known axioms for constitutive relations such as the principle of objectivity should directly be fulfilled. Considering nearly incompressible materials e.g., rubbers or biological tissues, it is advantageous to decompose the deformation gradient \mathbf{F} into an isochoric and a volumetric part according to Flory [4], where $J = \det \mathbf{F}$. The isochoric part $\bar{\Psi}$ of the strain energy function can be expressed in terms of the principal invariants of the right Cauchy-Green tensor $\bar{\mathbf{C}} = \bar{\mathbf{F}}^T \bar{\mathbf{F}}$ given by

$$I_{\bar{\mathbf{C}}} = J^{-\frac{2}{3}} I_{\mathbf{C}} \quad \text{and} \quad II_{\bar{\mathbf{C}}} = J^{-\frac{4}{3}} II_{\mathbf{C}}. \quad (1)$$

For hyperelastic materials, the first Piola-Kirchhoff stress tensor \mathbf{P} can be expressed by

$$\mathbf{P} = \frac{\partial \bar{\Psi}}{\partial \mathbf{F}} = 2 \left(\frac{\partial \bar{\Psi}}{\partial I_{\bar{\mathbf{C}}}} J^{-2/3} \mathbf{F} + \frac{\partial \bar{\Psi}}{\partial II_{\bar{\mathbf{C}}}} J^{-2/3} (I_{\bar{\mathbf{C}}} \mathbf{F} - J^{-2/3} \mathbf{F} \mathbf{C}) + \frac{\partial \bar{\Psi}}{\partial J} \frac{J}{2} \mathbf{F}^{-T} \right). \quad (2)$$

To obtain the stresses, it is necessary to determine the derivatives of the strain energy function with respect to $I_{\bar{\mathbf{C}}}$, $II_{\bar{\mathbf{C}}}$ and J . Certainly, this framework can be extended for anisotropic materials by introducing structural tensors $\mathbf{L}_r = \mathbf{l}_r \otimes \mathbf{l}_r$ for $r = 1, \dots, R$ with $\|\mathbf{l}_r\| = 1$ as presented for example in [5]. Additionally, it is possible to extend the framework by introducing other physical parameters e.g., temperature.

3 Constitutive Neural Networks and Symbolic Regression

For constitutive neural networks and symbolic regression, the main goal is to find the strain energy as a mapping between invariants and stresses. For artificial neural networks (ANNs) an initial data set is provided to determine the internal parameters of the neural network. Note that the universal approximation theorem states that any continuous function can be approximated by ANNs. The approach with symbolic regression is similar but different to ANNs. In general, regression is a mathematical method to find the relationship between specified independent variables and a single dependent variable. Symbolic regression is a special case where this relationship is found in a form of a mathematical expression. The goal of this evolutionary algorithm is to find an expression optimal with respect to simplicity and precision in comparison to the specified data set. Both approaches perform the same purpose, but ANNs represent “black box” models whereas symbolic regression is considered as a “white box” model. Hereby, the benefit of symbolic regression is that the model is physically interpretable and is easier to integrate into a commercial FE-software like LS-DYNA.

Nevertheless, the incorporation of a continuum mechanical framework is useful for ANNs as well as symbolic regression. By this means, one can simulate a general 3d loading case and predict arbitrary deformation states. Both procedures are visualized in Fig.1.

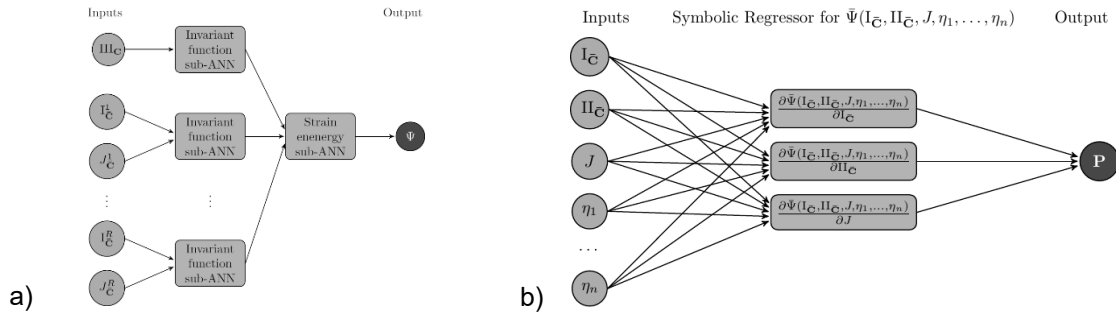


Fig.1: a) Procedures for CANNs [1] and b) symbolic regression [3] for determining the strain energy function depending on I_C , II_C , J as well as the generalized invariants I_C^r and J_C^r for $r = 1, \dots, R$.

4 Application to a Temperature Dependent Data Set Using Symbolic Regression

To investigate the performance of such approaches a temperature dependent data set has been studied using symbolic regression. Stress strain responses of a thermoplastic polyester elastomer Hytrel 4556 with nine stress-strain curves for different temperatures between -40°C and 120°C have been considered. A total of five curves have been used as a training set, the remaining four curves served as a test set. The strain energy function was determined by

$$\bar{\Psi}_{\text{Hytrel}} = I_{\bar{C}} \exp \left(\sqrt{\left(-\bar{T} + \exp \left(1.41 \sqrt{(0.5 \log \bar{T} - 1) \log \bar{T}} \right) - 1.0 \right) \log^2 \bar{T}} \right) + 0.131 I_{\bar{C}} \log \bar{T} - 2.0 II_{\bar{C}} \log \bar{T} + \exp(41.19 \exp(-II_{\bar{C}})) \log \bar{T} \quad (3)$$

where \bar{T} is a scaled temperature with $\bar{T} = \frac{T}{400} + \frac{1}{2}$ for the temperature range $T \in [-40^\circ\text{C}, 120^\circ\text{C}]$. The corresponding predictions for the training set as well as the test set are visualized in Fig.2.

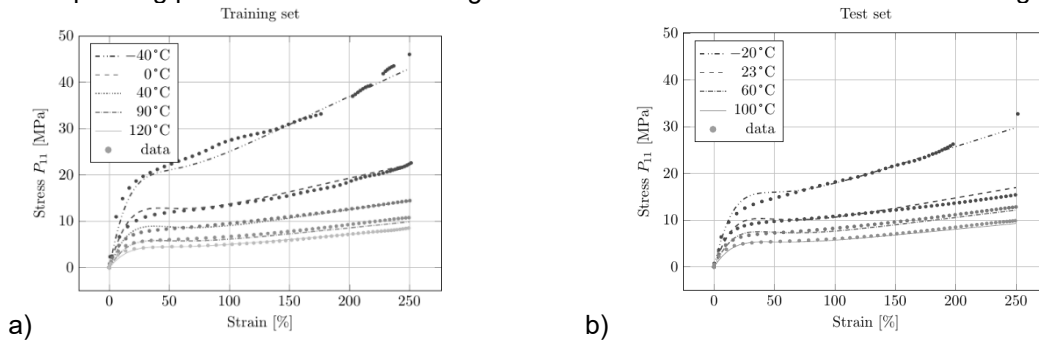


Fig.2: Stress-strain curve responses for a) training and b) test for strain energy from equation (3).

5 Summary

In this work, we investigated the applicability of constitutive artificial neural networks as well as symbolic regression in the context of finding new material models through suitable strain energy functions. The necessary continuum mechanical framework as well as the procedure for both approaches were presented. Additionally, the application to a temperature dependent data set for the case of symbolic regression was shown.

6 Literature

- [1] Linka et al.: "Constitutive artificial neural networks: A fast and general approach to predictive data-driven constitutive modeling by deep learning", Journal of Computational Physics 429, 2021, 110010
- [2] Kabliman et. al.: "Application of symbolic regression for constitutive modeling of plastic deformation", Applications in Engineering Science 6, 2021, 100052
- [3] Abdusalamov et. al.: "Automatic generation of interpretable hyperelastic material models by symbolic regression", arXiv preprint, 2022
- [4] Flory: "Thermodynamic relations for high elastic materials", Transactions of the Faraday Society 57, 1961, 829
- [5] Ehret et. al.: "A polyconvex hyperelastic model for fiber-reinforced materials in application to soft tissues", Journal of Materials Science 42, 2007, 8853–8863

Efficient Gradient-Enhancement of Ductile Damage for Implicit Time Integration

Johannes Friedlein¹, Julia Mergheim¹, Paul Steinmann¹

¹Institute of Applied Mechanics, Friedrich-Alexander-Universität Erlangen-Nürnberg

1 Introduction

Metal forming processes involve complex loading paths and large plastic strains. The latter is typically intrinsically linked to the generation of ductile damage [1]. To reliably simulate such processes, accurate material models are needed to reproduce these plastic as well as damage evolutions. Once the softening effect of the latter becomes relevant, it needs to be modelled in a coupled sense [1]. However, the strong coupling of plasticity and damage causes a pathological dependency on the mesh size and orientation [2]. This unphysical behaviour for softening can be cured by regularisation techniques introducing an additional internal length. In contrast to typically expensive non-local integral methods [3], the implicit gradient-enhancement requires merely an additional scalar field and governing equation for the non-local variable. Such two-field problems can, for instance, be implemented in commercial software by user-defined elements [2]. Due to the monolithic solution of thermomechanical problems in ABAQUS, the thermal solver can be utilised together with a user-defined material model (UMAT) for regularisation and is therein equivalent to a monolithic user-element, such that existing gradient formulations can directly be applied [4].

2 Gradient-enhancement for implicit time integration in LS-DYNA

We propose a gradient-enhancement of softening material models based on the weakly staggered thermomechanical coupling on global level. In contrast to existing theories, such as [5], we account for a finite time step size on the local material point level enabling the use for implicit time integration. Tools for the implementation can be found on GitHub (see user "jfriedlein").

2.1 Global level: Substitution model using the thermal solver for regularisation

The gradient-enhancement of the damage variable (gradient-damage) is incorporated by the following partial differential equation (PDE) of Helmholtz type in eq. (1)a, compare [2].

$$(a) \ c \Delta_x \bar{d} - \beta [\bar{d} - d] = 0 \rightarrow (b) \ d = \beta^{-1} d^{\text{loc}} + [1 - \beta^{-1}] \bar{d} \rightarrow (c) \ l^2 \Delta_x \bar{d} - [\bar{d} - d^{\text{loc}}] = 0 \quad (1)$$

with the regularisation parameter c related to the internal length and the penalty parameter β . Based on [6], we distinguish between a purely non-local damage \bar{d} , a truly local damage variable d^{loc} , and a local damage variable d , which are related by the affine combination in eq. (1)b. Consequently, eq. (1)a can be reformulated, "eliminating" the penalty parameter β , and replacing the regularisation parameter by a length parameter l as in eq. (1)c. The latter equation is like the stationary heat conduction [4] being solved by the thermal solver in LS-DYNA with the following replacements [5] ($temp \hat{=} \bar{d}$) in the Fortran subroutine *thumat1x*

$$c1 = l^2; c2 = c3 = cvl = 0; ihsrcl = 1; hsrcl = -[temp - d^{\text{loc}}]; dhsrcl = -1$$

To be able to access the truly local damage d^{loc} , which is part of the mechanical history variables (named *hsv* in subroutine *umat4x* and *hsvm* in *thumat1x*), the option *IHVE=1* needs to be activated in ***MAT_THERMAL_USER_DEFINED**. This option is currently limited to selected elements in LS-DYNA, see LS-DYNA manual appendix H. Moreover, the following keywords are additionally necessary: ***CONTROL_SOLUTION**, ***CONTROL_THERMAL_SOLVER**, ***CONTROL_THERMAL_TIMESTEP**.

2.2 Local level: Coupling of truly local, local and non-local damage

Gradient-damage achieves regularisation by altering the damage evolution. In areas of localisation, the damage growth is limited, whereas in the periphery of the localisation zone, further damage is motivated spreading to the desired finite width. This altering of the damage evolution is not inherent in the usual (truly local) damage law but must be incorporated based on the non-local damage. For explicit time integration [5], the local damage variable in the UMAT was simply replaced by the previously computed non-local damage. Therein, this was sufficient due to the small explicit time steps. Therefore, the non-local damage, which is computed based on the "old" results from the previous time step, did not introduce a noticeable delay or time step size dependency. For implicit time integration with finite steps, however, the use of the "old" non-local variable causes a perceptible time step dependency. To avoid

this, we utilise the linear character of eq. (1)c. A damage distribution $d^{\text{loc}}(X)$ scaling linearly, results in a linear increase in the non-local variable and therefore a constant ratio $\bar{d}/d^{\text{loc}} \equiv K_{\text{NL}}$, compare [7]. This linear relation is assumed to hold during implicit finite time steps, leading to the following relation eq. (2)a

$$(a) K_{\text{NL}} \equiv \frac{\bar{d}_n}{d_n^{\text{loc}}} \approx \frac{\bar{d}_{n+1}}{d_{n+1}^{\text{loc}}} \rightarrow (b) \bar{d}_{n+1} \approx K_{\text{NL}} \cdot d_{n+1}^{\text{loc}} \rightarrow (c) d_{n+1} = \max(\max(d_n, \bar{d}_n), \bar{d}_{n+1}) \quad (2)$$

This approximate relation is utilised to project/extrapolate how the non-local variable in eq. (2)b is expected to change during the current mechanical time step. Consequently, we can – to some degree – compensate for the delay that is incorporated by the weakly staggered coupling. Moreover, regularisation needs to spread damage, which must also be possible in areas with stagnating or zero truly local damage. Therefore, we use relation eq. (2)c to ensure that damage can also spread to the old non-local damage, but never decrease. Therein, eq. (1)b is idealised by $\beta \rightarrow \infty$ to $d_{n+1} \approx \bar{d}_{n+1}(d_{n+1}^{\text{loc}})$.

3 Numerical example and results

We consider a plane strain shear band specimen with geometrical imperfection from [4], shown in Fig.1 (left). The material parameters for elasticity and plasticity are taken from [8] as identified for the dual-phase steel HCT590X. The geometry is discretised by 3D hexahedral elements (ELFORM=-1) with suitable boundary conditions for plane strain. The damage evolution law and parameters are chosen as $d^{\text{loc}} = \langle [\varepsilon^{p,\text{acc}} - 0.01] / [0.4 - 0.01] \rangle^2$ [3] with the Macaulay brackets $\langle \cdot \rangle$. For the local plasticity-damage model (cyan), damage localises mesh-dependently in a limited number of elements in Fig.1. The force-displacement response in Fig.1 (right) exhibits a strong mesh-dependency and tends to converge to a brittle-like failure. In contrast, plasticity - gradient-damage (dark green) with a length parameter $l = 1$ mm converges to a finite damage zone width and a physical system response. Here, the medium mesh (dotted) is sufficient to capture the system behaviour, where even the coarse mesh already predicts the damage zone width well. The final load is applied in less than 200 implicit time steps.

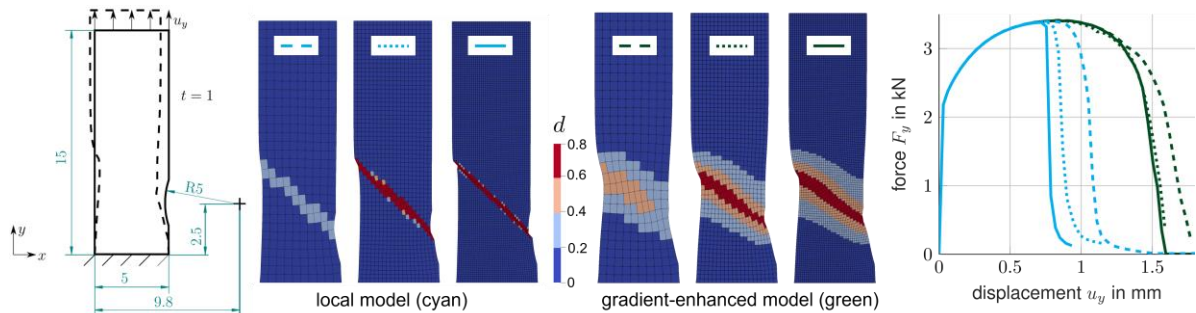


Fig.1: Shear band specimen. The local model (cyan) gives mesh-dependent responses, whereas the developed gradient-enhancement (dark green) renders the softening model mesh-objective.

4 Summary

We proposed a gradient-enhancement of softening material models, which is well suited for implicit time integration, based on the weakly staggered thermomechanical coupling. The latter is akin to a post-processing step, making the approach efficient and easy to incorporate into existing material models.

5 Literature

- [1] Tekkaya, E., et al.: "Damage in metal forming", CIRP Annals, 2020, 600-623
- [2] Kiefer, B., et al.: "A gradient-enhanced damage model coupled to plasticity—multi-surface formulation and algorithmic concepts", Int J Damage Mech, 2018, 253-295
- [3] Nahrman, M., Matzenmiller, A.: "Modelling of nonlocal damage and failure in ductile steel sheets under multiaxial loading", Int J Solids Struct, 2021
- [4] Seupel, A., et al.: "An efficient FE-implementation of implicit gradient-enhanced damage models to simulate ductile failure", Engineering Fracture Mechanics, 2018, 41-60
- [5] Matzenmiller, A., Schmidt, H., Nahrman, M.: "Gradient enhanced damage: modelling, implementation and applications", 13th European LS-DYNA Conference, 2021
- [6] Friedlein, J., Mergheim, J., Steinmann, P.: "Anisotropic plasticity-damage material model for sheet metal—Regularised single surface formulation.", PAMM, 2021
- [7] Andrade, F.X.C., Vogler, M., Cesar de Sa, J.M.A., Andrade Pires, F.M.: "User-Defined Nonlocal Models in LS-DYNA", 8th European LS-DYNA Users Conference, 2011
- [8] Friedlein, J., Mergheim, J., Steinmann, P.: "Inverse parameter identification of an anisotropic plasticity model for sheet metal.", IOP Conf Ser: Mater Sci Eng, 2021

Method Development Characterization, Modeling and Simulation of Hygro-Thermo Effects in Thick Layer Adhesives

Fabian Kötz¹, Anton Matzenmiller^{1,2}

¹Institute of Mechanics, Department of Mechanical Engineering, University of Kassel, Mönchebergstr. 7, 34125 Kassel, Germany

²Professor of Applied Mechanics

1 Introduction

Semi-structural bonded joints of steel components are exposed to long-term stresses consisting of water diffusion, temperature and external forces during operation. This hygro-thermomechanical loading leads to successive degradation of stiffness and strength due to damage resulting from chemical aging and fatigue processes, leading to failure of the bonded joint when its service life is reached. In the following contribution, a methodology is presented to predict the service life of hygro-thermo-mechanically loaded semistructural adhesive joints by unsteady FE simulation. The lifetime prediction is based on a concept that includes a viscoelastic and a damage part. The first part for viscoelasticity consists of the generalized Maxwell model, in which the effects of temperature and humidity on the viscoelastic properties of the adhesive bond are captured by the time-temperature and time-water concentration shifts. The second part for material damage is an ordinary differential equation. It consists of a creep and a moisture damage part for the damage developments, caused by the local water concentration due to mechanical stress and chemical aging. Both damage parts are multiplied by Arrhenius-type functions to account for the effect of temperature on defect growth. The interaction of the creep and the moisture damage parts is studied by using analytical and numerical solutions of the damage differential equation. All parameters of the damage model are determined by using fracture times from creep tests under different climatic conditions and loading levels. The local water concentration in the adhesive is calculated by Fick's model, based on a concentration boundary condition. The diffusion parameters are determined from gravimetric tests. A numerical example shows the lifetime prediction methodology and the influence of viscoelasticity on the predicted lifetimes for different hygro-thermo-mechanical loading cases.

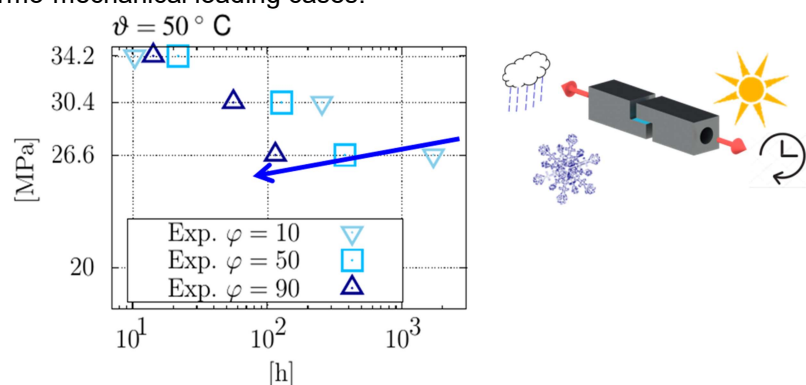


Fig. 1: Fracture times from long-term experimental tests [1] under different relative humidities (see shear test on the right); the blue arrow indicates the hygric influence on the fracture times

2 Modeling and simulation of moisture diffusion with LS DYNA

In the case of hygrothermomechanical loading, there is a so-called three-field problem with the three fields: hygric, thermal and mechanical. However, LS-DYNA does not have a diffusion solver, so the three-field problem is reduced to a two-field problem. This simplifying assumption is permissible, since the temperature field, in contrast to the other field, has adjusted itself quickly. For this reason, the temperature in the simulation at each node and the solution of the thermal field problem is omitted.

As a result, the **thermal solver** of LS-DYNA can be used for the solution of the hygric field problem, because the diffusion and thermal problems have analogous field equations and boundary conditions. This is shown in Table 1, which compares the equations of the two analogous field problems. The analogy is exploited by replacing the coefficients in the comparison performed in Table 2.

FICK's first law $\mathbf{J} = -D\nabla c$	FOURIERS heat conduction $\mathbf{q} = -k\nabla T$
continuity equation $\frac{\partial c}{\partial t} + \nabla \cdot \mathbf{J} = 0$	heat transfer $\rho C_p \frac{\partial T}{\partial t} + \nabla \cdot \mathbf{q} = 0$
FICK's second law $\frac{\partial c}{\partial t} = D\nabla^2 c$	heat equation $\frac{\partial T}{\partial t} = \frac{k}{\rho C_p} \nabla^2 T$

Table 1: Formulation of the analog equations [2]

concentration c	temperature T
mass flow \mathbf{J}	heat flow \mathbf{q}
diffusion coefficient D	thermal conductivity k
1	specific heat capacity C_p
1	density ρ

Table 2: Comparison of coefficients for the analogy of field problems as shown in Table 1

The parameter identification for the calculation of moisture diffusion is carried out with test data from gravimetric investigations on adhesive substance samples from [3] and inversely optimized with LS-Opt. Thus, the water absorption can be determined exactly for a certain adhesive and is used in a damage model as a damage-driving hygric parameter for the service life prediction in any adhesive compound sample or component.

$$\dot{D}_{ca} = \frac{1}{c_0} \left(\frac{\sigma}{\sigma_{ref}(1 - D_{ca})} \right)^n \exp \left(p_c \left(\frac{1}{T_{refc}} - \frac{1}{T} \right) \right) + B_a(1 - D_{ca}) \frac{c}{c_{\infty,ref}} \exp \left(p_a \left(\frac{1}{T_{refa}} - \frac{1}{T} \right) \right) \quad (1)$$

For the calculation of the service life prediction, the damage differential equation (eq. 1), which takes into account the temperature, the moisture concentration and the mechanical load in a ***usermat**, is implemented to calculate the service life satisfactorily with LS-DYNA (see Fig. 3).

Acknowledgement

We thankfully acknowledge the financial support through FOSTA of the AiF/IGF from the Federal Ministry for Economic Affairs and Energy for the funding within the framework of IGF project 2155 N (P 1496).

Literature

- [1] Bieker, C. (2006). "Methodenentwicklung zur Bestimmung des hygrothermo-mechanischen Langzeitverhaltens von strukturellen Klebverbindungen mit metallischen und mineralischen Untergründen". Schriftenreihe des Instituts für Werkstofftechnik Kassel. Shaker. Dissertation.
- [2] Crank, J. (1975). The mathematics of diffusion. Clarendon Press.
- [3] Kötz, F.; Matzenmiller, A.; Sander, S.; Meschut, G.; Damm, J.; Kaspar, Y.; Ummenhofer, T. (in progress). „Methodenentwicklung zur rechnerischen Auslegung geklebter Stahlverbindungen unter Alterungsbeanspruchung im Stahl- und Anlagenbau“. (FOSTA P 1496/15/2021 / IGF-Nr. 21555 N)

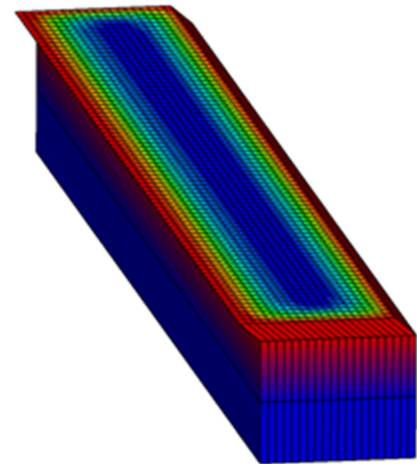


Fig. 2 Visualization of water diffusion as temperature in LS-PrePost for a tensile shear sample

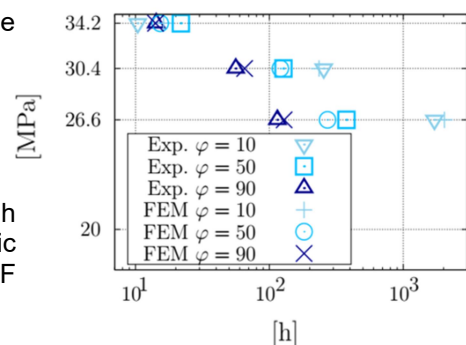


Fig. 3 Fracture times from long-term experimental tests under different relative humidities with FEM calculation

10 years human modeling at DYNAmore and future projects

A. Gromer, D. Fressmann (DYNAmore)

Simulation of Sheet Metal Forming – Current Developments

Dr. M. Fleischer, Dr. S. Sitz, F. Asen, P. Craighero, N. Paramasivam

¹BMW AG, Knorrstrasse 147, 80788 München

1 Introduction

The use of finite element (FE [12], [16]) simulations to conduct a virtual validation of the forming process for sheet metal parts has been introduced in the mid 1990s and is state of the art in the automotive industry today. Two challenging tasks for determination of feasibility of a tool design and its process parameters are feasible [17] are the prediction of the material behavior during the forming process and the springback of the final part [2,3,4].

In order to improve the predictive accuracy of the forming simulation, the level of detail has increased steadily regarding many aspects of the simulation model. For example, the material behavior during drawing is influenced by the preceding trimming operation as the latter causes damage at the trimmed edge. Furthermore, during the drawing the pressure distribution between the blank and the blankholder may vary significantly due to the deflection of the tool and the press. This can result in a disadvantageous restraining behavior. Considering these effects may lead to a further improvement of the simulation's accuracy.

As a result, the increase in data size and level of detail of the FE models poses a challenge for the future simulation systems and their application [5].

2 Forming simulation at the BMW Group – State of the art

Since the mid of the 1990s, forming simulation is state of the art in the tool development process and there are a lot of use cases today.

2.1 Simulation in the tool development process

The design process of a deep drawing tool is supported by FE simulation systems in many applications.

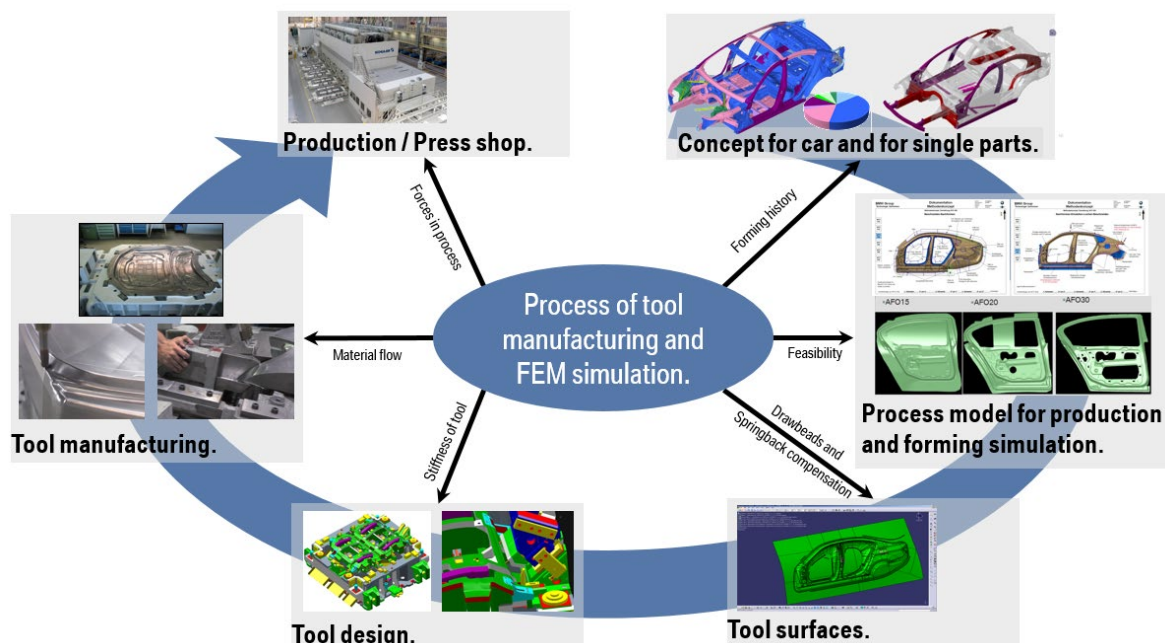


Fig. 1: Application of simulation in the tool development process – [5].

In the design process of the car body, the forming simulation supports the simulation of passive safety with the material history from the production process to give a better prediction of the structural behavior of the car body in crash simulations. The main usage of the forming simulation is to model the production process itself and to conduct design studies for feasibility. When a good geometrical design for the forming tools is found, the next step is the springback simulation and its geometrical compensation. One more use case for the simulation is the prediction of stiffness of the tool to support the CAD engineer. More key results from the forming simulation are the forces that occur in the production process in the press line and the material flow during the deep drawing. All these applications of the FE simulation support the engineers in the design process.

2.2 Software concept

To deal with all the challenges in the design process, a general software setup is used for forming simulation. The input consists of geometries, material data and process parameters. These are all part of the classical pre-processing. The application was realized with BMW's own software systems to provide a process orientation to the forming process in graphical user interfaces [2,3,4]. This approach enables every user to setup a metal forming simulation with the FE solver LS-DYNA [1,9]. In the next step, the solution is computed by the solver and the results can be analyzed.

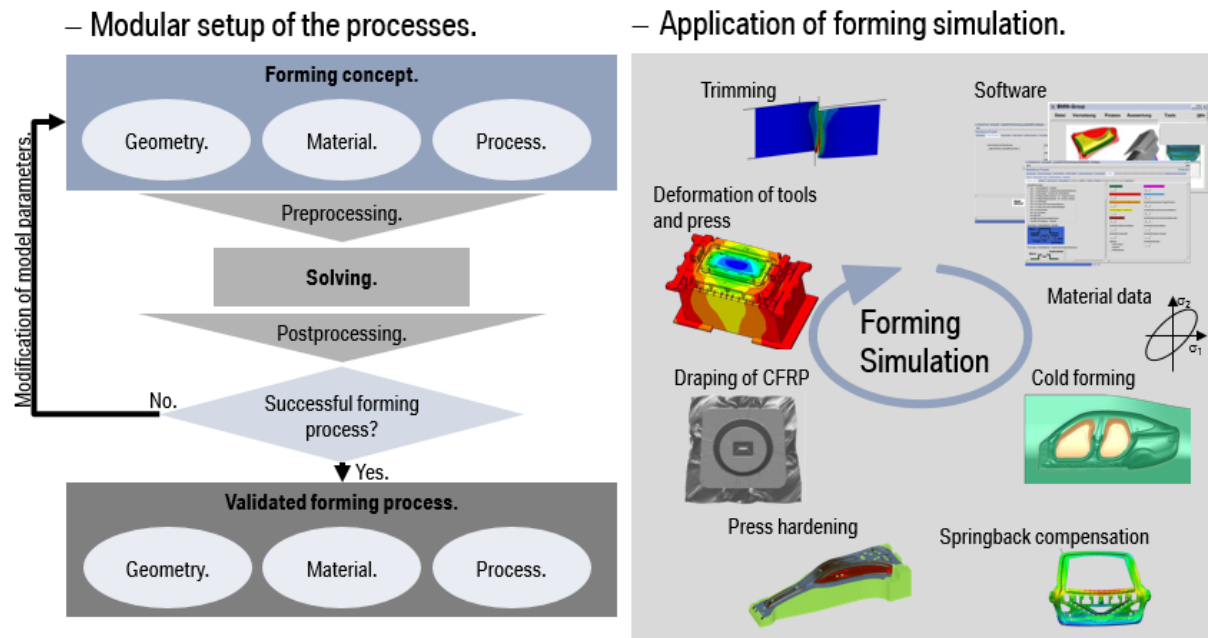


Fig.2: Software concept – [5].

This kind of simulation is used in a lot of cases in the engineering process, whereas cold forming simulation of automotive body parts is fundamental. After the cold forming simulation, the tools are springback compensated to reduce the final deviation from the target geometry. Further applications are indirect press hardening [13], draping of CFRP [14,15], calculation of the deformation of tools and the press at the end of the forming operation and the trimming.

2.3 Assumptions and limitations

The state-of-the-art simulation models for sheet metal forming have a lot of assumptions and restrictions. For example, assuming all the tool surfaces as well as the whole press as a rigid body, the simplification of the displacement curve for the punch, the evaluation of necking and fracture with the FLD – limited to linear strain paths and flat geometries, etc.

3 Current developments

In the following, an overview on four possible approaches improvement for accuracy and speed is given.

Having rigid tools is a state-of-the-art modelling procedure for the tool surfaces. An example of a fender is shown, where the blankholder is modelled as an elastic part. Due to this elastic behavior, we can see a direct possibility to influence the springback of a first drawn part. There are different ways which have been investigated, e.g., elastic modelling of the whole press-system or elastic modelling of just some tools.

The assumptions in the theory of shell elements [12], can be reduced by using solid elements for the sheet metal blank. In flat areas, we will not gain a better prediction for the drawing operation. But e.g., in sharp radii, the theory for shell elements is not any more valid. Therefore, we use solid elements for discretizing the door-handle geometry and we enhance the model with the ability for 3D flow rules. With solid elements, and in sharp radii, an FLD is no longer useful. Fracture models [10] for the material are a good choice to model the material behavior. One more strategy is to enhance the shell elements with less assumptions and increase the accuracy inside the finite elements itself. [18].

A few years ago, we published the “one input deck” strategy [8] – a way to model all 4 physical disciplines in an object orientated input deck structure that is easy to enhance. This was inspired by LSTC’s one code strategy. [19]. Coupling the structure and the thermomechanical problems like indirect press hardening is state of the art. A first prototype of a b-pillar is shown where the model was enhanced with a water-cooling system and coupled with fluid-dynamics simulation [20].

At the end, the improvements in simulation time with LS-DYNA [9] R12 vs R9.3 are shown on 3 sideframes. A time reduction of ca. 50% is possible with models that use h-adaptivity.

4 Summary

Shell element, rigid tools and the FLD have been state of the art for more than 10 years in evaluation of the forming simulation for the sheet metal blanks. In this presentation, some approaches that can enhance the simulation accuracy have been shown to benefit with better predictions. The next step is the implementation of these methods in a standard engineering process.

5 Literature

- [1] Livermore Software Technology Corporation, LS-DYNA KEYWORD USER'S MANUAL VOLUME I R12, 2020.
- [2] Meinhardt, J., Lipp, A., Ganser, M., Fleischer, M., Aspekte der Simulation Blechumformung im industriellen Umfeld, LS-DYNA Forum 2007, Deutschland.
- [3] Meinhardt, J., Lipp, A., Fleischer, M., Neue Prozesse im Bereich Simulation Blechumformung, LS-DYNA Forum 2009, Deutschland.
- [4] Fleischer, M., Panico, T., Meinhardt, J. Lipp, A., Anwendung der Simulation in der Technologie Umformen, LS-DYNA Forum 2011, Deutschland.
- [5] Fleischer, M., Lipp, A., Meinhardt, J., Hippchen, P., Heinle, I., Ickes, A., Senner, T., Usage of LS-DYNA in Metal forming, Europäische LS-DYNA Konferenz 2015, Deutschland
- [6] Fa. GNS, OpenForm, Europäisches LS-DYNA Forum 2013, England.; www.gns-mbh.com
- [7] Fleischer, M., Sarvas, J., Grass, H., Meinhardt, J., Umformsimulationen, Schnittstellen und Prozesse, LS-DYNA Forum 2016, Deutschland
- [8] Fleischer, M., Sarvas, J., Grass, H., Meinhardt, J., Forming simulation, meta language and input decks, LS-DYNA Conference 2017, Austria
- [9] <http://lstc.com/>, 2022
- [10] Livermore Software Technology Corporation, LS-DYNA KEYWORD USER'S MANUAL VOLUME 2 Material Models R12, 2020.

- [11] Livermore Software Technology Corporation, LS-DYNA KEYWORD USER'S MANUAL VOLUME 3 Multi-Physics Solvers R12, 2020
- [12] BELYTSCHKO, T., LIU, W.K., MORAN, B., Nonlinear Finite Elements for Continua and Structures. Wiley, 2008
- [13] Hippchen, P., Merklein, M., Lipp, A., Fleischer, M., Grass, H., Craighero, P., Modelling kinetics of phase transformation for the indirect hot stamping process, Key Engineering Materials, Vol. 549, pages 108-116, 2013
- [14] Senner, T., Kreissl, S., Merklein, M., Meinhardt, J., Lipp, A., A modular modeling approach for describing the in-plane forming behavior of unidirectional non-crimp-fabrics, Production Engineering, Volume 8, Issue 5, pp 635–643, October 2014
- [15] Senner, T., Kreissl, S., Merklein, M., Meinhardt, J., Lipp, A., Bending of unidirectional non-crimp-fabrics: experimental characterization, constitutive modeling and application in finite element simulation, Production Engineering, Volume 9, Issue 1, pp 1–10, February 2015
- [16] Wagner, M., Lineare und nichtlineare FEM, Springer Verlag, 2017
- [17] Birkert A., Haage, S. and Straub. M., Umformtechnische Herstellung komplexer Karosserieteile: Auslegung von Ziehanlagen. Springer, 2013.
- [18] Willmann, T., Bieber, S. Bischoff, M., Nonlinear Poisson Stiffening Effects in 3d-shell Models, WCCM-Konferenz, 2022
- [19] Hallquist, J., Recent Developments and Roadmap, 12th international LS-DYNA User's Conference, Detroit, 2012
- [20] Paramasivam, N., Modelling of the Thermo-mechanical Behaviour of the Deep Drawing Tools and Blank Sheet under Cyclic Loading in Production, Masterarbeit, RWTH Aachen, 2022.

Analysis of Global Sensitivities for One-Step and Multi-step Deep-Drawing Simulations

Tobias Lehrer^{1,2}, Arne Kaps², Tobias Daiminger¹, Ingolf Lepenies³,
 Marcus Wagner¹, Fabian Duddeck²

¹OTH Regensburg, Galgenbergstraße 30, 93053 Regensburg, Germany

²Technical University of Munich, Arcisstraße 21, 80333 Munich, Germany

³SCALE GmbH, Pohlandstraße 19, 01309 Dresden, Germany

1 Motivation

In practical use cases, simulation engineers are confronted with uncertainties in the simulation parameters. Normally, trust in a model is built from experience, practical assumptions, and parameter studies. This approach, though, is based on the assumption that few parameter combinations are sufficient to represent the whole design space. This lacks an appraisable mathematical basis.

To get insights into which parameters most strongly affect the results, a global sensitivity analysis can be conducted [2, 3]. The results are utilized to rank the most influential parameters and to filter less relevant ones. This gives feedback which improved set of input data will lead to more certainty in the simulation results. To enable this in the framework of multi-fidelity analysis and optimization, we compare here global sensitivities and uncertainties of the implicit One-Step approach (low-fidelity) with those of the explicit multi-step deep drawing approach (high-fidelity).

2 Simulation Models

Both simulation schemes regarded here share the same material model and boundary conditions. While the One-Step simulation works solely with the final part geometry and periphery nodes to represent the drawbead influence, the deep-drawing simulation is built with a die, punch, blank mesh, and slave node sets as drawbead geometry. The tooling and final part geometry share the same base parameters (e.g. die radius), see Fig. 1.

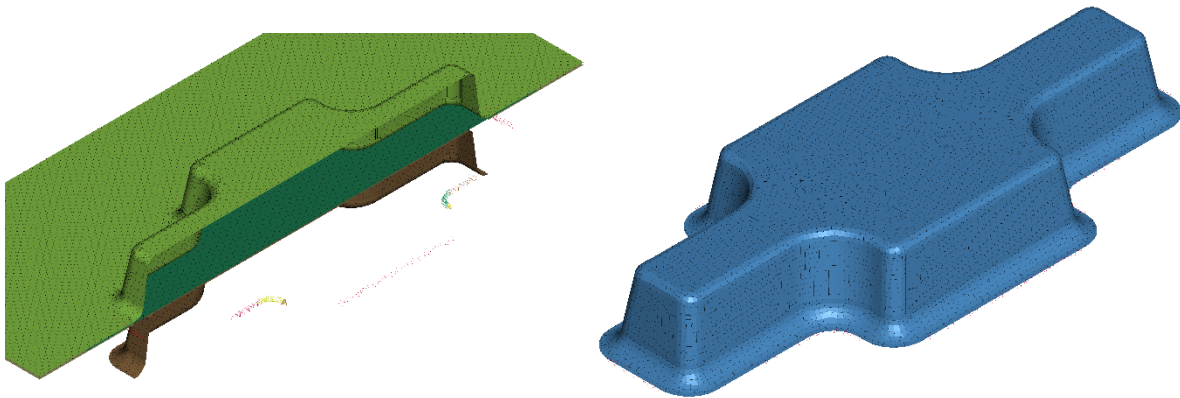


Fig. 1: Simulation setups for the multi-step deep drawing simulation (left) and the One-Step simulation (right).

3 Sensitivity and Uncertainty Analysis

As shown in Table 1, we investigate geometry parameters in cross-die tool examples, material parameters including hardening, as well as process parameters. The global sensitivities are calculated on the foundation of a Saltelli-extended Sobol sequence with respect to plastic strain [1]. We compare the sensitivity indices between One-Step and multi-step deep drawing simulation per design variable. In addition, we rank the sensitivities and analyze patterns for geometry, material, and boundary condition subdomains.

Table 1: Overview of parameters regarded in the sensitivity and uncertainty analysis

geometry	material	boundaries
sheet thickness	Lankford coefficient	coefficient of friction
slant depth	yield strength	blankholder force
die radius	Considère strain	drawbead cover ratio

4 Conclusion

To conduct global sensitivity analysis for One-Step or multi-step deep-drawing simulations with Sobol indices with multiple design variables, one needs to calculate several thousand numerical simulations for technical reliable confidence intervals. Hence, it is advantageous to combine sensitivity information from highly efficient low-fidelity models with those from cost-intensive high-fidelity simulations.

5 Literature

- [1] Herman, J. and Usher, W.. "SALib: An open-source Python library for Sensitivity Analysis". In: The Journal of Open Source Software 2.9 (2017), p. 97. doi: 10.21105/joss.00097.
- [2] Saltelli, A. ; Annoni, P.; Azzini, I. ; Campolongo, F. ; Ratto, M.; Tarantola, S. "Variance based sensitivity analysis of model output. Design and estimator for the total sensitivity index". In: Computer Physics Communications 181.2 (2010), pp. 259–270. issn: 00104655. doi: 10.1016/j.cpc.2009.09.018.
- [3] I.M Sobol'. "Global sensitivity indices for nonlinear mathematical models and their Monte Carlo estimates". In: Mathematics and Computers in Simulation 55.1-3 (2001), pp. 271–280. issn: 03784754. doi: 10.1016/S0378-4754(00)00270-6.

3D-Shell Elements for Improved Prediction Quality in Sheet Metal Forming Simulations

Maximilian Schilling¹, Tobias Willmann¹, Manfred Bischoff¹

¹ Institute for Structural Mechanics, University of Stuttgart
 Pfaffenwaldring 7, 70550 Stuttgart, Germany
 {schilling; willmann; bischoff}@ibb.uni-stuttgart.de

1 Introduction

For most sheet metal forming simulations Reissner–Mindlin shell elements are employed. These elements are based on the assumptions of zero transverse normal stress and cross-sectional material fibers remaining straight during deformation. However, for some critical applications, like bending with small radii or forming of thick sheets, this approach is not feasible, since warped cross-sections and a highly non-linear strain distribution in thickness direction can occur [1]. In those cases, the impact of the mentioned assumptions on the prediction quality can be significant. One approach to improve the prediction quality is to discretize the sheet metal with so-called higher order 3D-shell elements. These elements allow for cross-sectional warping and a higher order strain distribution with respect to the thickness coordinate [2].

In this contribution, we evaluate the results from a variety of simulations of critical forming processes. For this purpose, the stress and strain in higher order 3D-shell elements are studied in comparison to results from solid elements and various Reissner–Mindlin shell elements (Shell2, Shell6, Shell16). The solution with a fine mesh of solid elements will serve as the numerical reference solution. Lastly, computational efficiency of these formulations is also compared.

2 3D-shell element

The 3D-shell element utilized for the simulations in this contribution allows for cross-sectional warping and a strain field up to third order with respect to the thickness coordinate. This element is denoted as 3DBM-13. Figure 1 illustrates various components of the deformation.

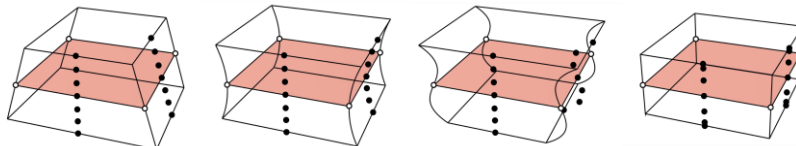


Fig. 1: Visualization of the deformation modes of 3DBM-13 including (from left) linear, quadratic, cubic deformations of cross-sectional fibers and a cubic strain field in thickness direction.

The assumed natural strain method is employed in order to prevent transverse shear locking [3]. More detailed information on 3DBM-13 can be found in [2]. In extension to this element formulation, in-plane shear locking and in-plane volumetric locking are prevented using reduced integration and hourglass control, Poisson thickness locking is prevented using the Enhanced Assumed Strain Method [4].

3 Evaluation of numerical tests

3.1 Tensile test of a thin sheet

In-plane locking effects impaired the analysis of tensile tests in [2]. As these are mitigated in this contribution, we can analyze differences in the prediction quality for tensile tests. These are critical as a three-dimensional strain state occurs after the beginning of necking of the specimen. For this a thin tensile specimen is subjected to a homogeneous Dirichlet boundary condition on the left side and an inhomogeneous Dirichlet boundary condition on the right side.

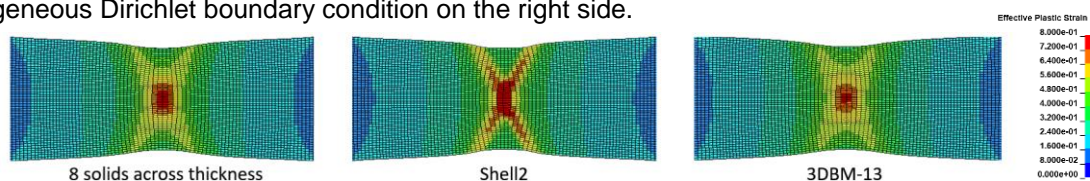


Fig. 2: Effective plastic strain for a tensile test of a thin sheet at the beginning of necking.

Figure 2 shows that the effective plastic strain in the tensile test specimen at the beginning of necking predicted by 3DBM-13 coincides much better with the reference solution than the results obtained with Shell2. Further analysis shows that for 3DBM-13 the stress in thickness direction of the sample are also closer to the reference solution.

3.2 Bending test of a thick sheet

One example of bending with small radii is a three-point bending test of an initially flat, thick sheet metal strip as shown in Figure 3. The middle loading pin is subjected to an inhomogeneous displacement boundary condition while the two outer supporting pins are fixed.

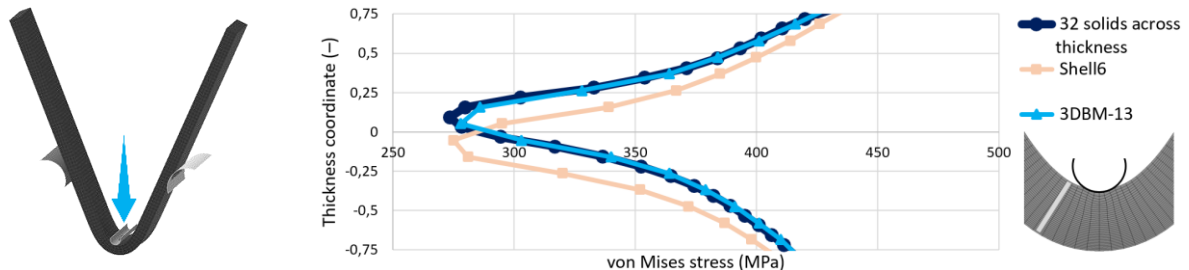


Fig.3: Three-point bending test (left) and von Mises equivalent stress in thickness direction (right).

Figure 3 indicates that 3DBM-13 is capable of predicting the equivalent stress across the sheet thickness near the punch closely to the reference solution, which is not the case for Shell6. This holds for all stress components and is an additional advantage to the superior geometry approximation [2].

3.3 Comparison of numerical efficiency

In order to make the element suitable for industrial applications, the performance of the element was improved by a more efficient implementation and using reduced integration. To measure the performance improvement, the computing time for 5000 time steps of a tensile test simulation is compared.

	3DBM-13 (from [2])	3DBM-13 (improved)	5 solids across thickness	Shell16
Abs. time in s / rel. time compared to solids	966 / 4830%	27 / 135%	20 / 100%	6 / 30%

Table 1: Comparison of computing time for 5000 timesteps of a tensile test simulation

Table 1 shows that the computing time for the improved 3DBM-13 element is in the order of magnitude of the computing time for five solid elements across the thickness of the tensile specimen and therefore in a range that is suitable for industrial applications.

4 Summary and Outlook

The improved prediction quality of a higher order 3D-shell element for stress and strain in sheet metal forming simulations is demonstrated. Results from numerical tests indicate that the element is able to represent the behavior in critical sheet metal forming simulations better than Reissner–Mindlin shell elements. The efficiency of the element is improved in order to achieve a computing time suitable for industrial applications. Further efficiency improvements are possible by applying mass scaling to the higher order degrees of freedom [5] and an improved time step estimation for the 3D-shell element [6]. The project was funded by the German Ministry for Economic Affairs and Climate Action based on a decision of the German Bundestag as IGF project no. 21466 N. This support is gratefully acknowledged.

5 Literature

- [1] Fleischer, M: “Absicherung der virtuellen Prozesskette für Folgeoperationen in der Umformtechnik”, Dissertation, Technische Universität München, 2009
- [2] Willmann, T., Wessel, A., Beier, T., Butz, A. und Bischoff, M.: “Cross-Sectional Warping in Sheet Metal Forming Simulations”, 13th European LS-DYNA Conference, 2021
- [3] Bathe, K.J., Dvorkin, E.N.: “A formulation of general shell elements – The use of mixed interpolation of tensorial component”, Internat. Journal for Numerical Methods in Engineering 22, 1986
- [4] Simo, J., Rifai, M.: “A class of mixed assumed strain methods and the method of incompatible modes”, International Journal for Numerical Methods in Engineering 29.9, 1990, p. 1595-1638
- [5] Research project “Verbesserte Blechumformsimulation durch 3D-Werkstoffmodelle und erweiterte Schalenformulierungen – Teil 2“, EFB 06/219, AiF 21466N
- [6] Willmann, T., Schilling, M., Bischoff, M.: “Data-driven analysis of LS-DYNA's time step estimates and a machine learning based estimate”, 16th LS-DYNA Forum, 2022

Recent Developments in Dynaform

J. Chen (eta)

Oil Flow and Cooling Analysis using Incompressible SPH

Edouard Yreux¹, Satish Pathy¹

¹Ansys, Inc.

Lubrication and thermal management of various mechanical devices relies on an oil flow around rotating and reciprocating parts. Due to the intricate nature of many of these devices, instrumentation and gathering of experimental data are difficult to achieve. However, analyzing the oil flow under various operating conditions is critical to optimize the performance of these devices in terms of lubrication, cooling, churning loss, etc. While numerical simulations can help evaluate and improve performance of a particular design, the rapid motions of the structures can be challenging for traditional CFD methods. Particle methods such as incompressible Smoothed Particle Hydrodynamics offer an interesting alternative.

In this presentation, we will study two industrial problems to illustrate the current capabilities of the incompressible SPH solver in LS-DYNA: A gallery-cooled piston in a diesel engine, and a gearbox lubrication study. A new workflow allowing to import geometries directly from Ansys SpaceClaim or other CAD handling software will be presented, eliminating the need for time-consuming FEA mesh generation. CAD geometries can be exported in the OBJ format, and imported directly within LS-DYNA using the `*DEFINE_SPH_MESH_OBJ` keyword. A new preprocessing tool will also be introduced, that can easily be parametrized to consume various OBJ geometry files. It will create a regular distribution of surface particles on the provided structures, generate parent rigid LS-DYNA parts, and attach OBJ geometries to these LS-DYNA parts. The tool then automatically creates LS-DYNA input files that contain all the relevant information for analysis. Fluid-Structure Interaction is handled directly within the SPH solver without the need for any contact setup, while the structural motion is prescribed with the usual LS-DYNA keywords.

While the geometry described in the OBJ files is not created as an LS-DYNA part in the input file, it can nonetheless be visualized in the *d3plot* results. Massflow sensors and vicinity sensors can be employed to monitor how much fluid goes through specific areas or gets in close proximity to specific parts. This information is then accessed through the *binout* file. An SPH interface file can also be created to visualize instantaneous wetness, accumulated wetness, coupling forces or instantaneous Heat Transfer Coefficient values. Time-averaged Heat Transfer Coefficient values can also be requested and can be output in a profile-file format that can be used in subsequent thermal analysis in Ansys Fluent or Ansys Mechanical. Finally, Ensight provides an easy solution to represent SPH particles as a continuous fluid without expensive free-surface reconstruction.

LS-DYNA Structured ALE Recent Progresses

Hao Chen

Ansys LST

1 Introduction

LS-DYNA ALE has been widely used to simulating moving fluids interacting with structures. Unlike CFD, the focus is rather on the structure response under dynamic loading from fluids, than the fluids' motion. Fluids are agitated by a high pressure gradient; and then hit the structure, carrying a large momentum. The key in successfully capturing the physics lies in the fluid-structure interaction algorithm. It needs to accurately predict the peak of pressure loading during the impact, which is characterized as a momentum transfer process. This request could only be fulfilled by a transient analysis with a penalty-based coupling between fluids and structure.

In 2015, LSTC introduced a new structured ALE (S-ALE) solver option dedicated to solve the subset of ALE problems where a structured mesh is appropriate. As expected, recognizing the logical regularity of the mesh brought a reduced simulation time for the case of identical structured and unstructured mesh definitions.

During the past years, effort has been made to expand the capability, improve the stability, enhance the efficiency. New features have been added; existing ones improved, either with a reduced running time or a less memory usage, or both. And more importantly, all developments aim to achieve an user-friendliness to reduce, if not eliminate, the long time compliants on error-prone ALE setups.

This presentation, first gives a brief description on the renewed S-ALE model setup process. Next on the new FSI keyword `*ALE_STRUCTURED_FSI`. And then some recently added features are described.

2 S-ALE model setup

Three step setup We follow a straight-forward three step setup. First, mesh; secondly, material properties of fluids; thirdly, filling the mesh with fluids. In this section, we describe the three keywords doing these three steps.

1. Mesh generation: `*ALE_STRUCTURED_MESH`
2. Material definitions: `*ALE_STRUCTURED_MULTI-MATERIAL_GROUP`
3. Volume Filling: `*ALE_STRUCTURED_MESH_VOLUME_FILLING`

One thing worth a special note here is that, in material step, PART definitions are dropped. And in return, model setup becomes much more conceptually clear. And referring AMMGs by strings rather than IDs reduced the chance of potential input mistakes greatly.

<code>*ALE_STRUCTURED_MULTI-MATERIAL_GROUP</code>							
<code>AMMGNM</code>	<code>MATID</code>	<code>EOSID</code>					<code>PREF</code>
Rod	1	1					0.0
Air	2	2					101325.0
Plate	3	3					0.0

3 S-ALE FSI keyword: `*ALE_STRUCTURED_FSI`

The major advantages of the new keyword, are:

1. Automate Everything:
 - All parameters are internally calculated, automatically chosen.
 - PFAC: Penalty stiffness is the only one users need to pick.
 - Automated Leakage control
 - Eroding option always on
 - Edges automatically generated and on
2. Better Performance:
 - Enhanced Leakage Control
 - Stable, Faster
3. MPP efficiency greatly improved; Nonblocking, Groupable MPP

*ALE_STRUCTURED_FSI							
LSTRSID	ALESID	SSTYP	ASTYP				MCoup
		PFAC			IFLIP		

4 New features

4.1 Mesh Trimming

S-ALE mesh needs to be regular, box-shaped. Elements far away from our point of interest not needed. The solution is to trim the S-ALE mesh at places irrelevant to the simulation to save the cost. The cost saving could be significant as the cost is proportional to the number of elements.

4.2 Mesh Motion

1. Symmetric Plane: ISYM → Set symmetric plane(s) to control S-ALE mesh motion.
2. Mesh expansion to cover Lagrange structure: COVER_LAG → to make the mesh follow the motion of a Lagrangian structure and expand/contract so that the Lagrangian structure is fully covered in the S-ALE mesh. It is most useful to model airbag deployment.

4.3 Enhanced Leakage Control in FSI

*ALE_STRUCTURED_FSI comes with a much better leakage prevention. It is achieved through the following improvements:

- Much more accurate at capturing fluid interface
- Not only process structure segments, but also edges, nodes.
- Enhanced leakage control algorithm
 - Better estimation of spring stretch
 - Innovative algorithm to achieve energy balance
 - New algorithm is order-free → more stable
- New MPP implementation (order-free calculation) → more stable

4.4 Added Thermal support for S-ALE

TOPAZ only supported ELFORM 5 and ELFORM 12 (single material with void). As heat capacity and thermal conductivity matrices only allows for 1 material per element. Now for S-ALE, we have an additional loop through each ALE multi-materials. FSI thermal support also added, to allow heat exchanges between fluids and structure (*CLIS, for now).

5 Resources

Example model input decks: https://ftp.lstc.com/anonymous/outgoing/hao/sale/models_R121/

Tutorials: <https://ftp.lstc.com/anonymous/outgoing/hao/sale/tutorials/>

Recent Developments in WB LS-DYNA

E. Plugge (Ansys)

Transitioning LS-DYNA workloads to the Cloud in the path to Digital Maturity

Iago Fernández¹, Daniel Dorribo¹

¹Gompute, Gridcore AB (Gothenburg, Sweden)

Abstract

Industries worldwide are going through a Digitalization process towards industry 4.0 where cloud resources play a key role, forcing a transition for CAE engineers from traditional, in-house HPC to more flexible solutions in the cloud.

On the digital maturity journey there are different dimensions to consider when transitioning a CAE team to the cloud as a permanent solution, being the needs and requirements of the different industries not always covered with a single solution, what requires an analysis of the different layers involved (IT/Network, Licensing, Security, Engineering).

Firstly, the Gompute team will cover an overview of the different options available in the market, and how those can be deployed for LS-Dyna users based on their needs. Secondly, the most important dimensions that any corporation will require on this transition: Performance and Security, for what Gompute will show the scalability results of LS-Dyna on different hardware types, and the most common set-ups to guarantee data protection both from on-premise or home offices.

1 Digital Maturity, Digital transformation and Cloud adoption

In order to define the role of Cloud adoption, we need to define what is “Digital Maturity”. There is not a single definition on the literature, but a common root in most of them is: “The capacity of an organization to adopt and take advantage of the digital technologies available”. Digital transformation, as part of the path to achieve Digital Maturity, is defined as “the application and use of modern technologies in the organization’s business processes to achieve its goals and increase efficiency” [1].

1.1 Company nature

As defined in Martec’s law, technology advances exponentially (Moore’s law) while organizations change logarithmically. This is setting up a challenge for organizations to absorb changes, so the gap trend to widen over time, and sometimes a organization “reset” is required, making it a complex process to achieve Digital Maturity [2].

Digitalization is just on the roots of any Startup or young company, being part of the company culture, while for multi-cultural companies operating over decades this is not a trivial task, with difficulties being directly proportional to the level of complexity of the organization, specially on large conglomerates result of merges and acquisitions, carrying legacy thinking and behavior, where implementing a digital transformation strategy adoption requires a special planning with longer timeframes than any smaller or homogeneous entity [3].

Any cataclysm event like the 2020 COVID-19 crises has speed-up digital transformation in most corporations, removing lots of barriers (budgetary, bureaucracy, time...) and becoming a priority in the general management agendas.

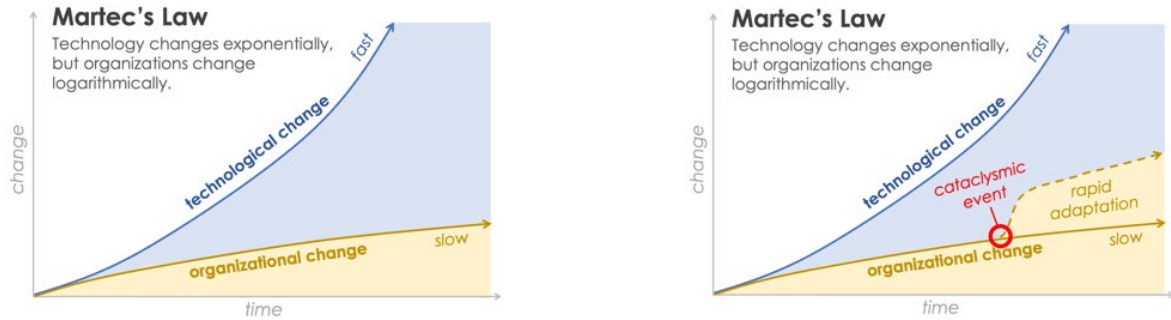


Fig.1: Martec's Law representation. On the right, including a cataclysmic event like the COVID-19 Pandemic. Source: Brinker S.

1.2 Cloud adoption

Cloud adoption is just a small part of the digital maturity journey of any organization, but a challenge for those Engineers that need to move CAE workloads. A real High-performance computing solution is required in order to reduce total simulation time and make the most out of the pre-invested software licenses.

When talking about HPC for CAE, different cloud models are available in the market, in order to fit the different company types. The alternatives can be classified based on different criteria, being the location of the resources the most common one. HPC cloud for CAE can be divided then in 4 main blocks:

In-house / Enterprise cloud	Hybrid cloud	Private cloud	Public cloud
Cloud is mounted on internal company systems, centralized on one or few sites.	An in-house cloud complemented with a private or Public cloud	HPC resources are located on a certain datacenter, with exclusive use of the enterprise during the contract period	General access cloud resources, mounted on multi-location providers.

Table 1: HPC Cloud types based on hardware location.

When moving to one of the options listed in Table 1, there are different criteria to choose one of the options in the list, summarizing:

- Data location: Company policies or end customer restriction might force enterprises to run in-house.
- Ownership and data management: Due to project or NDA regulations, in these cases Public cloud is not an option.
- Budgetary structure: Specially on large enterprises with subsidiaries managed by OPEX and CAPEX, owning hardware or part of it could be a requirement. A private cloud option sometimes fits, as all costs can be pre-defined.
- Management of internal resources: When an IT team is not available, external resources look like a more viable option.
- Electricity and hosting infrastructure: When the use of simulation grows, more space and power is needed. Allocating a space for this is not an option on certain locations, forcing companies to go for a private or Public cloud.
- Fluctuating needs: For those enterprises working per-project with a variable workload, there is a clear adaptation to pure cloud models.

As can be seen, several of the above listed options depend on legal or administrative requirements. During the last years and thanks to the pandemic push, there is a trend to change rules and make the move to the cloud easier for the end users.

2 Moving LS-DYNA loads to the cloud

There are 2 main decisions to take when moving the local simulations to any of the defined cloud options:

2.1 Performance

Performance of the simulation can be defined by the total time a simulation takes compared to a previous workflow (engineering performance), or the total elapsed time on the simulation run. In the first, the capacity of remote pre-post processing is key, so users just need to upload a CAD file and then the whole mesh can be created in the cloud.

For simulation performance of LS-DYNA, the next criteria need to be evaluated when choosing a certain hardware:

- Generation of the architecture: Vendors have different architectures available, that must be evaluated. A discounted price on a previous generation can offer the users to get more cores within a certain budget, sometimes sacrificing a small percentage in performance per core.
- Number of cores per node: The scalability and model sizes need to be evaluated in different architectures, always checking the license restrictions.
- Virtualization or bare-metal nodes: Virtualization might affect final simulation performance, so a bare-metal configuration is always preferred.
- Interconnect: When running multi-node, a fast interconnect is required in order to keep the scalability.
- Tuning: The installation and configuration needs to be tested and adjusted for a certain hardware type in order to get maximum performance.

Users must note that there is always a price driver on the decision making, so price-performance is one of the measuring units when evaluating a certain option.

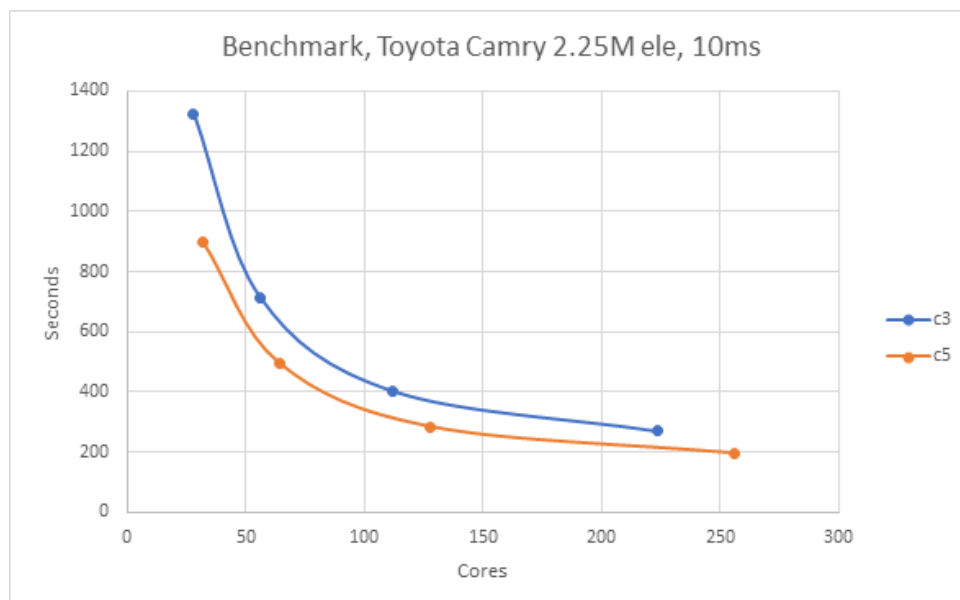


Fig.2: Benchmark representation on C3 nodes (Intel E5-2680v4) and C5 nodes (Intel Gold 6242).

2.2 Security and connectivity

Nowadays many psychological barriers on the cloud being insecure have been removed, and providers have options that can be customized to be an extension of the enterprise internal IT. In those cases where sensitive data is managed, having a dedicated file server is a preferred option, then a private cloud is usually a preference over a public cloud.

Direct	IP-Restricted	VPN	Private line
Access is available over the internet.	Only certain IPs can access the service. For users on home-office a static IP is required.	Customer enterprise is connected to the resources on a VPN. Users working from home need a VPN to their company to access the service.	Customer is accessing the service directly. Is the best-performing solution, price depends on distance to the data center.

Table 2: Connectivity options.

From the connection options, nowadays having a private line is becoming a popular solution when there is a decent amount of users, and the solution is available for a mid-long term due to the initial installation costs.

LS-DYNA requires a license to run, so the connection of a license server must be evaluated. Cloud hosting partners are allowed to host also the license on a cloud license server, but when users prefer to have a local license server installation, is required a stable connection to the cloud service.

3 Summary

Nature of the enterprise will be a key decision maker on the cloud model chosen, but in all cases a true HPC system is required when moving LS-DYNA workloads. Having remote visualization is a plus, as reduces the amount of data transferred, and opens the possibility to eliminate local storage of simulation databases, more than regular input files for back-up.

4 Literature

- [1] Aslanova, I.V., Kulichkina, A.I.: "Digital Maturity, Definition and Model", Advances in Economics, Business and Management Research, volume 138
- [2] Brinker, S. "Martec's Law: Technology Changes Exponentially, Organizations Change Logarithmically." Chief Marketing Technologist (blog), June 13, 2013. <https://chiefmartec.com/2013/06/martecs-law-technology-changes-exponentially-organizations-change-logarithmically/>
- [3] Kupilas, K., Montequín, V. & Álvarez-Pérez, C. & Balsera, J (2021). Industry 4.0 and Digital Maturity, Chapter 2.

Enabling Performance Isolation for LS-DYNA in Multi-Tenant Supercomputing Platforms

Gilad Shainer, [Ophir Maor](#), David Cho, Gerardo Cisneros-Stoianowski, Scot Schultz

HPC-AI Advisory Council

1 Abstract

High-performance computing has evolved to be the primary data processing engine for wide research and commercial use. The supercomputing platforms hosting HPC applications need to support a growing number of users and jobs and therefore designed for multi-tenancy. HPC applications, such as LS-DYNA or other scientific simulations demand extremely low communication latency and multi-process synchronizations. In an environment hosting multiple concurrent simulation jobs, each job may interfere with another job's performance as they all share the same interconnect infrastructure. This causes a significant difference in the simulation run time. New performance isolation features introduced in the NVIDIA Quantum InfiniBand network platform can provide predictive performance by ensuring that one job cannot impact another job's performance.

LS-DYNA is a general-purpose finite element program used to simulate complex real-world problems in the areas of automobile, aerospace, construction, military, manufacturing, bio-engineering, and more industries. This paper will review the InfiniBand performance isolation technology and its impact on LS-DYNA in a multi-tenant / multi workload supercomputing environment.

2 InfiniBand Performance Isolation

The heart of a supercomputer is the network that connects the compute elements together, enabling parallel and synchronized computing. InfiniBand, an industry standard developed in 1999, continues to show a strong presence in the high-performance computing market. It is deployed in many of the world's leading supercomputers based on the TOP500 supercomputer list. As a standards-based interconnect, InfiniBand enjoys the continuous development of new capabilities, better performance, and scalability.

The latest InfiniBand generations introduce a new element for performance isolation. Performance isolation aims to solve the negative performance impact between concurrent jobs sharing the same network. As examples, one job can cause network congestion due to path sharing, or many data sources to single data target (aka many-to-one), are cases which can delay data movement for other jobs sharing the same network. HDR and NDR InfiniBand include hardware-based performance isolation engines running on the InfiniBand adapters. These engines receive advanced telemetry information from the network – congestion and many-to-one indications from the network switches, data from round trip time sensors, and more. With this information, the performance isolation engines can control data injection rates of the network per job, and per destination, to ensure the ideal usage of the network, so that one job cannot negatively impact the network performance of another job.

Figure 1 showcases the InfiniBand performance isolation mechanism. The InfiniBand switches include a variety of sensors, such as congestion sensors and time sensors. The sensors' data, combined with congestion detection from the InfiniBand adapters, are being used to control the data injection rates into the network.

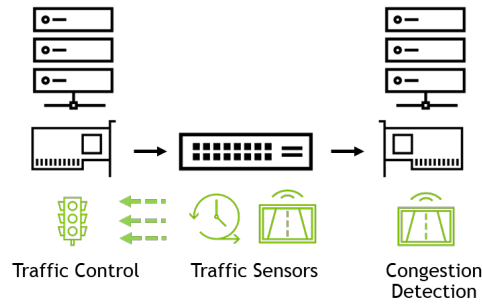


Fig.1: Illustration of InfiniBand performance isolation mechanism

3 LS-DYNA Performance with InfiniBand Performance Isolation

We have tested LS-DYNA performance in a multi-application / multi-tenant supercomputer platform comprised of 93 server nodes. The system hosted several workloads alongside LS-DYNA concurrently. We used the LS-DYNA '3cars' input and tested the following scenarios:

- LS-DYNA with 19 nodes, with the remaining 74 nodes in idle (Case #1)
- LS-DYNA with 19 nodes, with the remaining 74 nodes running different kinds of background applications, and InfiniBand performance isolation turned off (Case #2)
- LS-DYNA with 19 nodes, with the remaining 74 nodes running different kinds of background applications, and InfiniBand performance isolation turned on (Case #3)

Each case was repeated 60 times, and each time the nodes were selected randomly. The background applications included One-sided Remote Memory Access (RMA) $N \rightarrow 1$ incast and Alltoall network traffic patterns.

3.1 Cluster Setup

Hardware

- Compute - 93 servers
 - CPU: Intel Xeon E5-2697A v4 @2.6GHz (two sockets per node)
 - 256GB DDR4 2400MHz RDIMMs
 - NVIDIA ConnectX-6 HDR100 Adapter
- Network
 - NVIDIA Quantum InfiniBand two level network

Software

- Operating System: RHEL 7.6
- MLNX_OFED: 5.7-1
- Storage: NFS
- MPI: HPC-X v. 2.12
- LS-DYNA R.13.1
- Input: 3cars

3.2 LS-DYNA 3cars Performance Results

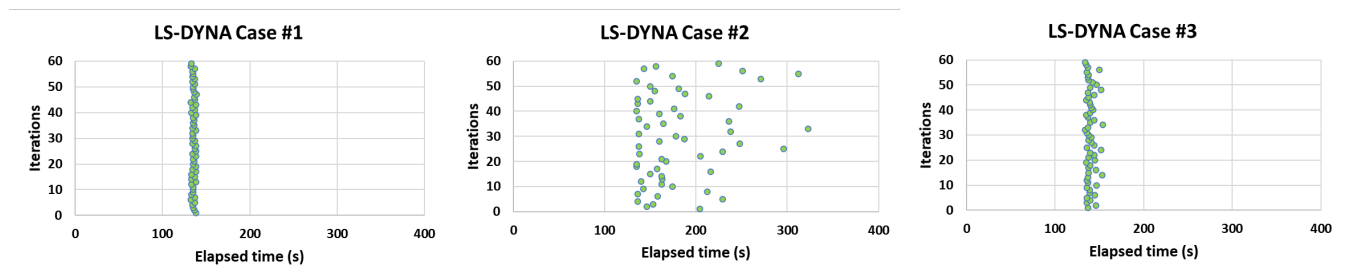


Fig.2: LS-DYNA 3cars performance results

As expected, the results of case #1 (no background application traffic) demonstrate the same runtime performance for each iteration. In case #2, with background application traffic, we can see the negative impact on the LS-DYNA runtime – each iteration resulted in a different performance outcome. In case #3, the InfiniBand performance isolation mechanism was enabled, nearly eliminating the negative effects of the additional background traffic, providing nearly the same performance results for each iteration.

4 Summary and Conclusions

Most supercomputers are required to simultaneously service multiple applications. The performance isolation technology in the InfiniBand network significantly reduces the performance impact of applications sharing the network concurrently. As a result, supercomputing administrators can guarantee performance, and therefore SLAs (Service Level Agreement), to their users.

In the future, we plan to repeat this testing on an NDR InfiniBand-based platform and review the results with the additional performance isolation capabilities included with that InfiniBand generation.

Drop Response Simulation of Balanced Armature Receivers for Hearing Aid and Professional Audio Applications

Mostafa J. Moghtader, Michele Colloca

Sonion Nederland BV, Hoofddorp, The Netherlands

1 Introduction

Balanced armature (BA) receivers are miniaturized loudspeakers used in applications where efficiency (battery life) and size are critical parameters, like hearing aid instruments, earphones and hearables. The armature (metal strip) is placed between two permanent magnets and a coil is wound around the armature. The armature tip is positioned exactly in the center between the magnets (balanced armature). Current through the coil will inject magnetic flux into the armature, setting it in motion. A drive pin connected to the armature on one end moves the membrane (diaphragm) on the other end producing sound [1]. In BA receivers, the mechanical failure of the armature where the magnetic motive force is converted into mechanical movement, needs to be prevented. Permanent deformations in the armature, will cause offsets between the magnets, hence significant levels of distortion or no sound amplification at all. During the transducer development, improving the reliability and robustness of BA receivers under shock and drop impacts has become a clear and significant goal for the developers in the audio and electronics industry [2].

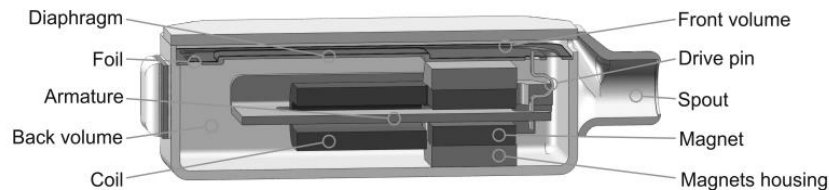


Fig. 1: Cross-sectional view of typical balanced-armature loudspeaker [1]

***KEYWORDS** balanced armature receiver, drop simulation, finite element method, transient analysis, hearing aid, earphone, hearable

2 Materials and Methods

In this simulation study, the nonlinear transient response of a typical BA receiver under drop load is predicted via the Ansys LS-Dyna software. The 3D FE model consists of case, cover, membrane, armature, drive pin, magnet housings, permanent magnets, bobbin and coil (Fig. 1). By exploiting the stress strain curves from experimental material testing, along with ANSYS Granta Materials Database inputs, the elastic-plastic material properties (multilinear and bilinear plasticity models) are adopted for all the transducer components except for magnets, bobbin, drive pin and coil. Effective plastic strains (EPS) and von Mises (VM) stresses in the transducer components are investigated in order to reveal the weak regions of the design and predict the failure mechanisms. Moreover, the amplitude and frequency of armature oscillations, as well as the contact forces between the back of the case and the ground are investigated to provide a better understanding of the drop response of the system.

3 Results and Discussion

The dynamic response of the receiver is investigated for different drop heights and angles to determine the worst case drop scenario (Fig. 2). The flat drop (angle of 0 degree with respect to the ground) is found to be the most severe drop situation (Fig. 2A). The regions of high stress and plastic strain concentrations in the armature are found to be around probe P1, P2 and P4 points (Fig. 2C & 2D). The flat drop of the receiver is further simulated for different drop heights. The gradual increase of the ground contact force and the plastic strains at probe points of the armature by increasing the drop height are shown (Fig. 2B-D). Another interesting investigation is related to the oscillations of the armature with respect to the magnets and the number of times the armature is in contact with one of the two magnets

(Fig. 2E & 2F), which can be used to improve the robustness of receiver by selecting shock absorbers. By increasing the drop height, the impact forces also increase and lead to higher frequency of the oscillations of the armature in the airgap.

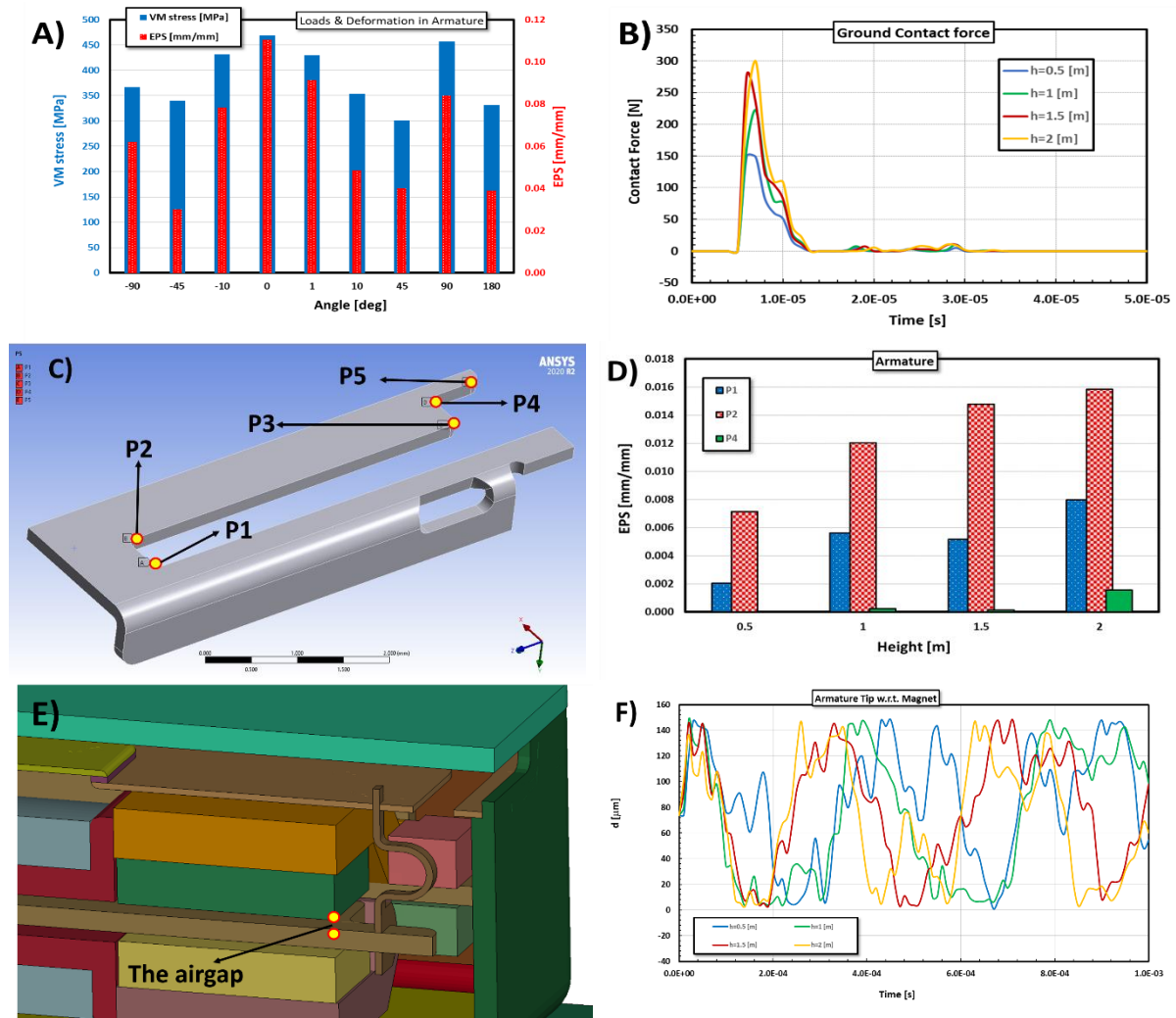


Fig.2: A: VM stress and EPS in the armature for different drop angles; B: ground contact force for different drop heights; C: probe points in the armature; D: EPS at probe points for different drop heights; E: distance between the upper surface of the armature and lower surface of the magnet (airgap); F: the evolution of the airgap over time.

4 Conclusions

The non-linear transient analysis shown in this study allows for identifying the regions of high stress and plastic strain concentrations in the armature and the potential failure modes of the device. In particular, the VM stress and EPS provide measures to compare loaded regions and plastic deformations in the armature for different drop heights, orientations, and designs. Furthermore, the oscillations of the armature between the two permanent magnets and the possible contact provide the developer with options on how to design shock absorbers as a countermeasure to improve the robustness and reliability of the receiver at early stages of the product development.

5 Literature

- [1] Jensen, J., "Nonlinear Distortion Mechanisms and Efficiency of Miniature Balanced-Armature Loudspeakers", Ph.D. thesis, Technical University of Denmark, 2014
- [2] Liu, Y., Qian, Q., Kim, J., & Martin, S. "Board level drop impact simulation and test for development of wafer level chip scale package", Proceedings 60th Electronic Components and Technology Conference (ECTC), 2010, 1186-1194, IEEE.

Development of Fall Strength Design Method for Portable Products

Yoshifumi Hasebe, Jun Morimoto

Toshiba Tec Corporation

1 Introduction

A product is required to have strength that does not break even if the user accidentally drops it. Especially, in the case of a portable product, we need to assume it would clash in various postures. For this reason, a strength design method is required that can predict the falling collision phenomenon and ensure strength even in the collision posture that is most likely to break it. Therefore, we have developed drop analysis using LS-DYNA® to evaluate strength considering various collision postures. As a result, we have been able to reduce the number of redesigns.

2 Development of drop analysis technology

2.1 Evaluation of damping factors

As shown in Fig.1, the strain in the second collision is added to the first one propagating with attenuation. So, depending on the collision posture, second one may cause more significant damage to a product than first one. In that case, we must simulate strength against not only first collision but also second one by using damping factors that express attenuation of strain.

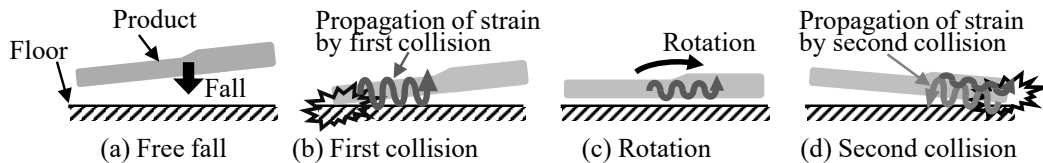


Fig.1: Phenomenon of oblique collision of a product

To represent attenuation simply in simulation, we selected Rayleigh damping that consists of two parameters; a mass damping constant α and a stiffness damping constant β . According to Wilson, the following empirical formula holds between α , β , the damping ratio ξ and the angular frequency ω ^{[1][2]}.

$$\xi = \frac{\alpha}{2\omega} + \frac{\beta\omega}{2} \quad (1)$$

We developed the original method of evaluating the constants by utilizing low frequency vibration test for α and high frequency vibration test for β ^[3].

2.2 Developing a pre-/post-processor function to detect postures that could break a product

To detect postures that are likely to break a product, we had to simulate many conditions of postures. In order to make many input data and evaluate many results automatically, we have developed new functions of the pre-/post-processor Jvision®^[4] for LS-DYNA®. GUI screen image is shown in Fig.2.

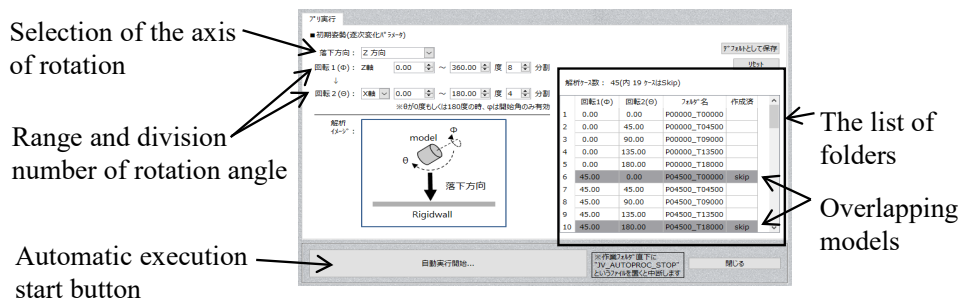


Fig.2: An example of GUI screen image of Jvision®'s pre-processor

3 Development of drop test technology

To let a product collide against the floor in the collision posture that might break it, we developed a drop tester that can control the posture. Fig.3 shows the structure and function of the tester^[5].

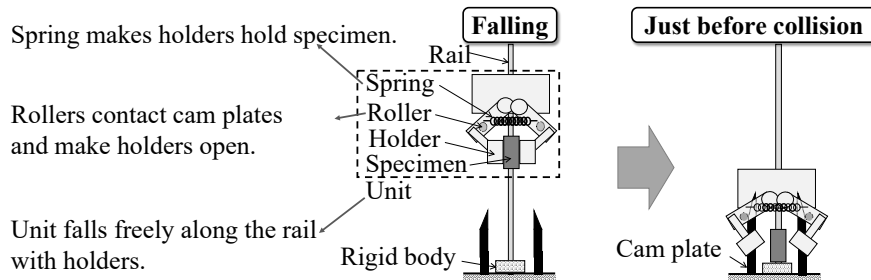


Fig.3: Structure and function of our drop tester

4 Application of simulation and test technology to product

Fig.4 shows a mobile printer to which we applied our simulation and test technology^[6]. A simulation was performed on 62 postures by using the developed pre-/post-processor, that made man-hours required for analysis reduced by 85% compared to the conventional method.

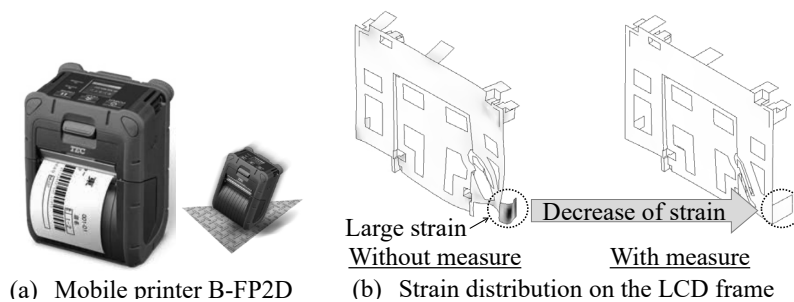


Fig.4: The product to which we applied our technology and the result of simulation

5 Summary

We developed the method of evaluating damping constants by utilizing high and low frequency vibration tests. In addition, by expanding the functions of the pre-/post-processor, it got possible to quickly evaluate the fall postures that could break a product and the strength of it. Furthermore, we developed an original drop tester. Toshiba Tec Corporation continues to apply these technologies to various products and provide highly reliable products to customers in a timely manner.

6 Literature

- [1] Wilson, E. L., "A Computer Program for the Dynamic Stress Analysis of Underground Structures," USAEWES, Contact Report No.1-175 (Jan.1968)
- [2] Washizu, K. and Miyamoto, H. and Yamada, Y., W., "Finite Element Method Handbook II Advanced Edition," BAIFUKAN (Jan.1983)
- [3] Nishimura, T. and Takahashi, F. and Morimoto, J., A study on Evaluation of Plastic Material Properties Against Impact Load for Molding of Outer Housings for Information Appliance Use, JSME International Journal, Series A, Mechanics and Material Engineering, Vol.66, No.641 (2000), pp.87–95
- [4] <https://www.jsol-cae.com/product/struct/jvision/feature/>
- [5] Morimoto, J. and Takahashi, F. and Tsushima, H., J., Drop Impact Test Apparatus, Japan patent 2002-174574
- [6] TOSHIBA B-FP Series (n.d.). Retrieved March 9, 2020 from https://www.toshibatec.com/cnt/products_overseas/printer2/mobile_printer/b-fp/

Drop Test Simulation of Short Fiber Composites with LS-DYNA in Ansys Workbench

F. Negri¹, S. Mendy¹, F. Pavia¹, S. Acharya¹, H. Mao¹, S. K. Meenakshisundaram¹

¹ANSYS, Inc.

1 Introduction

Drop impact performance is an important concern for the design of consumer devices. However, it is very expensive and time-consuming to conduct drop tests to experimentally detect the failure mechanisms and identify their drop behaviors. That is why finite element simulation is key to accurately capture drop impact behavior early in the design phase of the device. Here, we show a new Ansys Workbench workflow to simulate with LS-DYNA the drop impact of devices with injection molded short fiber reinforced components (for instance casings of electronics devices).

2 Short Fiber Composites Modeling in Ansys Workbench

Since release 2021 R1, a native workflow for the simulation of short fiber composites is available in Ansys Workbench. The workflow consists of three parts. First, using Ansys Material Designer homogenization technology, the anisotropic orientation-dependent elasto-plastic response of the composite material is characterized. Then, local fiber orientations, weld lines, and residual stresses predicted by the most popular injection molding tools (including Moldflow, Moldex3D, SIGMASOFT and CADMOULD) are imported into the Ansys Mechanical application, where they are mapped onto the structural model. Finally, the application combines and sends this data to the solver. While it first only supported the implicit Ansys MAPDL solver, the workflow has been recently extended to also support LS-DYNA. In the next sections, more details about the abovementioned steps are given.

2.1 Material Calibration in Ansys Material Designer

Modeling short fiber composites is particularly challenging because of their anisotropic, orientation dependent, and nonlinear behavior. To address this challenge, Material Designer combines micro-mechanical with phenomenological methods. Linear elastic and thermal material properties of the composite are obtained by homogenization using well established micro-mechanical methods. The plastic deformation behavior – yielding and hardening – is predicted by a phenomenological model calibrated against experimental data. Specifically, it combines an orientation dependent anisotropic Hill yield criterion with a nonlinear isotropic hardening law. Such nonlinear model is calibrated against uniaxial tensile curves from specimens milled out of an injection molded plate at 0° and 90° with respect to the main flow direction. Optionally, orientation tensor dependent, orthotropic, ultimate strengths can be calibrated to be later used into a Tsai-Hill type failure criterion. The resulting calibrated material can be saved and used for different type of analyses.

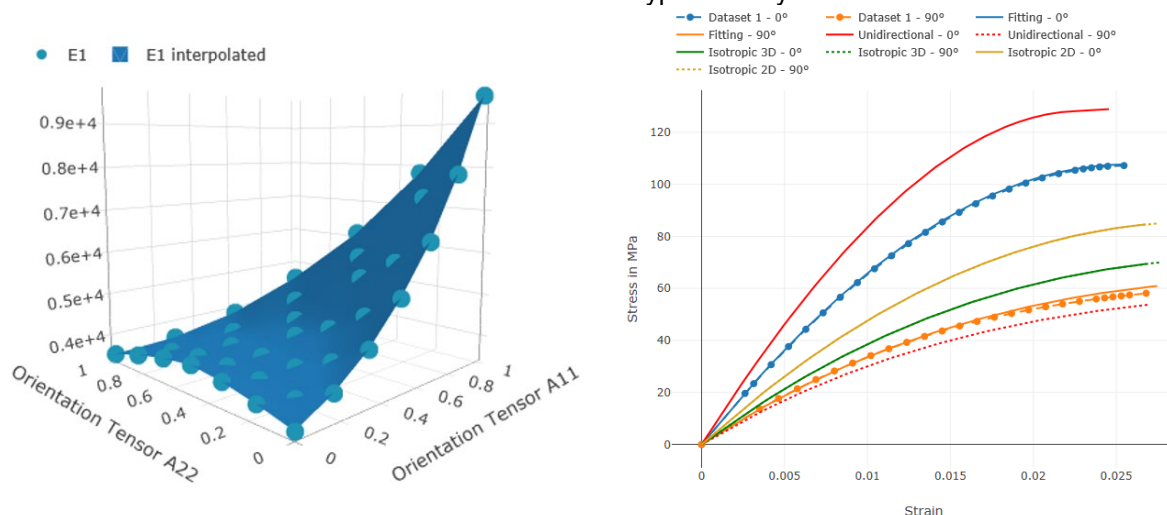


Fig.1: On the left: example of material property (Young modulus in the 1-direction) as a function of the eigenvalues of the fiber orientation tensor. On the right: comparison of experimental and calibrated uniaxial stress-strain curves.

2.2 Model setup in Ansys Mechanical

The FEA model of the structure at hand is prepared using Ansys Mechanical following common practice to create the mesh, define connections, rigid walls, initial conditions etc. To account for the effects of the manufacturing process, the fiber orientation tensor field predicted by injection molding simulation tools is imported and mapped onto the structural mesh. Finally, the application combines this information with the material model described in Sect 2.1. In the case of an LS-DYNA analysis:

- The elements coordinate system is set to coincide with the principal fiber directions using the ***ELEMENT_SOLID_ORTHO** keyword.
- The material model is translated into the ***MAT_ANISOTROPIC_ELASTIC_PLASTIC** keyword.
- Anisotropic stiffness coefficients, Hill yield ratios and optionally strength limits are overridden elementwise through history variables using the ***INITIAL_STRESS_SOLID** keyword.

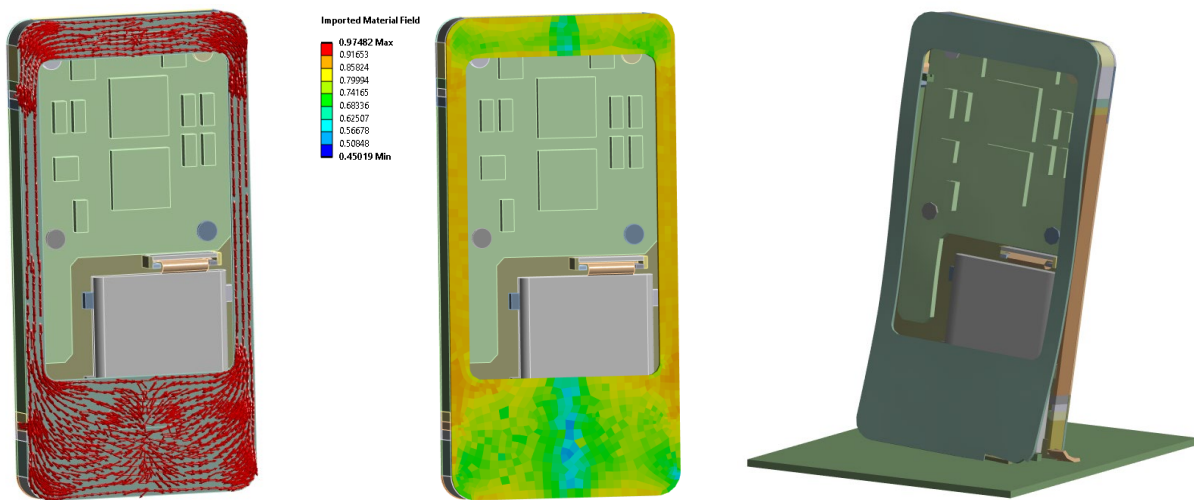


Fig.2: Drop test of a phone. Left: first principal fiber direction in the upper casing. Middle: largest eigenvalue of the fiber orientation tensor. Right: result of the impact with failure and erosion.

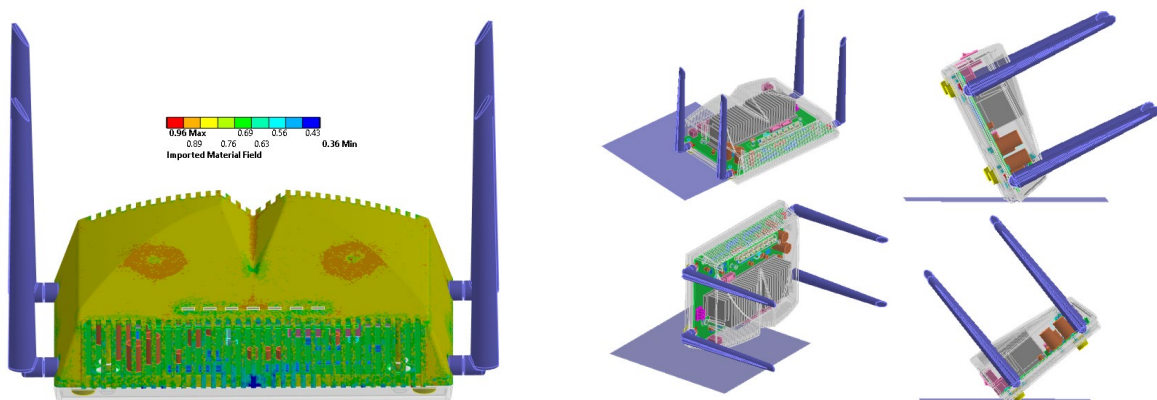


Fig.3: Drop test of a wifi router with a short fiber reinforced casing. Left: largest eigenvalue of the fiber orientation tensor. Right: multiple drop test scenarios.

3 Conclusions

Electronic devices as well as many other consumer goods often include components made of injection molded short fiber reinforced composites. A new workflow is available in Ansys Workbench to simulate their drop test behavior using the LS-DYNA solver. Existing isotropic models can be easily upgraded to account for the effect of fiber orientations and more accurately predict possible failures.

Cumulative Loading Methodology Development

Somnath Chavan¹, Shrikant Jagtap¹, Nikhilesh Wankhede¹, Amit Mandal², Krishna Kusupudi³

¹Lead Engineer, ²Senior Manager, ³Manager,

Whirlpool of India Ltd., Pune, India

1 Introduction

Whirlpool Corporation designs and manufactures appliances that are intended for household and commercial purposes and Stand Mixer is one such appliance. These Stand mixers may undergo specific levels of dynamic stresses during transit from the manufacturing plant to the customer's home such as stresses due to general handling, storage, and shipping stresses. To check all the potential failures during transit, Whirlpool has come up with the requirements to properly evaluate and approve finished goods product and packaging designs that flow through the standard distribution process. This process consists of a series of tests, for example, one of the sequences can be performing a flat drop from a certain height on all faces starting from the bottom face. The current simulation methodologies are very mature to mimic the individual drops but simulating sequential drops is a bit of a challenge due to the large deformations of packaging components, attaining equilibrium of stress levels, changing the loading and boundary conditions for the next drop, etc.

The objective of this paper is to develop a cumulative methodology that mimics the sequential tests in the physical world. This work helps to replicate the field failures in simulation, understand the load path, and finally improve the packaging to safeguard the product in sequential loading during transit. To simulate the sequential drops, the stresses and deformations shall be carried forward from one drop to another. Performing such steps manually is tedious and time-consuming. Also, it involves high memory usage, data loss, and manual errors. To overcome these challenges, a cumulative loading methodology is proposed with *CASE card.

2 Experimental Work

The experiments started with Expanded PolyStyrene (EPS) blocks of standard size to perform the sequential operations shown in Fig 2.1. The accelerometer is mounted on the impact hammer which impacts the block during each drop to capture the acceleration data. Accelerometer output is in the form of Acceleration vs. Time and the maximum 'g' level is used for correlation purposes.

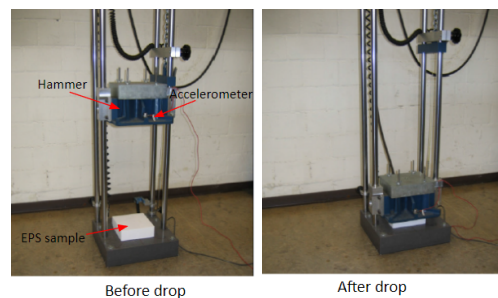


Fig.2.1: Experimental Test setup

3 Cumulative Methodology Development

With the Case File Approach, the results of each drop are taken further and the cumulative effect is captured. The *CASE command provides a way of running multiple LS-DYNA analyses (or cases) sequentially with a single input file. When *CASE commands are used to define multiple cases, some portions of the input will be shared by some or all of the cases and other portions will be unique to certain cases. Due to the sequential loading scenario, the results from one case, e.g. a dynain file, can be used in the analysis of a different and subsequent case. Case File Approach is shown in Fig 3.1. The Transformation function is used to position the product to the desired orientation as per the drop sequence. Include structure format used for multi-drop analysis for calling dynain as deformed input, position nodes, and impactor. The transform keyword file works with two basic commands, *INCLUDE_TRANSFORMATION and *DEFINE_TRANSFORMATION.

Parameter identification for process simulation of high-speed joining

Dr.-Ing. Michael Gerken

1 Introduction

This paper is about the numerical simulation of the car body joining technology high speed bolt joining (brand name RIVTAC) which was developed by the company Wilhelm Böllhoff GmbH & Co. KG from Bielefeld. First, the process and the resulting requirements are described. Then a part of the experimental investigations required for the simulation is presented.

2 Process description and characterisation requirements

High-speed joining is based on the push-rod principle. A piston is pneumatically accelerated and drives the tack into the parts to be joined. As the tack enters the metal sheet, most of the kinetic energy is converted into mechanical work or heat. The remaining surplus energy is absorbed by a rubber bump stop. A diagram of the tack-setting tool and the individual process stages is shown in Figure 1.

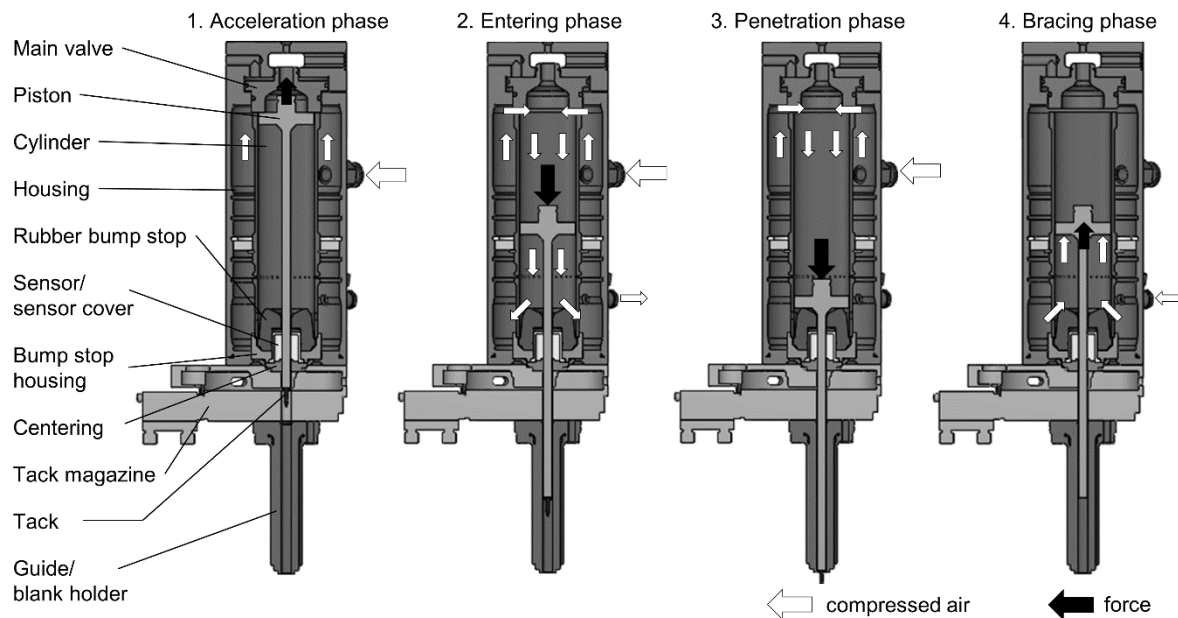


Fig. 1: Layout of the tack-setting tool and stages of the joining process [1]

The joining process itself only takes approx. 1 ms, so that adiabatic heating in the forming zone can be assumed. High degrees of deformation, strain rates and temperatures occur, which must be considered in the material description. The holding mechanism is based on a force and form fit, so the friction between the bolt and the sheet metal must also be characterised. In addition to the geometrical description of all relevant components, the following requirements exist for the experimental characterization:

- Joining process: velocity up to 40.000 mm/s
- Push-out process: relative velocity approx. 1 mm/s
- Strain rate: over 1.000 1/s (locally over 10.000 1/s)
- Temperatures: steel up to 800 °C, aluminium up to 400 °C
- Degrees of deformation up to 0.6

Essentially, the sheet metal material HC340LAD in $t = 1.5$ mm and the extruded profile EN AW-6060 T66 in $t = 3.0$ mm as well as the joining element RIVTAC with zinc-nickel coating were characterised. In the following, selected results for the necessary characterisation of materials and friction values are summarised. Details can be found in the dissertation [1].

3 Material characterisation

Different test setups were used for the material characterisation, which are summarised in Table 1 below.

Characterisation method	Component, specimen	Boundary condition
Standard tensile test	Metal sheets, Flat tensile specimen	Universal testing machine, GOM qs - 10 1/s, RT
High speed tensile test	Metal sheets, Mini tensile specimen	High speed testing machine, DMS 500 – 1.500 1/s, RT
High temperature tensile test	Metal sheets, flat tensile specimen	Universal testing machine with conductive heating, qs, max. 800 °C
High speed compression test	Metal sheets and tack, cylindrical specimen	Split Hopkinson pressure bar, approx. 15.000 1/s, RT
High temperature compression test	Tack, cylindrical specimen	Universal testing machine with solid carbide punch, inductive heating, qs, max. 800°C

Table 1: Overview of the test setup for the material characterisation of the metals [1]

In addition, the thermophysical properties, such as the temperature-dependent heat capacity, were calculated with JMatPro V10.2. [2]. The results of all material tests were evaluated and transferred into a material model according to Johnson Cook, cf. *MAT_TABULATED_JOHNSON_COOK [3]. Figure 2 shows the yield surfaces for the two joining partners.

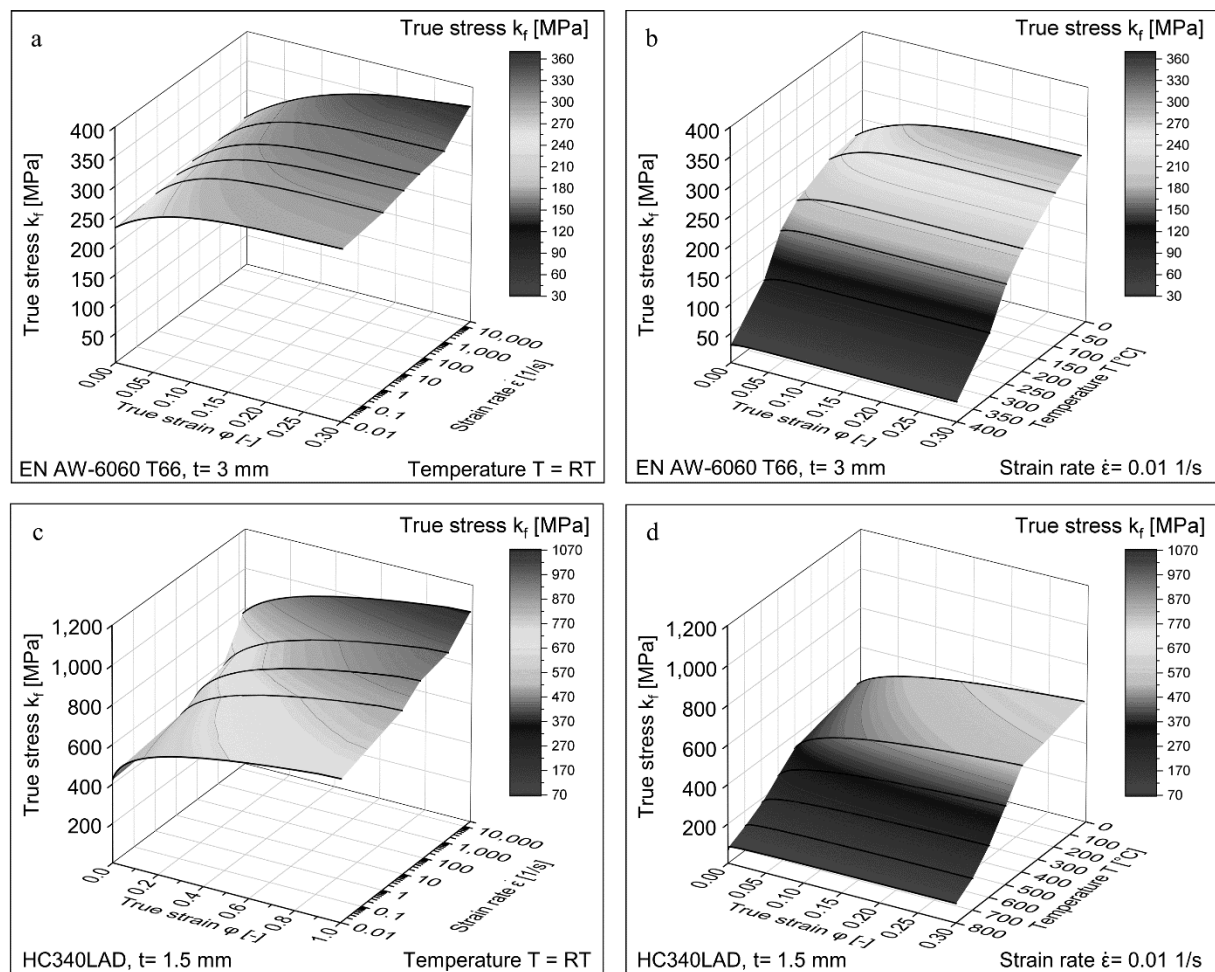


Fig.2: (a), (c) strain rate-dependent yield surface and (b), (d) temperature-dependent yield surface of EN AW-6060 T66 and HC340LAD [1]

4 Friction characterisation

The friction parameters must be differentiated in relation to the velocity of the joining process and the push-out process. The arrangement of the joining partners must also be taken into account. Due to the high surface pressure, the shear yield behaviour of the joining partners is also an important factor. For the characterisation of the friction behaviour, a test bench was developed according to the pin-on disk principle and a simulation-based inverse parameter identification was carried out. The data was used to build friction models for the different load situations, velocity levels and sheet metal arrangements. The velocity-dependent friction model, cf. formula (1), which is implemented in the contact keyword ***CONTACT_2D_AUTOMATIC_SURFACE_TO_SURFACE_MORTAR_THERMAL** by default, was used. [4]

$$\mu = FD + (FS - FD)e^{-DC|v|} \quad (1)$$

Table 2 below shows the friction parameters used. It should be mentioned that a coefficient for viscous friction VC and a heat transfer conductance H was also defined for each friction pairing.

Material combination	Process simulation				Push-out simulation			
	HC340LAD/ AW-6060 T66		AW-6060 T66/ HC340LAD		HC340LAD/ AW-6060 T66		AW-6060 T66/ HC340LAD	
Parameter	cover	base	cover	base	cover	base	cover	base
FS	0,196	0,167	0,206	0,24	0,158	0,167	0,341	0,240
FD	0,103	0,178	0,178	0,103	0,157	0,207	0,468	0,165
DC	0,0004	0,0004	0,0004	0,0004	3	7	8	7,5

Table 2: Overview of the friction parameters [1]

5 Summary

The most important finding of the investigations is that the thermomechanical effects and the different friction conditions must be considered in the simulations. There is potential for development in the coupling of material law and contact description with regard to the shear yield stress (cf. parameter VC) as well as a simplification of the material description, e.g. in the form of parametric model models. A challenge will be the transfer to the 3D simulation, as the material failure will then be required for the penetration of the sheets.

6 Literature

The contents of the abstract are based on the dissertation [1]. The dissertation was supervised by Professor Meschut at the Laboratory for Materials and Joining Technology at the University of Paderborn.

- [1] M. Gerken: „Entwicklung einer Methodik zur numerischen Simulation des Hochgeschwindigkeits-Bolzensetzen“, Dissertation, Shaker ISBN 978-3-8440-7583-0, 2020
- [2] Sente Software Ltd., Guildford, United Kingdom: [online], 2022. URL: <https://www.sentesoftware.co.uk/jmatpro> [Status: 02.09.2022].
- [3] LS-Dyna Keyword Users’s Manual Volume II- Material Models, LS-Dyna R10.0, (2017)
- [4] LS-Dyna Keyword Users’s Manual Volume I, LS-Dyna R10.0, (2017)

Framework for Automatic Numerical Sensitivity Analysis of Process Chains to Produce Complex Car Body Components

Sebastian Kriechenbauer¹, Ingolf Lepenies¹, Sebastian Hensel²

¹SCALE GmbH
²Fraunhofer IWU

1 Introduction

Most of the car bodies are assembled from different sheet metal parts. A lot of complex process steps are required to produce the whole body-in-white and body add-on parts. Today, sheet metal forming and joining processes are numerically simulated with finite element methods (FEM) to support the production development quite well.

If there are too many parameters influencing the design of the process chain, then the best design can be found with machine learning methods like variance-based sensitivity analysis with field meta models [1]. Field meta models describe the most important parameters, which helps to identify a suitable parameter set without an annoying trial-and-error search.

In computing the field meta model, the challenge is to spatially correlate the input and output of all simulations and experiments. For example, in deep drawing the outline of the resulting finite element mesh vary across different deep drawing simulations. For this reason, an automated workflow with different software tools was developed to calculate the field meta model [3].

2 Description of the developed framework

Figure 1 shows the developed framework for a process chain with deep drawing, clamping and joining of an assembly. The data driven pipeline consists of a pre- and postprocessor, which automate the generation of the simulation model and the result extraction respectively.

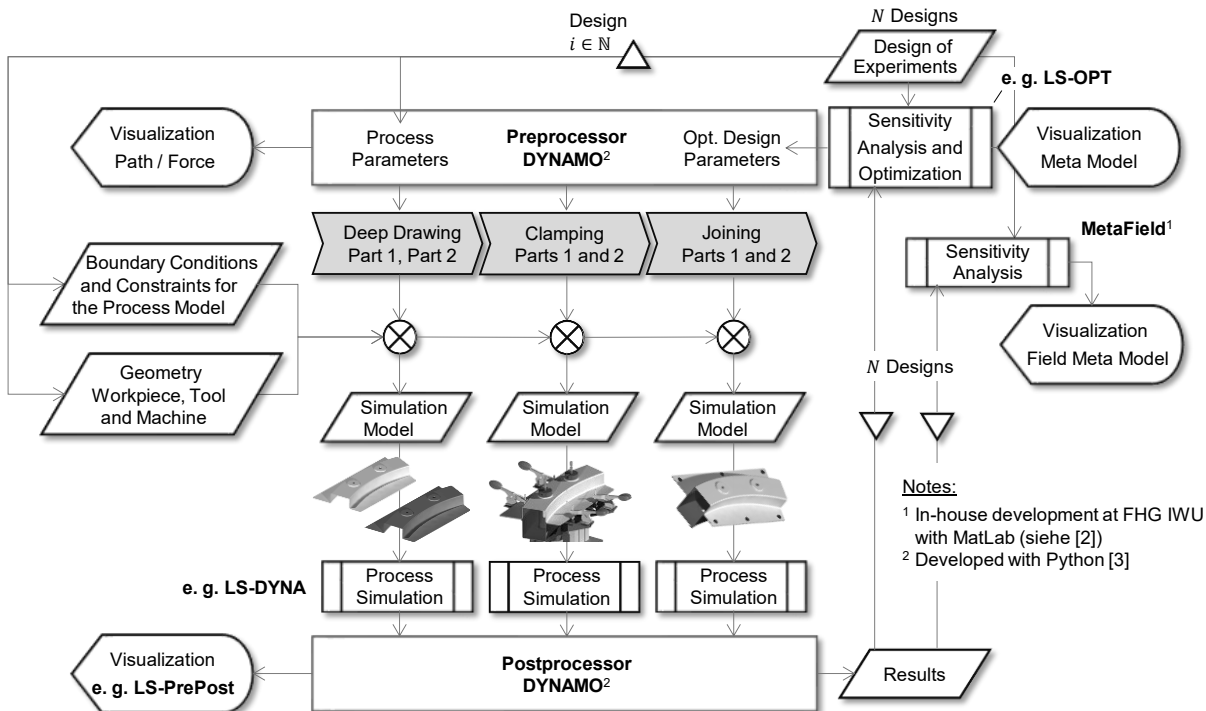


Fig. 1: Framework for the automatic field meta modelling and calculation of an example process chain with deep drawing, clamping and joining process

For the postprocessor it does not matter whether data from simulation or experiment are used. Here the simulation pipeline works with LS-OPT to build the design of experiments, LS-DYNA to simulate the manufacturing processes and LS-PrePost to visualize the data. The universal tool MetaField [2] calculates the field meta model and shows the prediction.

3 Summary

The developed framework automates numerical sensitivity analysis of process chains. The calculated field meta models can speed up the start of production of complex car body components. They show the most important influence parameters. That is why the complexity of the process chain is reduced. For optimization tasks designs can be quickly generated from the field meta model without the need for time-consuming simulations. The field meta modelling approach replaces process design based on trial-and-error.

4 Acknowledgments

The presented results are part of public research projects at Fraunhofer Institute for Machine Tools and Forming Technology IWU, which is in Chemnitz, Germany. The Projects 17058BR, 17488BR and 19007BR of the research association Europäische Forschungsvereinigung für Blechverarbeitung (EFB) e. V. were financed by the Arbeitsgemeinschaft industrieller Forschungsvereinigungen Otto von Guericke e. V. (AiF) as part of the program to support Industrial Community Research and Development (IGF) with funds from the Federal Ministry for Economic Affairs and Energy (BMWi) following an order by the German Federal Parliament. Further development and practical work were funded by the Federal Ministry of Education and Research (BMBF) as part of the research project ML@KaroProd. The financial support and cowork are gratefully acknowledged by the authors.

5 References

- [1] Wolff, S.: Random fields and field meta models – Correlation analysis in time and space. RDO-Journal 1, 2016. Downloaded on 01/09/2022 from https://www.dynardo.de/fileadmin/Material_Dynardo/dokumente/broschuere/JournalArtikel/RDOJournal_1_2016_Title_RandomFields_P_web.pdf
- [2] Schwarz, C. et al.: Principal component analysis and singular value decomposition used for a numerical sensitivity analysis of a complex drawn part. Int J Adv Manuf Technol, 94: 5-8. pp. 2255-2265, 2018. DOI: 10.1007/s00170-017-0980-z
- [3] Kriechenbauer, S.: Beitrag zur Analyse und Synthese von variablen Kraft- und Wegfunktionen beim Tiefziehen auf Servo-Spindelpressen. Dissertation, TU Chemnitz, 2022.

A Deep Learning Approach to Predict the Deviation of Sheet Metal Parts in Deep Drawing Process

Aida Farahani, Julien Vitay, Fred.H Hamker

Chemnitz University of Technology, Department of Computer Science, Lab of Artificial Intelligence

Deep neural networks have been recently applied to many domains and applications and offer new types of solutions for different problems. The power of neural networks in tasks such as classification, prediction, high dimensional data regression, data compression, and data generation could be employed for more efficient, accurate, and optimized solutions alongside or instead of classical approaches. This paper presents a deep learning approach trained on FEM simulations generated by LS-DYNA to predict the deviation of simulated metal parts in a deep drawing process. The presented method is capable of processing large meshes and predicting the final shape for unseen input process parameters with high accuracy, in a few seconds, instead of running a new FEM simulation.

Keywords: Geometric Variation Modeling, Deep Learning, FEM Simulations

1 Introduction

In recent years, different approaches have been introduced to process 3D data using deep neural networks (NN) for various purposes [1], such as object classification, segmentation, reconstruction, compression, etc. Contrary to other data types such as image, video, or text that usually have standard representations, the proper selection of 3D data representation for neural networks is crucial. It may cause the success or failure of the approaches. Explicit representations, such as meshes, should provide the whole structure to the network at once, drastically increasing the network size for large meshes. On the other hand, multiple meshes with different sizes and topologies are applicable for representing a single geometry. The exact shape would have a different mesh after each FEM simulation execution. This arbitrary property of mesh structure makes it incompatible with NNs that are usually fed with fixed-size data.

The combination of NN with implicit representations has received great attention recently and resolved some of the main issues of explicit methods [2]. DeepSDF, which was introduced in 2019, presents neural networks as an embedded representation of a single shape. The Signed Distance Function (SDF) is an implicit representation of 3D shapes in which every point in 3D has a distance value, depending on whether it is inside (-), outside (+), or on the shape surface (0). A deep neural network can be trained to estimate the SDF value of a shape S for each query input position in 3D space. This continuous interpretation of space makes it possible to reconstruct shapes at any desired resolution and to preserve shape deformations without large memory requirements. This method can effectively address the problem of efficient shape embedding, and the network size is comparable to classical approaches for processing arbitrarily large meshes with arbitrary topology.

2 Proposed Method

We have built on the idea of implicit representations to process the data obtained from deep drawing experiments. Our partners at Fraunhofer IWU, Dresden, produced 879 deep drawing simulations by varying a set of process parameters such as “sheet thickness”, “drawing depth”, “hold-down force”, “draw gap”, and “insertion position”, creating meshes with over 20,000 nodes that can be compared to a template to measure the deviation. The main advantage over explicit approaches is that we no longer have just a few hundred simulated experiments to feed the neural network (which will most likely lead to overfitting), but thousands of measurements per experiment, representing the thickness, thinning, plastic strain, etc., at individual locations. Instead of relying on the non-Euclidean structure of the input space and performing expensive operations such as convolutions on the entire input mesh [3], this approach ensures efficient regularization of the NN by using individual positions as training patterns and proved to be very robust for modeling FEM simulations in different dimensionalities.

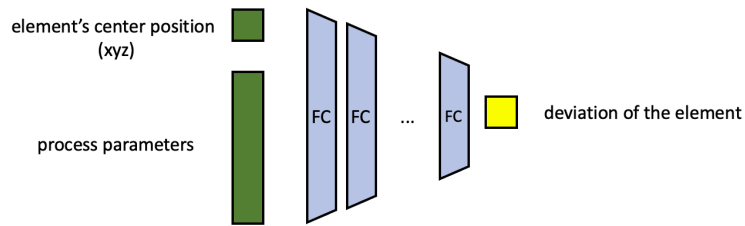


Fig.1: Network architecture (fully connected (FC) layers) – inputs and output of the network

The model is trained using the process parameters (which can be both numerical and categorical inputs) and the xyz coordinates of an element as inputs (Fig. 1). Using fully connected layers and modern optimization procedures (Adam optimizer, Bayesian hyperparameter search), the network learns to predict the deviation of the corresponding query point. After training, new values for the process parameters can be defined by the user. For each sampled input position, the corresponding simulations can be replicated by the neural network in a few hundred milliseconds without running the corresponding FEM simulation, allowing an engineer to perform thought experiments and robustness checks very quickly. As an example, a sample ground truth mesh and the corresponding network prediction are depicted in Fig.2.

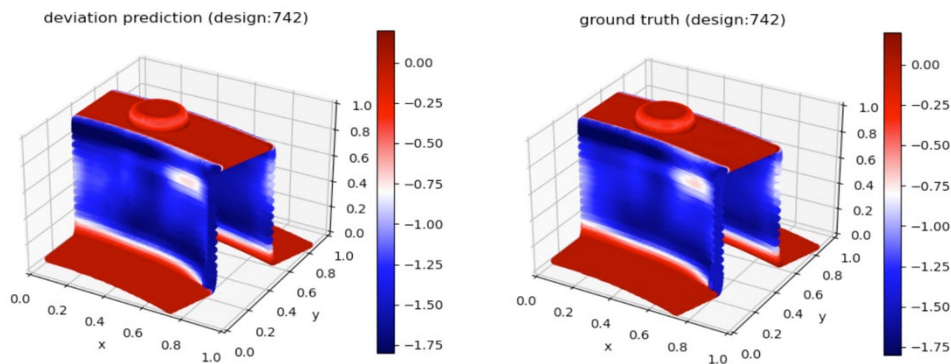


Fig.2: Deviation prediction for a design sample. The left plot is the network output, and the ground truth mesh is depicted on the right.

3 Summary

In this paper, we present a deep neural network trained on FEM simulated data from a deep drawing process. The proposed model is able to process large meshes and predict the deviation and thickness of the resulting mesh based on input process parameters. The results show that this method could be effectively combined with existing FEM methods to help engineers to refine the FEM simulations faster and tune the best process parameters more easily. To some extent, the model is also able to generalize to unseen data; for instance, the simulation result could be generated for a new initial sheet thickness value.

4 Acknowledgement

This work has been funded by the Federal Ministry of Education and Research (BMBF) - ML@Karoprod (01IS18055)

5 References

- [1] Ahmed, E., Saint, A., Shabayek, A. E. R., Cherenkova, K., Das, R., Gusev, G., Aouada, D., & Ottersten, B. "A survey on Deep Learning Advances on Different 3D Data Representations" (arXiv:1808.01462), 2019
- [2] Park, J. J., Florence, P., Straub, J., Newcombe, R., & Lovegrove, S. "DeepSDF: Learning Continuous Signed Distance Functions for Shape Representation." (arXiv:1901.05103), 2019
- [3] Ranjan, A., Bolkart, T., Sanyal, S., & Black, M. J. "Generating 3D faces using Convolutional Mesh Autoencoders." (arXiv:1807.10267), 2018

Connector Wear Modeling and Testing Validation of Server Hardware

Eric Campbell¹, Arshad Alfogaha¹, Kevin O'Connell¹, Mehdi Hamid¹, Shawn Canfield¹, Suraush Khambati¹

¹IBM Corporation

1 Introduction

Electrical connectors are used in a variety of applications in the electronics industry. Connectors consist of a separable pair of electrical conductor contacts that join to form an electrical circuit. The electrical conductors are typically constructed of conductive metal base material, such as copper, and have noble metal platings, such as gold, applied to portions of the conductor to prevent metallic corrosion at the contact interface, which could impact the electrical connection.

During dynamic conditions, such as when electrical hardware is shipped, relative motion between the mating connector contacts can be induced and cause wear of the noble metal platings. The amount of wear generated during a test is a function of the contact normal force, the hardness of the contacting materials, the contact geometry, the friction and lubricity of the contacting materials, and the relative sliding distance of the contact pair. If the wear of the noble plating layers is excessive, the underlying metal layers can become exposed to the atmosphere and prone to corrosion. An example of an electrical connector with worn gold contacts is shown in Figure 1. Understanding the amount of wear an electrical connector could experience in its life is necessary for determining the long-term reliability of the connector.



Fig.1: Example gold plated electrical contacts exhibiting connector wear after a vibration test

Methods for assessing connector wear in server hardware applications typically involve accelerated shock and vibration testing of the electronic hardware. These tests are expensive because the tests require prototype hardware to be built for each iteration. Also, the tests are often damaging and can destroy the hardware. To reduce the number of test iterations required to evaluate connector reliability, several predictive engineering modeling approaches using the finite element method (FEM) were developed for assessing connector wear of server hardware and are presented in this study. Testing was performed to validate and build higher confidence in these FEM models.

2 Testing Background

A high-end server (Server A) underwent shock and vibration testing during product qualification. During this test, the server was installed in a server rack, which is mounted onto a shipping pallet. Testing was performed using two different server racks (Rack T and Rack S). A server is considered to pass the test if the electrical connectors do not have excessive wear as determined through visual inspection and scanning electron microscopy (SEM) energy-dispersive X-ray spectroscopy (EDS) inspection. The test results showed that when the test was performed using Rack T, the power supply unit (PSU) electrical connectors passed internal metrics for connector wear. However, when the test was performed using Rack S, the PSU connectors failed the connector wear inspection.

3 Macro-level FEA Model Setup

Finite element methods were developed to simulate connector wear and the product qualification vibration testing. These methods were applied to the Server A that underwent vibration testing in Rack T and Rack S. ANSYS SpaceClaim and ANSYS Explicit Dynamics (LS-DYNA Export) tools were used to create the 3D FEM-optimized CAD of the server assemblies, and to build the FEM models for

simulation [1-3]. The simplified 3D CAD model is shown in Figure 2. Two different random vibration profiles were applied as the loading constraints in the FEM model that corresponded to acceleration data collected during the server testing in Racks T and S. The random vibration profiles were applied to the rack mounting points of the server enclosure. The resulting FEM models were exported as an LS-DYNA input file (*.k file) and solved using the nonlinear, explicit solver [1].

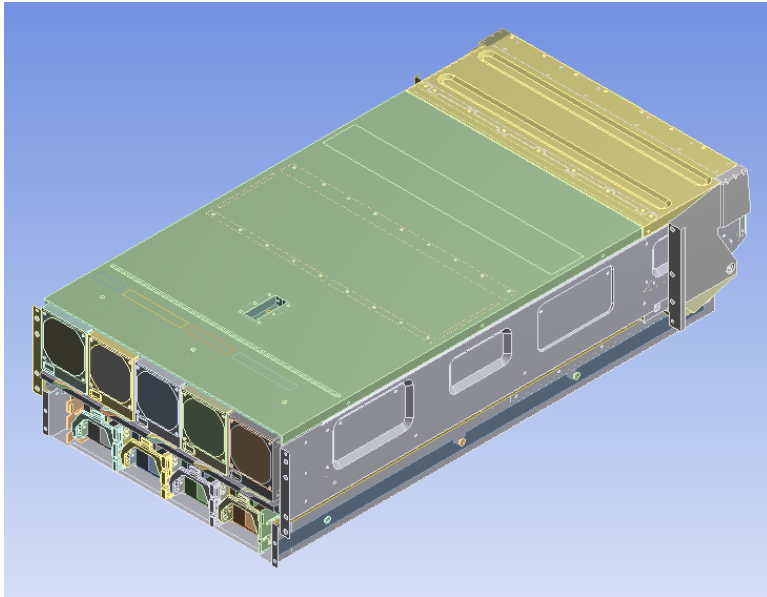


Fig.2: Simplified 3D CAD of Server A.

4 Macro-level Sum of Delta Displacements Method

To assess the potential of connector wear for a given connector, a “Sum of Delta Displacements” post processing method was applied to the FEM model results. This method quantifies the total travel distance the connector header/receptacle pair moves relative to one another (i.e. contact pair sliding distance). The total travel distance (i.e. sum of delta displacements) was calculated for the FEM models by probing the results and extracting the displacement between the PSU header and receptacle and inputting the displacement data into Equation 1. The displacement vs. time for the PSU connectors for both configurations are shown in Figure 3. The simulated total travel distance results for the PSU connector in Rack T and Rack S are shown in Figure 4.

$$\sum_{t=0}^{t=\infty} |X_{t+1} - X_t|, \text{ where } t = \text{time and } X = \text{displacement} \quad (1)$$

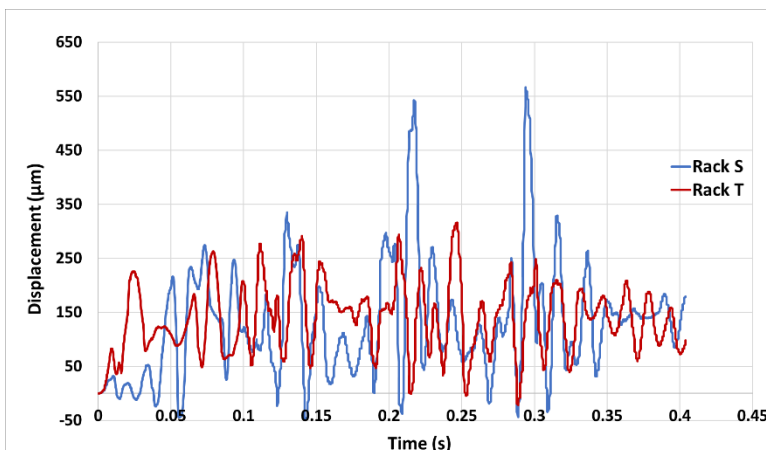


Fig.3: The displacement results of the PSU connector versus time for the Rack T and Rack S FEA models.

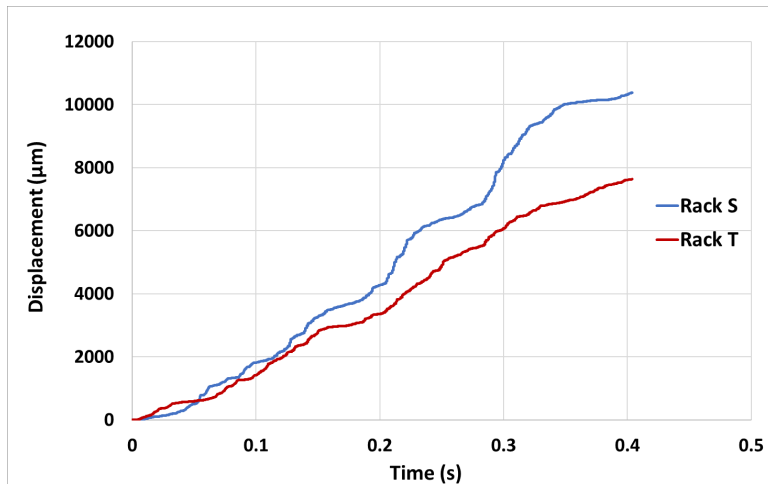


Fig.4: The total travel distance of the PSU connectors for the Rack T and Rack S FEA models.

5 Macro-level Sum of Delta Displacements Results

The sum of delta displacements results, shown in Figure 4, revealed that the total travel distance for Rack S was 36% higher than Rack T. This coincides with testing, where the Rack S hardware had more connector wear than Rack T. The connector hardware used between the two tests was identical, so the contact normal force, the hardness of the contacting materials, the contact geometry, and the friction and lubricity of the contacting materials can be assumed to be relatively similar between the two tests. This assumption leads to the conclusion that the contact sliding distance (i.e. total travel distance / sum of delta displacements) is the main factor influencing connector wear differences between the two tests.

6 Modeling of Connector Wear

The modeling of physical connector wear can be achieved by implementing Archard’s wear model [4], shown in Equation 2, and applying it to a simplified model of a connector contact pad/pin pair. For Archard’s wear model, Q is the total volume of wear debris produced, K is a dimensionless constant, W is the contact normal force, L is the sliding distance, and H is the hardness. An example of the simplified connector model is shown in Figure 5. For this model, the pad is fixed, the pin is in contact with the pad, and a displacement is applied to the pin to simulate the pin sliding on the pad. The relative displacement of the connector pair shown in Figure 3 can be used as the input for the displacement applied to the pin. For this model, the hardness was assumed to be 38,328 Pa, the normal force was 0.74 N, the friction coefficient was assumed to be 0.2, and the wear coefficient, K, was assumed to be 6.3x10⁻⁷. The results of this model are shown in Figure 6, where the wear thickness is plotted vs. time. As expected, the wear thickness versus time shown in Figure 6 matches the trend of displacement versus time shown in Figure 4. The connector wear model simulated 0.4 seconds of vibration testing. The measured wear thickness was extrapolated linearly to 15 minutes, which corresponds to the duration of the typical vibration test. The estimated wear thickness at 15 minutes is shown in Table 1 for both Rack T and Rack S. The estimated wear thickness of 0.63 µm for Rack S would fail internal pass/fail conditions, while the estimated wear thickness of 0.47 µm for Rack T would pass. This result confirmed the trend seen in testing. Additional physical testing needs to be completed on connector hardware to verify the hardness and wear coefficient for Au-on-Au connector contacts.

$$Q = \frac{KWL}{H} \tag{2}$$

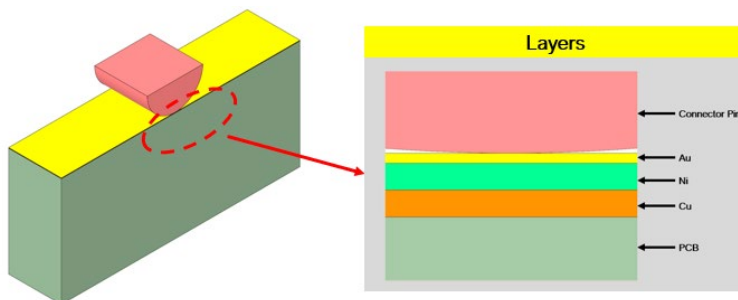


Fig.5: Simplified model of the connector contact pad/pin pair.

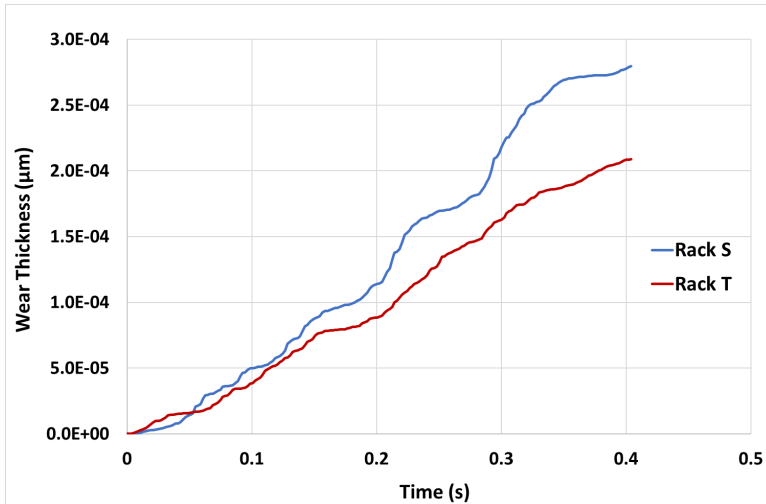


Fig.6: Connector wear modeling results showing the wear thickness vs. time for the PSU connectors.

	Wear Thickness (µm)	Duration
Rack S	2.8E-04	0.4 sec
	6.3E-01	15 min
Rack T	2.09E-04	0.4 sec
	4.7E-01	15 min

Table 1: Wear thickness of Rack T and Rack S at the end of the FEM model (0.4 seconds) and the estimated wear thickness at after 15 minutes.

7 Use of Sum of Delta Displacements Method in Other Applications

The sum of delta displacements method was applied for three other server applications (Servers B, C, and D). For those applications, the PSU connectors were of interest and the relative total travel distance was modeled and calculated for each application. Figure 7 shows a comparison of the relative total travel distance of Servers B, C, and D vs. Server A. These results show that the total travel distance for the Servers B, C, and D was less than Server A, and thus less connector wear was expected in Servers B, C, and D. Shock and vibration testing of Servers B, C, and D corresponded with the trend observed in modeling, where all three servers passed the test and did not have excessive wear.

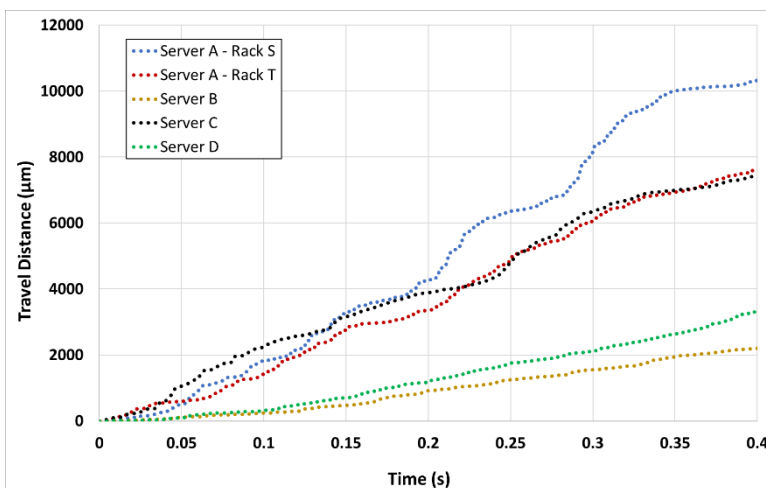


Fig.7: The total travel distance of the PSU connectors in three other server applications vs the original server application with Racks T and S.

8 Literature

- [1] "LS-DYNA Keyword User's Manual Volume 1", Livermore Software Technology Corporation, 2017
- [2] "ANSYS Mechanical User's Guide Release 18.0", ANSYS, Inc., 2017
- [3] "ANSYS Theory Reference Release 5.6.", ANSYS, Inc., 1999
- [4] Shen, X., Cao, L., Li, Ruyan.: "Numerical simulaiton of sliding wear based on archard model", International Conference of Mechanic Automation and Control Engineering, 2010

Simulation based distortion management for multiple stage assembly of welded structures

Tobias Loose¹, Sujit Chatterjee²

¹Dr. Loose GmbH, ²Jaguar Land Rover Ltd

1 Introduction

The avoidance of shape deviations and material changes due to welding is an interesting and challenging issue, which often leads to difficulties to solve in practice. With welding simulation, it is possible to calculate welding distortion, residual stresses and microstructural changes in advance. Welding assembly often takes place in several stages. For multi-stage weld assemblies, the deformations from previous sub-assemblies must also be considered in the simulation. This extends the welding simulation to a manufacturing simulation. The FabWeld software was developed by Dr. Loose GmbH to setup multi-stage assembly simulations for LS-DYNA.

2 Assembly simulation of welded structures

In order to obtain accurate results when simulating the welded assembly, the clamping process with the resulting distortions must be mapped correctly. If individual components or subassemblies already deviate from the nominal geometry, clamping distortion occurs when they are clamped in the fixture. Welding generates the thermal distortion. When the clamping forces are released during unclamping, unclamping distortion occurs, which represents spring back. All distortion components together result in the final distortion. The clamping process must be mapped realistically in the simulation in order to achieve exact calculation results. The simulation of the assembly requires a multi-stage simulation. In the simulation, as in reality, components or subassemblies are added, clamped and welded from manufacturing station to manufacturing station.

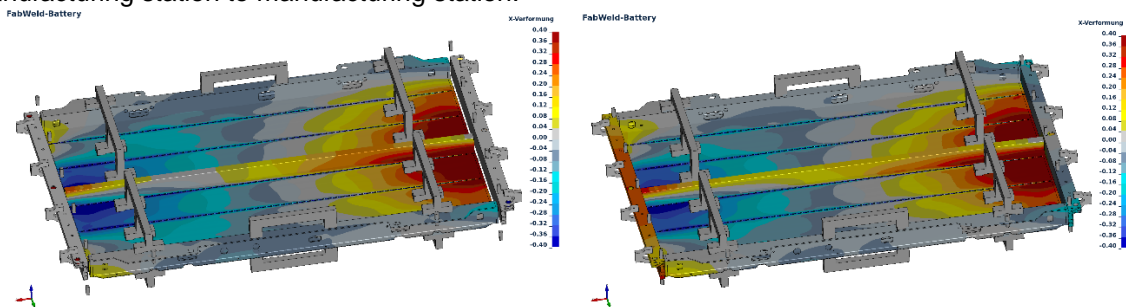


Fig. 1: Longitudinal distortion before (left) and after (right) clamp closing

Fig. 1 shows a battery tray in the 2nd manufacturing stage, where the subassemblies cross member and bottom plate are added. Both plots show the longitudinal distortion in the X-direction. Fig. 1 left represents the situation before insertion and clamping of the cross members. The bottom plate shows deformations in the X-direction. During clamping, the cross members are pressed onto the bottom plate and deformed in the process due to the imperfection of the bottom plate. During welding, this deformation component is frozen (Fig. 1 right).

Critical points can be analyzed from the assembly simulation. By calculating the welding distortions, it can be determined in advance whether the insertion of further components is possible or whether fit conflicts will occur. Fig. 2 left shows such a fit conflict. The cross member has the length of the CAD nominal geometry. Due to the welding of the frame from the previous production stage, the side profiles have warped inward to such an extent that it is not possible to insert the cross member. Here, the simulation shows in advance that measures must be taken to enable trouble-free insertion.

The assembly simulation can be used to analyze whether critical gaps occur during production. When the bottom profiles of the battery carrier example are welded together, a gap occurs toward the end between the center profile and the adjacent profile. The gap forms in both the vertical and lateral directions (Fig. 2 right). The vertical gap can be significantly reduced by optimizing the clamp position.

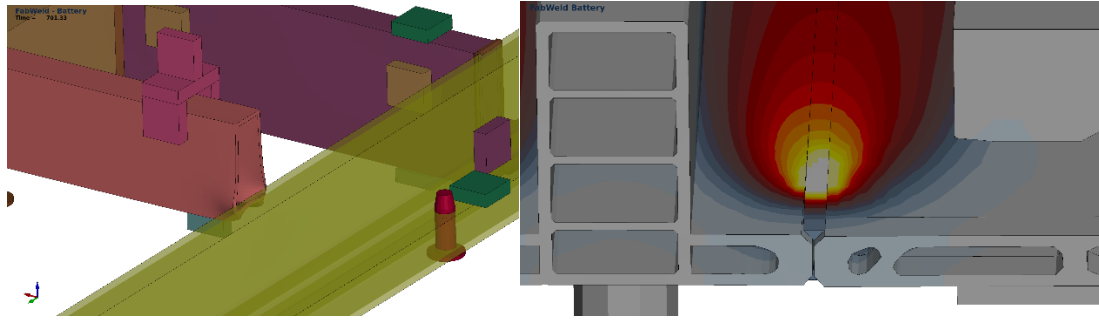


Fig.2: Left: conflict at insertion, right: gap during welding

3 Improvement for a battery tray

A battery tray for electromobility is manufactured from extruded aluminum profiles. An MSG cold wire process is used. Assembly takes place at three stations with a substation:

Station 1: Assembly of the base plate, Substation 1.1: Subassembly of bushings to outer cross members

Station 2: Assembly of base plate with outer cross members

Station 3: Assembly of inner cross members

For this battery tray, the distortion that occurs during the welding assembly is calculated. As described above, the deformations from the previous welding station are considered in this simulation.

For the center section two design Variants are discussed. Variant 1 represents the original design. The center section is designed with the bottom section as an extruded section. This profile is welded to the other profiles in station 1 to form the base plate. Variant 2 represents the optimized construction. The profile is divided into a floor profile and a longitudinal member profile. The bottom profile is installed in station 1, while the longitudinal member profile is not added until the third and final station.

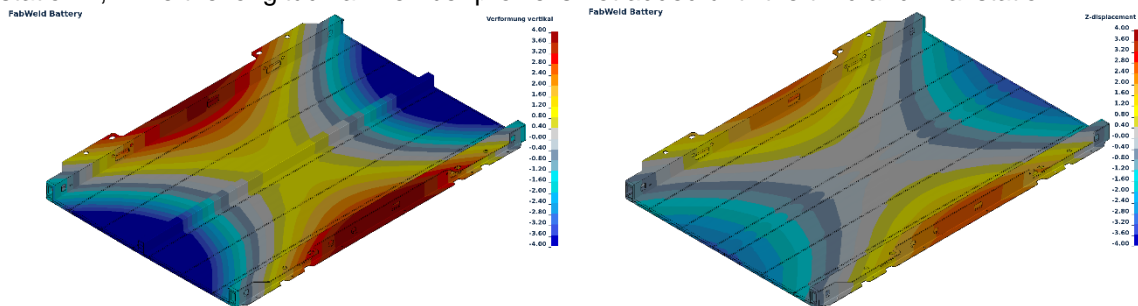


Fig.3: Vertical distortion after Station 1. Left Variant 1, right Variant 2.

From the multi-stage assembly simulation, the station where the greatest distortion occurs can first be determined. In our example, this is station 1 with the welding of the floor profiles. Fig. 3 left shows the vertical distortion of variant 1 after unclamping and intermediate cooling shortly before clamping in station 2. The station at which the greatest distortion occurs is also the station at which the compensation measures are most effective. Fig. 3 right shows the vertical distortion of variant 2 after station 1. A clear distortion minimization can be seen. Finally, this leads also to significant distortion minimization after final assembly (Fig. 4).

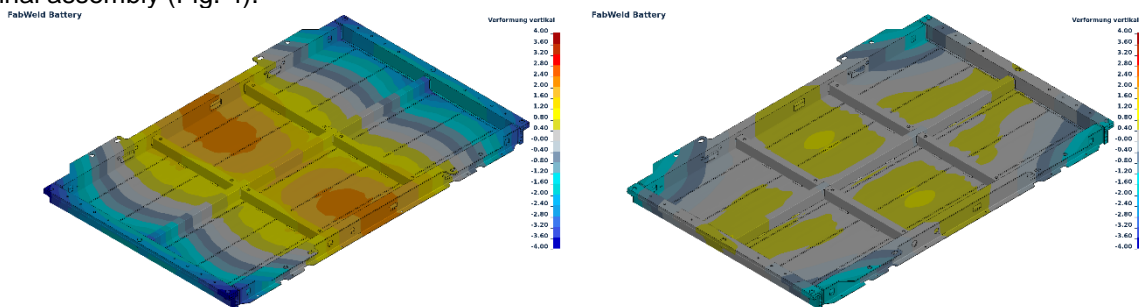


Fig.4: Final distortion. Left Variant 1, right Improvement Variant 2.

This example clearly shows how profitably assembly simulation can be used in the design phase. If the welding distortion is determined precisely at this early stage, it is possible to minimize the welding distortion efficiently with geometry changes that do not require much effort.

Consideration of Bake Hardening by a phenomenological model

Martin Hofmann¹, Andre Oeckerath², Klaus Wolf², Thomas Wallmersperger¹

¹Institut für Festkörpermechanik, TU Dresden

²Fraunhofer SCAI, Sankt Augustin

1 Introduction

The steadily increasing demands on the crash safety of automobiles with simultaneous weight reduction also mean higher requirements for crash simulation. In addition to manufacturability, the focus in component dimensioning is increasingly on crash properties. In order to improve the predictive accuracy of crash simulation, the individual process steps must be coupled in the simulations. To increase the quality of the predictions, thermal treatments such as curing of the paint, which normally takes place at 170 °C for around 20 minutes, should also be taken into account. In many steels, the so-called Bake Hardening effect occurs. This leads to an increase in the yield stress due to the fact that solved carbon atoms diffuse into the dislocations that result from the pre-deformation. The change of yield stress after a pre-deformation of 2% is analyzed in the standard DIN EN 10325 [1]. But the increase of yield stress also depends on the pre-deformation. For example, in [2] experimental results show a change of this yield stress increase for different biaxial pre-deformations. Hardenable Aluminum shows a similar increase of yield stress due to this heat treatment too, but this effect results from the formation and growth of precipitations. Here some experimental findings around this effect will be shown and a simple phenomenological model for including this effect in the simulation of the process chain will be given accompanied by a simple numerical demonstration example.

2 Experimental results

Here three high strength steel grades were analyzed in detail. Special attention was given to the nature of the yield strength increase due to the heat treatment. For this, special non proportional tensile tests have been carried out, where in a first step, a large tensile specimen was brought to a defined elongation and then secondary micro tensile specimen were cut out with angles of 0°, 45° and 90° to the initial loading direction. Some of the secondary specimens have been subjected to standard heat treatment of 170° C for 20 minutes, before the secondary loading while the rest remained untreated. By comparing the stress strain curves of the treated and untreated specimen the change of yield stress can be evaluated for the different secondary loading directions. Even so there are quite large measuring errors in the change of yield stress, it can be concluded that the bake hardening is of isotropic hardening type as can be seen in Fig. 1 left.

3 Model

From the resulting information of the experiments it can be assumed that the increase of yield stress behaves like isotropic hardening. Therefore, it is possible to describe the change of yield stress depending on the effective plastic strain ε_{eff}^{pre} that was reached before the heat treatment and the overall effective plastic strain ε_{eff}^p during the secondary loading. For this we propose three phenomenological ansatz formulas. One describes the change of yield stress directly the other describe the new hardening behavior directly:

$$\Delta\sigma = A - B(1 - \exp [m_1(\varepsilon_{eff}^{pre})^{n_1} + m_2(\varepsilon_{eff}^p)^{n_2}]) \quad (1)$$

The second ansatz bases on a gosh hardening law, where the parameters are depending on ε_{eff}^{pre} via an error function Erf that can have asymptotical constant behavior for low and high values of ε_{eff}^{pre} . It has high flexibility but also needs a lot of experimental data for calibration

$$\begin{aligned} \sigma &= A(\varepsilon_{eff}^{pre}) - (B(\varepsilon_{eff}^{pre}) - A(\varepsilon_{eff}^{pre}))(1 - \exp [m(\varepsilon_{eff}^{pre})[\varepsilon_{eff}^p]^{n(\varepsilon_{eff}^{pre})}]) \\ A(\varepsilon_{eff}^{pre}) &= k_{1A} + \frac{k_{2A}}{2} [1 + \text{Erf}(-m_A \varepsilon_{eff}^{pre} - c)]; \quad B(\varepsilon_{eff}^{pre}) = k_{1B} + \frac{k_{2B}}{2} [1 + \text{Erf}(-m_B \varepsilon_{eff}^{pre} - c)] \\ m(\varepsilon_{eff}^{pre}) &= k_{1m} + \frac{k_{2m}}{2} [1 + \text{Erf}(-m_m \varepsilon_{eff}^{pre} - c)]; \quad n(\varepsilon_{eff}^{pre}) = k_{1n} + \frac{k_{2n}}{2} [1 + \text{Erf}(-m_n \varepsilon_{eff}^{pre} - c)] \end{aligned} \quad (2)$$

The third ansatz is like ansatz 1 but approximates the hardening curve directly.

$$\sigma = \bar{A} - \bar{B}(1 - \exp[\bar{m}_1(\varepsilon_{eff}^{pre})^{\bar{n}_1} + \bar{m}_2(\varepsilon_{eff}^p)^{\bar{n}_2}]) \quad (3)$$

The three ansatz functions have been calibrated on the experimental data by nonlinear regression using Mathematica [3]. For the analyzed DP600HF Fig. 1 right shows the calibrated ansatz function of Eq. (1) that agrees well with the experimental data.

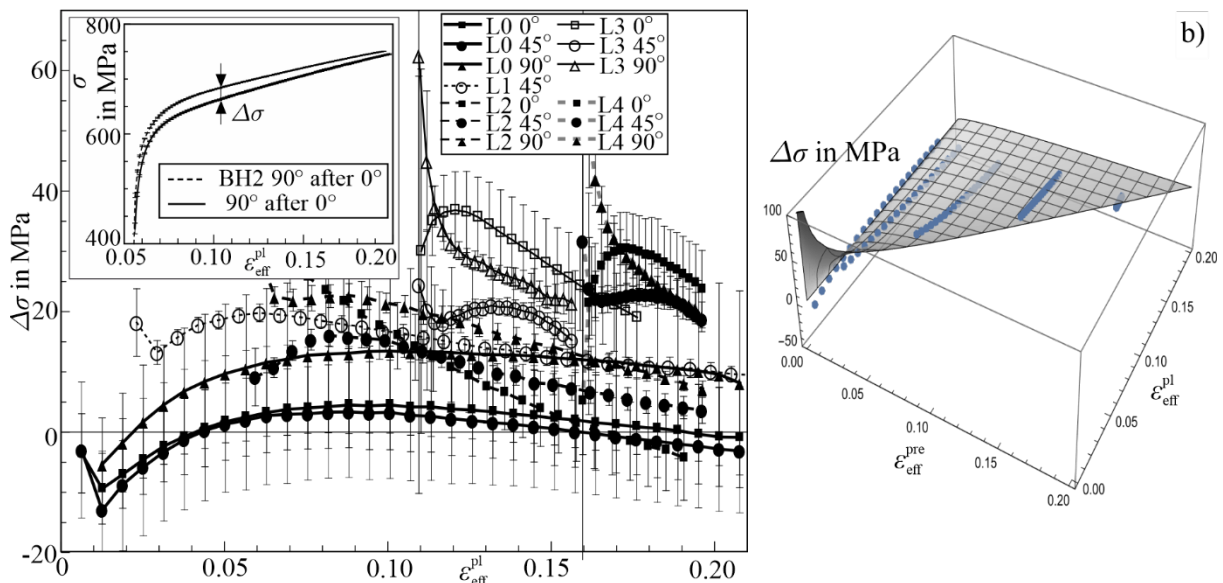


Fig. 1: Left: Change of yield stress between untreated and heat-treated material for different levels of pre-deformations (L0 - 0%; L1 - 1.9%; L2 - 5.5%; L3 - 10.7%; L4 15.7%) for DP600HF. Right: Calibrated ansatz function depending on pre-strain and plastic strain compared to experimental yield stress change.

4 Simulation at demonstrator part

Since the resulting effects at the analyzed three high strength steels in the overall behavior are rather small, we here show a simulation of a deep drawn cup with curved bottom made out of an hardenable aluminum alloy (AA6014), where similar effects occur during the paint drying process. We use the MpCCI-Mapper of the Fraunhofer SCAI [4] to segmentize the part in regions of different material behavior. But the use of MAT251 would be possible too. The force-displacement curves of the model agree well with the experimental results.

5 Summary

The presented results show that the Bake Hardening effect is mainly of isotropic nature. For the inclusion of this behaviour in the transformation of the material behaviour between the manufacturing and loading simulation (e. g. Crash simulation), three phenomenological ansatz functions are proposed. For the three analysed steel grades, all ansatz functions show good agreement with the experimental data. An example simulation of an indentation test of a deep drawn cup specimen shows good agreement of the simulation with the experimental results.

6 Literature

- [1] DIN EN 10325: „Bestimmung der Streckgrenzenerhöhung durch Wärmebehandlung (Bake-Hardening-Index)“, 2006.
- [2] Palkowski, H. and Anke, T.: „Bake hardening of hot rolled multiphase steels under biaxial pre-strained conditions“, *Steel Research International*, Bd. 77, p. 675–679, 2006.
- [3] *Wolfram Mathematica R 11.3.0 Copyright 1988-2018 Wolfram Research*, Champaign, Illinois, USA.
- [4] Fraunhofer SCAI, "MpCCI Mapper," Fraunhofer SCAI, [Online]. Available: <https://www.mpcci.de/en/mpcci-software/mapper.html>. [Accessed 09 02 2022].

Multi-Shape Modeling of Line Welds in Crash Models using ANSA

Dr. Niels Pasligh¹, Thanassis Fokylidis²

¹ Ford-Werke GmbH, Research and Innovation Center Aachen

² BETA CAE Systems SA

1 Introduction

One of the most critical processes during the manufacturing of a vehicle is its assembly. Similarly, during the setup of the virtual model of a vehicle, the assembly process holds a key role in CAE. This is because numerous different parts must be brought together with high accuracy. This is accomplished with the use of various types of joints. Line welds are one of the often-used types of joints exemplarily laser weld or gas metal arc weld lines.

The current presentation demonstrates a new CAE modelling approach using line welds with the aid of the ANSA pre-processor. Highlights of this new process include: the way the CAD information is translated into CAE data, the automated assembly process of the full vehicle, the adaptation of the Heat Affected Zone concept in the process, and the treatment of legacy models (CAE models assembled differently in the past).

2 CAE modelling approach

Line welds are much used at Ford, in several applications during production with highly predictive approaches. The currently developed approach of laser and gas metal arc weld lines target full vehicle models. There are three types of FE-representations in CAE that will be approached depending on the type of the connection. These are butt, edge, overlap or t-joints. As a result, the weld lines are represented either by shell elements only, by a single row of solid elements, or by a cluster of cohesive and continuum mechanics elements. Also, the developed approach is applicable to several shapes of geometries such as, overlap joints from stitch to complex 2-D shaped forms.

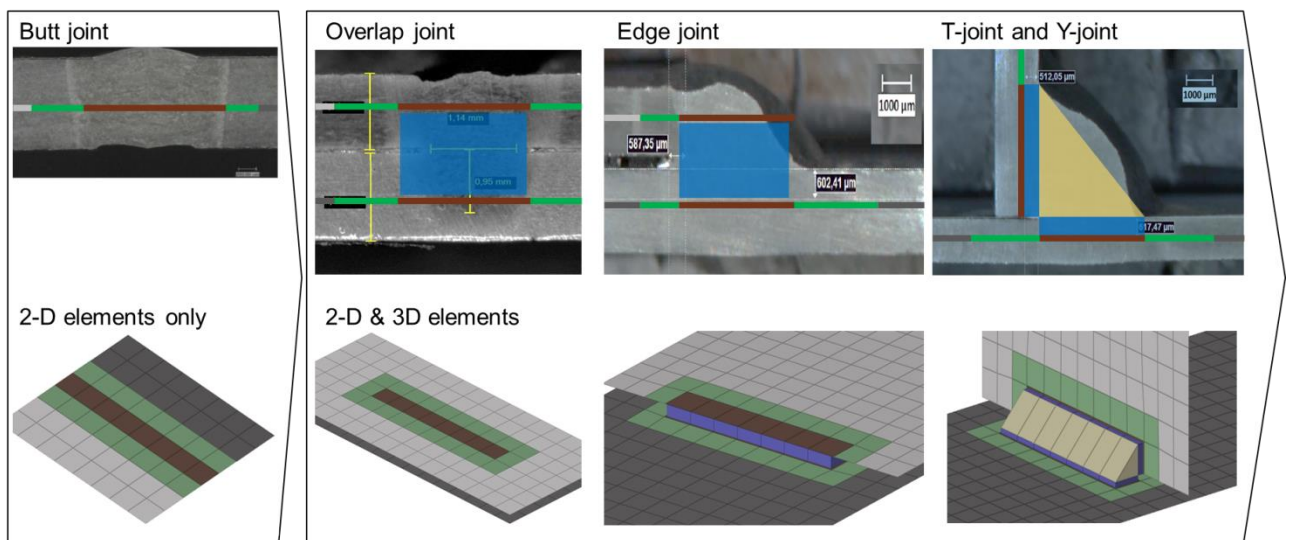


Fig.1: Physical x-sections and the respective CAE line welds

3 Automated Pre-Processing of seamlines in ANSA

Product development teams require a thorough yet efficient and user-friendly pre-processing application. Resulting from the cooperation between Ford and BETA CAE Systems, ANSA has been enhanced and can now capture all requested features such as, types of line weld shapes and

configurations. Following the main steps of the process in ANSA, one meets the translation of the CAD data to CAE ones, the ANSA connections templates and finally the development and realization of the main FE-Representations used in the current process.

3.1 CAD to CAE

CAD represented seamlines can be imported in ANSA. The user can easily convert the CAD data to CAE connection lines and proceed with the assembly process of the seamlines within ANSA. Another way of handling the connection information coming from CAD is with the use of an xml file. Having already the desired FE model in ANSA, the user can import the connection's file (xml) and ANSA will create the connection lines (seamlines) while maintaining all the necessary information such as, the connection name, the connectivity parts and connection position (x, y, z coordinates) which are mandatory for the connection lines realization.

3.2 ANSA connection templates and FE-Representations

For the current seamlines assembly process, the development of special FE-Representations took place following the FORD specifications. Each FE-Representation has specific settings that each time need to be applied on the FE model. Since the process addresses the full vehicle and the different FE-Representations have to be re-used several times, the connection's settings are saved in ANSA connection templates. The connection templates are the basis of the current automated assembly process. Every time that the user needs to assemble a model, the connection templates are automatically loaded in ANSA and distributed according to specific criteria (e.g. connection name). As a result, the user can realize massively all the connection lines of the CAE model through a properly defined assembly scenario decreasing the process time to its minimum.

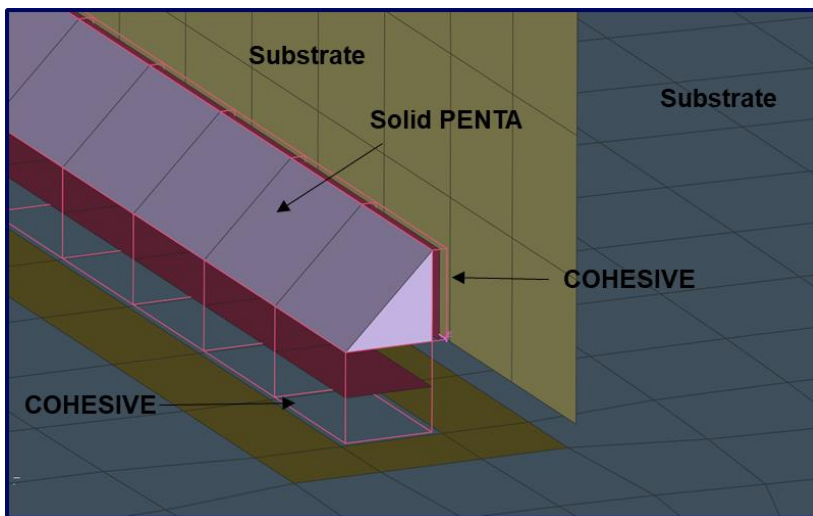


Fig.2: Example of a T-Joint realized in ANSA

4 Heat affected zones assignment

It is worth mentioning the special effort put, in the FORD seamline assembly process, to represent a real connection in the CAE world as accurate as possible. During realization, the HAZ assignment is made possible to each substrate per case in the connection area. This way, the re-crystallization areas of the flanges are represented with different ***PART** (material). As a result, special failure settings are automatically assigned according to the FORD material specifications.

5 Legacy models treatment

The legacy models' treatment was another accomplished aspect of this assembly approach. Line connected models have been imported in ANSA and ANSA connection lines have been created in pure keyword files with no ANSA information yet. Then the line elements (e.g. ***ELEMENT_BEAM**) could be

directly transformed into *ELEMENT_SOLID (COHESIVES) to follow the current assembly approach and continue to the respective analysis in LS-DYNA®.

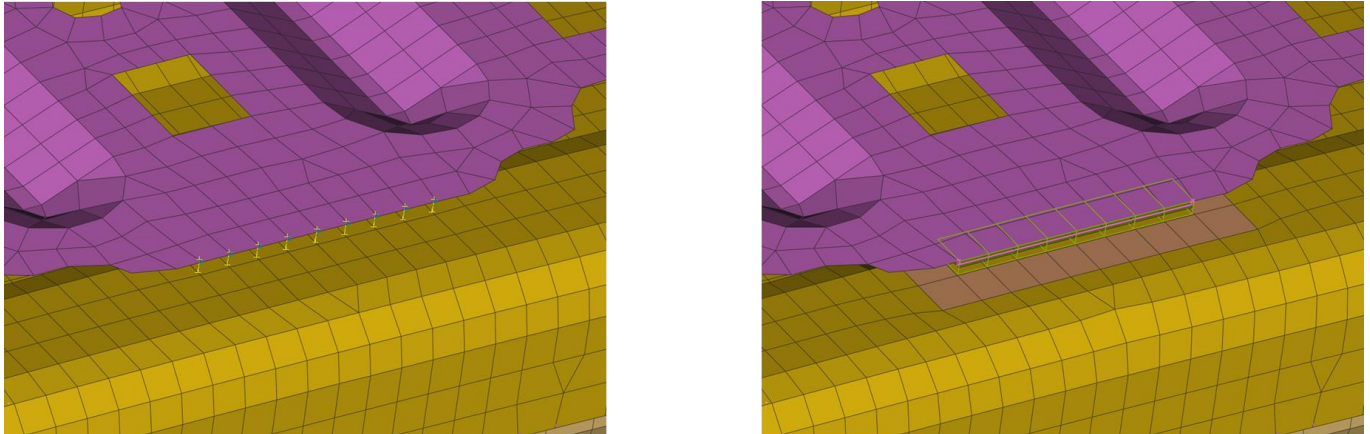


Fig.3: Transform a line connection to a solid one

6 Literature

[1] ANSA User's Guide v22.1.x

[2] META User's Guide v22.1.x

[3] Halquist, J.O., LS-DYNA® Keywords User's manual Version 971 R9.0, Livermore Software Corporation, Livermore, 2016

Towards Faster 3D Simulations of CFRTP Induction Welding

Miro Duhovic, Stefano Cassola, Thomas Hoffmann, Peter Mitschang

Leibniz-Institut für Verbundwerkstoffe GmbH, Technische Universität Kaiserslautern, Erwin-Schrödinger-Straße 58, 67663 Kaiserslautern, Germany

1 Introduction

Imagine the process design space of joining two material partners together via electromagnetic induction where one of the most important joining parameters is the temperature field within the joining zone. The input parameters for the process are the induction coil power input (alternating current amplitude), welding speed, induction coil to consolidation roller distance, induction coil to work piece offset distance, material partner one thickness, material partner two thickness, material partner one material properties (heat capacity, electrical and thermal conductivities), material partner two material properties (heat capacity, electrical and thermal conductivities) and top surface cooling rate. This already results in a whopping 13 variable parameter set, resulting in the seemingly impossible computing task (13 factorial solutions or 635,013,559,600 different possible simulation combinations!) in terms of process design variable optimization. This parameter set grows even further when anisotropic materials (such as carbon fiber reinforced thermoplastics (CFRTPs)) are considered and the electrical and thermal conductivities are separated into their directional components. In addition, the simulation of any single arbitrarily chosen parameter set can take several days to compute using even today's high powered computing resources, not due to model size (e.g. number of elements in the model), but due to the complex interacting multi-physical phenomena (and their resulting differential equations) which need to be solved in parallel. Using MSC Software's ODYSSEE CAE, this challenging optimization task is simplified through powerful reduced order modelling (ROM) and machine learning (ML) technologies. The software speeds up the generation of results by several orders of magnitude after an initial training phase using only a small number of full model training sets, dependent on the number of parameter variables considered in the model. In the current work, the software's capabilities are initially demonstrated on the application case of CFRTP electromagnetic induction welding parameter set optimization. In this study, five key parameters have initially been chosen, namely the *power input*, *welding speed*, *top surface cooling rate*, laminate fiber in-plane electrical conductivity, $K1/K2$ and laminate electrical conductivity transverse to the fiber direction, $K3$. For each of these parameters, a realistic range (max. and min. possible values) is defined. This is used to create the design of experiments (DOE) based ROM training data which can then be used to predict the output of the simulation model, in this case, the maximum temperature achieved anywhere at the welding interface over the entire duration of the welding process.

2 Basis model description

The typical setup for the continuous joining of two composite laminates is illustrated in Figure 1.

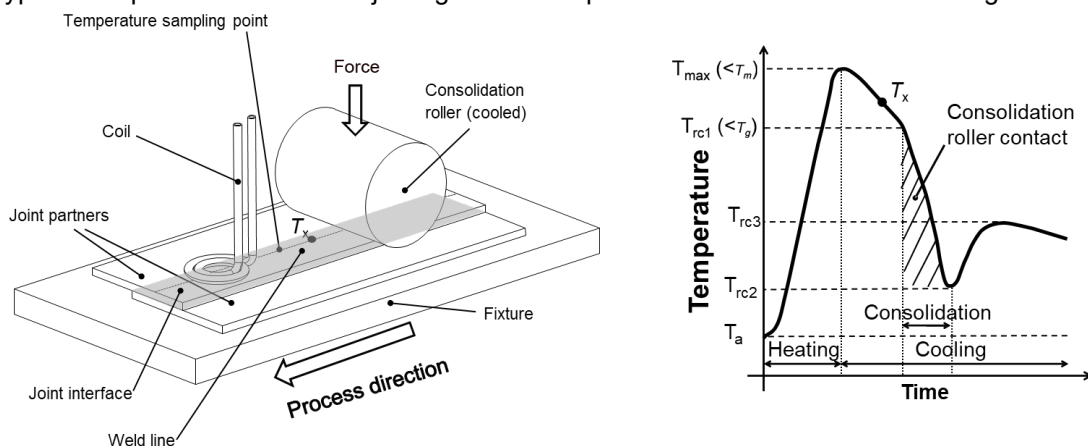


Fig. 1: Basic setup of the continuous induction welding of two composite panels (left) and simplified temperature versus time profile on the top surface of the laminate stack (right).

The graph shown in Figure 1 (right) represents the temperature profile of a single fixed point on the top surface of the laminate stack during the induction welding procedure. In Figure 2 (left), results from a simulation show the temperature development across the entire width of the weld with respect to time. To prevent overheating on the top surface of the laminate stack, cooling is applied via an air-jet nozzle blowing air through the center of the coil. An example of the maximum temperature reached at any time at the joint interface during the entire induction welding process with applied top surface cooling is shown in Figure 2 (right). Further details on such continuous induction welding simulation models can be found in references [1] and [2].

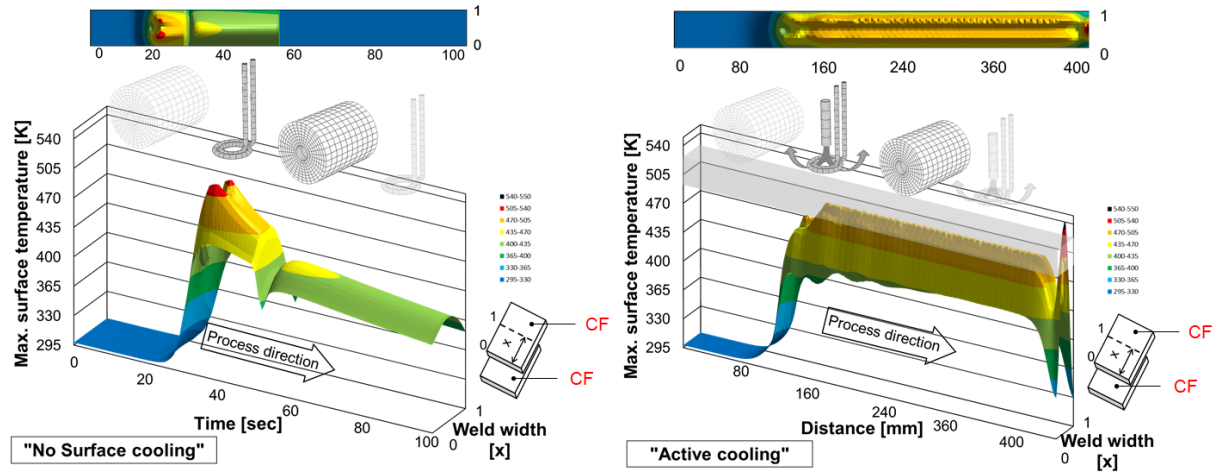


Fig.2: Examples of induction welding surface plots of the top surface temperature development over time (left) and the maximum achieved temperature at any point at the joint interface during welding (right).

The latter forms the basis of the results dataset (Y database) used to create the ROM in ODYSSEE CAE's Lunar module. The DOE, which is also generated in Lunar uses the parameter set shown in Table 1 and provides the input database, (X database) for the ROM. A total of 42 simulations are carried out considering DOEs generated using the Latin Hyper Cube approach starting from 21 to 42 DOEs in steps of 3 for the sake of ROM training improvement. Command scripts have been written to automatically extract the maximum temperature data on all nodes at the joint interface for each LS-DYNA® model.

Priority	Parameter	Min value	Max value
1	Welding speed (m/min)	0.1	0.5
2	Power (current amplitude) (A)	70 (10% Power)	700 (100% Power)
3	Top surface cooling rate (W/m ² K)	0	10000
4	Laminate in-plane electrical conductivity, K1/K2 (combined) (S/m)	16000	30000
5	Laminate through thickness electrical conductivity, K3 (S/m)	0.03	10

Table 1: Possible process and material input parameters and their ranges that define the DOE and model input database (X database) for the ODYSSEE CAE Lunar reduced order model.

The data from the surface plots are arranged into the Y database .csv file required by Lunar as a single row of data (per DOE parameter set) which is obtained from each LS-DYNA® simulation model output. Each simulation takes an average of 12 days to solve using 4 Cores of an Intel® Xeon® Ice Lake Gold 6326, 2.9 GHz, 16-Core CPU. Due to the complexity of the physics involved rather than model size, the best strategy to generate the ROM training set is to run as many simulations as possible in parallel rather than use more CPUs per simulation. The models were solved using the new monolithic EM solver *EM_SOLVER_FEMBEM_MONOLITHIC and LS-DYNA® R13 SMP. More details regarding the monolithic EM solver can be found in reference [3].

3 ODYSSEE CAE

The creation and analysis of the ROM accuracy is carried out in ODYSSEE CAE's Lunar module (v2022.2). The user provides file paths to the X and Y .csv database files together with the type of solver

desired (POD (all modes) with ARBF is used in this work). Additionally, validation sets can be given to check the accuracy of the ROM with parameter sets (Xn database) not used in the training, but which have been run separately in LS-DYNA® (Yn database). The directory containing the training models is also given together with the "LS-DYNA® animation file base name" e.g. d3plot, of a training model, which is used by the software to generate new complete LS-DYNA® output data for a desired model input parameter set. Figure 3 shows a screenshot from Lunar and the base curves for an initial DOE study consisting of 25 training models. It can be seen that the 4 predicted output curves (colored solid curves) fit reasonably well with the 4 imported validation curves (colored dotted curves) generated from joint interface temperature data obtained from LS-DYNA® simulations not used in the training DOE.

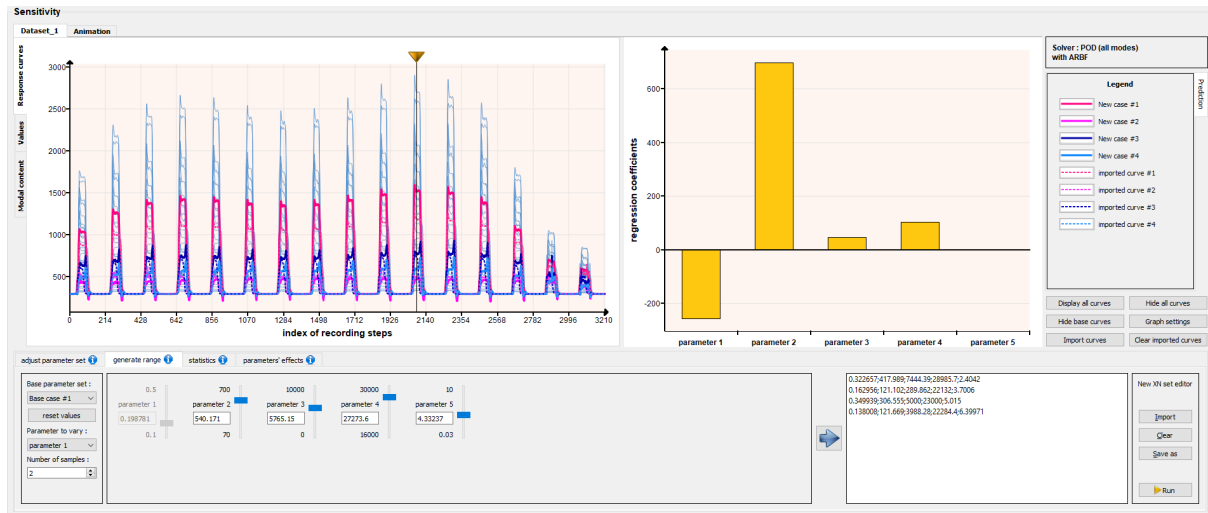
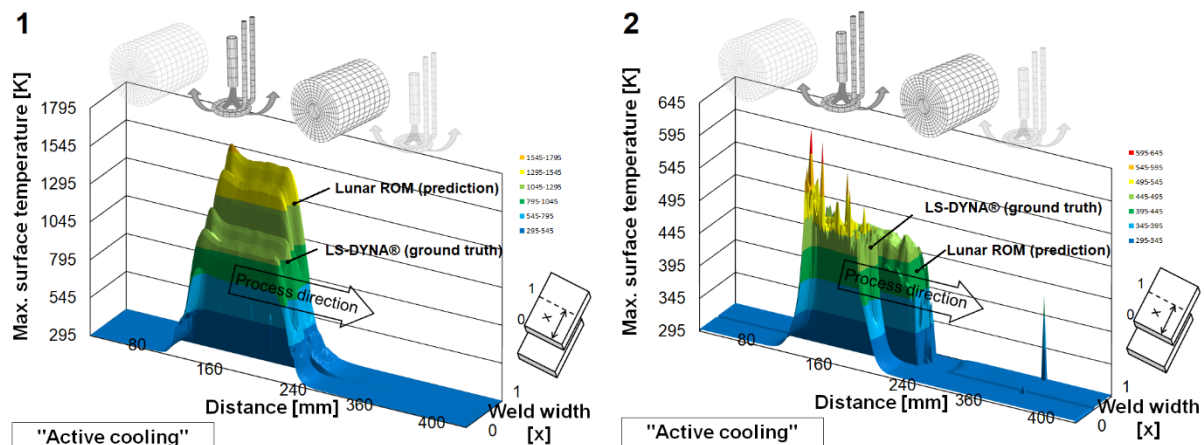


Fig.3: Validation of ROM temperature response curves of maximum temperature achieved during induction welding in ODYSSEE CAE's Lunar module together with regression coefficients for the five considered welding parameters.

Further training sets, in particular for regions of the DOE exhibiting a highly non-linear response are required in order to improve the ROM prediction accuracy. Through the slider bars in the sensitivity tab, one is able to change any of the parameters and then instantly generate data for a new parameter set which can again be reconstructed and visualized as 3D surface plots. The regression coefficients show that the coil current (*parameter 2*) followed by the welding speed (*parameter 1*), the in-plane electrical conductivity (*parameter 4*), top surface cooling (*parameter 3*) and the through thickness electrical conductivity (*parameter 5*), have the most influence on the temperature field in this order according to the individual ranges chosen (see again Table 1). This means that a narrowing of the induction coil current input to a more reasonable range (i.e. 700 A coil input current seems far too high) will most likely help improve the ROM accuracy and avoid the necessity of additional training. Full simulation results (d3plots) can also be recreated in a fraction of the time (<2 minutes rather than 12 days) compared to complete individual LS-DYNA® runs. An export of the ROM generated data can also be transformed back to 3D surface plots allowing better visualization of LS-DYNA® versus Lunar ROM predicted results.



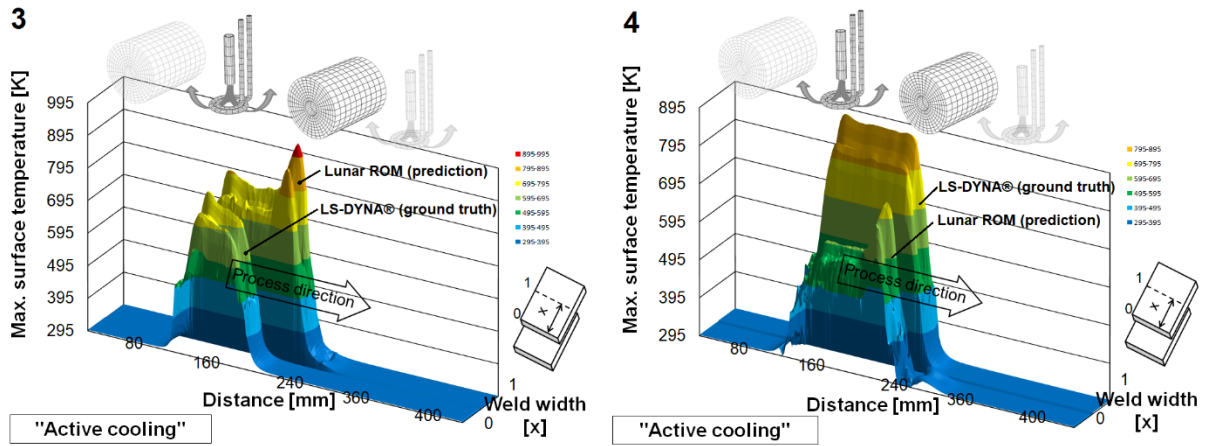


Fig. 4: A comparison of the maximum welding temperature surface contours obtained from LS-DYNA® (ground truth) and Lunar (predicted) ROM for the selected validation parameter sets 1 to 4.

Figure 4 shows the LS-DYNA® (ground truth) versus ODYSSEE CAE's Lunar ROM (predicted) results for four selected validation sets (see Table 2) and their corresponding surface plots placed side-by-side on the same graph. It can be seen that overall good results have been achieved considering the limited number of training sets. For cases where the coil current strongly dominates or when the combination of parameters results in the coil current becoming the dominating factor, accuracy is lost.

Parameter	Val. Set 1	Val. Set 2	Val. Set 3	Val. Set 4
Welding speed (m/min)	0.322657	0.162956	0.349939	0.138008
Power (current amplitude) (A)	417.989	121.102	306.555	121.669
Top surface cooling rate (W/m ² K)	7444.39	289.862	5000	3988.28
Laminate in-plane electrical conductivity, K1/K2 (combined) (S/m)	28985.7	22132	23000	22284.4
Laminate through thickness electrical conductivity, K3 (S/m)	2.4042	3.7006	5.015	6.39971

Table 2: Parameter sets used to validate the trained ODYSSEE CAE Lunar reduced order model.

4 Summary

ODYSSEE CAE's Lunar module is a powerful ROM parameter optimization tool, which can be used to create ROMs of even extremely complex multi-physics simulation scenarios (in this work electromagnetic, thermal and structural). Once validated, accurate instances of the full 3D models can be recreated in close to real-time allowing for digital twin type implementation of the induction welding process in order to help plan and optimize the process. A first attempt at creating a ROM for the induction welding simulation models shows that some of the parameter ranges need to be refined, in particular the coil current, in order to allow a more accurate ROM with a manageable model training set size.

5 Acknowledgements

The authors would like to thank Nikolay Lazarov and Steffen Frik for their technical support and MSC software for providing the ODYSSEE CAE test license.

6 Literature

- [1] Duhovic M., Hausmann J., L'Eplattenier P., Caldichoury I. A Finite Element Investigation into the Continuous Induction Welding of Dissimilar Material Joints. In: Proceedings of the 10th European LS-DYNA® Users Conference, Process VII – Welding, 15.-17. June, 2015, Würzburg, Germany.
- [2] Duhovic M., Caldichoury I., L'Eplattenier P., Mitschang P., Maier M. Advances in Simulating the Joining of Composite Materials by Electromagnetic Induction. In: Proceedings of the 9th European LS-DYNA® Users Conference, Electromagnetic(2), 2-4. June, 2013, Manchester, UK.
- [3] Duhovic M., Caldichoury I., L'Eplattenier P., Nguyen T., Hausmann J., Kielhorn L., Rüberg T., Zechner J. Applications of the new magnetostatic solver/ AMS preconditioner in LS-DYNA®. In: Proceedings of the 13th European LS-DYNA® Users Conference, 5.-7. October, Ulm, Germany, 2021.

Automatic Outlier Detection for Crash Simulation Results

Dominik Borsotto¹, Vinay Krishnappa¹, Clemens-August Thole¹, Kirill Schreiner¹,

¹SIDACT GmbH

1 Introduction

To cope up with the ever growing amount of simulation runs being performed, tools and techniques are needed to make use of the huge amount of simulation data being stored. While current Simulation Data Management systems and the IT infrastructure already allows to store and access huge datasets and would facilitate putting this into action for analysis, the user usually only has tools and the time to make rather straight forward model to model comparisons between current model versions and their immediate predecessors. To take analysis capabilities and model development a leap forward it is necessary to also make use of whole model development branches to learn from the gathered simulation information

2 Analysis Database

In order to make use of all simulation results during model development a database has to be deployed which grants access to every result also at a later stage of development.

2.1 Compression

To being able to analyse hundreds of simulations against each other a compressed database is key here. With SDMZIP it is possible to compress thousands of simulations together in a database while making use of already archived simulations, so that just the differences have to be added which eliminates data redundancy. This database was the enabler for the development of Eventdetection.

2.2 Mapping

One of the biggest challenges next to compressing data is the actual mapping between simulations to make analysis possible over the whole development branch. Some of the challenges to cope with during the model development process are e.g. PID changes, altered parts, different meshes, additional parts and many other part changes, without losing relationship between predecessor parts. To do so a sophisticated mapping approach between the simulations has been developed, in which groups of parts are treated together. These form components to be used for the mapping procedure. Compared to single PID mapping this allows to cope with the above mentioned challenges.

3 Eventdetection

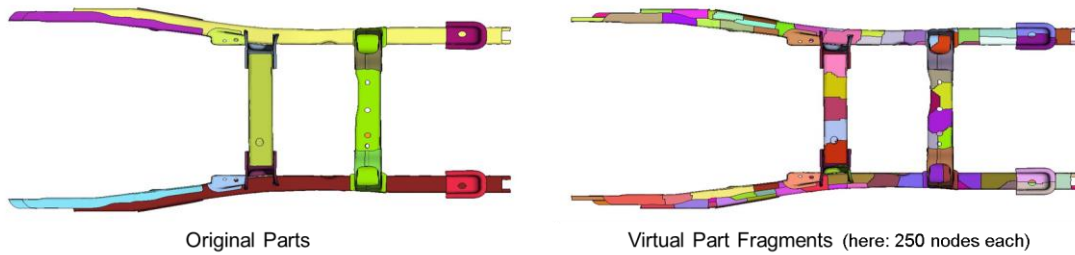
The tool Eventdetection was developed with the emphasis to automatically spot unknown behaviour in new simulation runs. It allows detecting new behaviour/events within the current simulation compared to all predecessors and automatically raises this to the engineer.

3.1 Eventscore

The before mentioned detection of new events is based on a PCA related outlier score computation. This results in an event score in the range from [0:2] for every part and time-step, defining how much of an unknown behaviour this event represents. This also gives feedback to the engineer right away about how strong the outlier is, depending on the value of the event score. A score below 1 represents known behaviour, while scores above 1 represents unknown behaviour. The higher the score, the stronger the outlier.

With respect to the challenge of analysing crash structures it is mandatory to not only highlight complete parts which are conspicuous, but also the local segment of the part which showed the behaviour, which is why internally Eventdetection splits parts into fragments to also support a high

geometrical resolution and detect local events. Additionally, next to the geometry also all post-values, as e.g. strains and stresses, as well as failure are being analysed.



"The model has been developed by The National Crash Analysis Center (NCAC) of The George Washington University under a contract with the FHWA and NHTSA of the US DOT" <http://www.ncac.gwu.edu/vml/models.html>

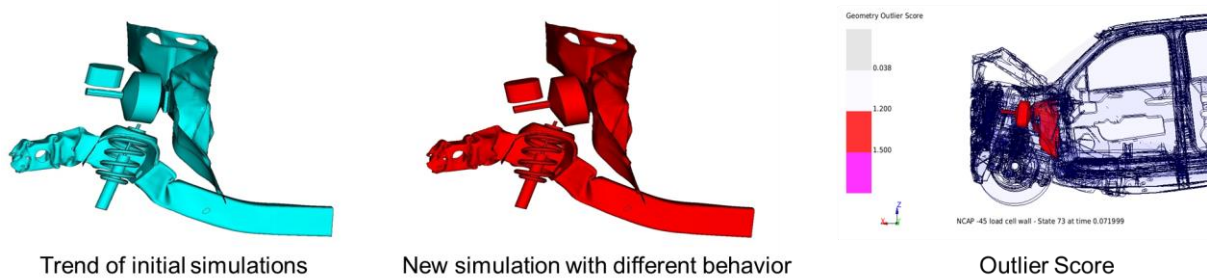
Fig.1: Exemplary part fragmentation to being able analyse local effects

3.2 Event Propagation and Clustering

To not only detect single part differences the event computation incorporates an event clustering. Based on the neighbourhood and the propagation of the deformation, parts are clustered together, forming Events which also represent the propagation over time and space.

4 Example Case

To being able to benchmark and evaluate Eventdetection a well-known data set was chosen. 30 simulation runs of the Chevrolet Silverado Model ("The model has been developed by The National Crash Analysis Center (NCAC)) with thickness variations, which have been analyzed in the past by means of robustness, where known to show a clear bifurcation. While for some simulation runs the break-booster hooked up to the suspension, being pushed into the firewall, for others there was no such hook-up. Therefore the test scenario shown here consists of a set of simulation runs with similar behavior of no hook-up and a newly analysed simulation containing the hook-up.



"The model has been developed by The National Crash Analysis Center (NCAC) of The George Washington University under a contract with the FHWA and NHTSA of the US DOT" <http://www.ncac.gwu.edu/vml/models.html>

Fig.2: Test scenario: Chevrolet Silverado deformation @ State 80 [ms]

Analysing the set of simulations runs with the tool Eventdetection automatically highlighted the areas of interest and pushed the attention immediately to the new behavior at the break-booster

5 Summary

In this abstract we illustrated how the Eventdetection tool can automatically spot and highlight new behaviour. A compressed database with a sophisticated mapping approach is the enabler to analyse new simulation runs against all predecessors and highlight unknown behaviour to the engineer automatically.

Future Engineering Data Management: Data-driven product development with a single system for all engineering data

Christopher Woll

GNS Systems GmbH

Customer and market requirements are changing rapidly. Accordingly, product life cycles have shortened and companies need to develop faster and more efficiently. The traditional time-intensive development cycle is thus obsolete - today it is all about bringing products to market in the shortest possible time with simulation-based design and digital twin. At the same time, companies are facing the challenge of mastering a growing amount of data. Dealing with LS Dyna in particular also requires consistently linking simulation results with experimental engineering data from a wide variety of sources in a sustainable manner.

With the Platform for Digital Engineering, GNS Systems precisely meets these requirements. The open platform integrates distributed data silos and allows efficient data management from product development involving R&D digital twin to product practice. The centralized platform for engineering offers consistent access to the growing number of data types and systems for the necessary Big Data Management. It supports developers in using even complex data correlations for product development across system boundaries. Through the seamless integration of specific tools, such as LS Dyna for complex crash and forming problems, CI/CD pipelines, and data integration layers, engineers can process simulation, test, and field data in equal measure. Highly complex scenarios can be simulated and validated in the shortest possible time using the platform as an information hub.

Likewise, developers benefit from the enormous process reliability and high flexibility offered by an integrated system for managing engineering data. The resulting trust in the company-wide data repository as a single point of truth (SPOT) encourages developers to make data-driven decisions and drive product innovation. Integrated AI-based analytics of the datasets further increase efficiency by identifying valuable information and patterns that can be used profitably.

1 Summary

Data-driven product development is not only dependent on selecting and implementing the right IT system. Rather, it is a matter of establishing a coherent strategy for an environment that addresses the challenges of handling engineering data (for example, data storage and management, optimal data access, and traceability) in a forward-looking approach. Using a use case, the experts from GNS Systems show how the Platform for Digital Engineering addresses all aspects of cost reduction, reliability, and flexibility. Integrating standardized processes and fully automated workflows via a CI/CD pipeline supports companies in significantly reducing the time between development, testing, and implementation.

Introduction to Machine-Learning Capabilities in d3VIEW for Numerical, Categorical, and 2D Data Learn and Predictions for Data-Science and non-Data-Science Engineers

Suri Bala¹

¹d3VIEW Inc. + legal form

Abstract

This paper will demonstrate the newly integrated d3VIEW's Machine-Learning capability that augments the visualization library. With this new capability, data can be imported, visualized and now ML-models can be built for use in prediction. The paper will show example applications to learn and predict using a variety of models available in d3VIEW.

Towards the Isogeometric Aero-Engine

Markus Kober¹, Bernd Beirow¹, Kai Singh²

¹Brandenburgische Technische Universität Cottbus – Senftenberg,
Lehrstuhl für Strukturmechanik und Fahrzeugschwingungen

²Rolls-Royce Deutschland Ltd & Co KG

1 Introduction

The need for more efficient and environmentally friendly aero-engines powering aircrafts leads in the development process to more and more detailed thermomechanical simulation models in order to better understand and optimize the behavior of the engine during different flight conditions. Currently, classical finite element models are used for these computations. Since a high degree of accuracy is necessary, the engine models contain almost no simplifications or idealizations. By this, the effort for the model generation in terms of mesh quality is very high. Additionally, in many regions a very fine mesh is necessary since a coarse mesh could prevent a kinematically correct rotation of parts against each other due to the faceting of the contact surfaces for example in bearing regions [1].

Isogeometric Analysis (IGA) offers the possibility of an exact geometry description e.g. for curved structures also in the computational domain although a coarse mesh can be used. As shown in [2,3] this leads to much more realistic results, for example for the contact forces in bearings. Moreover, the process of creating a CAD model and a finite element model can be combined since the IGA uses as basis functions for the finite elements so-called Non-Uniform Rational B-Spline functions (NURBS) which are also used for the geometry description in CAD tools.

2 Generation of Solid IGA Models

Unfortunately, the pre-processing capabilities for the generation of solid IGA models in commercial tools as LS-PrePost are still limited. Here, we present a possibility to generate at the same time a CAD model and a computational IGA model for LS-DYNA by using a simple Python CAD tool, described in [4], and our own Python translation tool which transfers the generated CAD NURBS data automatically into a LS-DYNA IGA model which is ready for computation without further meshing. The model generation process is very similar to a classical CAD construction procedure. For example, a simple casing part of an aero-engine can be created by defining the cross section of the part and revolving this cross section. By this, we get the co-called coarsest mesh of the part (Fig. 1a), which exactly represents the geometry with the minimum number of necessary control points, which correspond to the nodes in the classical FEM. Often, it is necessary to refine the coarsest mesh in order to get an improved mass distribution or a better resolution of stresses. For this purpose, the required algorithms are already implemented in LS-PrePost and mesh refinement is performed automatically by just changing the number of elements or increase the order in a certain direction without changing the geometry (Fig. 1c).

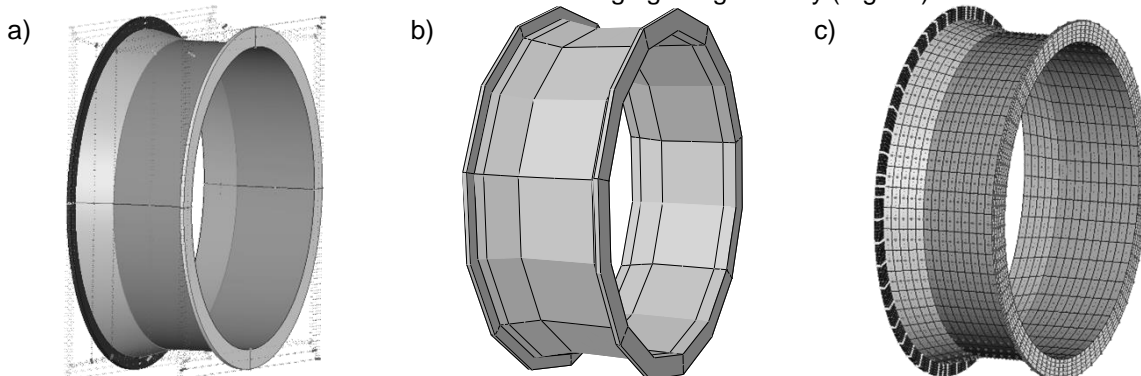


Fig. 1: Coarsest mesh of casing part with 2nd order NURBS elements (a), classical 2nd order finite element mesh with similar number of degrees of freedom (b) and refined NURBS mesh (c)

3 Isogeometric Dummy Engine Model

By using the described methodology of generating isogeometric models we were able to create a simplified whole-engine model of an aero-engine (Fig. 2). This fully isogeometric model is used for different implicit transient computations as well as for explicit simulations.

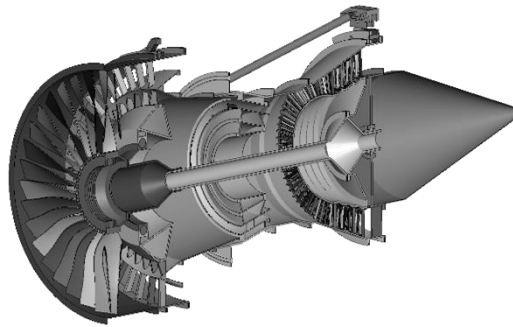


Fig.2: Section cut of isogeometric Dummy Engine Model

4 Computational Costs

When using a new technique like isogeometric analysis it is also interesting to consider the computational costs in comparison to the classical FEM. Doing so, it is important to distinguish between different types of analysis (implicit, explicit, ...). Fig. 3 shows the ratio of the computational time for an IGA model in comparison to a classical FEM model (for one iteration) with the same number of degrees of freedom (both second order). All implicit computations were performed with the default direct solver. Obviously, the ratio of computational times between IGA and FEM is always greater than one which means that the solution process for an IGA model with the same number of degrees of freedom is slower than for a classical FEM model. This is caused by an IGA stiffness matrix which has the same maximum bandwidth for the same element order as for classical FE elements but less zero entries. Nevertheless, by using IGA much time can be saved during the model generation and meshing process which is for real parts mostly a multiple of the actual computational time.

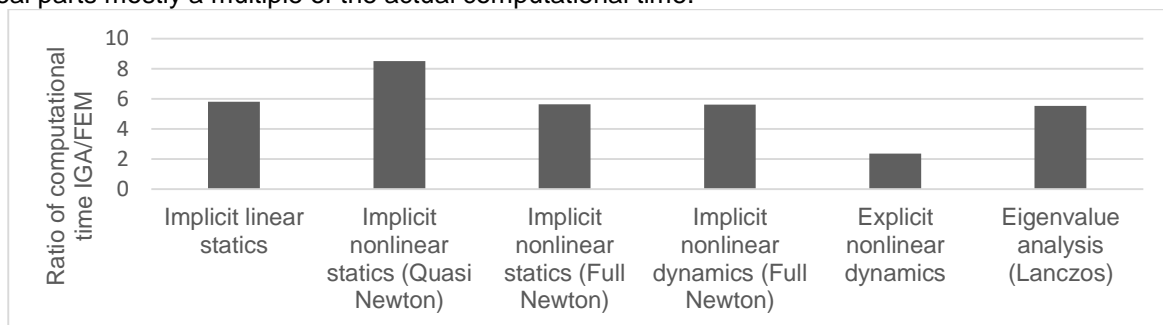


Fig.3: Ratio of computational time of IGA/FEM for different analysis types

5 Summary

Creating solid IGA models is still not state of the art in commercial tools. By using the presented process, we are able to generate almost arbitrary complex geometries and IGA models at the same time. The generated IGA models are automatically translated into the LS-DYNA format and used for all types of simulations. Since the meshing step in the model generation procedure can be skipped, much time is saved although the pure computational time can be higher than for classical FE models. Additionally, IGA is able to exactly represent the geometry with less degrees of freedom than classical FEM.

6 Literature

- [1] Kober, M., Kühhorn, A., Steldinger, E. and Keskin, A.: "Considerations about the Necessary Mesh Density of Bearings in Detailed Finite Element Models", Proceedings of ASME Turbo Expo, 16-20 June 2014, Düsseldorf, Germany, Paper GT2014-25624.
- [2] Naveed, Z., Kühhorn, A., Kober, M.: "An Isogeometric Based Study of Contact Behaviour for Rotating Structures", 14th World Congress on Computational Mechanics (WCCM)-ECCOMAS Congress 2020, Virtual Conference 11-15 January 2021.
- [3] Naveed, Z., Kühhorn, A., Kober, M.: "Contact Behaviour of Isogeometric Analysis for Rotating Structures and its Industrial Application by Coupling to the Classical Finite Element Method", VII International Conference on Isogeometric Analysis, 18-20 September 2019, München, Germany.
- [4] Johannessen, K.A. and Fonn, E.: "Splipy: B-Spline and NURBS Modelling in Python", Journal of Physics: Conference Series, Volume 1669, EERA DeepWind'2020, 15-17 January 2020, Trondheim, Norway.

Isogeometric Analysis in ANSA, challenges and solutions

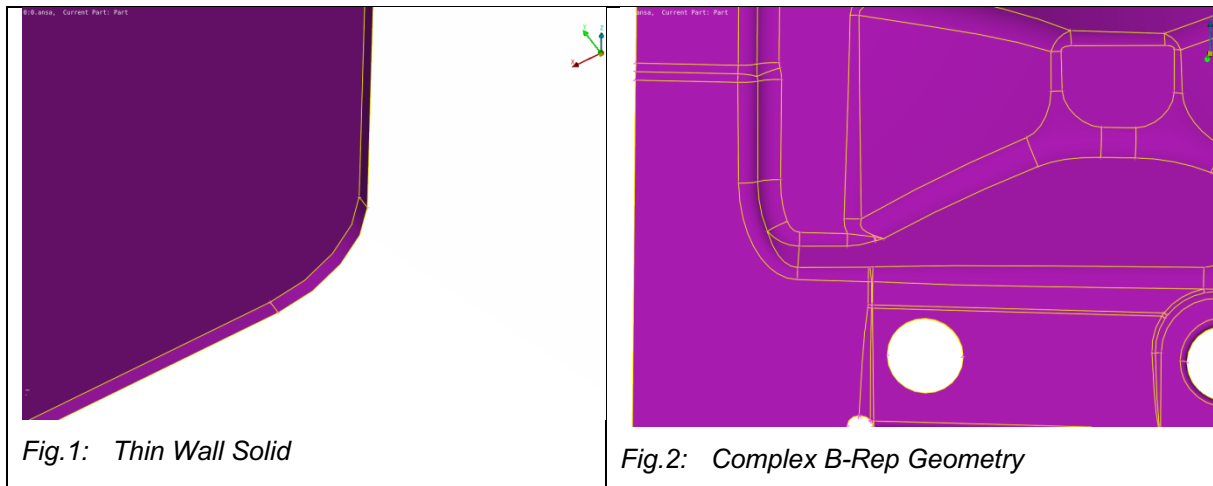
Lambros Rorris¹, Ioannis Chalkidis²

¹BETA CAE Systems International AG

²BETA CAE Systems SA

1 Introduction

Isogeometric Analysis (IGA) is maturing fast and offers certain advantages over classic FEA that makes it useful for large deformation dynamic analyses such as Crash applications in the automotive industry. CAD-CAE integration is yet another motivation for ANSA to introduce Isogeometric Analysis in pre-processing model simulations. Initial CAD designs, however, describe the boundary representations of complex solid parts with high level of detail in particular areas and a large number of undesired, in terms of analysis, faces (triangular – needle faces). Moreover, especially in automotive parts a large number of small holes appear quite often.



2 Creation of Analysis suitable geometry

During the last years the capabilities of both LS-DYNA and ANSA, in the creation and analysis of IGA crash models, have been under continuous development.

Coming up with a ready to solve IGA model for such complex geometries is a quite challenging process whether the target is a single trimmed patch or a set of connected untrimmed patches. Powerful fitting algorithms together with powerful CAD functionality are essentials to exploit the full potential of IGA.

The focus of our efforts has been the efficient generation of trimmed NURBS-based multi-patch surfaces that can represent parts of shell structures for the analysis in LS-DYNA. The transformation of CAD B-Rep data into Analysis suitable patches needed the development of algorithms that close the gaps of a B-Rep and result into a watertight model and at the same time merge them into just a few patches with the desired polynomial degree.

3 Unstructured Splines

As for unstructured patches, resulting from body fitted methods, ANSA supports pre – processing Bezier extraction files using LS – DYNA keywords. These body fitted methods seem to be an alternative to avoid the bottleneck of creating trimmed, watertight patches caused by the immersed boundary methods, but in this case a retopology tool of the initial geometry coming from CAD is essential. This

approach has many challenges but gives us a way to calculate Bezier extraction operators for complex existing geometries.

4 Model quality, model creation and assembly

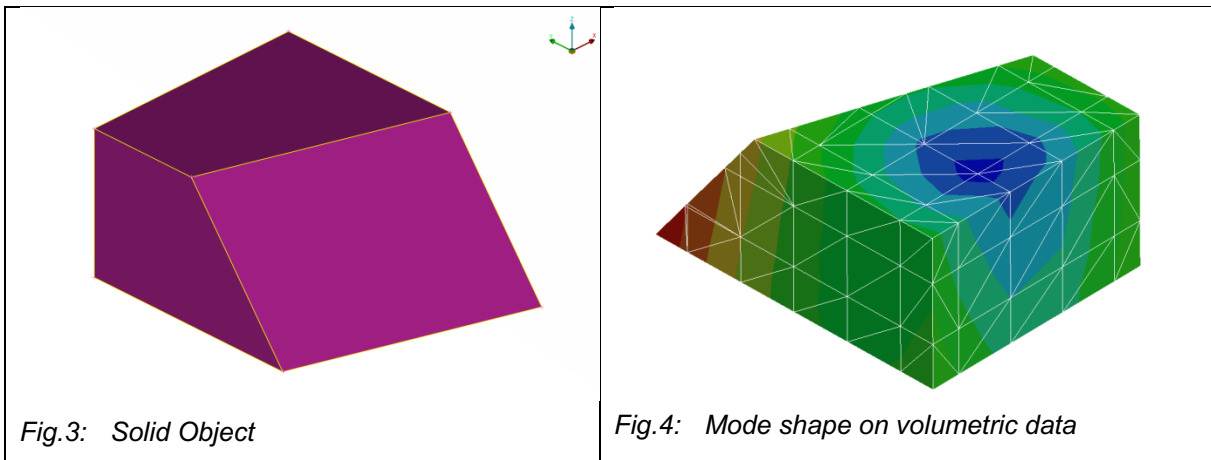
Another challenging task though is to bring together all the pieces of the building process of a complex model. Well defined NURBS geometries are rarely analysis suitable, since describing the shape of a part has completely different requirements than performing an analysis. Analysis suitable patches, though add an extra challenge to the pre-processor which has to be in position to warn about potential errors on the solver side, providing statistics and visualizing IGA entities in detail at the same time. Several parameters and metrics like the Jacobian, calculating the element length, the time step, the internal loops in knot span boxes etc. should be defined in order to ensure successive LS-DYNA results.

Another important requirement is to be able to define trimming areas and apply boundary conditions on them so all BCs and ICs can be applied on geometric entities.

Continuous integration with existing FE models and easy creation of Hybrid FE – IGA is another key target for the introduction of the new method in the current workflows and processes of such a demanding sector as the automotive, where tight schedules and fast development is common.

5 Solids

Classical boundary representations, as already mentioned, describe a solid only by its boundary faces and do neither provide any physical nor geometrical description of the interior. Solid Isogeometric Analysis brings as a new challenge, which is the recognition and conversion of closed volumes into trimmed trivariate B-Splines and in addition to that, the calculation of the corresponding volumetric data needed by the solver. Even though Analysis of solid structures is far more demanding, several developments towards this target have already started.



6 Summary

BETA CAE Systems has been actively developing and supporting IGA methodologies for the creation of IGA suitable geometry.

ANSA is continuously being updated with all functionality needed, for pre-processing and assembly of IGA or Hybrid FE-IGA automotive models.

Isogeometric Shell Components in Full Vehicle Crash Simulations: Hybrid Modeling

Lukas Leidinger¹, Stefan Hartmann¹, Dave Benson², Attila Nagy², Liping Li², Marco Pigazzini², Lam Nguyen², Frank Bauer³

¹DYNAmore GmbH, Industriestr. 2, 70565 Stuttgart, Germany

²ANSYS LST, 7374 Las Positas Road, Livermore, CA 95411, USA

³BMW Group, Knorrstraße 147, 80788 Munich, Germany

1 Abstract

Isogeometric Analysis (IGA) [1] uses higher-order and higher-continuity spline basis functions known from Computer Aided Design (CAD) for the description of model geometry and solution field. This not only facilitates a tighter design-analysis connection and faster development processes, but also provides benefits such as a more accurate geometry description, a smooth solution field, and larger time steps in explicit dynamic analysis [2].

The joint effort on trimmed isogeometric shells made by LS-DYNA development (DYNAmore, ANSYS LST), preprocessor development (e.g. ANSA), industry partners (e.g. BMW) and academia (e.g. TUM) in recent years, has now enabled full vehicle crash simulations of hybrid IGA/FEA models. More specifically, IGA shell components generated with ANSA can now be easily inserted into existing Finite Element (FE) vehicle models via a one-to-one component exchange without (or only minor) modifications, see Fig.1. Thus, applying and testing IGA in LS-DYNA within a productive industrial setting is now strongly facilitated.

The aim of this contribution is to demonstrate the IGA capabilities in LS-DYNA, some requirements for hybrid IGA/FEA modeling and first successful applications.

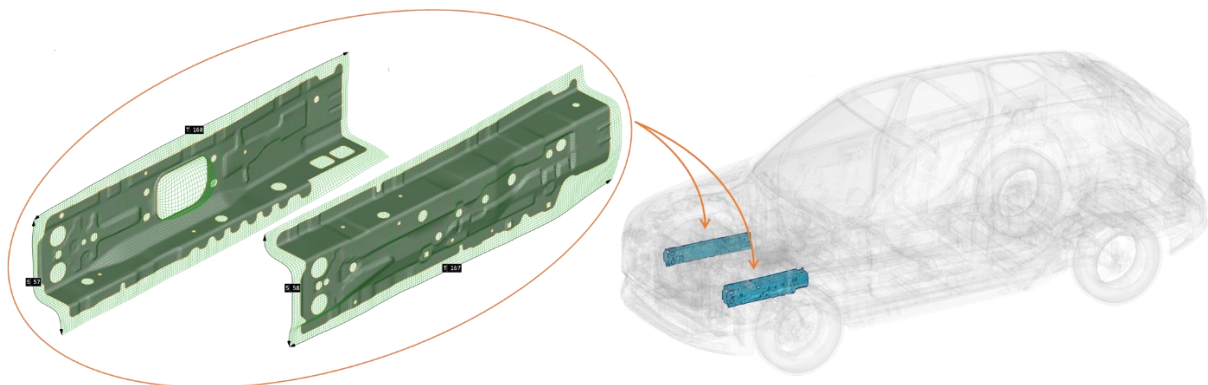


Fig.1: Hybrid IGA/FEA vehicle model: Replacing FE components with trimmed isogeometric shells.

2 Hybrid Modeling for Vehicle Crash Simulations

LS-DYNA can run hybrid (vehicle) models consisting of standard FE and isogeometric components. The ideal scenario is a one-to-one exchange of an FE component with the corresponding isogeometric component without further modifications. This can be achieved by using PID-based connection modeling techniques. The following list provides an (incomplete) overview of LS-DYNA functionalities and connection modeling techniques crucial for hybrid vehicle crash simulations, see also [3]:

- CAD-inspired *IGA keyword structure including geometry and topology information for trimmed multi-patch shell models.
- Crash-specific features such as (i) elasto-plastic material behavior including damage modeling via DIEM, (ii) contact treatment via FE interpolation mesh, (iii) enhanced time step estimation accounting for element continuity, and (iv) mass scaling.
- Robust stabilization of small trimmed elements.
- Initialization of material history data.
- Compatibility of IGA with standard FEA settings.

- Connection modeling for isogeometric shells:
 - Spotwelds via `*CONSTRAINED_INTERPOLATION_SPOTWELD` with PID-based definition.
 - Connections via `*CONTACT_TIED_SHELL_EDGE_TO_SURFACE_BEAM_OFFSET` (e.g. bolts) with PID-based definition. Penalty-based tied contacts for IGA are available, constraint-based tied contacts for IGA are under development.
 - Node-based connections in the FE model (e.g. for nodal rigid bodies) should be avoided, but could be replaced via a node projection onto isogeometric shells using `*IGA_POINT_UVW`.

3 Application to Full Vehicle Crash Simulations

Simulation results of a hybrid IGA/FEA full vehicle model with isogeometric longitudinal members in a front crash scenario are shown in Fig.2 and Fig.3. As can be seen, the deformation pattern and the resultant barrier force over time plot show good agreement between the pure FEA (red/left) and the hybrid IGA/FEA model (blue/right).

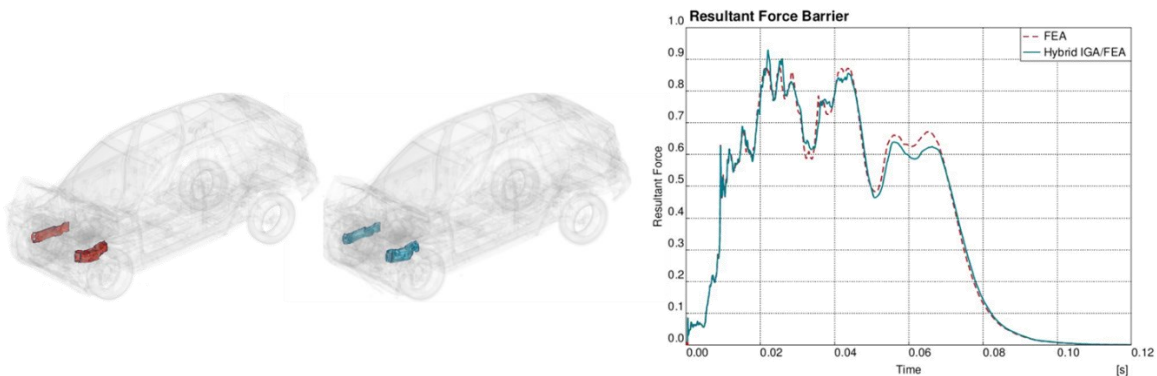


Fig.2: Front crash: Pure FE model (left), hybrid IGA/FEA model (right) and barrier force comparison.

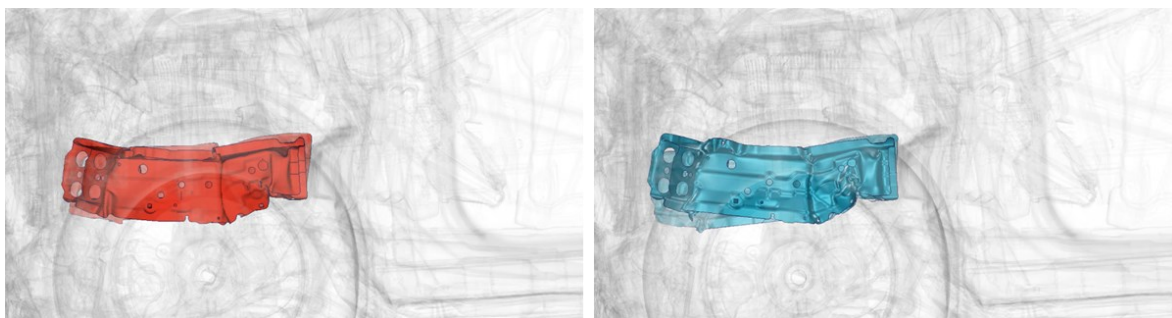


Fig.3: Front crash: Comparison of longitudinal member deformation for FEA (left) and IGA (right).

4 Summary and Outlook

Starting from version R13, LS-DYNA is able to perform large-scale crash simulations with IGA shell components. With the increasing number of industrial applications, users, and requests, the IGA capabilities in LS-DYNA will improve and expand further. Next steps are (i) detailed component studies to gain deeper knowledge about damage and failure modeling with IGA, (ii) improve modeling of discontinuities like notches and cracks, (iii) implementation of trimmed B-Spline solids, (iv) increase numerical efficiency, and (iv) feature-based modeling techniques.

5 Literature

- [1] Hughes, T.J.R., Cottrell, J.A., Bazilevs, Y.: "Isogeometric Analysis: CAD, finite elements, NURBS, exact geometry, and mesh refinement", Computer Methods in Applied Mechanics and Engineering, Vol. 194, 2005, 4135-4195.
- [2] Leidinger, L., "Explicit Isogeometric B-Rep Analysis for Nonlinear Dynamic Crash Simulations", PhD Thesis, Technical University of Munich, Germany, 2020.
- [3] Leidinger, L., Hartmann, S., Benson, D., Nagy, A., Rorris, L., Chalkidis, I., Bauer, F.: "Hybrid IGA/FEA Vehicle Crash Simulations with Trimmed NURBS-based Shells in LS-DYNA", 13th European LS-DYNA Conference 2021, Ulm, Germany

Analysis of 3D structures using IGA solids: Current status and future directions

Lukas Leidinger¹, Stefan Hartmann¹, Manuel Meßmer²
David Benson³, Attila Nagy³, Liping Li³, Marco Pigazzini³, Lam Nguyen³

¹DYNAmore GmbH, Industriestr. 2, 70565 Stuttgart, Germany

²Technical University of Munich, Chair of Structural Analysis, Arcisstr. 21, 80333 München, Germany

³ANSYS LST, 7374 Las Positas Road, Livermore, CA 95411, USA

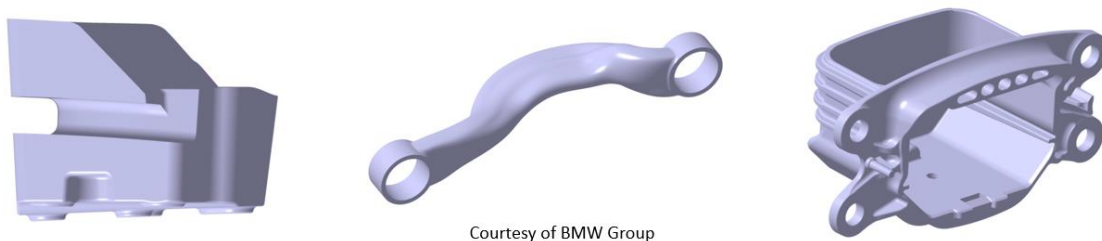
1 Abstract

The journey of the *Finite Element Analysis* (FEA) methodology *Isogeometric Analysis* (IGA) started with the paper by Hughes et al. [1] in 2005. The main difference of IGA compared to standard FEA is the choice of shape functions that are used for the approximation of the geometry and solution fields. While standard FEA mainly uses low-order Lagrange polynomials, IGA uses spline-based shape functions, that are also used in the *Computer Aided Design* (CAD) environment. This may lead to a leaner workflow going from design to analysis and back and to superior analysis properties, using higher-order and higher-continuity basis functions.

Over the last few years, the development of the IGA technology in LS-DYNA was very active and mainly focused on thin-walled structures. However, recent, prototypical developments in cooperation with the Technical University of Munich have shown, that IGA may beneficially be used also for the analysis of bulky, volumetric engineering parts.

2 Motivation

Although the majority of engineering parts may be classified as thin-walled structures, the interest in efficient and accurate analysis tools for volumetric engineering parts (see Fig. 1) is increasing.



Courtesy of BMW Group

Fig.1: Volumetric engineering components: CAD models.

Using standard finite elements in LS-DYNA, the analysis of such parts is not always straight forward and trivial. In terms of the quality of solid finite elements, it would be preferred to use hexahedral solid elements. However, it may be a difficult task to automatically generate a hexahedral mesh for any kind of 3D geometry. Therefore, one is typically forced to generate and work with a tetrahedral mesh. As low-order tetrahedral elements usually perform rather poorly, one either needs to choose higher-order tetrahedral elements or one would need to use a relatively fine mesh. Both choices increase the computational effort in solving the problem.

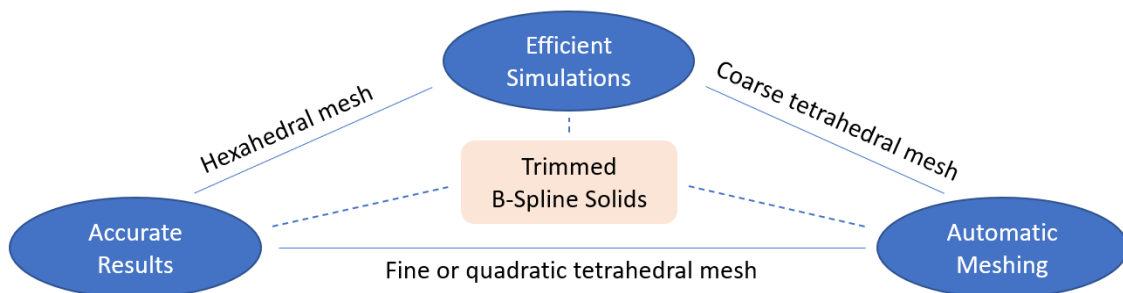


Fig.2: Conflict of interest within the analysis of 3D solid components.

In Fig. 2, this conflict of interest using standard solid finite elements is sketched. A solution to this dilemma may be the use of trimmed B-Spline solids, which will be described in the next section.

3 Trimmed B-Spline Solids

The main idea of using trimmed B-Spline solids is similar to so-called immersed methods. Thus, the actual geometry of the solid structure is embedded into a regular hexahedron discretized with higher-order B-Splines, as shown in Fig. 3.

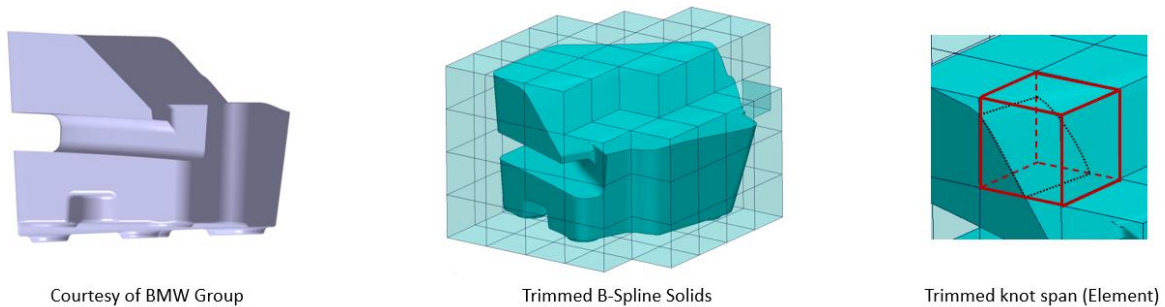


Fig.3: Embedding of the geometry into a hexahedron B-Spline.

The background hexahedron is subdivided in so-called knot spans, which, like in standard FEA, can be interpreted as elements. Due to this embedding process different types of elements will result: Elements that are fully embedded (untrimmed), elements that are only partly embedded (trimmed) and elements that are completely outside of the material domain (inactive). Inactive elements will be ignored, untrimmed elements are treated in a standard manner, and for trimmed elements an individual numerical integration scheme is specified.

Highlights of this trimmed B-Spline solid approach:

- Fully automatic “meshing”.
- Feasible time step size in explicit analysis, independent of the trimmed element size (ratio btw. trimmed and untrimmed element size), due to the higher-order *and* higher-continuity B-Spline background discretization. This is not the case for C^0 elements used in standard FEA.
- Decoupling of the actual geometry description (can be arbitrarily fine) and the mechanics background discretization (only as fine as required for the specific load case).
- Higher continuity across element boundaries.
- Efficient numerical integration rules.

First results computed with LS-DYNA are shown in Fig. 4. More detailed information about this method including efficient numerical integration schemes can be found in the papers by Meßmer et al. [2,3].

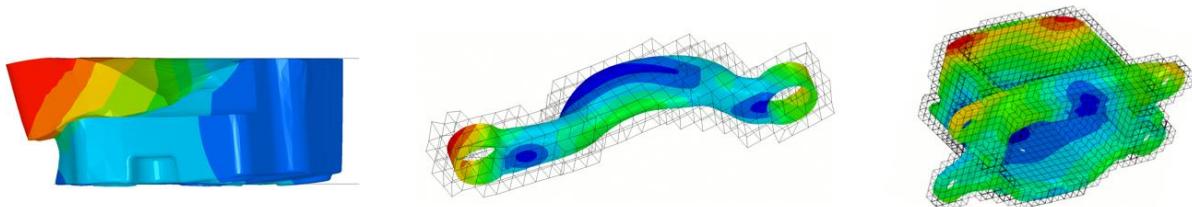


Fig.4: Volumetric engineering components: Trimmed isogeometric B-Spline solids in LS-DYNA.

4 Summary

First studies using trimmed B-Spline solid IGA elements in LS-DYNA have shown, that this methodology may represent a sound alternative to the existing standard FEA approach. More details and additional information will be given in the actual presentation.

5 Literature

- [1] Hughes, T.J.R., Cottrell, J.A., Bazilevs, Y.: "Isogeometric Analysis: CAD, finite elements, NURBS, exact geometry, and mesh refinement", Computer Methods in Applied Mechanics and Engineering, Vol. 194, 2005, 4135-4195.
- [2] Meßmer, M., Leidinger, L., Hartmann, S., Bauer, F., Duddeck, F., Wüchner, R., Bletzinger, K.-U.: "Isogeometric Analysis on Trimmed Solids: A B-Spline-Based Approach Focusing on Explicit Dynamics ", 13th European LS-DYNA Conference 2021, Ulm, Germany.
- [3] Meßmer, M., Teschemacher, T., Leidinger, L.F., Wüchner, R., Bletzinger, K.-U.: "Efficient CAD-integrated isogeometric analysis of trimmed solids", Computer Methods in Applied Mechanics and Engineering, Accepted Manuscript.

GISSMO 1: A short introduction to the basic options

D. Koch (DYNAmore)

GISSMO 2: Application to metallic materials

Prof. A. Haufe (DYNAmore)

GISSMO 3/3: Application to polymers

Sergio Conde¹

¹DYNAmore GmbH

1 Abstract

In the last years, the demand of the modelling of polymers has steadily increased due to its widespread use in industry. The modelling must be not only able to predict the main aspects of the polymer behavior but also to keep computation times under control from a practical application point of view. The latter still makes the use of von Mises plasticity, i.e., *MAT_024 in LS-DYNA, necessary, although many arguments can be found in the literature that warns about the inability of von Mises plasticity to model polymers. Nevertheless, we show in this work that many aspects of a typical polymer response can still be covered to a satisfactory extent. Two main aspects make polymers extremely challenging when it comes to its modelling: a highly strain-rate sensitivity and an absence of metal-like necking due to the plastic process not being isochoric anymore whilst a stress-softening may show up. These two features demand a proper description of the von Mises surface for the model to be able to provide a good correlation in terms of global stress-strain response and local deformation process. Based on tensile and bending tests performed at different velocities we show how to deal with a successful calibration of the plastic behavior of a standard polymer that in turn results in a suitable starting point for the modelling of the strain-rate dependent failure. To this end, the stress-based criterion proposed by Cockcroft and Latham (1968) is used due to the current lack of reliable tests for different triaxiality ratios on polymers. Finally, this criterion is translated into a GISSMO card where the strain-rate sensitive failure can be easily implemented.

Automated material model generation in VALIMAT – AUTOFIT & AUTOFAILUREFIT

B. Hirschmann¹, C. Schober¹; B. Jilka¹; H. Pothukuchi¹

¹4a engineering GmbH

1 Background and Motivation

4a engineering GmbH developed the software solution VALIMAT[®], which helps the user to calibrate FEM material models to measurement data with a reverse engineering process. For some material models automated workflows were defined¹⁾. They state the necessary measurements and have parameterized material models and define how the parameters are optimized. These workflows did not support the fitting of a failure model. The introduction of the AutoFailureFit feature should also automate this step and with that reduce the required time and lead to more reproducible results.

2 Material and Failure Models

Currently material and failure modeling in crash simulations typically deal with simple von Mises viscoplasticity (*MAT_024) and equivalent strain failure criteria. For the description of the complex material behavior of unreinforced thermoplastics (like tension-compression asymmetry) *MAT_187/*MAT_187L are commonly used^{2) 4)}. In the present work, an emphasis has been placed on using *MAT_ADD_EROSION failure models which can be added to other material models³⁾.

3 Failure Fit Implementation

An additional Failure Evaluation model setting was added to VALIMAT[®]. It simulates the linked load cases with the found material model parameters and calls a python post processing script, which performs the following tasks:

1. Data Extraction

- a. Element Histories: Extract for all integration points in the simulation model without failure criterion in the area of interest the history variables necessary for the failure model (stress state metrics: pressure p , Von Mises stress σ_{VM} , stress triaxiality η , Lode angle θ_{Lode} ; strain metrics: volumetric strain ε_{vol} , equivalent plastic strain ε_p , maximum principal strain ε_i ; equivalent plastic strain rate $d\varepsilon_p/dt, \dots$)
- b. Evaluation Times: Define/find when failure occurs in the given measurement

2. Failure Model Evaluation

- a. Failure Target Points: Combine Evaluation Times with Element Histories
- b. Failure Modell: Selected failure model in a parameterized form
- c. Fitting: Find the best parameters for the Failure Modell to get minimal differences to the Failure Target Points.

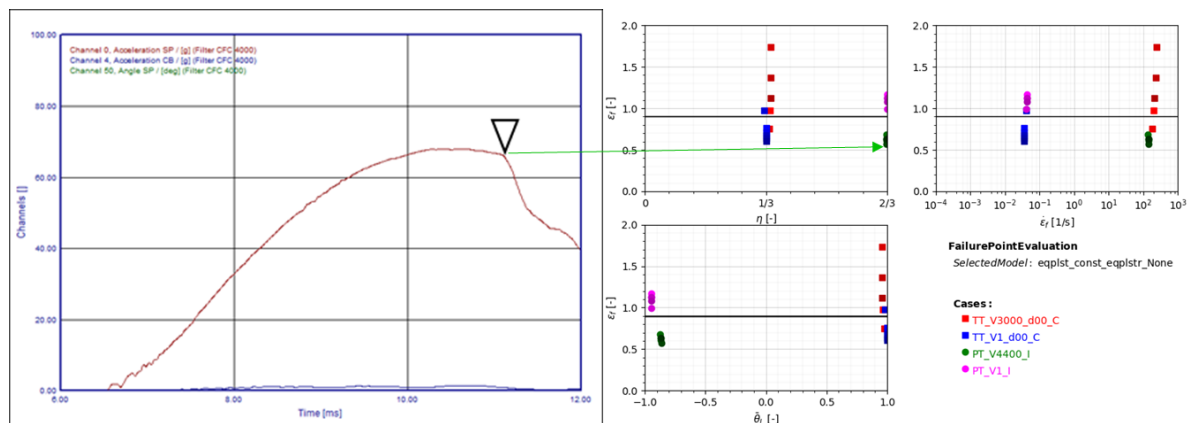


Fig.1: Measurement channels of a dynamic puncture test with marked failure time (Evaluation Times) [left]; Failure Target Points displayed in $\varepsilon_p(\eta)$ [right, upper left], $\varepsilon_p(d\varepsilon_p/dt)$ [right, upper right] & $\varepsilon_p(\theta_{Lode})$ [right, lower right] with the fitted Failure Model displayed with a black curve

4 Results and Outlook

For an impact modified polypropylene, the whole material calibration workflow isoP_Pro was done with and without the developed AutoFailureFit feature while recording the process step times. Fig. 2 shows in general a good correlation between the *MAT_187L+*MAT_ADD_EROSION (DIEM) material model to the measurement curves.

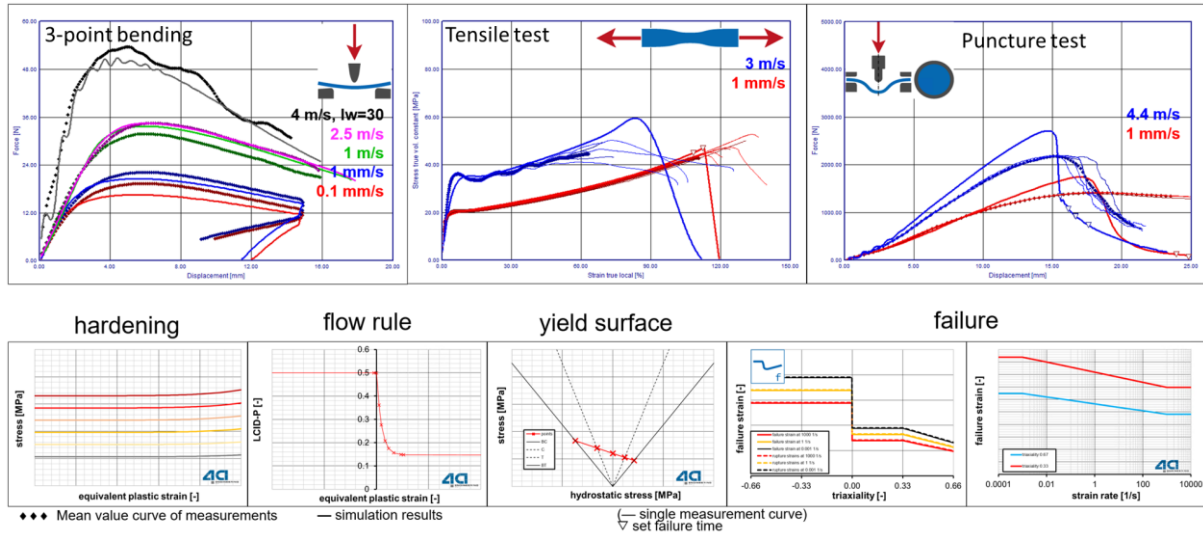


Fig.2: A comparison between the measurement and the simulation for 3-point bending, tensile test and puncture test at different loading conditions can be seen above. The calibrated material model curves can be seen below.

The introduction of the AutoFailureFit feature reduces the required time to calibrate a material model by roughly 10% of total process time. The material testing is a separate process from the simulation and the reporting. With respect to the simulation times, this additional feature contributes to a reduction of 30% in the total simulation time for a material model calibration process (see Fig. 3). The addition of this feature in VALIMAT® enables a complete automation of the material model calibration process including failure. These workflows are currently under further development regarding their robustness and accuracy.

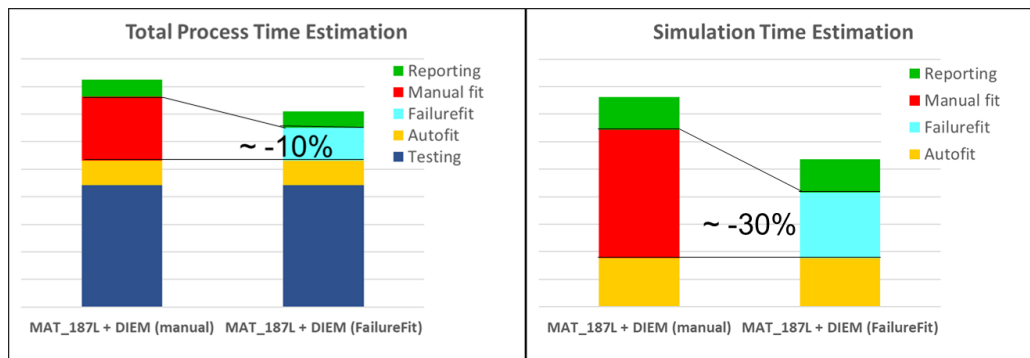


Fig.3: A comparison between the total process times with and without the FailureFit feature (left). The Simulation Time Estimation removes the Testing Process Times from the comparison (right).

5 Literature

- [1] 4a test packages, <https://www.4a-engineering.at/downloads/testpackages.pdf>
- [2] Reithofer. P et.al: “Failure modeling of Unreinforced and Fiber reinforced Thermoplastics”, 12th European LS-DYNA Conference, Koblenz, 2018
- [3] Fertschej. A et.al: “Failure models of plastics – material characterization for *MAT_ADD_EROSION (DIEM)”, 11th European LS-DYNA Conference, Salzburg, 2017
- [4] Kolling. S et.al, SAMP-1: A Semi-Analytical Model for the Simulation of Polymers, 4th LS-DYNA Anwenderforum, 200

A robust method for identifying GISSMO regularization behaviour

Ninad B. Kulkarni¹, Sebastijan Jurendic²

¹RWTH Aachen University

²Novelis Deutschland GmbH

1 Introduction:

When using shell elements to simulate the failure of thin-walled structures, mesh size regularization is one of the major components governing the element erosion behaviour of the GISSMO damage and failure model [1]. A hybrid experimental-numerical approach for identifying the regularization curve of the GISSMO model at shell element sizes typically used in automotive crash test simulation is proposed and evaluated on a AA6000 series aluminium case study. The main objective of the work is to improve the accuracy of material failure prediction, specifically using the GISSMO model as implemented in the R9.3.1 revision of LS-Dyna using the “MAT_ADD_EROSION” material model extension.

2 Constitutive model and base GISSMO model characterization

The elasto-plastic material model used in this work consists of the Von Mises yield locus together with a combined Swift-Hockett-Sherby hardening law, fit to measured material hardening behaviour based on uniaxial tensile test and equi-biaxial hydraulic bulge test measurements Figure 1-a.

The triaxiality dependant localization and fracture loci used in the GISSMO model were identified using established methods of determining the local fracture strain at different stress triaxiality ratios using proportional loading experiments [2, 3]. The measured fracture and localization loci for the considered AA6000 series aluminium alloy are shown on Figure 1-b.

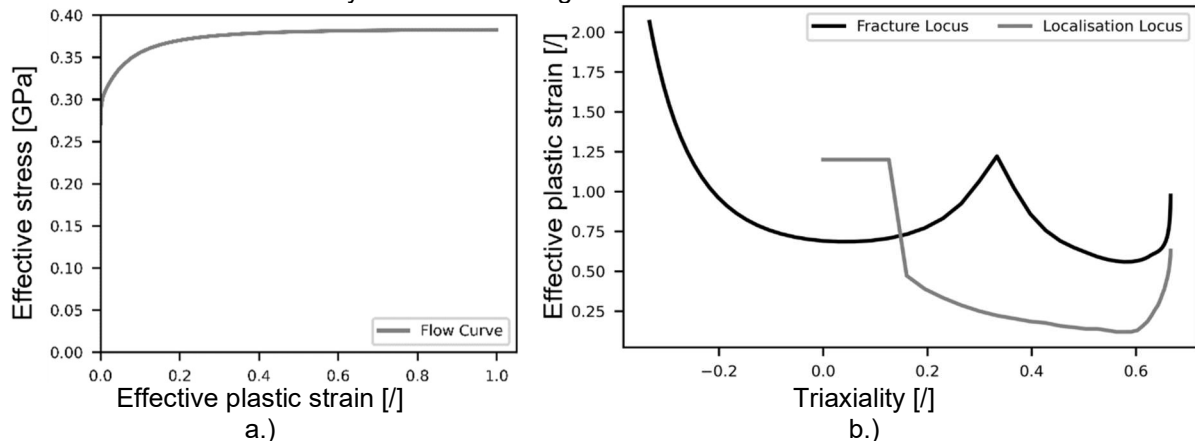


Fig.1: a.) Extrapolated flow curve and b.) Localization and fracture loci for the tested aluminium alloy.

3 Regularization

A logarithmic relationship between the regularization factor f_{reg} and the element size is proposed based on simplified assumptions about the necking deformation: a.) deformation up to necking is homogenous on a length scale similar to the element size, b.) after the onset of necking, all deformation is contained in the necking region and c.) the necking region is smaller than the element size.

$$f_{reg}(elsize) = \frac{\ln\left[K + \frac{A}{elsize}\right]}{B}, \quad (1)$$

where K, A and B are parameters of the regularization equation.

To evaluate the material model behaviour at various shell element sizes, large tension coupons were developed for the plane strain and uniaxial stress loading conditions. The coupon geometries are shown below on Figure 2. These were then strained to failure and the global elongation at failure was noted. An average of at least three repeats is taken as the reference failure elongation, for the plane-strain and uniaxial tension tests respectively.

Finite element meshes of these geometries were generated at different element sizes, ranging from approximately 3 mm to approximately 9 mm in 1 mm increments. Particular care was taken to ensure mesh uniformity in the primary deformation zones.

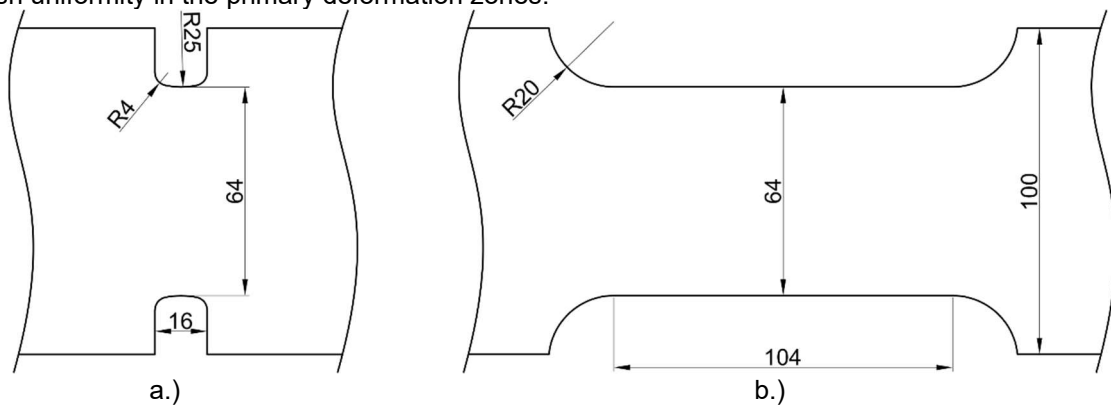


Fig.2: a.) Large scale plane-strain notch specimen and b.) Large scale uniaxial tension specimen.

The parameters of the regularization equation were identified using an inverse optimization scheme by minimizing the error between the measured global elongation to failure and simulated global elongation up to the point of first element erosion, for the plane-strain and uniaxial tension conditions and for all element sizes simultaneously.

4 Results

The resulting regularization curve determined using the described method is shown on Figure 3-a and the corresponding load vs. global strain behaviour of the test and the simulations at different element sizes are shown on Figure 3-b.

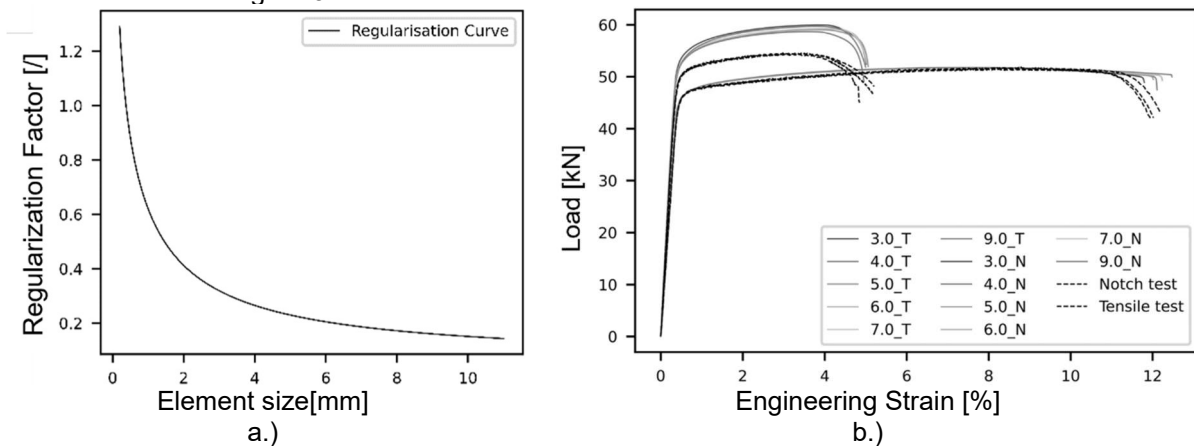


Fig.3: a.) Identified regularization curve and b.) Load vs. global engineering strain behaviour of the large scale tests and corresponding simulations.

Good agreement between the test and the experiment with mean average errors in elongation to failure over all the element sizes of 1.52% and 1.38% for the plane-strain and uniaxial tension tests respectively. Note: the load discrepancy between the tested and simulated behaviour of the plane-strain tension specimen is attributed to the Von Mises yield locus assumption.

5 Summary

A method for characterizing the regularization behaviour of shell elements for sheet metal failure prediction is presented, along with a proposed phenomenologically derived regularization equation. The combined experimental-numerical inverse method for identifying the regularization parameters shows good results and consistent fracture behaviour could be achieved over a wide range of shell element sizes.

6 Literature

- [1] Andrade, F. X. C., Feucht, M., Haufe, A., Neukamm, F., "Int. J. Fract", 200, 2016, pp. 127-150
- [2] Abedini, A., Butcher, C., Worswick, M.J., "Int J Solids Struct", 144, 2018, pp.1-19
- [3] Roth, C. C., Mohr, D., "Int. J. Plast.", 79, 2016, pp. 328-354

Development of component tests to reproduce the bending of seatbelt webbing under transverse load

Oliver Schoeneich¹, Carsten Meinel²

¹IAT mbH

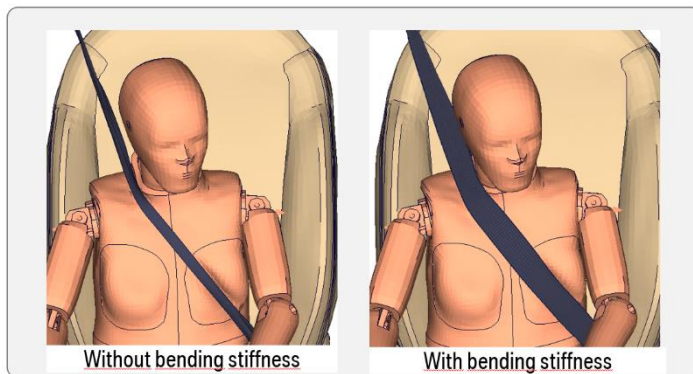
²BMW AG

1 Abstract

To improve actual and to evaluate future modeling techniques concerning the bending behaviour of seatbelt webbing, two component tests for evaluating the bending stiffness have been developed.

2 Introduction

Using 2D seatbelt elements without bending stiffness can lead to unrealistic behavior of the seatbelt



webbing if transverse forces are introduced, resulting in the complete folding of the webbing and therefore in an unrealistic prediction of the dummy kinematics and the corresponding injury values (figure 1).

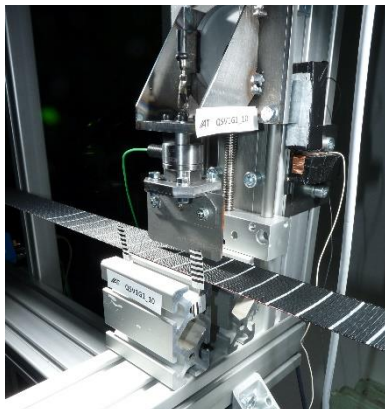
Workarounds exist to introduce bending stiffness adding either a layer of transverse beam elements or a thin shell layer on the commonly used 2D-seatbelt elements.

Fig.1: *Folding of Seatbelt webbing*

Trying to calibrate this workaround, it soon became clear that not sufficient knowledge existed how a seatbelt bends, what the folding characteristic looks like and what is the influence of the preload due to the acting belt force. Thus, a set of component tests was developed that should capture those aspects, having a high degree of reproducibility and a low degree of complexity so that these tests could easily be integrated in the product development cycle.

3 Test setup

The two tests - a bending test and a shear test – share the same setup.



In both configurations the belt is stretched over a length of ~2m and in the middle of the setup an impactor is applying a bending or shear force. The impactor feed rate is low so that a quasistatic loading condition of the belt can be assumed.

By applying weights a constant force level of the axial preload is realized (Seatbelt webbing has the tendency to creep). To simulate a loading situation comparable to the situation in the product development a preload of 2, 4, 6 and 8kN was applied (this represents the usual load limiting level).

Load cells were applied to the belt fixation to measure the axial force and to the impactor to measure the bending or shear force (Figure 2)

Fig.2: *Test rig*

3.1 Bending test

In this test a flat impactor is “pushing” the seatbelt in a gap between two blocks provoking the bending of the seatbelt which can be evaluated visually. Furthermore, the resistance of the webbing against a orthogonal force can be evaluated in dependency of the preload (Figure 3).

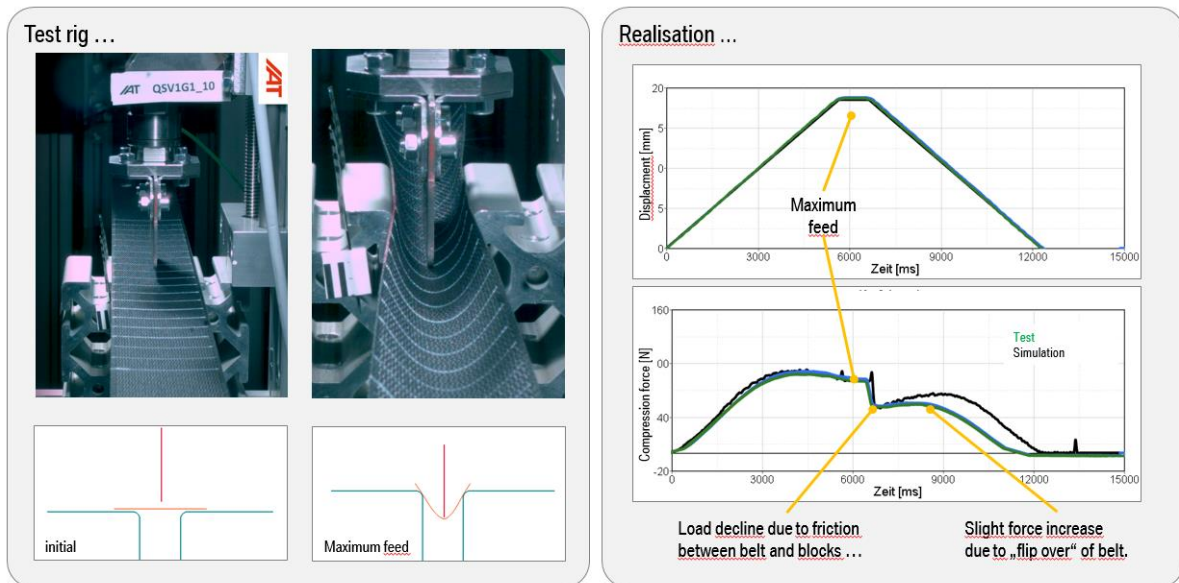


Fig.3: Bending test

3.2 Shear test

In this test a “L-shaped” profile slowly pushes the belt sideways. This way a shear force is applied that gradually forces the belt to fold. Once the first fold develops the impactor is stopped (Figure 4).

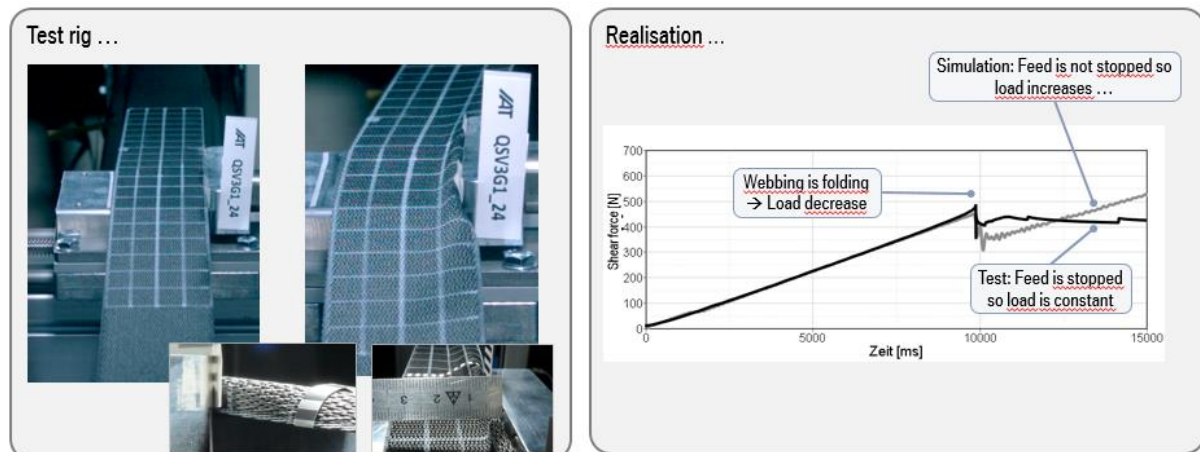


Fig.4: Shear test

Next to the evaluation of the force on the profile the geometry of the belt-fold can be measured and compared with different FE-modelling techniques (Figure 5).

Beltforce [kN]	Test		Simulation (Beam)	
	Height [mm]	Width [mm]	Height [mm]	Width [mm]
2	5	12	5	10
4	4,5	8	5	6,5
6	4	5	3	4
8	4	4	3	3

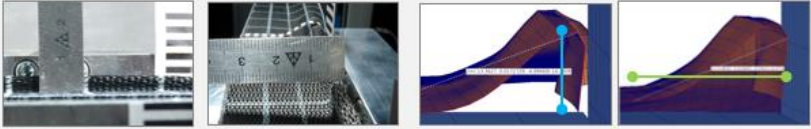


Fig.5: Folding characteristic of seatbelt webbing

4 Modelling technique

Different modelling techniques were evaluated to introduce bending stiffness in the seatbelt webbing.

- “plastic beams” a layer of beam elements in the transverse direction
- “shell layer” an additional shell layer accounting for the bending stiffness

In both approaches elements of the type *ELEMENT_SEATBELT are used to model the axial stress components (figure 6).

Modelling technique	Slip Ring applicable?	Compression test		Shear test			conclusion
		Loadcurve: charakteristik & niveau	Visual: bending line belt	Loadcurve: charakteristik & niveau	Loaddrop: time & niveau	Visual: bending line belt	
shell layer	N	Y	Y	(Y)	(Y)	N	due to slipping demand not pursued
plastic beams	Y	Y	Y	(Y)	(Y)	Y	Alle relevant demands fulfilled

Fig.6: Modelling technique

Best results were achieved modeling the close bends of the seatbelt webbing using an elasto-plastic material law for the beam elements (figure 7).

First tests to generate this type of a “plastic hinge” with the “shell layer” approach did not proof as successful as with the beam approach. This and the fact that the shell layer is incompatible with the use of 2D- Sliprings led to the decision to focus on modelling the bending behavior using elasto-plastic beam elements.

Webbing is modelled as a superposition of ...

- beam elements → bending stresses ⁽¹⁾
- membran elemente → „in plane“ stresses ⁽²⁾

(1) Elastoplastic beam elements form a plastic hinge.
Verification using the „bending line“ of the webbing & loadcurves of the component tests.

(2) Membran elements validated by the suppliers.
The elongation in axial direction is hardly influenced using the transvers beam elements.




Fig.7: Modelling approach using elasto-plastic beam elements

5 Calibration of material parameters and discretization

A simple elasto-plastic material law is applied (`*MAT_PLASTIC_KINEMATIC`). It was “straight forward” to define the relevant parameters from the test data

- bending test: varying the young’s modulus the slope of the load curve and the maximum load are determined.
- shear test: varying the yield stress sets the timing when the belt is folding

The above mentioned parameters were defined with one load level for the axial force and then verified with the other preload-levels.

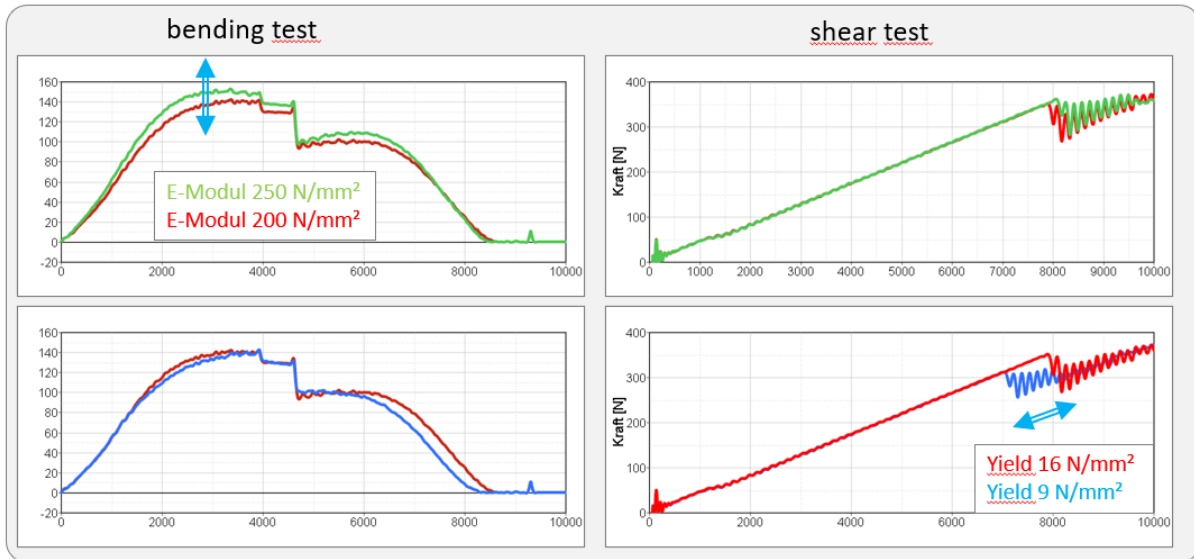


Fig.8: Verifikation of material parameters

To examine the influence of the discretization on the bending characteristic different element lengths were evaluated by visually comparing the deformation pattern of the seatbelt webbing with the results from the shear test (figure 9).

The following element lengths were examine: 1mm, 2mm and 4mm (The average distance between warp threads of the webbing material used in the hardware tests was $\sim 0.7\text{mm}$).

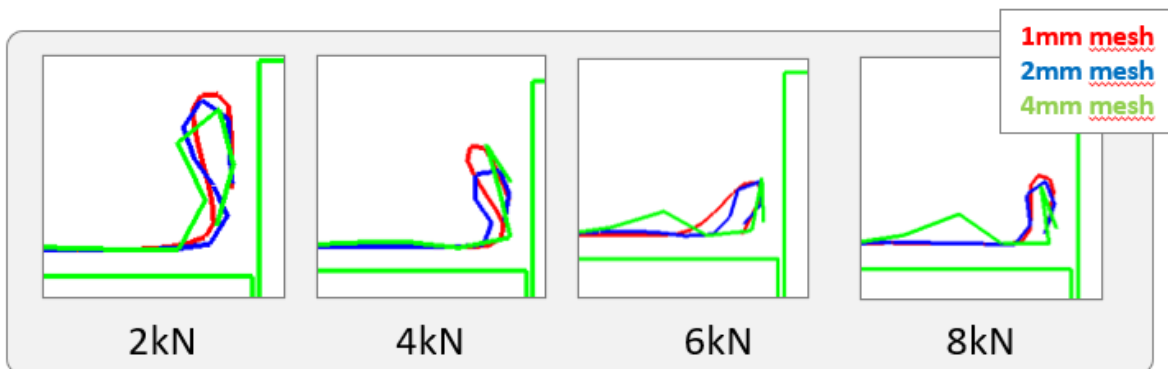


Fig.9: Bending characteristic under shear load

Focusing on the final position of the 1mm and 2mm mesh a similar folding pattern for all preloads is developing which is comparable to the pattern observed in the hardware tests. This pattern differs strongly for the 4mm mesh starting with a preload of 6kN.

A novel method for characterizing seatbelt webbing bending response under tension force

Stefan Schilling; Dr. Anurag Soni; Dr. Tom-Michael Voigt; Felix Manneck; Stephan Gathmann

Autoliv B.V. & Co. KG, North Germany

1 Introduction

Inadequate modelling of seatbelt webbing bending response often results in a rope-like folding deformation in the lap belt during passive safety crash simulations. This causes loss of contact area and eventually increases the risk of incorrect pelvis coupling and submarining prediction. To improve predictions of webbing folding, the webbing bending stiffness was quantified in a cantilever test setup with a tension-free webbing specimen [1]. In contrast, during a crash, the lap belt experiences a tension force while bending. Therefore, characterizing webbing bending response as a function of tension force is important. This paper presents a novel method for characterizing bending in seatbelt webbing under varying tension force. The method was conceptualized using simulations and thereafter a physical proof of concept was created.

2 Method

The setup mimicked the loading and boundary conditions experienced by the lap belt in a crash while restraining the occupant. Therefore, the webbing sample was wrapped around two rigidly fixed support structures 500 mm apart, like a lap belt routed across the pelvis. The ends of the webbing sample were fastened and tightened to set the required tension force in the webbing.

A FE model of the conceptualized test setup was created (figure 1). At first, tension on the webbing (force levels: 0 N, 125 N, 400 N and 1000 N) was achieved by applying a ***BOUNDARY_PRESCRIBED_MOTION** (0 mm, 0.5 mm, 1 mm and 2 mm displacement ramped up in 250 ms) to the webbing free ends. Subsequently, bending was introduced: a rigid cylindrical actuated pin moved 20 mm within 250 ms, to load the webbing in the transverse direction, while the bottom edge was supported by a fixed pin. The webbing between the pins was pushed out-of-plane by a convex-shaped structure to introduce an imperfection, necessary for a controlled the bending. The convex-shaped structure was pushed by 2 mm in the out-of-plane (Z) direction of the webbing. The webbing was modelled using ***MAT_FABRIC** with an element edge length of 3 mm [1], whereas all other structural parts were modelled using ***MAT_RIGID**. For all the contact definitions a friction coefficient of $\mu = 0.3$ was applied as a starting point. For result assessment, the tension force, the bending force, and the deformation pattern were recorded. The belt force data was filtered with CFC 60 according to SAE J211 [2]. LS-Dyna R931 SVN 140922 was used.

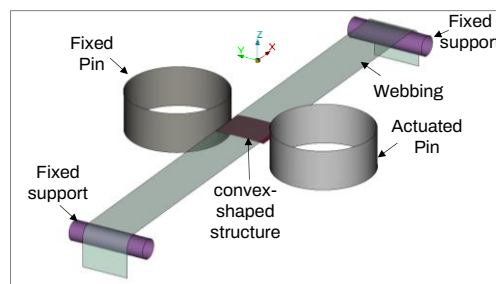


Fig.1: Conceptual CAE model for webbing bending in tension loading

3 Results

Figure 2 shows the belt tension force, bending force and the webbing deformation pattern for the simulated belt tension force variations. Both the bending force and the deformation pattern were found to be dependent on the belt tension force. The peak bending force reached up to 30 N, 50 N, 60 N and 80 N for the 0 N, 125 N, 400 N and 1000 N belt tension, respectively. This also resulted in further increase in the belt force: 150 N, 200 N, 100 N and 140 N increase, respectively. While the webbing was bent in an asymmetric arc-shape for the 0 N belt tension, the apex of the arc-shape was no longer showing a continuous deformation gradient rather than a sharp edge of the 125 N belt tension load case.

For the higher belt tension cases (i.e., 400 N and 1 000 N), the belt deformed in an accordion-shape (i.e., bending occurred along the element edges).

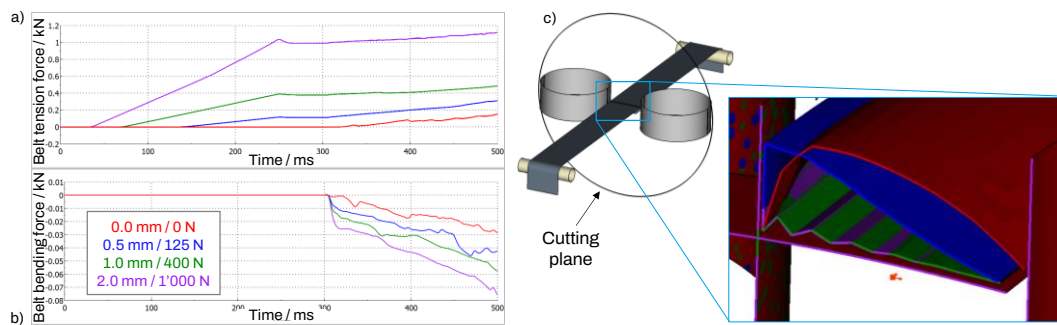


Fig.2: Belt tension force (a), bending force (b) and deformation pattern at 500 ms (c) for conceptualized setup with variation in belt tension force

4 Discussion

A novel method of seatbelt webbing bending stiffness characterization under tension loading was presented. The conceptualized setup successfully captured the effects of belt tension on the webbing bending response. The webbing deformation pattern varied with tension force. However, the expected arc-shape bending mode occurred only in the two lower tension force load cases (0 N, 125 N). Whereas, an accordion-shape bending occurred in the two higher tension force load cases (400 N, 1000 N). Based on the simulation outcome, a physical proof-of-concept was built, and the first set of tests was conducted with varied belt tension force from 100 N to 900 N (figure 3). Here, the phenomena of the webbing edge sliding on the actuated and fixed pin was observed, in contrast to simulation. Interestingly, in all the tests, the webbing deformation pattern resulted in the arc-shape. This indicates remaining limitations in the webbing modelling.

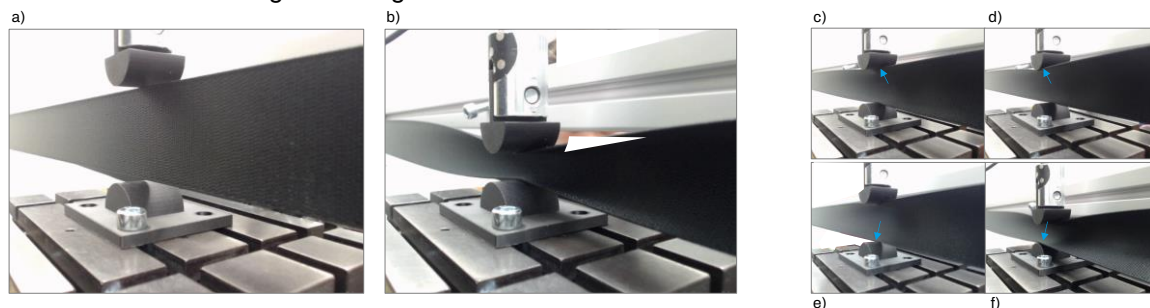


Fig.3: Initial setup (a) and arc-shaped deformed state (b) of the webbing for 400 N preload. Figures c to f show test the results of 900 N belt tension force, where sliding of the webbing edge on the actuated and fixed pin was observed. Sliding on the actuated pin before (c) and after sliding (d). Same observation of for the fixed pin, before sliding (e) and after sliding (f).

Further improvements to the physical test method are required to achieve repetitive, robust, and reliable results. In the future, test results will be utilized to optimize the coating parameters available in ***MAT_FABRIC** and ***MAT_SEATBELT_2D** material models in LS-Dyna solver. Therefore, the controlled bending deformation of the webbing should ultimately help in improving the procedure for validating the webbing response in simulations. With such extended validation procedure, webbing folding in crash-simulation could be predicted more precisely.

5 Conclusion

A novel test method was conceptualized using CAE methods and recreated in physical testing. The test method seems promising to address current shortcomings in the webbing modelling, incorporating for the first-time tension-dependent bending stiffness characteristics.

6 Literature

- [1] Soni, A.: "Parameter Identification of Coating Parameters to Improve Webbing Bending Response", 13th European LS-DYNA Conference 2021, Ulm, Germany
- [2] SAE J211-1: Instrumentation for Impact Test, Part 1, Electronic Instrumentation

6 Verification

To verify the modelling approach the results have been compared with data from existing car projects. The generated seatbelt folding patterns have a closer match with reality but still the results must be interpreted with care. The above-described approach can model crumpling of a seatbelt but from our estimation can not predict it.

A seat belt webbing consisting of the interwoven warp- and weft- thread has a much more complicated structure than it can possibly be modelled using the above-described approach consisting of 2D seatbelt elements with a bending stiffness added. Nether the less for a lot of applications on a macroscopic scale - like they exist in “normal” occupant safety simulation demands – a “sufficient” prediction quality can be achieved.

7 Conclusion

Two component tests that measure the resistance against a transverse load and the force initiating a fold in seatbelt webbing have been set up and investigated in hardware using different preload levels.

Those component test have been used to determine the material parameters for existing workarounds to integrate bending stiffness in belt models.

Furthermore, the test results were used to evaluate the influence of belt discretization on the folding patterns of the seatbelt webbing.

Occupant Safety Prediction

Drougkas Dimitrios¹, Tzolas Nikolaos¹

¹BETA CAE Systems S.A.

1 Introduction

One of the most common finite element analyses in vehicle development is designed to study the passengers' safety during a front crash using a sled test. In this test the vehicle's front structure dynamics during a crash is simulated whereby restraint systems such as airbag and seatbelt are also modelled. The dummy kinematics are highly affected by the various restraint systems' parameters which can result in great variation of the measured occupant's injury criteria, like Head Injury Criterion (HIC 15/36), Brain Injury Criterion (BRIC), upper body parts' acceleration and load absorption etc. To predict and control this variation, Design of Experiments (DOE) or "what if studies" can be set up exploring the different parameters combination. However, the calculation time of the full FE analysis restricts the number of experiments that can be realized.

This study presents the use of Machine learning models for such an analysis. Trained Machine Learning models can help predict the FE model's behavior and results like accelerations, deformations, or injury criteria without the need of running the time-consuming full FE analysis. These capabilities enable multiple "what if" studies without the expense in analysis and design time. Additionally, such trained predictive models are used for optimization purposes as response surface models, increasing the optimization speed and achieving improved designs faster.

The example case used is a sled test with a restraint system (airbag, seatbelt) and the occupant, represented by the THOR-50M Anthropomorphic Test Device (ATD). The simulation of the vehicle-human interaction during such an accident and its actual consequences on the human body are used to train Machine Learning models and predict the occupant's safety. The study focuses on the effect of the various restraint systems' parameters on the occupant's injury criteria.

2 Parametric model - DOE

Four parameters were defined on the FE model (Fig.1) to control:

1. Seatbelt's slip-ring position along the Z-axis,
2. Friction coefficient between the seatbelt and the dummy
3. Airbag's venting trigger time and
4. Seatbelt's sensor trigger time.

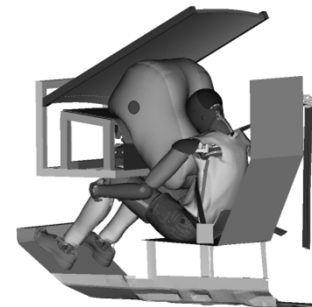


Fig.1: Sled test with restraint and airbag.

A Design of Experiments (DOE) was defined using the Optimization tool using "Uniform Latin Hypercube" DOE Algorithm to generate 25 experiments in total. The FE model LSDYNA analysis ran with the design variable values of each one of the 25 experiments in a completely automated procedure. The Occupant Injury Criteria tool was used in META post-processor, to extract occupant injuries from the ATD. The extraction of the results, the reporting and the output were driven from a META session file and thus, the whole process run automatically in batch mode for each experiment of the DOE. The created data were saved in a DM container system with specific structure and hierarchy.

3 Machine Learning

The 'Design Variable based' Machine Learning was used as the training method, using the 25 available Simulation Runs to train a group of predictive models (Predictor) in order to generate

predictions for the injury criteria or other results. Different groups of predictors are defined for the different categories of responses, listing each predictor that corresponds to a single response. A predictor entity provides the direct prediction of the respective response, based on any configuration of design variables' values. Thus, the prediction of a model's response can be done much faster than the actual FE analysis, leading to a significant decrease in the computational time.

4 Optimization

The created predictor was used in the optimization of the responses as a response surface model, speeding up the optimization progress. The objective of this problem was to minimize the HIC15 value. For this optimization setup, the Simulated Annealing optimization algorithm was selected and the BRIC and HIC 36 were constrained to specific limits.

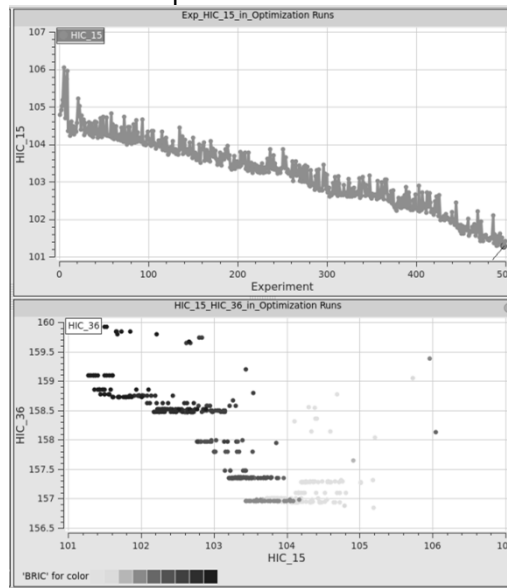


Fig.2: Optimization results. Top: HIC15 vs experiment Bottom: HIC36 vs HIC15 vs BRIC(color)

5 Prediction Validation

The optimum experiment was selected and evaluated to validate the predictor's accuracy. The predictions showed small error values that were within the Mean Absolute error and the confidence bounds of the predictor.

2D Plot and 3D field scalar results were predicted using a machine learning model trained by the initial 25 simulation runs. History Curves, displacements and other scalar values of theoretical experiment were predicted for all time steps of the sled test simulation with good accuracy.

6 Summary

In this study a parametric FE model was used in order to create a dataset to train machine learning models. The trained machine learning models were used in order to predict the results of various designs, performing what if studies while exploring the design space. Such predictive models were also used in finding the optimum design through an optimization study. The predicted results were evaluated compared to an FE analysis and shown very good accuracy, concluding that the use Machine learning can assist in speeding up optimization and design exploration.

7 Literature

- [1] Fokylidis.T., Tzolas.N.: "Performing DOE Studies in Occupant Protection Using BETA CAE Tools", CAASE20, June 16-18
- [2] Ljungqvist.C., Wass.C., Tzolas.N., Appelgren.P.: "Occupant Injury Criteria, a Complete Solution for the Evaluation of Occupant and Structural, Simulation and Physical Test Results in META", 5th LS-DYNA International Conference & Users Meeting, June 10-12.
- [3] ANSA v23.0.x User Guide June 2022

Adaption and integration of CORA in the validation process of occupant safety simulations

Oliver Schoeneich¹, Carsten Meinel²

¹IAT mbH

²BMW AG

Automotive Occupant Protection pre and post ADAS event using a LS-DYNA/Carmaker Co-simulation Approach with Model Center Integrate

A. Nair, Z. Zhang, S. Choudhary (Ansys)

LS-OPT[®] Pro Status Update

Nielen Stander¹, Anirban Basudhar¹, Imtiaz Gandikota¹,

Katharina Liebold², Åke Svedin², Charlotte Keisser², Lars Gråning³

¹Ansys, Livermore, CA

²DYNAmore GmbH, Stuttgart-Vaihingen, BRD

³Dynardo, Weimar, BRD

1 Introduction

The goal of LS-OPT is to facilitate product development using efficient and accurate optimization and reliability assessment methods. To further this goal, one of the focuses of LS-OPT development is to also integrate other Ansys products, where applicable. The current work serves three purposes: (i) to expand the scope of the mode tracking feature of LS-OPT, (ii) to improve the surrogate modeling for optimization and reliability and (iii) to enable the construction of substructures as substitutes for LS-DYNA[®] FE components. The work is therefore also important for LS-DYNA functionality. The two main metamodel features being added are (i) Ansys Twin Builder and (ii) the Metamodel of Optimal Prognosis method adopted from Ansys optiSLang, but with the legacy LS-OPT metamodels incorporated. As a preparation for these improvements, the LS-DYNA fields and field-histories have been enhanced to support part selection. This paper presents some of the early examples tested using both of the new metamodeling features. Additionally, mode tracking is being extended to problems with shape and mesh changes by mapping the nodes of varying designs to the baseline.

2 Mode Tracking for Shape Optimization

Mode tracking for shape optimization with frequency criteria requires a special methodology for comparing modes of different designs. In this case different designs typically have different FE topologies that must be matched in terms of the eigenvectors. A Point Set Registration method has therefore been implemented to map the reference (baseline) eigenvector to that of each design.

3 LS-DYNA Fields and Field histories

Fields and field history results were implemented for the purpose of generating Twin Builder input. All the LS-DYNA fields such as displacements, strains and stresses are supported for shells and solids. The element-based quantities are mapped to the nodes using element averaging. Part sets can be selected to generate substructure or component ROMs.

4 Twin Builder

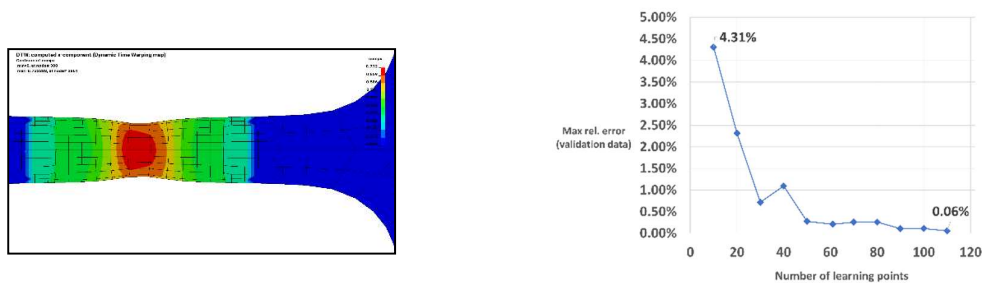


Fig. 1: Finite Element model of a tensile test and ROM prediction accuracy as a function of the number of training (sampling) points

Twin Builder is a design modeler principally based on Reduced Order Modeling (ROM). ROMs are built from simulation data to provide additional metamodel types for the LS-OPT process flow in order to accelerate optimization. A goal is also to enable ROMs to be used as accurate LS-DYNA models or component (substructure) predictors that can be incorporated to accelerate analysis. Applications with particular potential in LS-OPT are material calibration using standardized testing and also applications

in the biomedical industry. The example (Fig. 1) shows a steel coupon loaded in tension with two material constants for which a full-field history ROM model was built. There are 122 sampling designs each with 81 time frames. The ROM model animation will be shown in the presentation. A current LS-OPT feature uses the field or field-history databases to generate the ROM input for Twin Builder based on part selection. Integration into the optimization cycle is targeted for the next release.

5 Metamodel of Optimal Prognosis (MOP)

In the previous LS-OPT version the optiSLang MOP method for automated metamodel selection was implemented and illustrated using the crash model (Fig. 2) [1] shown here. The model has been assigned 22 design variables consisting of thicknesses and material properties. In the previous study, metamodels were compared using 1200 test designs and 800 training designs. To extend the earlier results, further testing has now been done to investigate the effect of the number of training points [100, 200, 400] (see Fig. 3). The similarity of the LS-RBF and MOP performances is notable. The MOP technology is currently being extended by incorporating these LS-OPT metamodels (Radial Basis Function Networks, Feedforward Neural Networks, Support Vector Regression and Kriging).

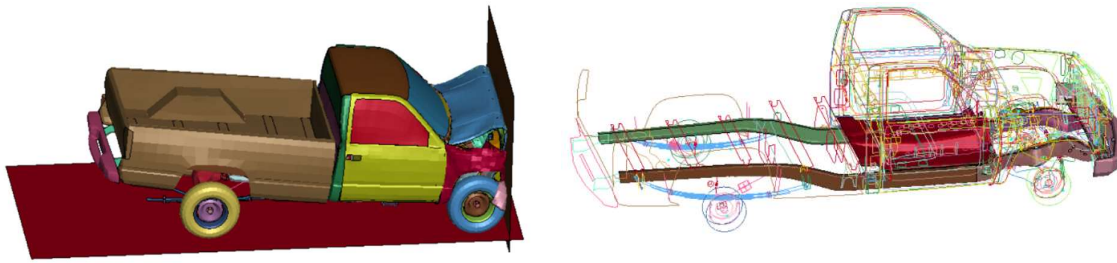


Fig.2: Truck frontal impact showing design components (NHTSA)

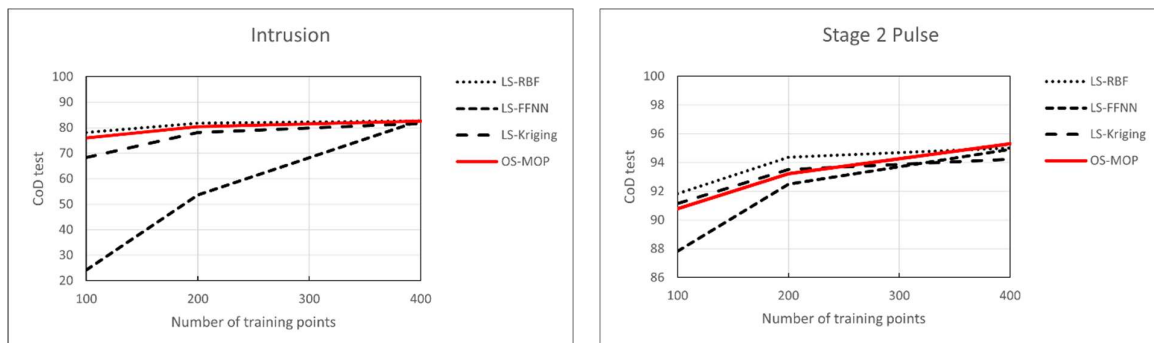


Fig.3: 22-Variable truck: Comparison of MOP (optiSLang) (solid line) with LS-OPT metamodels (dotted lines): Coefficient of Determination (test) for responses Intrusion and Stage 2 Pulse

6 Summary

A number of new features have been added to LS-OPT namely enhanced mode tracking for shape optimization as well as several improvements to metamodeling which are in progress. The early results of the metamodel testing have shown that the LS-OPT metamodels, particularly the Radial Basis Function Network model, have the potential for further improving the current MOP system for automatically selecting the best metamodel. This should benefit both LS-OPT and optiSLang.

7 Acknowledgements

We are grateful to Ansys Dynardo (Weimar, Germany) who contributed to the crash test analysis and to Ansys Digital Twin (France) for providing Twin Builder ROM results for the coupon problem.

8 References

[1] Stander, N., Basudhar, A., Liebold, K., Keisser, C., Svedin, Å, LS-OPT Status Update. Proceedings of the European LS-DYNA Conference, 2021

Graph and Heuristic based Topology Optimization of 3D crash structures - Presentation of all essential modules of the fully automatic process

Axel Schumacher, Florian Beyer

University of Wuppertal

1 Introduction

The graph and heuristic-based topology optimization (GHT) has been researched for about 15 years. The main area of application is the topology optimization of cross-sections of crash-loaded profiles such as those used in vehicle rockers or vehicle side members [1,2].

The GHT has been expanded in the last 3 years so that the method can now also be used to generate optimal three-dimensional frame structure for crash load cases (GHT-3D) [3,4]. This option is of great importance for the automotive industry, because new vehicle concepts are currently giving rise to new design freedoms that should be used optimally. Due to the highly complex mechanics of the crash processes, it is not possible to deal with the optimization task using purely mathematical methods. Linear methods of topology optimization cannot be used. For this reason, the idea of GHT-3D is the use of heuristics generated from expert knowledge, which find optimal layouts in combination with mathematical optimization processes.

Chapter 2 of this contribution presents all essential modules of the fully automatic process. Chapter 3 gives some results of the layout optimization with GHT.

2 Essential modules of the fully automatic process

For the use in automatic structure optimization, the GHT modules are programmed in such a way that they run reliably in the batch process.

2.1 Use of mathematical graphs to a flexibly building of complex 3D frame structures

The mathematical graph is used to describe the layout of a frame structure and the cross-sections of its profiles. It is used for the manipulation of the geometry and to check various geometrical constraints like minimum distances or connection angles.

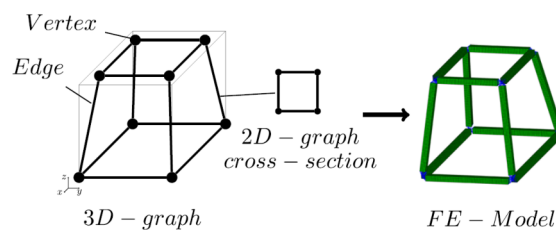


Fig.1: From the graph to the finite element model

2.2 Automatic generation of geometry details

The modelling of the relevant details is essential for the prediction quality of the crash simulation. In addition to the modeling of the profiles, the connection nodes are modeled as realistically as possible.

2.3 Automatic generation of the LS-DYNA models

The geometry can be exported with an interface (e.g. to a STEP-file), so that state of the art finite element pre-processor can manage the meshing. With the include strategy of LS-DYNA the part to be optimized is integrated into the overall crash model.

2.4 Automatic evaluation of the results of the LS-DYNA crash simulations

The heuristics need an automatic evaluation of the crash simulation. Self-developed programs are used together with commercially available post-processors.

2.5 Module of heuristics

The heuristics for the topology optimization of 3D frame structures are generated from expert knowledge. More than 10 heuristics are currently used. As an example, Fig. 2 show the heuristic "Support Fast Deforming Edges" which improves the topology of the structure with regard to global buckling.

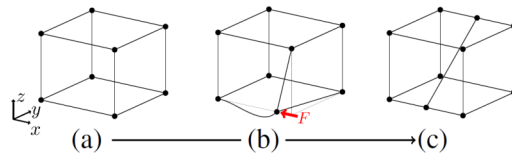


Fig.2: Example of the scheme of the heuristic "Support Fast Deforming Edges". Initial design (a). Fast deformation under loads (b). New structure with supported edge (c)

2.6 Mathematical algorithms for shape optimization and dimensioning

LS-OPT is used for all necessary optimization beside the changings generated by the heuristics.

2.7 Module for control and manage of large computing clusters for time-consuming crash simulations

In each iteration, all heuristics provide design suggestions, of which a certain number (e.g. 5) are pursued. This results in a large number of necessary LS-DYNA simulations. If shape optimization and dimensioning are added, hundreds of simulations are necessary. Controlling a computing cluster is necessary.

3 Application examples of the layout optimization process

Fig 3 shows some typical designs generated by GHT.

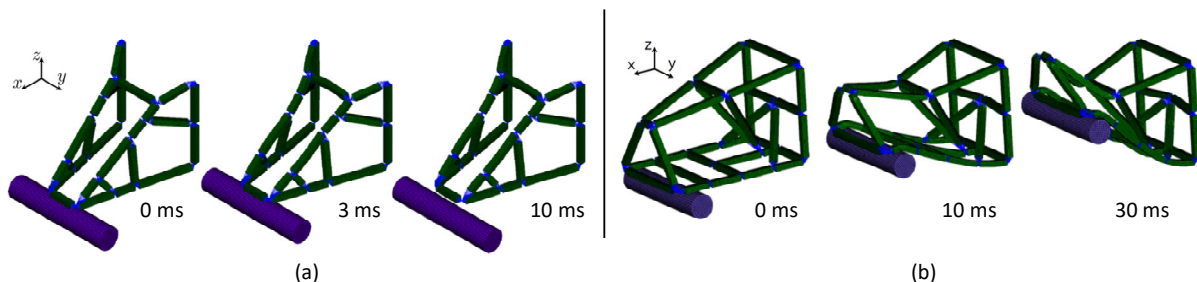


Fig.3: Optimum design examples: Minimize the intrusion with a mass constraint and manufacturing constraints (a), Minimize the contact force with manufacturing constraints (b)

4 Acknowledgement

The work is being carried out as part of a project of the Research Association of Automotive Technology (FAT). The project is carried out in the framework of the industrial collective research programme (IGF no. 21621 N / 1). It was supported by the Federal Ministry for Economic Affairs and Climate Action (BMWK) through the AiF (German Federation of Industrial Research Associations eV) based on a decision taken by the German Bundestag.

5 Literature

- [1] Ortman, C.; Schumacher, A.: "Graph and heuristic based topology optimization of crash loaded structures", Structural and Multidisciplinary Optimization (2013) 47:839–854
- [2] Ortman, C., Sperber, J., Schneider, D., Link, S., Schumacher, A.: Crashworthiness design of cross-sections with the Graph and Heuristic based Topology Optimization incorporating competing designs, Structural and Multidisciplinary Optimization (2021) 64:1063-1077
- [3] Schumacher, A., Beyer, F.: Untersuchung zu den Einsatzmöglichkeiten der Graphen- und Heuristikbasierten Topologieoptimierung zur Entwicklung von 3D-Rahmenstrukturen in Crashlastfällen, FAT-Schriftenreihe 329, ISSN 2192-7863, 2020
- [4] Beyer, F., Schneider, D., Schumacher, A.: Finding three-dimensional layouts for crashworthiness load cases using the graph and heuristic based topology optimization, Structural and Multidisciplinary Optimization, (2021) 63:59-73

Creation of 3D geometry from topology optimization results for thin-walled structures

Alexandros Kaloudis¹, Alexander Malotka²

¹BETA CAE Systems International AG

²BETA CAE Deutschland GmbH.

1 Introduction

The interpretation of density-based topology optimization results is one of the most challenging tasks in the workflow of generative design that engineers follow nowadays in order to achieve the optimum design of their product. The aim is to transform the results with jagged and not well-defined boundaries into smooth parametrized 3D geometry. This presentation shows an automatic process for creating such geometry for structures consisting of welded stamped metal sheets. The individual steps of this process consist of tasks such as cross section's creation and parametrization, automatic recognition of the structure's skeleton from the topology optimization results, automatic adjustment of the selected cross-sections to these results, creation of 3D geometry and editing and fine tuning of the resulting geometry.

2 ANSA Cross Section : the basis of the process

The basic entity of the process for this kind of structures is the ANSA cross section. It can be created either from scratch by using 2D curves, or from already existing model/s by performing a "Plane Cut" on it/them. This cross section can be parametrized in order that it can be adapted during the process to the required size and/or be able to function properly in the context of a parametrical optimization regarding geometry.

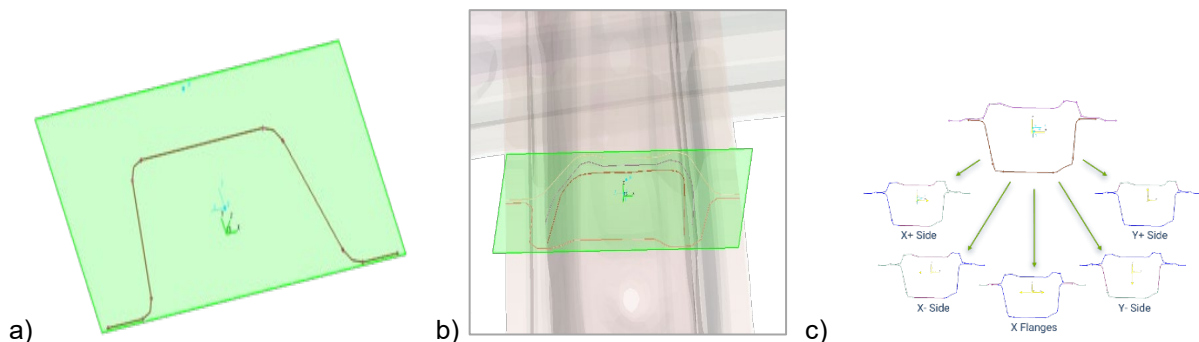


Fig. 1: Cross section created by a) 2D curves, and b) by "cutting" an FE Model. c) Parametrizing a cross section.

3 The process for automatic creation of 3D geometry.

The process that we have developed can create 3D geometry, fully automatically, based on one selected ANSA cross section and on a selected group of elements of the organic mesh model (Fig.2). The main advantage of the process is that all the following steps are performed automatically: 1. selection of the needed number of intermediate cross sections, 2. positioning of all these cross sections along the selected area of the organic mesh model, 3. adjustment of the cross section in order to be similar to the cross section of the organic mesh model at the same position, 4. alignment of the adjusted cross sections in order to produce a smooth geometry, 5. creation of the actual 3D geometry (faces).

4 Additional geometry-editing functionality.

In addition to the above automatic process, we have developed functionality in order to fine tune the resulting geometry. The tasks that we have covered till now are: 1. remove cross section/s from the

definition of the geometry, 2. rotate a cross section for fine tuning the geometry, 3. radial alignment of cross sections, 4. geometry elongation on demand, 5. connection of two different member geometries

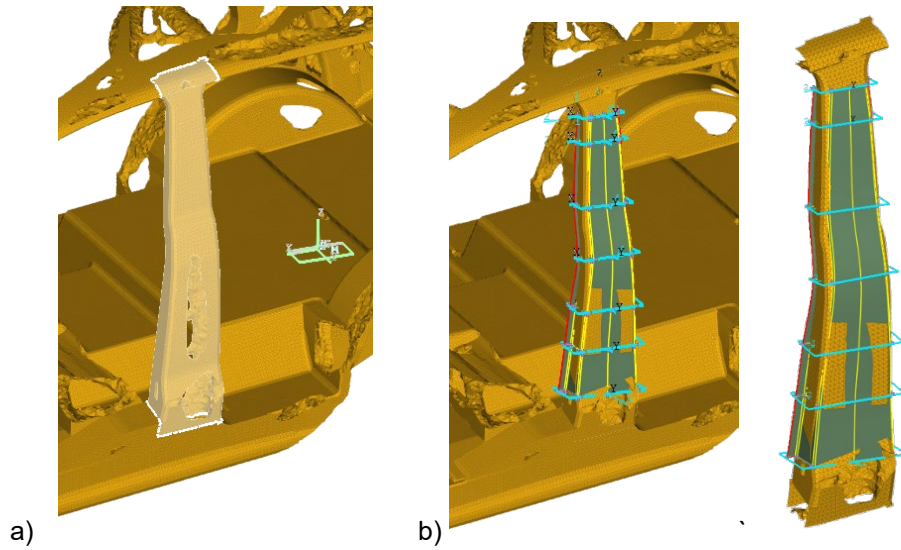


Fig.2: a) Selected area of the organic mesh model. b) Resulting 3D geometry.

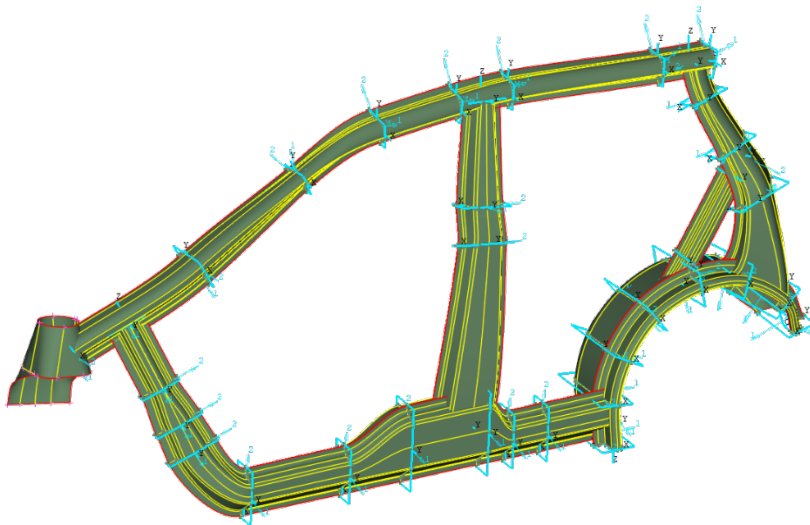


Fig.3: Final result of the process for the side structure of a vehicle's BiW.

5 Summary

Using the ANSA cross section and ANSA standard functionality we have created an automatic process that creates CAD geometry from topology optimization results for welded stamped metal sheets. The result for this process is shown in Fig.3, for the side structure of a vehicle's BiW.

Rapid Next Generation Material Calibration for LS-DYNA using Workflows for Metals, Elastomers, Polymers and Foams in d3VIEW in on-Premises and/or Cloud Platforms

Suri Bala¹, Paul DuBois¹

¹d3VIEW Inc. + legal form

¹Paul DuBois + legal form

Abstract

Simulations require calibrated material models that can reproduce observations in test-labs under different stress-states and for different mesh-densities. Manual calibrations are time-consuming and error prone. This paper presents a workflow-based material calibration in d3VIEW that accelerates the development of calibrated material models. The paper will demonstrate the unsupervised data management of test-data, automated data cleaning and transformation to formats required by simulations. The paper will present challenges in automating material calibrations and available solutions in d3VIEW.

Mode Tracking Using LS-OPT®

In the Presence of Shape and Mesh Changes

Anirban Basudhar¹, Katharina Liebold², Imtiaz Gandikota¹, Nielen Stander¹

¹Ansys, Livermore, CA

²DYNAmore GmbH, Stuttgart-Vaihingen, Germany

1 Introduction

Optimization or reliability assessment using modal analysis often requires tracking of the mode number corresponding to a particular shape of interest. As the design configuration varies for different samples, the mode number corresponding to the shape of interest may also change. The mode tracking feature available in LS-OPT identifies the closest matching mode shape for each design based on the Modal Assurance Criterion (MAC) [1]. Thus, optimization or reliability assessment can be performed using the response values (e.g. frequency) corresponding to the automatically identified modes of interest. However, the method is limited to problems with identical meshing. In this work, the feature will be extended to problems with re-meshing, which may sometimes be required due to shape or topology changes. The new method is based on a point set registration method named Coherent Point Drift (CPD) [2] to map the nodes of the different designs to the baseline nodes before application of the MAC criterion on comparable point sets.

2 Modal Assurance Criterion

The modal assurance criterion (MAC) is a statistical indicator used to determine the similarity between two mode shapes defined by the eigenvectors of the finite element (FE) models. It is defined as:

$$MAC_j = \frac{\varphi_0^H \varphi_j \varphi_j^H \varphi_0}{\varphi_0^H \varphi_0 \varphi_j^H \varphi_j} \quad (1)$$

The MAC value is 1 if there is a perfect match between two mode shapes or eigenvectors and takes smaller values up to 0 if the shapes are different. In order to track a specific mode shape, the corresponding mode number is provided a priori for the baseline or starting design. For a subsequent design sample, the best matching mode is automatically identified in LS-OPT as the one having MAC value closest to 1 for that design.

It is evident from Equation (1) that the calculation of MAC requires the eigenvectors of the two designs to be comparable. For this, in the context of FE models, the two designs must have the same number and ordering of nodes. There are, however, cases where this requirement may not be met. More specifically, if there's remeshing due to shape or topology changes then both the number and ordering of nodes may vary. Therefore, it is necessary to have an additional step that makes the node or point sets comparable before applying the MAC criterion.

3 Interpolated Modal Assurance Criterion (IMAC)

In this work, the Interpolated MAC (IMAC) criterion is proposed to address the issue of non-identical FE meshes. In this new approach, the CPD point set registration method based on a Gaussian mixture model is used to map each sample geometry to the baseline geometry. The output of the CPD algorithm includes a transformation matrix that transforms the baseline point set to the different shapes as well as the pairwise probabilities of association between the nodes of the two FE models. The transformation matrix is of primary importance in many point set registration applications. However, in this work the probabilities are used as the interpolation weights to calculate the eigenvector components at a fixed common set of points. While the baseline eigenvectors are used in their original form, the equivalent eigenvector components of the other designs at the baseline node locations are obtained using interpolation based on the probability weights and the original eigenvector components for those designs. The eigenvector component of the j^{th} mode of an arbitrary design with M nodes mapped to

the n^{th} node of the baseline design, p_{in} being the probability of association between the i^{th} node of this design and the n^{th} node of the baseline, is as follows.

$$\hat{\phi}_{jn} = \frac{1}{\sum_{i=1}^M p_{in}} \sum_{i=1}^M p_{in} \phi_{jm} \quad (2)$$

The revised similarity measure is:

$$IMAC_j = \frac{\phi_0^H \hat{\phi}_j \phi_j^H \phi_0}{\phi_0^H \phi_0 \hat{\phi}_j^H \hat{\phi}_j} \quad (3)$$

An example of mapping different shapes with different number of nodes is shown in Fig 1.

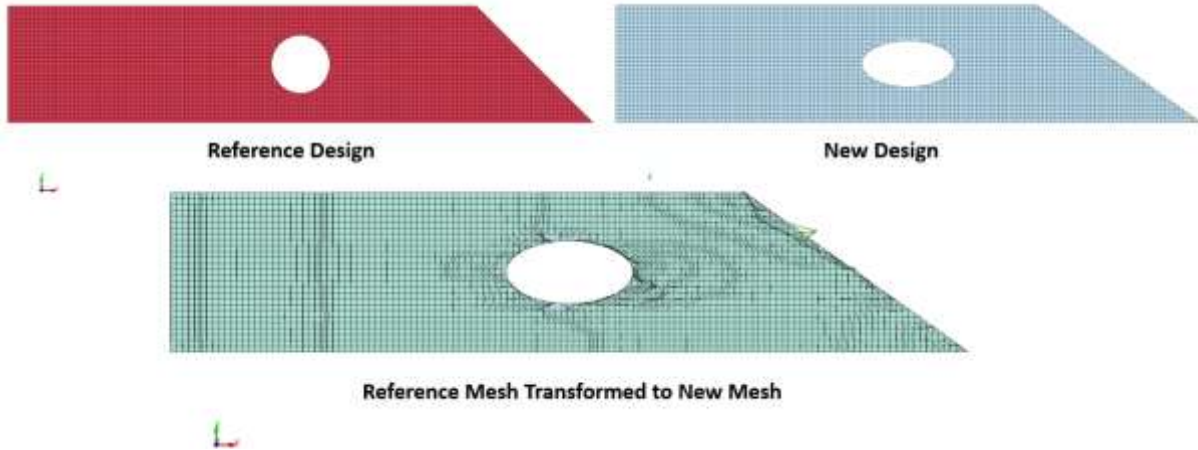


Fig.1: Baseline geometry transformed and superimposed on a different FE model.

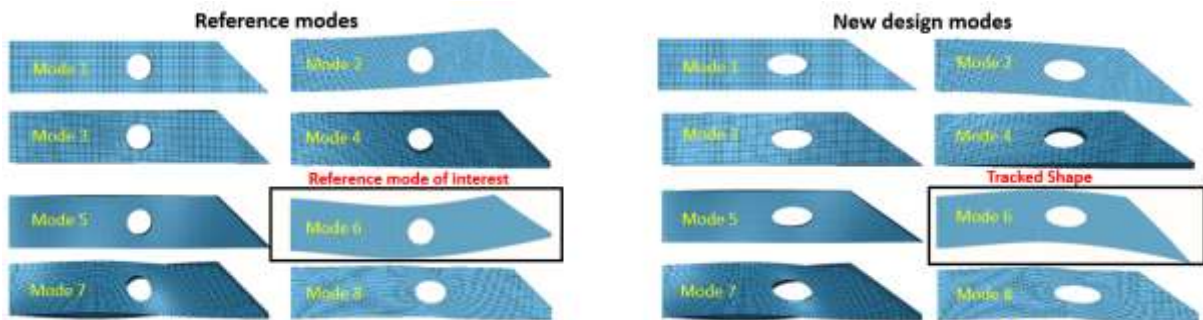


Fig.2: Mode tracking using mapped mesh for varying shapes. Although the baseline and the other design have the same mode number for the shape of interest, the modes may switch in the general case. The proposed method identifies the correct mode number and shape after mapping.

4 Summary

The current mode tracking feature of LS-OPT is limited to problems with comparable meshing, i.e. identical number and ordering of nodes. As demonstrated, the proposed approach based on CPD point set registration and interpolated MAC can be applied to problems with shape variations and different number and order of nodes. Thus, the new feature is more general and can be applied to a wider array of problems. The feature is expected to be released in the version 2023 R1. Currently additional work is being done to improve the efficiency of the shape matching algorithm and will be part of a later version.

5 References

- [1] Stander N, Basudhar A, Roux W, Liebold K, Eggelston T, Goel T and Craig K 2020 LS-OPT Users Manual Version 7.0
- [2] Myronenko, A. and Song, X., 2010. Point set registration: Coherent point drift. IEEE transactions on pattern analysis and machine intelligence, 32(12), pp.2262-2275.

Improvements of LS-DYNA ICFD's steady state solver

I. Caldichoury, F. del Pin, R. Paz, P. Huang (Ansys)

New Developments in LS-DYNA ICFD for the R14 Release

Facundo Del Pin, Rodrigo R. Paz, Peggy Huang and Iñaki Çaldichoury

Ansys

1 Abstract

The ICFD solver in LS-DYNA brings some new features and improvements to R14 that will be introduced in this presentation. As usual feature additions result from customer demand and ongoing development of existing tools. Among the new additions featured in this presentation will be a SIMPLEC steady state CFD solver for the prediction of steady state solutions, a gap closure model to predict the sealing in valves or FSI problems that restrict the flow passage, the addition of a species transport model for applications like drug delivery systems and the computation of a new scalar called residence time for the prediction of stagnation regions valuable in healthcare applications like heart valves simulation.

There are also several enhancements and bug fixes that will be addressed like the addition of FSI boundaries with one way coupling, the initialization of level sets using a single part or the use of inactive surfaces which are used to output fluid results like fluxes.

2 Introduction

To provide a more comprehensive view of the new features including keywords please refer to the release notes: <https://ftp.lstc.com/anonymous/outgoing/support/FAQ/ReleaseNotes/>

In what follows a high-level description of the new features will be presented. For a quick overview refer to Table 1.

New feature	Description
Linear Solvers	<ul style="list-style-type: none"> New Block Low-Rank factorization for both continuity and momentum equations. Scales very well in parallel.
Gap Closure	<ul style="list-style-type: none"> Allows complete closure using a user defined threshold, that prevents flow through a gap.
Residence Time	<ul style="list-style-type: none"> A new metric for flow stagnation. Useful in healthcare hemodynamics applications to predict regions of thrombosis.
Species Transport	<ul style="list-style-type: none"> Provides a tool to track drug delivery using intradermal injections.
Boundary Layer Meshing improvement	<ul style="list-style-type: none"> Improved quality close to surfaces with poor quality. Adaptive velocity of layer inflation.
New Steady State solver	<ul style="list-style-type: none"> Added a new SIMPLEC steady state algorithm adapted for FEM.
DEM coupling for FSI interface	<ul style="list-style-type: none"> New FSI interface representation using DEM particles on beams and shells. New coupling formulation that uses the fluid pressure gradient instead of the velocity drag. Added buoyancy effects.

Table 1: Summary of new feature for ICFD in R14.

3 Linear solvers

Our default solver for the continuity equation is Preconditioned Conjugate Gradients, where the preconditioner is a simple incomplete factorization of each local problem. For external aerodynamics

problems, this preconditioner is not always strong enough and convergence can be slow. In R14 we added an option to use MUMPS as a preconditioner. MUMPS [1,2] is a sparse direct solver and preconditioner that makes use of so-called Block Low-Rank (BLR) compression techniques. Tests were run for the standard DrivAer external aero model with 3.5M *d.o.f.* where the pressure solve showed a significant decrease in the computational time (see Table 2).

Preconditioner	Setup time [s]	Solve time [s]	Total time [s]	Iterations per solve
Default	13.7	210.0	223.7	351
MUMPS	30	26.5	56.5	3

Table 2: Results showing the performance of the MUMPS solver compared to the default preconditioner.

4 Gap closure

This feature is used to isolate regions of the domain that are in close proximity to each other. The algorithm detects elements in the proximity region and remove them from the analysis. The main applications involve valve closures and contact (see Fig 1).

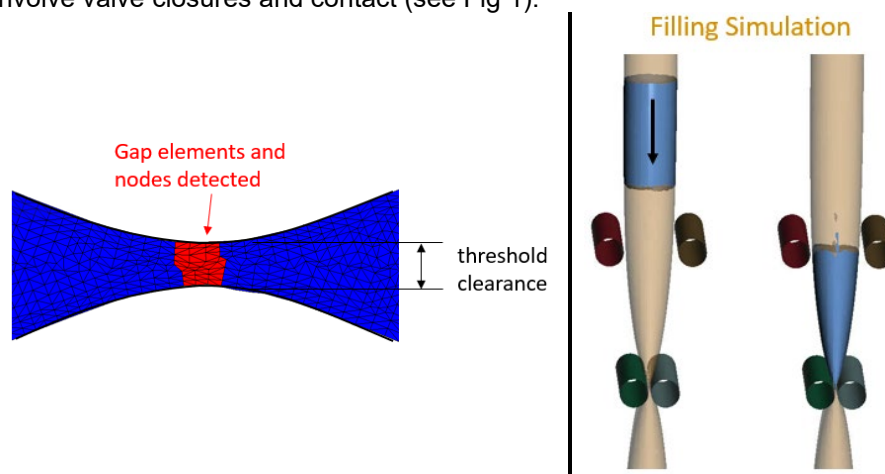


Fig.1: Elements detected by the Gap Closure algorithm in red.

5 Species transport

A species transport model was introduced to model intradermal injections and drug delivery systems in the context of Fluid Structure Interaction (FSI). In these applications the initial bulging of the skin and subsequent diffusion of the drug are important modeling aspects of the problem (see Fig. 2).

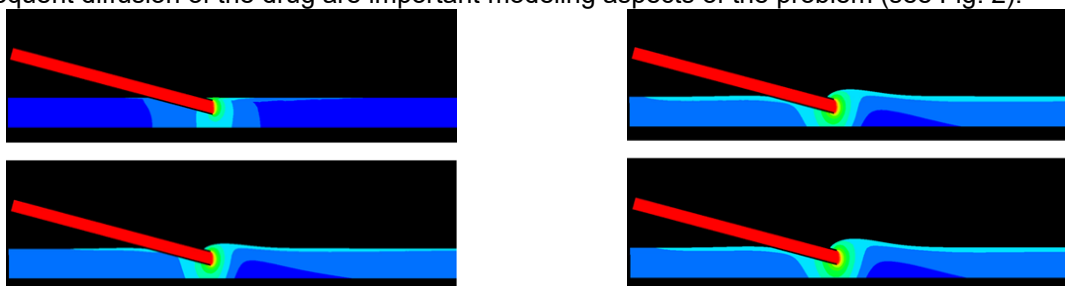


Fig.2: Example of an intradermal injection simulation using species transport and FSI.

6 Steady state simulations

A new SIMPLEC steady state formulation adapted for the ICFD FEM implementation replaces the old pseudo-steady state solver. It accounts for implicit relaxations for the momentum and continuity equations as well as the RANS solvers. It has applications in internal and external flows and it is a good tool to initialize FSI simulations.

7 DEM coupling for FSI interfaces

In this new feature DEM particles are used to represent FSI interfaces. The particles are placed inside shell and/or beam elements. The aim of this feature is to track FSI interfaces that are hard to track using a body fitted methods. These situations usually involve complex contact between solid parts. The DEM coupling method can be used in combination with body fitted methods. In Fig. 3 the suspension lines of a parachute are represented using DEM particles to account for the drag of the lines.

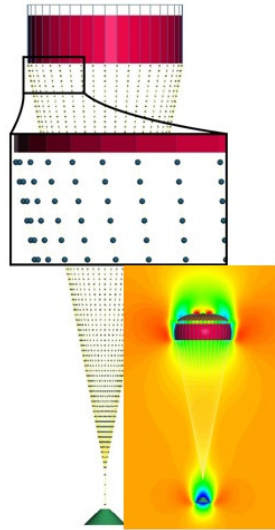


Fig.3: Parachute simulation using implicit FSI coupling with DEM particles on the beams representing suspension lines to transfer momentum to the lines and from the lines to the fluid.

8 Summary

In this paper a highlight of the new features that are part of the R14 release in ICFD were presented. For a more comprehensive list with keywords please refer to the release notes.

9 Literature

- [1] P. R. Amestoy, I. S. Duff, J. Koster and J.-Y. L'Excellent, A fully asynchronous multifrontal solver using distributed dynamic scheduling, SIAM Journal on Matrix Analysis and Applications, Vol 23, No 1, pp 15-41 (2001).
- [2] P. R. Amestoy, A. Buttari, J.-Y. L'Excellent and T. Mary, Performance and scalability of the block low-rank multifrontal factorization on multicore architectures, ACM Transactions on Mathematical Software, Vol 45, Issue 1, pp 2:1-2:26 (2019)

Fluid-structure Interaction Simulation of a Patient Specific Heart Model with Automated Segmentation Using Simpleware™ ScanIP

Chien-Jung (Peggy) Huang¹, George Hyde-Linaker², Chris Goddard², Facundo Del Pin¹, Christoph Maurath¹, Rebecca Bryan², Thierry Marchal¹

¹ ANSYS, Inc

² Synopsys, Inc

1 Introduction

The in-silico studies with the help of numerical simulation on the cardiovascular system can be helpful on the prediction of solid mechanics and fluid dynamics in the heart. The patient-specific geometry in the simulation is crucial in the studies for individual patients. However, in the workflow from the medical image data to high quality mesh for simulation, a large amount of labor work and time is usually needed. The goal of this work is to establish a workflow that needs minimum manual work from the medical image data to the mesh for LS-DYNA analysis by the software Simpleware™ ScanIP (Synopsys, Mountain View, CA) [1]. This nearly automated process enables a route to application within large scale multi subject analysis. Efforts were made to optimize the workflow within ScanIP, generating an optimal surface mesh and model setup for ICFD or fluid-structure interaction (FSI) simulations with LS-DYNA.

2 Methodology

The Simpleware™ ScanIP software offers automated segmentation solutions that are able to convert medical image data, from CT or MRI, to high-quality patient-specific models, extracting regions of interest, performing segmentation, and generating simulation ready meshes. In the beginning, the generated mesh has problems of skewed elements, intersecting surfaces, and un-smoothed complex geometries. It cannot be used in LS-DYNA simulations and needs huge amount of manual editing or smoothing, which can lead to defeature of some important details. After improvement on the workflow within ScanIP, more simulation ready models can be generated. The model includes the surface shell mesh of the left and right atrium and ventricles, aorta, valves for flow analysis and solid mesh of myocardium. The mesh quality is good and smooth. Moreover, different parts of the heart are labeled in different ID numbers for the convenience of simulation setup. The model is stored as Nastran format and is then imported into LS-Prepost for model setup and mesh conversion. With the help of command recording feature in LS-Prepost, it takes less than one minute from the ScanIP generated model to simulation ready model, and the workflow can be easily applied on different heart model with minimum preparation time.

3 Results

3.1 Two heart geometries

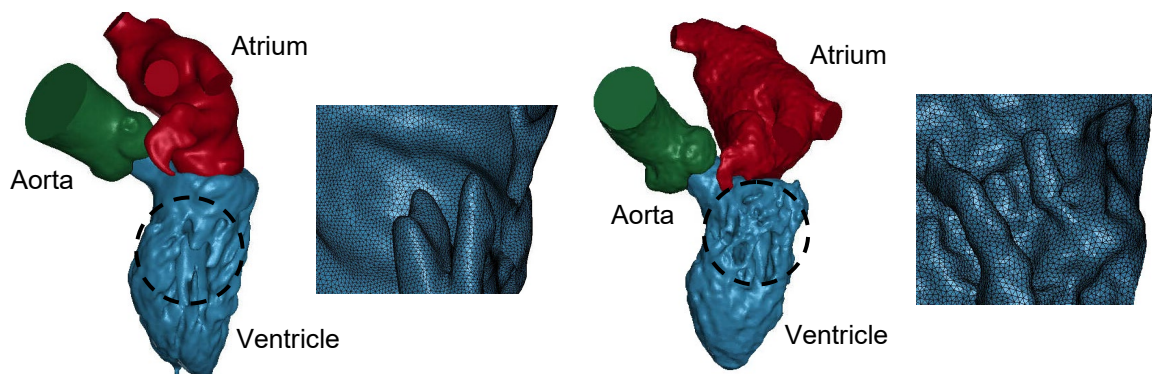


Fig. 1: Two different left heart geometries A (left) and B (right) and their mesh inside of the ventricle.

Two distinct heart geometries at the stage before the ventricular contraction are segmented from the CT scans. The surface mesh obtained has good quality. The fine structures of the surface of the left ventricle were represented by smooth triangular meshes (Fig. 1). The two meshes can be imported into LS-DYNA and high quality tetrahedra mesh can be generated. The ICFD simulation can be performed without any issue.

3.2 Moving heart simulation

For the heart geometry A, the surface meshes at different stages of a cardiac cycle were generated from the 4D cardiac CT scans. The nodes between different frames have one-to-one correspondence, so the motion of the heart wall can be calculated. The simulation is setup with 1-way FSI simulation, which the shell structure of the heart wall with prescribed motion transfers its displacement to the pressure driven flow inside. The results at the early stage of ventricle contraction are shown in Fig. 2.

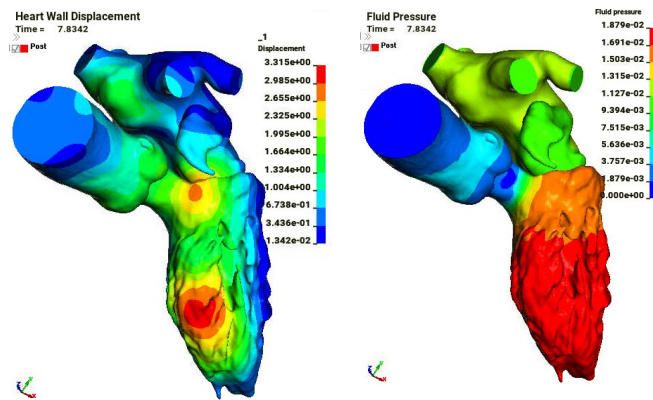


Fig.2: The displacement field of the wall of the left heart (left) and the computed pressure distribution of the interior flow (right) at the early stage of the ventricular contraction.

3.3 Fluid-structure interaction of prosthetic aortic valve

A prosthetic aortic valve is placed at the center of the aortic valve obtained from ScanIP. The prosthetic valve has an outer rigid ring and three axisymmetric leaflets. The FSI simulation of the rubber valve and fixed heart wall with time varying pressure profile at atrium is performed (Fig. 3). This is an example of FSI simulation of valvular system with the heart geometry obtained from ScanIP.

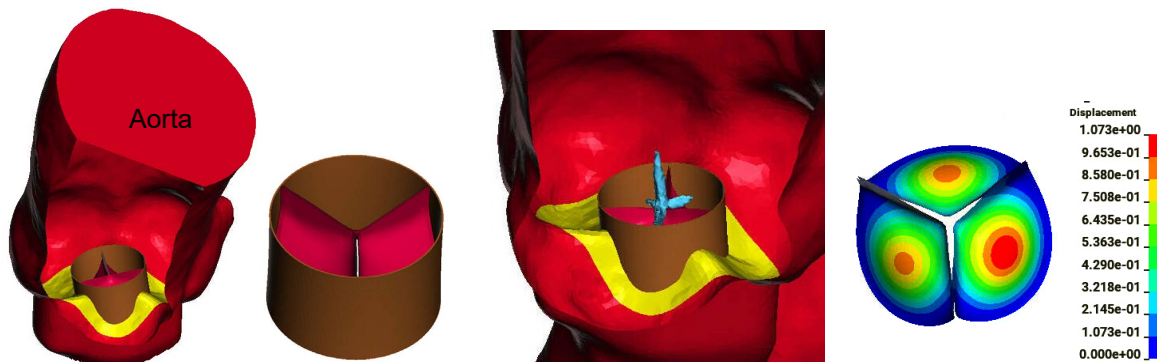


Fig.3: The geometry of the prosthetic aortic valve and its placement (left two). The iso-surface of velocity field and the displacement of the leaflets when the valve is about to open (right two).

4 Summary

In this work, the automated workflow from medical images to LS-DYNA model for ICFD or FSI analysis by the software Simpleware™ ScanIP has been established and optimized. The workflow can be applied on different heart geometries with minimum manual effort. The obtained model can also be applied on the simulation of the CFD analysis of a pumping heart and FSI study of the valve.

5 Literature

- [1] 3D Image Segmentation Software: Simpleware ScanIP
<https://www.synopsys.com/simpleware/software/scanip.html>

Overview of dual-CESE Solver in LS-DYNA and Its Applications

Zeng-chan Zhang¹, Grant Cook Jr¹ and Kyoung-Su Im¹

¹Ansys, Inc, Livermore, CA 94551, USA

The compressible fluid CESE/dual-CESE solver in LS-DYNA is based on the Conservation Element and Solution Element (CESE) method [1-2]. The CESE method is quite different from the traditional CFD method and has a lot of nontraditional features, including (i) a unified treatment of space and time (thereby ensuring good conservation in both space and time); (ii) a unified treatment for arbitrarily shaped polygonal mesh elements; (iii) a simple but efficient discontinuity (shock) treatment. This method is especially useful for high-speed compressible flows with complex flows patterns including shock waves and/or detonations.

Implementation of the dual-CESE solver in LS-DYNA started several years ago. It is an improved version of the regular CESE solver. The main difference between the CESE solver and the dual-CESE solver is: in the regular CESE solver, flow variables are solved and stored at one set of solution points that are the element centers; while in the dual-CESE solver, the flow variables are solved and stored at two sets of solution points of element centers & element vertices in two successive time steps. Fig.1 show the difference between these two methods.

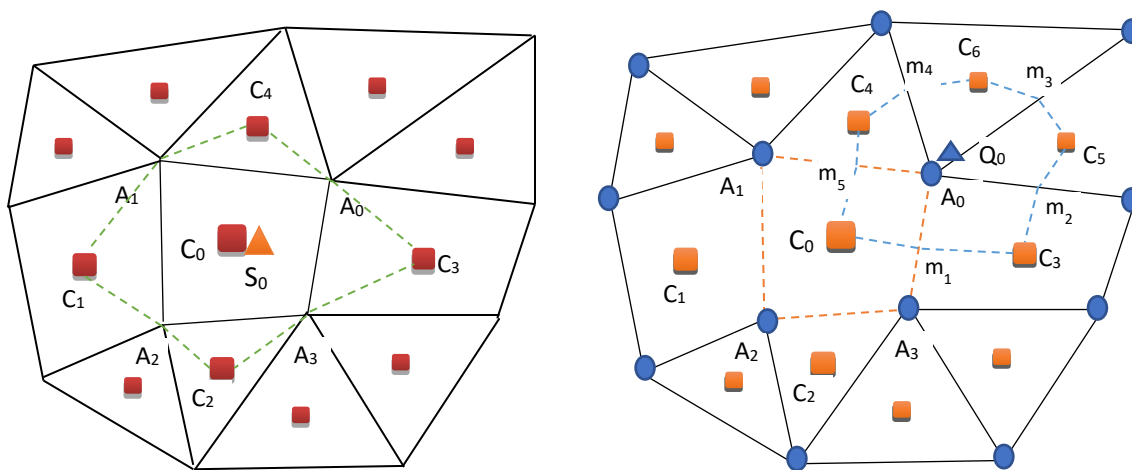


Fig.1 schematic of conservation element (CE) and solution element (SE) under (left) standard CESE and (right) dual CESE solver

Because of the differences in the calculation strategies, compared to the regular CESE solver, the dual-CESE solver is more accurate and stable when employing the same mesh. This is particularly true for triangle (2D) /tetrahedral (3D) meshes, while requiring a little more CPU time to compute the solution. Note that this does not mean that the mesh can be of poor quality and still obtain good results. That is, the mesh should still be smoothly varying from one region to another, with no large aspect ratio elements.

Now most of the regular CESE solver capabilities have been ported into the new dual-CESE solver, and table-1 shows the current status of these two solvers.

Table 1: current status of the regular CESE and dual-CESE solvers

Application models	CESE solver	dual-CESE solver
CFD solver (2D, 2D-axisymmetric, 3D) - general purpose transient compressible fluid solvers	✓	✓
FSI solvers: - FSI-ibm - FSI-mmm	✓	✓
Conjugate heat transfer (CHT)	✓	
Cavitation flow solver	✓	✓
Chemical reaction flow solver	✓	
Stochastic particle solver	✓	
Multiphase flow solver: (for condensed explosives)		✓
Phase-change flow solver		✓

Both the regular CESE solver and dual-CESE solver are coupled with the LS-DYNA structural FEM solver to solve different fluid/structure interaction (FSI) problems. We provide two FSI strategies, one is the immersed boundary method (ibm) and the other is the moving mesh method (mmm). In the ibm solver, the fluid mesh is fixed, and structural parts can move through the fluid domain. On the other hand, in the mmm solver, the fluid mesh will follow the motion of the structural boundaries (interfaces). The ibm method is more suitable for large deformation FSI problems, while the mmm method is more useful for small deformation FSI problems and is the more accurate method. But the cost of the mmm method mesh morphing grows significantly with the number of mesh elements, and mesh morphing is usually required every few time steps. Fig. 2 is an FSI-ibm example showing the process of three flimsy structural parts being lifted up by a vacuuming tube, while Fig. 3 shows the flow mesh and flow field changes inside a valve chamber driven by a simplified piston motion.

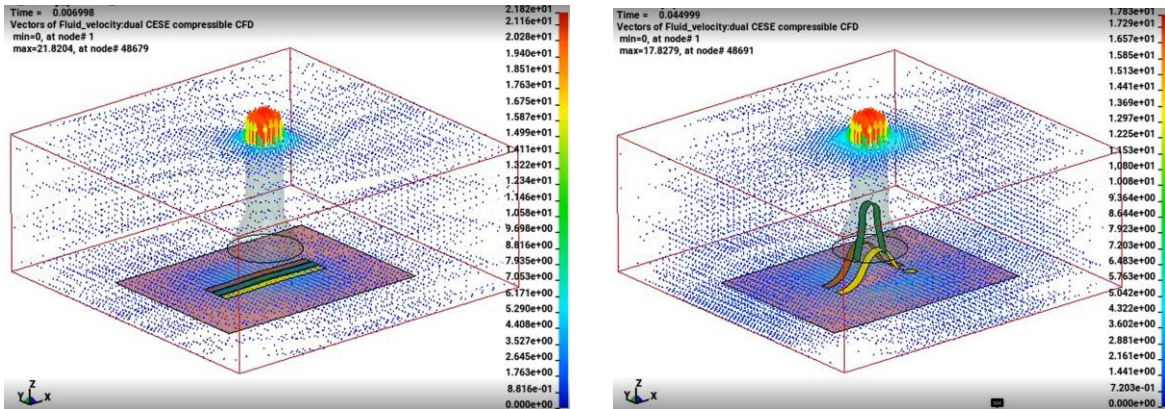


Fig. 2 flimsy movement sucking by a vacuum tube

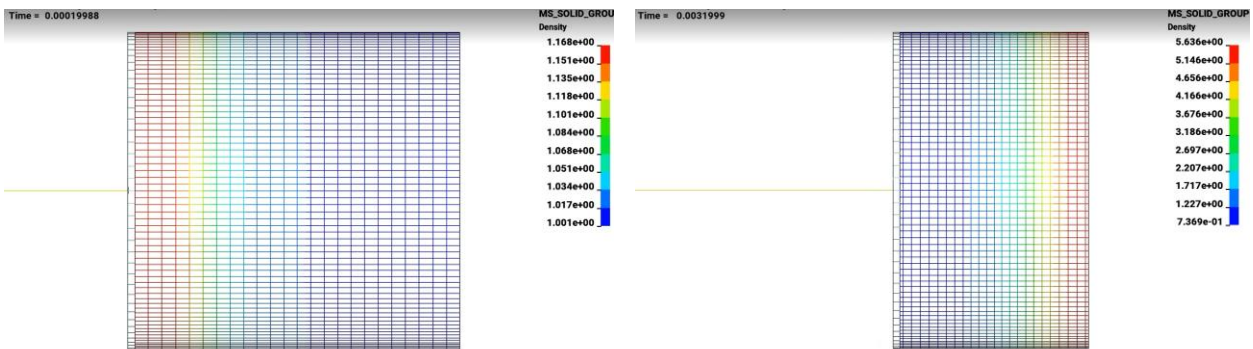


Fig. 3 fluid mesh and flow field change inside a piston chamber

Currently, no new capabilities are being added to the regular CESE solver. New features are added only to the new dual-CESE solvers. The following are some of the new features that we have added to the new dual-CESE solver:

1. Hybrid multiphase flow model ^[3]

In this model:

- a. Three materials can be used (one is an inert material, and the other two materials are a mixture of explosive materials (reactant and product)).
- b. Many realistic EOSes (such as Mie-Gruneisen type EOS) can be used, those implemented include: JWL EOS; Cochran-Chan EOS; generalized Van der Waals EOS and stiffened gas EOS, and, of course, ideal gas EOS can be used too, because it's one of the simplest Mie-Gruneisen type EOSes.
- c. Arbitrary (pressure- or temperature-based) **reaction-rate laws** can be used. At this time, we support: ignition and growth (I&G) model; simplified I&G model, and simple pressure dependent reaction rate law.

Application:

This model is targeted to the condensed phase explosives, such as:

- combustion and transition to detonation of condensed-phase explosives

- propagation of detonations in compliantly confined charges
- shock-induced cavity collapse in liquid explosives

Fig.4 shows a JWL rate stick inside a cylinder container, where an explosive material is initiated by the booster, forms a detonation wave, and propagates through the slab of reactive material. The high pressure behind the detonation wave forces the container to deform (expand).

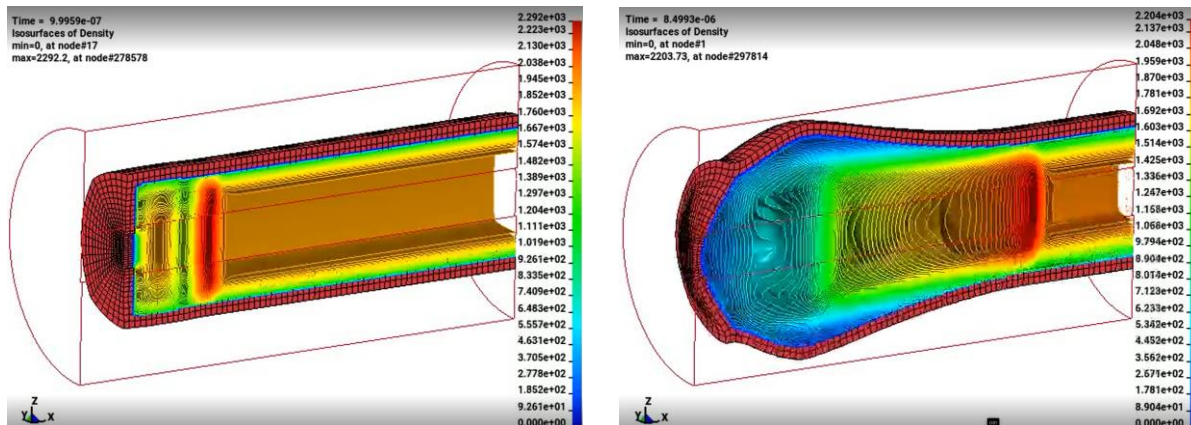
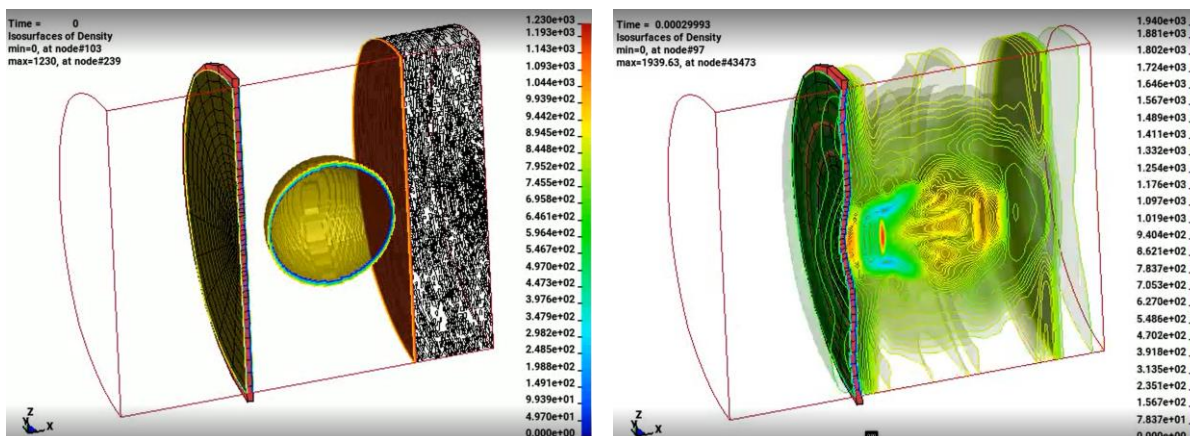


Fig. 4 explosive detonation wave propagating inside a cylinder container

2. Two-phase model

This is a reduced model of the above hybrid model, where two immiscible materials can be used, and the number of control equations is also reduced to five. Fig. 5 shows a left-moving shock wave propagating in a cylinder first hitting a stationary bubble, which gains speed and loses its circular shape. After the shock wave hits the bubble, circular pressure waves are created that keep moving forward and hit the structural panel, causing the panel to deform.



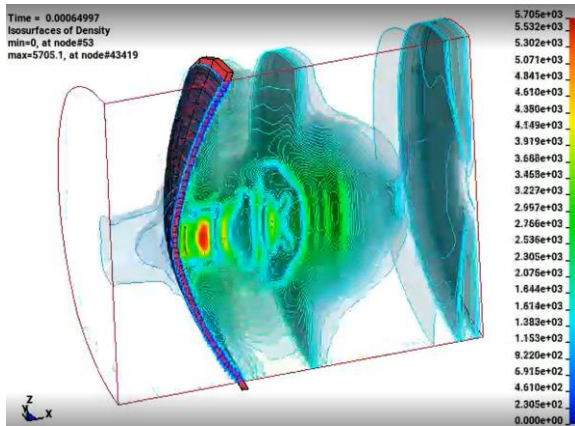


Fig. 5 Shock-bubble-structure interaction process

3. Phase-change model

Here we implemented is a Homogeneous Relaxation Model (HRM) or so-called 4-equation model that is extended to model liquid in equilibrium with multicomponent gases. A thermochemical relaxation algorithm is applied to achieve the phase transition. For the details of this model, please refer to ref. [6]. Fig. 6 shows an evaporating liquid jet in a cryogenic rocket engine during the ignition phase.

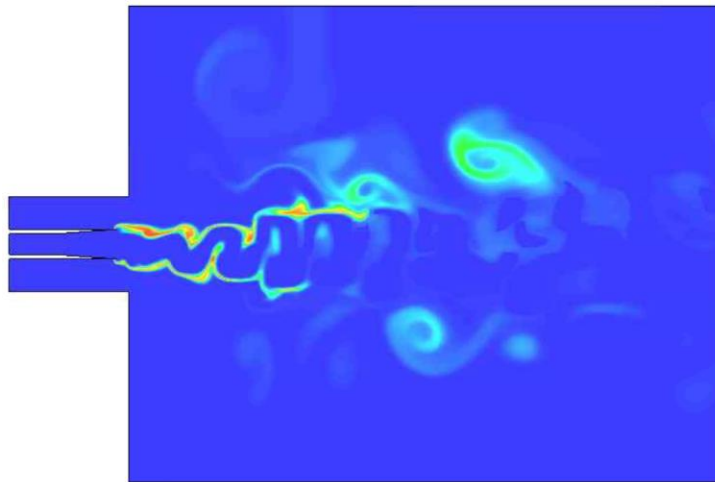


Fig. 6 vapor mass fraction distribution of the liquid jet in a nozzle

4. Future Capabilities

The dual CESE Solution Explorer will soon be in LSPP, and it will enable users to setup the fluid aspects of a dual CESE problem in a graphical way, including the mesh-related aspects. Fig. 7 shows the main input or dual CESE model editing panel of this Solution Explorer.

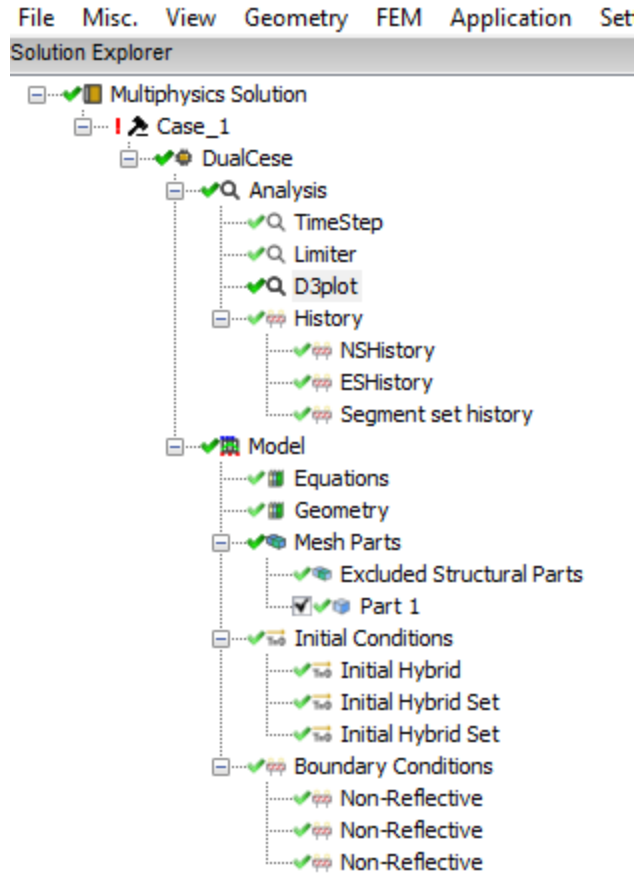


Fig. 7 The main tree view of the LSPP dual CESE Solution Explorer for a hybrid multiphase model.

Time history output from the dual CESE solver is now being output to ‘binout’ using the following keyword cards that are new in the R14 release of LS-DYNA:

- *DUALCESE_DATABASE_HISTORY_ELEMENT_SET
- *DUALCESE_DATABASE_HISTORY_GLOBALS
- *DUALCESE_DATABASE_HISTORY_NODE_SET
- *DUALCESE_DATABASE_HISTORY_POINT_SET
- *DUALCESE_DATABASE_HISTORY_SEGMENT_SET

A future version of LSPP should be able to plot this time history data.

References

[1] S.C. Chang, “The space-time conservation element and solution element – a new approach for solving the Navier-Stokes and Euler equations,” J. Comp. Phys. 119 (1995) 295-324

- [2] Z.-C. Zhang, S.T.J., Yu and S.-C. Chang, “A space-time conservation element and solution element method for solving the two- and three-dimensional unsteady Euler equations using quadrilateral and hexahedral meshes,” *J. Comp. Phys.* 175 (1) (2002) 168-199
- [3] L.Michael, N.Nikiforakis, A hybrid formulation for the numerical simulation of condensed phase explosives, *J. Comp. Phys.* 316 (2016) 193-217.
- [4] G. Allaire, S. Clerc, S. Kokh, A five-equation model for the simulation of interfaces between compressible fluids, *J. Comput. Phys.* 181(2) (2002) 577-616
- [5] J.W. Banks, D.W. Schwendeman, A.K. Kapila, W.D. Henshaw, A high-resolution Godunov method for compressible multi-material flow on overlapping grids, *J. Comp. Phys.* 223 (2007) 262-297
- [6] A. Chiapolino, P. Boivin, R. Saurel, A simple and fast phase transition relaxation solver for compressible multicomponent two-phase flows, *Computers & Fluids* 150 (2017) 31–45.

Development of a two-way flow Chinese-dome digester (TWF-CDD) for enhancing anaerobic digestion performance

Mfor Ebot^{1*}, Masaaki Fujiwara¹, Tatsuki Toda¹

¹Graduate School of Science and Engineering, Soka University, 1-236 Tangi-machi, Hachioji 192-8577, Tokyo, Japan.

1. Introduction

The Chinese dome digester (CDD) is a low-cost and most widely applied household digester in rural areas of developing countries, given its energy-efficient self-mixing process, reliability, low maintenance, and long lifespan, making it suitable to meet the energy requirement for cooking applications at the domestic and community levels [1]. When the biogas produced accumulates and is stored in the headspace above the slurry, the stored gas results in a pressure build-up and pushes part of the slurry into the expansion tank. During gas release through a valve, the slurry flows back into the main digester, thus, creating a mixing regime [2]. Fig. 1 illustrates the self-mixing process in a CDD. The major hindrance to achieving sufficient biogas production in CDD is the formation of scum at the surface of the slurry. Scum represents a severe technological challenge because it hampers the release of biogas and can reduce the available digester capacity by 30% [3]. The reason why scum is formed at the surface of slurry is attributed to dead zones created due to structural design of CDD which can limit mixing [2, 4]. CDD has a complex structure with a hose connecting the main digester and the expansion tank at the bottom and the back flow of slurry from the expansion tank (during gas release) only mix the bottom part, leaving dead zones at the upper part where scum could be nurtured. Addition of a hose to connect the expansion tank and main digester from the top, enabling two-way flow can be a long-term solution (Fig. 2). Since the presence of the dead zones in CDD leads to the formation of scum, advanced modeling and simulation techniques such as CFD could be employed.

Therefore, the objective of this study is to evaluate the mixing performance of a two-way flow Chinese dome digester (TWF-CDD) by using CFD simulations. A second simulation will be performed in a conventional CDD to compare the mixing performance of the two models.

2. Materials & Methods

The modeling and simulations of TWF-CDD were performed in ANSYS Workbench (v. 21.1). The CDD was constructed from PVC materials, with a digester volume of 15 L and an expansion tank of 2 L for slurry displacement and outlet [4]. The 3D geometry was developed in ANSYS SpaceClaim (v.21.1) as shown in Fig. 3 (a). Mesh independence analysis was performed on the TWF-CDD. The user-defined mesh used was primarily tetrahedral (5-cell, triangular pyramid) with minimal skewness (Fig. 3 (b)). The total number of elements was 312924. The discretized (meshed) 3D model was simulated by using Ansys Fluent software (v.21.1). The CFD simulation was performed on CDD for the gas release

process. The multiphase phase was performed (solid, liquid, gas) with a 12% TS concentration [18] and the flow was laminar [4].

3. Results and discussions

Characterization of mixing in TWF-CDD by CFD simulation

The velocity data of the model are captured from the simulation results. The results show the values of the slurry hydrodynamic inside CDD, as velocity profiles. Fig. 4 (a) shows the velocity contours in the TWF-CDD during gas release process. The contours show that the flow begins at the top (the surface where scum could be formed) with higher velocity to the bottom of the digester. The velocity vectors in Fig. 4 (b) shows that the fluid rotates in a circular motion with high velocity at the top, $H=20$ cm (3.5 ± 1.9 m s⁻¹), in the middle, $H= 10$ cm (3.8 ± 1.7 m s⁻¹) and bottom (3.4 ± 1.6 m s⁻¹). The results of velocity contours and vectors show that there was no difference in the velocity magnitude at the top, middle and bottom of TWF-CDD, implying that the digester was mixed homogeneously (Fig. 5). Notably, CDDs usually have dead zones at the top which can nurture scum and hinder methane yield. However, Structural modification of CDD to a TWF-CDD could allow slurry flow from the expansion tank directly to the slurry surface, eliminating dead zones and scum. The trend of mixing in the present study is similar to Jegede et al. [4] who performed 2D, three-phase simulation and evaluated the hydraulic characteristics of a CDD and an optimized CDD. The results of the optimized CDD with baffle plates showed high velocity magnitude at the top compared to the normal CDD. 3D simulations are usually efficient and represents the actual mixing process in CDD. However, Jegede et al. [9] did not focus on the relationships between scum formation and fluid characteristics which vary in the different parts of the CDD. Fig. 6 shows the solid-liquid interaction in the TWF-CDD at 3 seconds simulation time.

4. Summary

This study investigated the mixing performance of a TWF-CDD in comparison with conventional CDD. Slurry flow from the expansion tank to the surface could eliminate dead zones and prevent scum formation. The mixing intensity increased in the TWF-CDD, and mixing was homogeneous in all parts of the digester.

5. References

1. Cheng S, Li Z, Mang HP, Huba EM (2013) A review of prefabricated biogas digesters in China. *Renew Sustain Energy Rev* 28:738–748. <https://doi.org/10.1016/J.RSER.2013.08.030>
2. Jegede AO, Zeeman G, Bruning H (2019) Development of an optimised Chinese dome digester enables smaller reactor volumes; pilot scale performance. *Energies* 12:.. <https://doi.org/10.3390/en12112213>
3. Raman P, Rao VVR, Kishore VVN (1989) A static scum-breaking net for fixed-dome biogas plants. *Biol Wastes* 30:261–273. [https://doi.org/10.1016/0269-7483\(89\)90055-4](https://doi.org/10.1016/0269-7483(89)90055-4)
4. Jegede AO, Gualtieri C, Zeeman G, Bruning H (2020) Three-phase simulation of the hydraulic characteristics of an optimized Chinese dome digester using COMSOL Multiphysics. *Renew Energy* 157:530–544. <https://doi.org/10.1016/j.renene.2020.05.011>

DYNAmore ECO SYSTEM – News on DYNAmore’s LS-DYNA-Tools

Steffen Mattern¹, Kurt Schweizerhof¹

¹DYNAmore GmbH

1 LS-DYNA Tools – status-quo before 2022

Since many years, DYNAmore develops a family of small, command-line based tools to support the engineer’s daily work with LS-DYNA. These “little helpers” provide functionalities such as compress and modify d3plot databases, extract sub-models from d3plot files, collect and group warnings from message files, summarize model content, and many more. The development of new features has mainly been funded by German automotive OEMs, where some of the tools are strongly integrated in the simulation process chain of pre-processing, solving and post-processing. For more than 20 years (until July 2022) the tools had been free-of-charge for DYNAmore’s customers.

2 DYNAmore ECO SYSTEM

2.1 What’s new?

Due to an increasing number of users, also beyond the automotive industry, together with a corresponding effort for maintenance and technical support, it has recently been decided (and announced in [1]) to introduce a small license fee from now on, to be able to maintain good performance and high quality of the software. Together with more recently developed software products for special applications such as model checking, mapping of results or conversion of LS-DYNA output, the tools are grouped into five packages, that can separately be licensed. Major contributors to the development of the original tools, i.e., individual automotive OEMs, will still be allowed to use them without additional costs.

2.2 Available packages

2.2.1 General information

The different tools, the traditional LS-DYNA-Tools as well as further software products related to LS-DYNA, are now available in five different packages, each of which can be booked separately [2].

2.2.2 DYNAmore.pre

Contains five of the traditional LS-DYNA-Tools, mainly relevant for pre-processing tasks, model preparation or model analysis. The tools are in particular

- DM.plot2bc ... generate boundary conditions set of nodes from d3plot
- DM.check-hsp ... extract model information from d3hsp file
- DM.check-c ... scan mes-files for all kinds of contact messages
- DM.seghandle ... list, visualize and manipulate binary interface files (INFMAK)
- DM.plot2coor ... extract nodal coordinates of deformed geometry from arbitrary plot state

2.2.3 DYNAmore.post

Contains seven of the traditional LS-DYNA-Tools, mainly for post-processing tasks, including manipulation of LS-DYNA output files. The tools are in particular

- DM.plotcpvs ... manipulate, remove, or select data from d3plot file
- DM.check-failed ... collect info about failed elements and NaN values from message-files
- DM.check-binout ... repair corrupt LSDA-file, e.g., binout
- DM.d3plot-head ... manipulate d3plot header (title)
- DM.plotintrusion ... calculate maximum intrusion of a subset of nodes
- DM.plot2nodout ... extract nodout data from d3plot for a given node set
- DM.hsp-tailor ... cleanup d3hsp or message files to keep the files small

2.2.4 *DYNAmore.quality*

Contains DM.inspect [3], a batch program allowing customized quality control for LS-DYNA input files. The software requires the individual definition of quality criteria by the user rather than providing any pre-defined checks. This modularized approach allows the application of DM.inspect for various simulation disciplines, typically having different modeling requirements. The check procedure performed by DM.inspect can be divided into three subsequent phases. An optional pre-phase where checks from a pre-processor can be applied, a simulation-phase performing an LS-DYNA initialization run and a post-phase with various checks based on the LS-DYNA input and output files. In the last phase, DM.check-hsp is used to create an XML-file containing model information from LS-DYNA's output files. DM.check-hsp therefore is also included in this package. Finally, DM.inspect writes a report containing the results of the performed quality checks. DM.inspect can be used as a stand-alone tool as well as integrated in a simulation data management environment.

2.2.5 *DYNAmore.mapping*

Contains Envyo [4], a multi-purpose mapping tool dedicated to LS-DYNA. It allows for the transfer and manipulation of simulation result data between differently discretized meshes and from different solvers to an LS-DYNA specific input format. Furthermore, mapping of arbitrary point cloud data (e.g., experimental results) provided in CSV format or clustering methods based on grayscale images is available. Envyo provides a wide range of possibilities to consider any kind of preliminary results in a following numerical simulation to cover the complete process with LS-DYNA. Some standard and more automatized transformation options allow for the consideration of different length scales and coordinate systems.

2.2.6 *DYNAmore.testing*

Contains DM.binout2isomme (DM.b2i), a command-line based tool to convert selected LS-DYNA results from the binout database in an ISO-MME structure, as used in automotive industry to store experimental results from crash tests. The tool entirely works in batch mode expecting a configuration file. It provides channel modification (differentiation/ integration, offsetting and scaling of time and values, filtering) and channel aggregation (sum, mean). It is also possible to append channels and data to an existing ISO-MME data structure. DM.binout2isomme allows storage of LS-DYNA simulation results exactly the same way as experimental data and therefore enables applying the same templates for post-processing and visualization.

3 What's next?

In the future, DYNAmore is planning to assure and further extend the functional range of the introduced packages by maintaining and enhancing existing tools or adding new applications for specific tasks. A new tool to support creating and handling encrypted LS-DYNA input files – DM.keyword-crypt – is soon to be released. Also, a unified strategy regarding licensing is currently under discussion, since as of today, different tools still use individual licensing approaches. The major goal is and will be to support the daily work with LS-DYNA and help engineers to prepare, analyse, improve, and process simulation data.

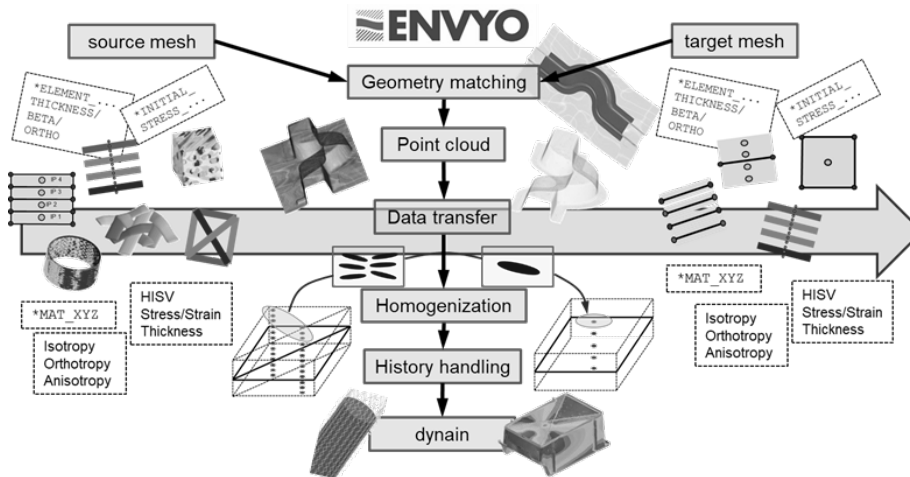
4 References

- [1] 158 Issue DYNAmore Infomail:
<https://www.dynamore.de/en/news/dmnews/2022/158-issue-dynamore-infomail>
- [2] DYNAmore ECO SYSTEM website:
<https://www.dynamore.de/en/products/pre-and-postprocessors/tools>
- [3] Mattern, Steffen: DM.inspect: customizable quality control of LS-DYNA input files, 13th European LS-DYNA Conference 2021, Ulm, Germany
- [4] DYNAmore GmbH: "Envyo User's Manual", DRAFT, Oct. 2022.

Recent developments in Envyo®

Christian Liebold, Tolga Usta¹

¹DYNAMore GmbH



Abstract

The mapping software Envyo [1] developed by DYNAMore GmbH is a multi-purpose mapper dedicated to LS-DYNA users. In comparison to our competitors, we focus on a solution which provides the transferred input data specifically in LS-DYNA ***KEYWORD** [2] format and related binary containers such as Isda, except for the new VMAP standard [3]. With different user commands which can be directly defined within the ascii-based input file or through the provided graphical user interface (GUI), users may manipulate the transferred data based on their application requirements, vary search radii, or apply different homogenization and averaging schemes to the data. The data itself may come from different sources such as simulation results from LS-DYNA, but also other solvers either through their native format or through the VMAP interface. Furthermore, Envyo supports the transfer of experimental data based on a gray-scale mapping algorithm, allowing users to increase the accuracy of their digital twin. A strong collaboration with customers allows identifying possible mapping approaches and ensures that solutions can be provided based on the individual problem.

Within the presentation, a basic introduction into Envyo will be given, covering licensing schemes for individual users as well as company license management systems on both, Windows and Linux operating systems. This is followed by an overview on recent enhancements to Envyo being made within research projects and based upon customers requests. The topics covered are:

- General enhancements
- Enhancements for molding result consideration
- Grayscale mapping for adhesives
- Plybook considerations
- Developments on homogenization across different length scales (micro-meso-macro)
- Stochastic analysis setup

The presentation will conclude with an outlook on upcoming developments and the introduction of a software release plan, enhancing customer access to bug-fix versions and new releases.

1 Literature

- [1] DYNAMore GmbH: "Envyo User's Manual", DRAFT, Oct. 2022.
- [2] Livermore Software Technology (LST), an ANSYS Company: "LS-DYNA® Keyword User's Manual – Volume I", Livermore, CA, USA, 2022.
- [3] Wolf, K., Gulati, P., Duffet, G.: "VMAP enabling interoperability in integrated CAE simulation workflows", 13th European LS-DYNA Conference, Ulm, GER, Oct. 2021.

DYNAmore ECO SYSTEM

The artists formerly known as LS-DYNA Tools

Max Hübner¹, Tobias Graf¹, Alexander Schif¹

¹DYNAmore GmbH

When simulating problems with LS-DYNA a vast amount of information and simulation data is being generated. Especially in the case of large models like full car crash models the extraction of the desired data might cause some effort itself. The DYNAmore ECO SYSTEM provides tools which will help to find and extract the desired data quickly. Most of the tools are being continuously developed and improved over the last 20 years and have been adapted for the special requirements of our customers.

The tool DM.check-hsp for example provides you with general information about the model as well as detailed information about the used material models, element formulations, contact definitions and much more. DM.check-c allows the user to easily gather a broad range of information, e. g. all recognized penetrations or untied nodes, about any contacts used in the model. This presentation will provide a closer look into the use of some of the tools like DM.check-c, DM.check-hsp and DM.check-failed. Their usage will furthermore be demonstrated by their practicable application.

New Features of the Latest LS-PrePost

Philip Ho¹

¹Ansys

1 Abstract

In this presentation, we are going to show the latest features and capabilities in the released version and the development version of LS-PrePost. We are going to emphasize the Solution Explorer for pre-processing and the Post Explorer for post-processing. The Solution Explorer is designed to help the user to setup the LS-DYNA input file without knowing all the details of the keyword input. The user just needs to know his application and the physics of his problem. The Solution Explorer will ask the user to enter parameters related to the problem and guide the user on what to input; it will create all the necessary keyword cards for the specific problem. The Post Explorer is a new way of doing post-processing for LS-DYNA results. Each Fringe plot and history graph will have its own properties. Many operations on one of such plots can be easily copied and transferred to another plot. The whole post-processing session also can be saved to be reused in the future for the same problem or a different problem.

Positioning Human Body Models based on experimental data

Maria Oikonomou¹, Athanasios Mihailidis¹, Johan Iraeus², Lambros Rorris³, Athanasios Lioras⁴

¹Aristotle University of Thessaloniki

²Chalmers University of Technology

³BETA CAE Systems International AG

⁴BETA CAE Systems SA

1 Introduction

Crash Simulation and Analysis aims to protect a variety of dissimilar road users. Numerous studies examine occupants' and pedestrians' motion and their potential injuries. However, a few analyses have been conducted about other vulnerable road users, such as motorcyclists and bicyclists, although bikes and generally two-wheel vehicles are common personal transportation. Thus, studying their kinematic behavior in multiple collisions will enable safe and convenient travel.

These road users can adopt an extensive range of non-standard seating choices, leading to different kinematic behavior. So, analyzing crash simulation results extracted from unique initial positions is critical to protect humans in out-of-position load cases.

Since dummies are established for specific crash situations, Human Body Modeling and Simulation is the most accurate way to reproduce humans' motion and predict their potential injuries in different crash scenarios. However, Human Body Models (HBMs) are developed only for the seating and standing postures, representing the occupant and pedestrian accordingly. Therefore, there is a need to move HBMs to adopt the desired position.

This study aims to develop a method that positions the HBMs in a target posture defined by experimental data. The positioning process of HBM was developed in ANSA python scripts and using the Ansa HBM Articulation tool.

Due to the expanding use of bicycles and increased bicycle traffic accidents, data from a typical bicyclist posture are extracted to illustrate the positioning tool.

2 Methods

The reproduction of body posture is the accurate positioning of HBM to replicate the experimentally derived Subject's position. This procedure is based on the precise positioning of specific anatomical landmarks, which characterize the whole body's position. The anatomical landmarks are easily identified and palpated points of human bones and are selected via literature. Therefore, an essential step in producing an identical pose of the HBM and the reference Subject is the definition of corresponding anatomical points on the Subject's and HBM's Bones.

Skin markers and imaging techniques are the most common ways to extract the coordinates of the Subject's landmarks. Imaging techniques can directly determine the position of bones as required, while skin markers do not. Thus, conducting a skin marker method requires further measurements of the Volunteer's skinfold thickness. Therefore, the coordinates of skin markers are modified as if they were set on the Volunteer's bones.

Although, due to anatomical differences between the HBM and the Subject, the HBM's articulation cannot occur by directly using the coordinates of the previously defined Subject's anatomical points. Thus, the goal is to articulate HBM to achieve the same slopes between its successive points with the Subject's successive markers.

So, an optimized repetitive articulation method is built to calculate the slopes' differences in each articulation step. The articulation Procedure uses ANSA python scripts and the Ansa HBM Articulation tool. The final HBM position is chosen as the one with the minimum slope error.

3 Implementation

An experiment using a Skin Markers technique was conducted to implement the above-described methodology. The investigation involves a racing bicycle with known typical dimensions. The selected for positioning HBM is the THUMS AM50 Occupant. A volunteer with similar characteristics (height and

weight) rides the bike, and skin markers are placed in its final position. In addition, a caliper measures skinfold thickness on the markers' positions. Pictures of the whole experimental setup are captured. The data collection is performed using a photogrammetric method by examining photos. The first step is the computation of camera intrinsic and extrinsic parameters, and the second is calculating the coordinates of the markers. The whole analysis is operated through python's OpenCV library. Finally, the HBM is moved to the reference bicyclist posture, as determined by the explained methodology, and an equivalent bike is constructed using the ANSA Bicycle Configurator Tool. Therefore, examining bicyclists' behavior in different crash situations using HBMs became feasible.

4 Discussion

This study develops a method that positions the HBM in a target posture defined by experimental data. The data can be derived from any volunteer matching the features of the to-be-positioned HBM. Consequently, unique initial positions can be examined to protect the occupant in non-standard load cases.



Fig.1: Reference Bicyclist Posture.



Fig.2: HBM Final Posture.

5 Literature

- [1] Makia, T., Kajzerb, J.: "The behavior of bicyclists in frontal and rear crash accidents with cars", JSAE, 2001, 357–363.
- [2] Peng, Y., Chen, Y., Yang, J., Otte, D., Willinger, R.: "A study of pedestrian and bicyclist exposure to head injury in passenger car collisions based on accident data and simulations", Safety Science, 2012, 1749-1759.
- [3] Siegler, S., Allard, P., Kirtley, C., Leardini, A., Rosenbaum, D., Whittle, M., D'Lima, D., Cristofolini, L., Witte, H., Schmid, O., Stokes, I.: "ISB recommendation on definitions of joint coordinate system of various joints for the reporting of human joint motion—part I: ankle, hip, and spine", Journal of Biomechanics, 2002, 543-548.
- [4] Wu, G., Van der Helmb, F., Veeger, H., Makhsous, M., Van Roy, P., Anglin, C., Nagels, J., Karduna, A., McQuade, K., Wang, X., Werner, F., Buchholz, B.: "ISB recommendation on definitions of joint coordinate systems of various joints for the reporting of human joint motion—Part II: shoulder, elbow, wrist and hand", Journal of Biomechanics, 2005, 981-992.
- [5] Klein, C., González-García, M., Weber, J., Bosma, F., Lancashire, R., Breiffuss, D., Kirschbichler, S., Leitgeb, W.: "A Method for Reproducible Landmark-based Positioning of Multibody and Finite Element Human Models", IRCOB Conference, 2021.
- [6] Frostell, A., Hakim, R., Thelin, E., Mattsson, P., Svensson, M.: "A Review of the Segmental Diameter of the Healthy Human Spinal Cord ", Frontiers in Neurology, 2016.
- [7] Gilad, I., Nissan, M.: " Sagittal evaluation of elemental geometrical dimensions of human vertebrae", Journal of Anatomy, 1985, 115-120.

Biofidelic positioning, pre-processing and post-processing of Human Body Models with ANSA and META

Lambros Rorris¹, Nikos Tzolas², Athanasios Lioras², Athanasios Fokylidis²

¹BETA CAE Systems International AG

²BETA CAE Systems SA

1 Introduction

HBM's have become a much-needed tool for the safety simulations of the automotive industry. Out-of-position load cases for passengers and drivers and simulations for other vulnerable road users, like pedestrians and cyclists are increasingly needed, and HBM's can address this need. Nevertheless positioning, pre-processing and post-processing of these models on a level suitable for industrial use is not straight-forward. During the last years a lot of research and development effort has been put in the ANSA pre-processor and META post-processor to develop the needed software tools to the engineers so they can handle these complex models.

2 Positioning and Pre - processing methods

To solve the positioning problem, we followed a novel approach based on two main technologies. Advanced Multi Body Dynamics Solver for the model kinematics in parallel with morphing algorithms.

The first step includes building a kinematic model of the human body that can predict the actual movement of the skeleton when positioning the limbs.

The second step is to find all the tissues affected by the movement and apply morphing algorithms on them, so they follow along and adapt at the same time to the new bone positions.

Based on the technologies mentioned, engineers are provided with a software tool that allows real time articulation and positioning of an HBM within an easy user interface. While the user just articulates the human model with the mouse in a most direct way, the biofidelic joint modelling guarantees realistic model movements and the generation of a ready-to-run model without the need of pre-simulation. All popular HBM's such as GHBMC, THUMS, SAFER and VIVA+ are supported and importantly for any solver that they are available, LS-DYNA, ESI VPS and RADIOSS. All the meta-data needed for the various HBM models are produced by BETA CAE Systems and are distributed along with the models.

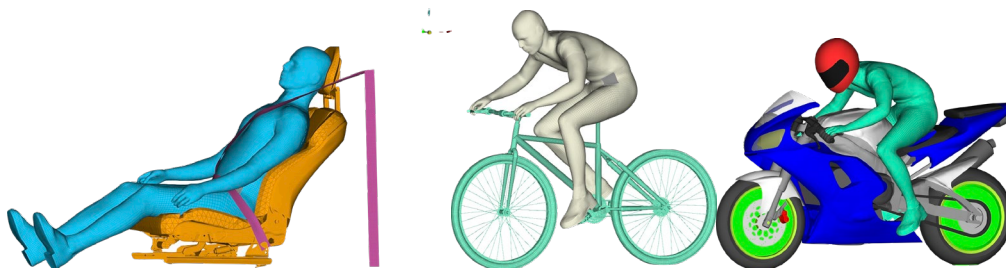


Fig.1: Positioning an HBM in various postures.

3 Vulnerable road users

Extending on vulnerable road users like cyclists and pedestrians was the next logical step of our development efforts. Starting either from the seated or the upright (pedestrian) posture it is possible to flex the spine so the model can move to a riding posture. Morphing of the internal organs in the abdomen results in a penetration free mesh.

To offer a complete solution to the analysts, we also developed a complementary tool that can be used to setup a bicycle for use with an HBM. Specifically, the tool can morph a bicycle model to different sizes and adapt the moving parts of a bicycle like saddle height, handlebar position and pedal position.

Thus, both the bicycle and the rider can be positioned on the desired position easily while robustness studies can be performed for different pedal or handlebar positions.

Various bike types (City, MTB, e-Bike) can be configured with the software.

4 Post-processing

On the post-processing side, running interactively or in batch mode, the META HBM tool automatically creates PPTX and PDF reports including videos and images of HBM's kinematics, strain contour plots, elements erosion identification, chest-bands deformations, and injury criteria calculations (Brain CSDM, Abdominal soft tissue organs SED, etc.).

Moreover, time history results can be extracted from the Occupant Injury Criteria tool. Injury criteria like HIC, BrIC, Nij, etc. are calculated. The extracted and calculated results can be compared to corresponding results of Anthropomorphic Test Devices (ATDs), while it is also easy to make comparisons between multiple HBMs simulation runs or between results from different solvers.

We have developed the software tools needed for the HBMs positioning and post-processing, offering the liberty to the engineers to perform the analysis they wish and giving them a transparent interface across all ATD and HBM models. In this presentation, all these exciting developments are demonstrated.

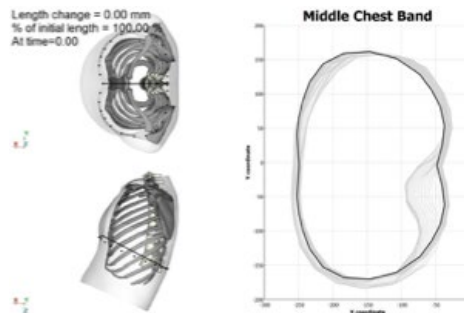


Fig.2: Post processing tools specifically developed for HBMs

5 Next Steps

We continue our research in many directions,

- Better kinematics and modelling of the human body joints especially in extremities.
- Morphing and mesh reconstruction in case of large deformations.
- Experimental studies of seated and riding postures so we can create a library of ready to use postures that are tested and validated.
- Use of morphing for creation of HBM variants, altering the BMI of an existing HBM.

6 Summary

BETA CAE Systems have been actively developing software tools in ANSA and META that let engineers use HBM models in an easy way both on the pre-processing and the post-processing side. There is currently support for almost all HBM models (GHBMC, THUMS, SAFER, VIVA+) both for LS-DYNA but also for ESI VPS and RADIOSS where applicable.

Moreover, we offer tools and integration not only for occupant loadcases (seat positioning, restraining etc), but also for cyclists (bicycle configuration and sizing), covering all possible needs.

7 Literature

- [1] GHBMC M50-O Version 5.1.1 User's Manual,2020, Elemance LLC
- [2] THUMS Version 6.1 Documentation, 2021, Toyota Motor Corporation

Virtual simulation of side sled testing

Jakub Prchal, Alžběta Kafková

TÜV SÜD Czech, Novodvorská 994/138,

1. Introduction

This work describes an advanced approach to sled testing, which combines virtual simulation and physical testing. Sled tests like every other component test can dramatically reduce the costs of development and help to test more setups than complete crash tests. Sled testing is a well-known testing method mainly for front-impact crashes. In those cases, sled-tests are common and have comparable results with crash tests. Side sled testing is more complex testing, mainly because of high intrusions into body-in-white. Because of that, there are problems with accuracy and repeatability of tests. There exists a lot of approaches for side testing methods mentioned by Chung et al.[1], Stein [2], Aekbote et al. [3], Miller II et al. [4], Owen [5], Aekbote et al. [6] and Chou et al. [7]. These attempts were side sled test experiments, where the intended deformations were obtained by the impact of the sled into either barrier or pole substituent. Later Lee et al. [8] came up with semi-controlled door intrusion, followed by Dix et al.[9], Lessley et al.[10], Kinoshita et al. [11], Liu et al.[12], Kinoshita et al.[13] and Janca et al.[14]. The solution described in this article uses two devices IST CSA Advanced Acceleration System, further in text referred to as catapult and ENCOPIM ALIS, further in the text referred to as ALIS. A combination of these two solutions and virtual simulations helps to accurately simulate all the types of standard side crash tests as IHS side barrier tests or UN/ECE 95, 135 and every non-standard test.

The goal of this article is to describe this methodology and show how can be the use of sled testing extended and how can be improved by virtual simulations. This article uses knowledge from the work of Jelinek J. [15],[16], but it examines the process from a different perspective and adds here new knowledge and trends for the next work.

2. Testing lab instrumentation

2.1 IST CSA Advanced Acceleration System (Figure 1.)

For a better understanding of the system, it is necessary to describe the devices used for the physical sled testing. The catapult is installed in the laboratory DYCOT_(Dynamic Component Testing) in Bezděčín near Mladá Boleslav. This device has the maximal force of 2.5 MN and can accelerate 1000kg object to 90g or 5000kg object to 35g. The maximal speed is 100km/h and the maximal gradient is 14 g/ms. This device has a repeatability of 0.5 km/h or 1g. This device is used to accelerate the whole ALIS system and the sled with the testing samples and necessary equipment for the test.



Figure 1. IST CSA Advanced Acceleration System

2.2 ALIS (Active Lateral Intrusion Simulation)

This paragraph describes the next device used for this sled test, which is called ALIS Figure 2. This device uses 3 pneumatic actuators controlled by hydrodynamic brakes which enable control of the actuators throughout the whole length of the stroke. Actuators are in two configurations 60 or 120 KN and the maximum stroke is 550 mm. Actuators are fully controlled during the whole stroke by PID regulation which can be set up for acceleration, velocity, displacement, or a combination of these attributes. This PID setup is individual for each new project and leads to great accuracy of the system.

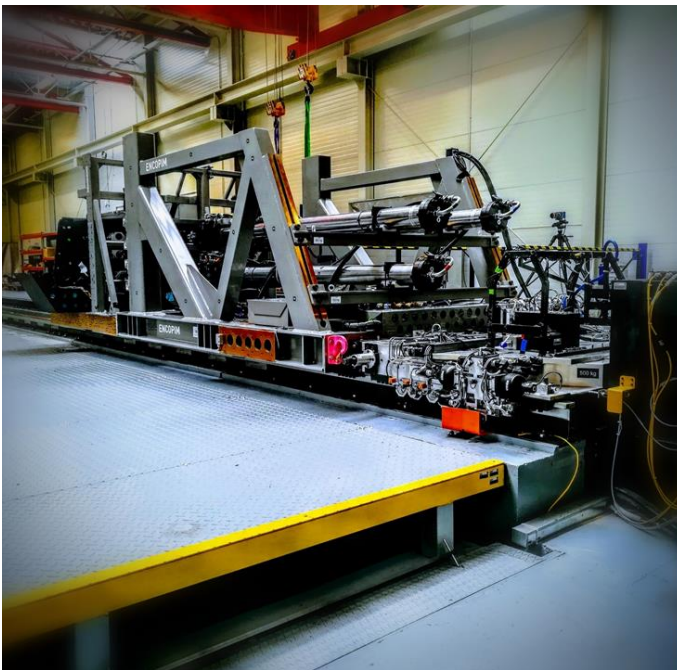


Figure 2. Active Lateral Intrusion Simulation (ALIS)

3. Methodology

2.1 Virtual simulation decomposition

This paragraph refers to the way, how to get an accurate representation of physical crash tests in the sled test environment. In the process of creating a very accurate model it is necessary to understand the base model of the full crash and decompose this model into smaller specific parts (Figure 3.). For each of these parts it is necessary to decide if it will be used or not. To control if moving these parts to the reduced model of sled test can't influence its functionality is also important in this process. Extremely sensitive are the rupture models, connection points, and simplified representations, for all these mentioned areas, it is better to use some type of the validation or to increase their control during whole validation of sled simulation.

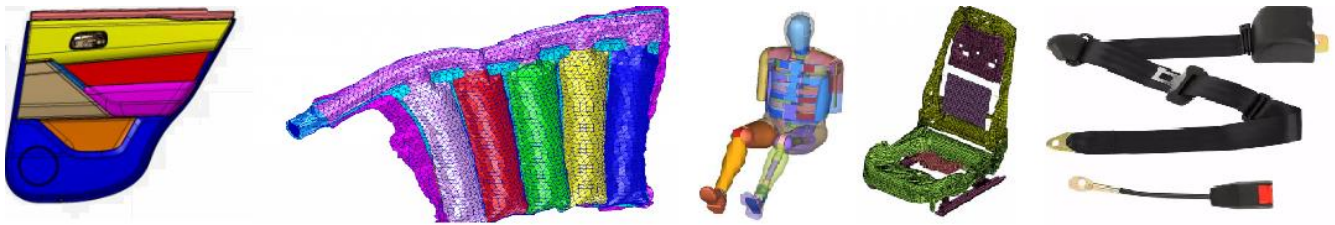


Figure 3. Decomposition of FE car model [17]

2.1 Virtual simulation validation

After decomposition of the simulation model, it is necessary to prepare a sled test tool, which is further referred to as an intrusion mechanism. Considering the deformation of the structure, dummy kinematics and bio-mechanical load, an original intrusion mechanism is prepared. This mechanism is the result of the sequences of simulations which combine original parts from the FE full crash model and newly designed TUV-SUD parts. All parts, deformation elements, joints and their position are also designed based on the simulations. This process is unique for every project and every issue which can occur during the development process of the car. Whole process is customized to get the best accuracy in the tested area. Figures 4.-5. demonstrate how the accuracy of the model changed during the process. After this process it is necessary to prepare the command pulses for the sled test and actuators. This process is iterative and can consist of an unspecified number of variables. In this process the validity of the simulation model is crucial. The final ALIS model can be accurate only if the base simulation is also accurate. To this process the real crash test data can be implemented, if they are available. This data improves the validity of results and predictability of the system during the physical testing stage.

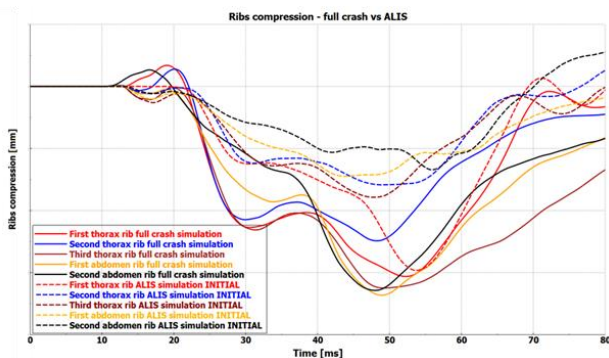


Figure 4. : Comparison of rib compression for full crash and sled simulation

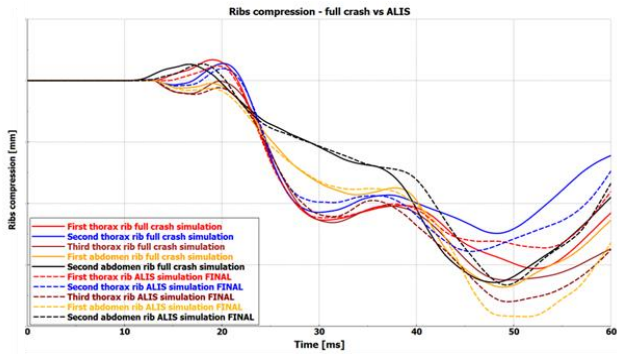


Figure 5. : Comparison of rib compression for full crash and final sled simulation

2.2 Design of Experiment (DoE)

To speed up the whole process, the DoE analyses can be implemented into it. However, it is necessary to choose the right responses, tune the system setup and choose the variables which will be used for system response improvement. As an example, the table of variables for the simulation with World Sid dummy (Table 1.) is added below. This method spares time, but it is also very sensitive to the independence and credibility of variables used in the system. The right setup of variables and responses can shorten the development stage of setup by weeks. However wrong usage can lead to a completely wrong setup.

ID	Type	Name	Component	Units
10061	1D el.	First thorax rib	Compression	mm
10062		Second thorax rib	Compression	mm
10063		Third thorax rib	Compression	mm
10064		First abdomen rib	Compression	mm
10065		Second abdomen rib	Compression	mm
10001	NODE	Head acc	Acceleration, velocity	mm ms ⁻² / mm ms ⁻¹
10002		T1 Lower neck acc	Acceleration, velocity	mm ms ⁻² / mm ms ⁻¹
10003		T4 first thorax acc	Acceleration, velocity	mm ms ⁻² / mm ms ⁻¹
10004		T12 second abdomen acc	Acceleration, velocity	mm ms ⁻² / mm ms ⁻¹
10005		Pelvis acc	Acceleration, velocity	mm ms ⁻² / mm ms ⁻¹

Table 1. List of responses

2.3 Physical testing

This paragraph describes the next stage in this testing process which is the physical stage. All the components are manufactured and installed on the sled and connected to the ALIS system. The control pulses for the sled and actuators are converted to the systems of the sled and ALIS. These systems are learned to perform these pulses. These test setups consist of intrusion mechanism, sensors, door and car trim parts, safety equipment, a seat and a test dummy (Figure 6.). The results from this test which consist of videos, bio-mechanical load, acceleration of structures, and results from 3D photogrammetry are recorded and validated with a simulation model. If the data from the physical crash test is available, it is possible to do more tests and adjust the test setup closer to these results. After the reference test, which results represent the deformation of the car at the required level, it is possible to change trim parts, seats, and restrain systems and evaluate the effect of these changes on the bio-mechanical load

and dummy kinematic. If the simulation models of changed components are available, validation of these models is also possible. Besides, it is possible to test how the bigger deformation influences the results of bio-mechanical load.



Figure 6. Complete ALIS test setup with all equipment (Courtesy of TÜV SÜD Czech and Škoda Auto)

2.4 Simulation Validity

One of the most important parts of every simulation is its correlation to real tests. Standardly every part which is included in the test is validated separately as the behavior of the whole system is unpredictable. The validity of every component is based on the correlation between the condition during validation and the condition of the test. Standardly the final validated ALIS sled test has a good correlation between the full crash test and sled tests (Figure 7.). The correlation of curves depends on the deploying space for airbags but also on the influence of the restraining system on the dummy and on exact interior intrusion. This correlation guarantees that every change in the ALIS simulation model will have similar consequences in the full-scale model. Other advantage of validation on the sled test model is that only the tested parts have not fully controlled deformation. The kinematics of the structure is described by accelerometers mounted on it, the sensors in the ALIS system and the deformation of the deformation elements which can be easily tested and described and make FE validation. Besides, dynamic 3D photogrammetry can be used on the dummy and trim parts which help to describe the tested area deformation. The sled tests enable to validate the bio-mechanical load, as well as the trim cracks in critical areas and the seat deformation.

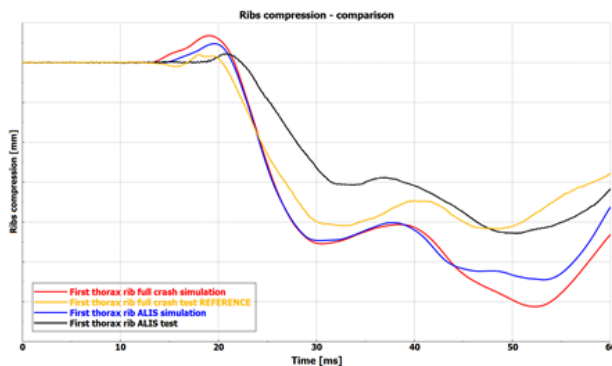


Figure 7. : Comparison of rib compression – first thorax (correlation between the simulation and real tests)

2.5 Out of position in sled test (OoP)

The sled tests can be also easily used for the performance of OoP tests. The high adjustability of construction helps to create special conditions for every position. Besides in the sled test, you can test the position which you are not able to implement to the car structure, such as moving and rotating seats in every direction and so on. In our study, we tested the dependency of a bio-mechanical load on seat position in the car. In the sled test simulation is possible to test the variety of seat positions without the long dummy repositioning and fitting of other restrain systems. For this study, the repositioning of seat in the X and Z direction and also the tilting of the backrest (Figure 8.) was used. For the evaluation of results, the DoE method was used. The aim of this study is to check if the system is safe for all seat positions.

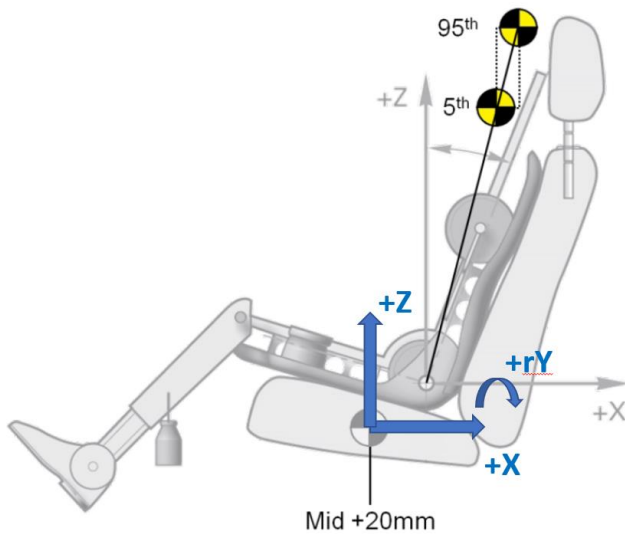


Figure 8. : Starting point and test matrix for OoP analyses [18]

3. Conclusion

It has been shown that the ALIS methodology has got sufficient accuracy between full crash test and sled test. Even though it is not possible to achieve the same conditions in sled test as in a full crash, accurate results for the critical areas can be still obtained. The focus area must be defined at the beginning of the project so that the project can obtain the required response and accuracy. The sled testing with the ALIS system has got a vast potential to be used in combination with full crash testing to reduce costs and gain maximum safety. It allows to get the assessment of initial restraint system performance very soon and hence speeds up the development process. The article describes the application of DoE in the validation process and also in the process of testing the robustness of the system. Because of good knowledge of the system the sled test is appropriate for validation of simulation models of the restraining system, trim parts and seat.

The variability of the system gives space for the next works focused on response curve matching or OoP testing.

References

- [1] Chung J. et al. „Development of a Sled-to-Sled Subsystem Side Impact Test Methodology“, SAE Paper No.970569
- [2] Stein D., „Apparatus and Method for Side Impact Testing“, SAE Paper No.970572
- [3] Aekbote K. et al. „A New Component Test Methodology Concept for Side Impact Simulation“, SAE Paper No.1999-01-0427
- [4] Miller II P. et al. „A Compact Sled System for Linear Impact, Pole Impact, and Side Impact Testing“, SAE Paper No.2002-01-0695
- [5] Owen G. „Demand Drivne Side Impact Restraint System Development Method“, 9th International LS-DYNA Users Conference 2006
- [6] Aekbote K. et al. „A Dynamic Sled-to-Sled Test Methodology for Simulating Dummy Responses in Side Impact“, SAE Paper No. 2007-01-0710
- [7] Chou C. et al. „A review of side impact component test methodologies“, International Journal of Vehicle Safety, Vol 2, Nos.1/2,2007, pp.141–184
- [8] Lee H. et al. „Simplified Side Impact Test Methodologies for Door Interior Trim Armrest in Automotive Vehicle“, SAE Paper No.2007-01-3722
- [9] Dix J. et al. „A Validated Oblique Pole Side Impact Sled Test Methodology“, SAE Paper No.2009-01-1433
- [10] Lessley D. et al. „Whole-Body Response to Pure Lateral Impact“, Stapp Car Crash Journal 54, Paper No.2010-22-0014, 2010, pp. 289-336
- [11] Kinoshita A. et al. „Development of a Side Impact Sled Test Method using Multiple Acutators, 22nd Enhanced Safety of Vehicle Conference 2011, Paper Number 11-0072
- [12] Liu Z. et al. „Study on One Kind of Test Method of Simplified Side Impact Using Sled Test“, Advanced Materials Research Vols. 301-303, 2011, pp 1249-1253
- [13] Kinoshita A. et al. „Development of Pole Side Impact Sled Test Method using Multiple Actuators for EuroNCAP“, SAE Paper No.2012-01-0095
- [14] Janca, S., Shanks, K., Brelin-Fornari, J., Tangirala, R. et al., „Side Impact Testing of the Near-Side, Rear Seat Occupant Using a Deceleration Sled“, SAE Technical Paper 2014-01-0547, 2014, doi:10.4271/2014-01-0547
- [15] Jelinek J., Růžička M. „New advanced methods in side crash testing“, MECCA: Journal of Middle European Construction and Design of Cars 2021; DOI: 10.14311/mecdc.2020.02.01
- [16] Jelinek J., Růžička M., Kafková A. „New methods in side sled crash testing“, International Journal of Crashworthiness; 2021, ID: 1904651 DOI:10.1080/13588265.2021.1904651
- [17] multicorpos, <http://multicorpos.com/portfolio-posts/dytran-en/>
- [18] EURO NCAP, Side Oblique Pole Test Protocol v7.1.2, <https://cdn.euroncap.com/media/67260/euro-ncap-pole-protocol-oblique-impact-v712.pdf>

Robustness Analysis of Passenger Airbag Out-of-Position Deployment using Ansys LS-DYNA and DIFFCRASH

Masahiro Okamura¹, Toru Ishizuka¹, Richard Taylor²

¹JSOL Corporation
²Arup

1 Introduction

In recent years, the demand for robustness in products has increased. Airbags are essential restraint devices that are indispensable for crash safety in automobiles. However, various factors affect their deployment, and deployment repeatability is still an issue^[1], especially in the out-of-position case where contact with the occupant occurs during deployment.

2 The target load case

In this study, an Out-of-Position case of a child dummy was used as an example. The model is based on the 2012 Toyota Camry model developed by the Center for Collision Safety and Analysis^[2]. The vehicle model was cut down to the front passenger side occupant compartment. The body and the seat surface were made rigid to save computation time. The dummy model was positioned using ARUP-PRIMER dummy positioning as shown in Fig. 1.

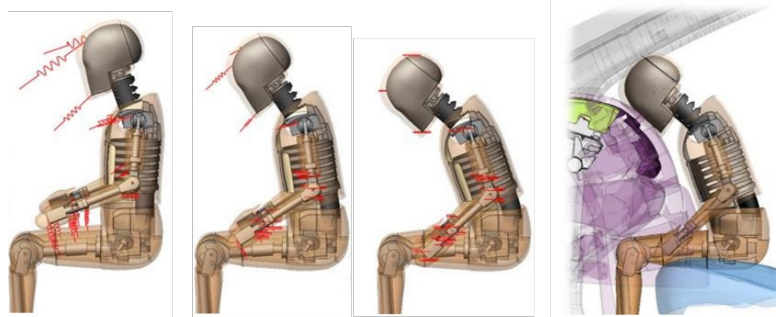


Fig.1: Dummy positioning and load case set up for the OoP simulation

3 Robustness and sensitivity analyses using DIFFCRASH

In this study, a quasi-Monte-Carlo simulation was conducted using LS-OPT. In order to take into account the physical scatter and conduct a sensitivity analysis, the friction between the airbag and dummy and the dummy position was varied. The result was processed with principal component analysis using DIFFCRASH^{[1] [3]}. Fig. 2 shows the PCA results of the deformation and travel of the dummy head part processed with DIFFCRASH. Fig. 2(a) indicates that the 1st mode is dominant in this case. Each plot in Fig. 2(b) represents a single simulation result, and two major clusters and several outliers are found on the plot.

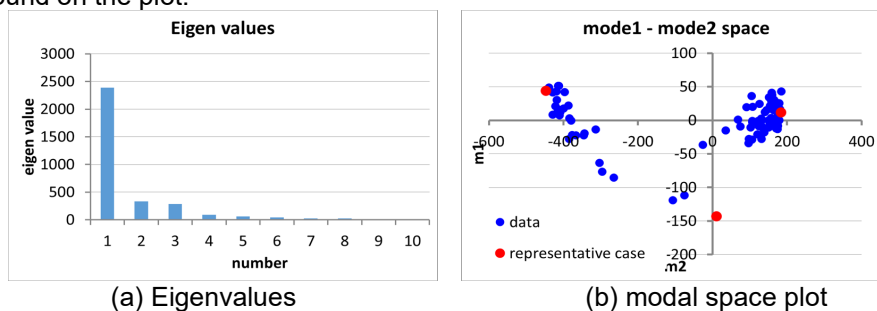


Fig.2: Load case set up for the study

A sensitivity analysis was conducted by regression analysis between input scatters and the coordinate of the plots on the modal space. The regression analysis showed that the lower position and lower friction coefficient induce the left mode, and the behavior is stable. However, a slight change in position and higher friction coefficient makes the behavior unstable, and the mode starts to bifurcate.

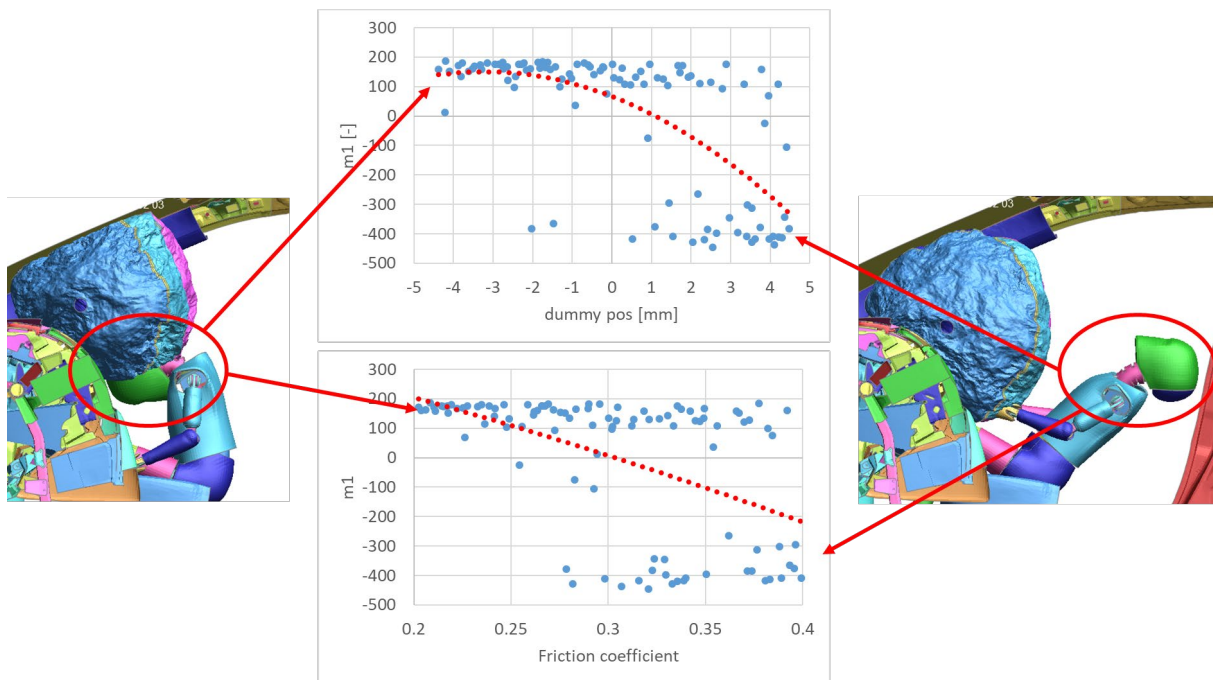


Fig.3: Regression analysis result between dummy position and the 1st mode

4 Summary

In this paper, results of multiple Out of Position cases with different friction levels and other influencing factors such as dummy positions were processed with principal component analysis and regression analysis. As a result, the relationship between the main modes of behavior and their influencing factors was visualized. In case the behavior is unstable and the system's robustness is low, the chance of unexpected results in physical tests will increase, so it is essential to detect robustness issues in the early stage of airbag system development with helps from effective and easy-to-use CAE tools such as DIFFCRASH.

5 Acknowledgment

The authors would like to acknowledge technical support and use of the DIFFCRASH license for this study to Mr. Dominik Borsotto and Mr. Clemens-August Thole of SIDACT GmbH.

6 Literature

- [1] R. Brown, M. Bloomfield, C. Thole, L. Nikitina, "Analysis of the Scatter of a Deploying Airbag", 12th International LS-DYNA® Users Conference, 2012
- [2] D. Marzougui, et al., "Development & Validation of a Finite Element Model for a Mid-Sized Passenger Sedan", 13th LS-DYNA Users Conference, 2014
- [3] D. Borsotto et al.: "Improving robustness of Chevrolet Silverado with exemplary design adaptations based on identified scatter sources", 10th European LS-DYNA Conference, 2015

Modeling terminal ballistics of 25x137 mm M791 APDS-T Ammunition

Mert Can Simsek¹, Dr. Murat Büyük²

¹Nurol Teknoloji, Turkiye

²Middle East Technical University, Turkiye

1 Abstract

Testing terminal ballistic events are both challenging and expensive. The work needed exponentially increases as the threat i.e., kinetic energy of ammunition gets bigger, thus a numerical approach is inevitable. The aim of this study is to obtain a reliable numerical terminal ballistics model of 25x137 mm M791 APDS-T via LS-DYNA. The numerical model is validated with previous work which can be found in literature and used to find ballistic limits for armor configurations to achieve NATO STANAG 4569 Level 5 protection. For different angles of impact, configurations with different areal weights are established. Material model parameters from the literature are employed, and numerical results are discussed vis-à-vis test results.

2 Introduction

Ballistic protection levels of armored vehicles are specified in the widely used NATO STANAG 4569 standard. STANAG 4569 defines 6 levels of protection against different threats. Level 5 protection requires protection against 25x137 mm ammunition (PMB 090 and PMB 073). In this study, PMB 073 version of the ammunition is investigated against different armor configurations consisting of ceramics, ballistic composites and armor steel.

Terminal ballistics of 25 x 137 mm APDS-T (PMB 073) ammunition against different armor steels and ceramics was previously investigated in [1] and [2] by Weiss et.al. Numerical model of 25 x 137 mm APDS-T used in this study is validated for the critical ricochet angles found in mentioned studies. Experiments were conducted for two different armor configurations with different critical impact angles, which are identified by the help of validated numerical models.

3 Numerical Modelling

25x137 mm APDS-T ammunition consists of a WHA penetrator core and a mild steel windshield as illustrated in Figure 1. The core and windshield are discretized with fully integrated hexahedral elements and 1-point nodal pressure tetrahedron elements, respectively. The edge length of the elements vary between 0.5 mm to 1.0 mm. Material models used for WHA and mild steel are modified Zerilli Armstrong with Gruneisen equation of state.

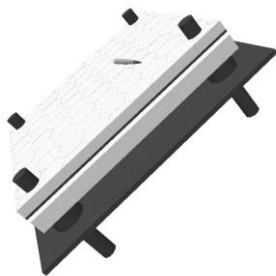


Fig.1: Numerical model of armor target

Figure 2 illustrates the armor with respect to the ammunition. The elements used in 500 BHN armor steel are also fully integrated hexahedral elements and the material model is Johnson Cook with Gruneisen equation of state. The contact algorithm used in all cases is ERODING_SINGLE_SURFACE with SOFT option 2. The material model of ballistic composites are MAT_221_ORTHOTROPIC_SIMPLIFIED_DAMAGE while ceramics are modeled with MAT_110_JOHNSON_HOLMQUIST_CERAMICS.



Fig.2: Numerical model of ammunition

4 Validation

Weiss et.al. [1] has found that for 25 mm APDS-T ammunition, the critical ricochet angle against 500 BHN armor steel is 81°. The ammunition model was tested to hold this condition. Figure 2(a) illustrates the initial stage of the setup, Figure 2(b) shows the ricochet as a result and Figure 2(c) illustrates the tests reported in [1]. It is found that the model shows good agreement with the test result.

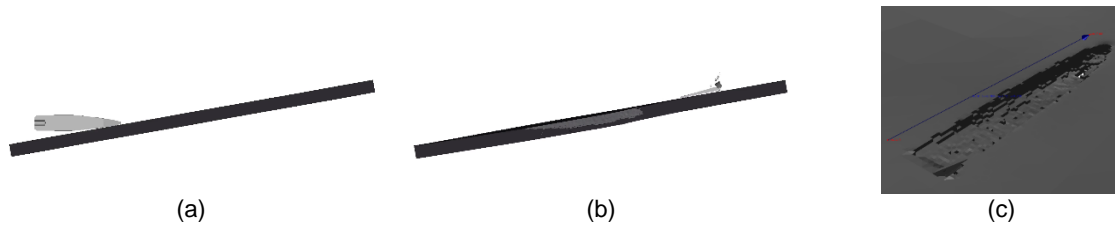


Fig.4: Validation of the model: (a) Initial stage, (b) Final stage, (c) Resultant deformation on HHS

Also, as stated in the [3] a complete penetration against 25 mm thick 500 BHN armor steel with 60° impact angle and a partial penetration result against 40 mm thick 500 BHN armor steel with the same impact angle was accomplished by the models as illustrated by Figures 3(a)-(b) and 3(c)-(d) for 40mm and 25mm respectively.

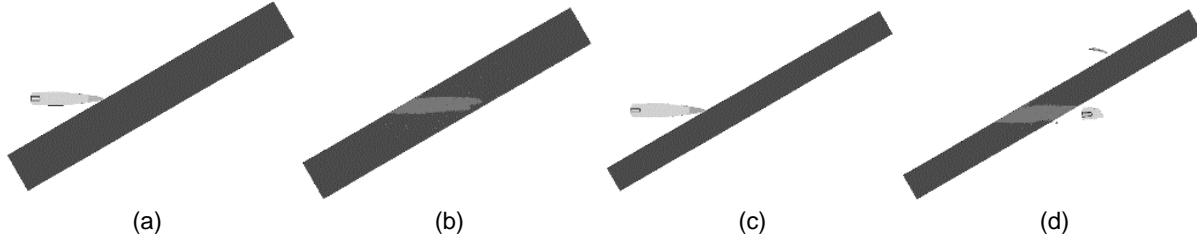


Fig.3: Validation of the numerical model. (a) Initial stage-40mm, (b) Final stage-40mm, (c) Initial stage-25mm and (d) Final stage-25mm.

5 Experiment

Two different armor configurations with different areal weights were tested in accordance with NATO STANAG 4569. The angle of impact was determined via critical impact angles found by numerical models. The target was 30 m away from the muzzle and a Doppler radar was utilized to measure impact velocity. The results are listed in Table 1.



Fig.5: Numerical model of ammunition

6 Comparison

The numerical models are in full agreement with the test results in terms of penetration ricochet characteristic behavior. It can be seen in Figure 4 that the deformation on ballistic composites and deformation on HHS are extremely similar with the experimental results.

Target	Impact Angle	Add-on Armor Areal Weight (kg/m ²)	Result	Model
Configuration - 1	55°	150	Ricochet	Ricochet
Configuration - 2	45°	180	Ricochet	Ricochet

Table 1: Test results compared with Numerical Model

7 Summary

The highly destructive ballistic test of 25x137 APDS-T ammunition was accurately simulated with LS-DYNA. Number of tests were significantly reduced with numerical models and a framework to achieve an optimal protection design was established. It was also shown that by using the add-on armor solutions, the 81° critical impact angle of 10 mm thick 500BHN armor steel can be improved up to 45° with minimal additional areal weight.

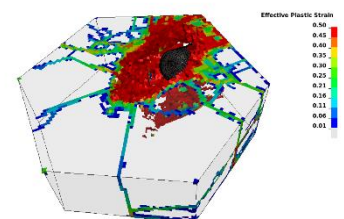


Fig.6: Plastic strain field during impact on ceramics

8 References

- [1] Weiss, A., Borenstein, A., Paris, V., Ravid, M., & Shapira, N. (2019). Evaluation of Critical Ricochet Angles for 25mm APDS-T Projectile on Metallic Targets - Modeling and Verification. *2019 15Th Hypervelocity Impact Symposium*. doi: 10.1115/hvis2019-069
- [2] WEISS, A., BORENSTEIN, A., STAN, G., RAVID, M., & SHAPIRA, N. (2017). Ballistic Performance of Ceramic Targets against 25mm APDS-T Projectile. *30th International Symposium on Ballistics*. doi: 10.12783/ballistics2017/16975
- [3] ATK Medium Caliber Ammunition Manual - Release to Public Domain- 04-S-3025/A1 — 108124

The use of blast load simulation to manage risks.

A. Sean Duvall¹, Jon Squire²

¹Nuclear Transport Solutions (NTS)

²Sellafield Ltd (SL)

1 Introduction

UK Nuclear Site License companies have a responsibility to manage the risk of deliberate acts of sabotage across their facilities. In the absence of engineering data these risks are often managed through the use of personnel.

The Nuclear Decommissioning Authority (NDA), as the parent organisation, has initiated a series of tests designed to understand the behaviour of on-site transport packages against an explosive device.

In order to improve the effectiveness of the tests, LSDYNA is used to predict likely outcomes. The physical tests are then used to validate the modelling.

This presentation demonstrates the approaches used, the current state of validation achieved and the likely impact on the testing.

2 Background

A series of tests are currently underway in the UK where a range of nuclear transport packages and internal transport containers are being subjected to explosive blast loads. These range from small, single walled cans to items the size of a large oil drum. Further testing including items within an ISO container are planned. These transport packages are expensive to manufacture, therefore testing should be optimized to give useful information. It is pointless to completely obliterate an item, instead the tests should give information that can be measured and quantified. This is an ideal situation where finite element analysis can be used to assist in and drive some of the testing.

A set of finite element analyses, using LSDYNA, were completed in parallel to the initial testing.

3 Analysis approach

Initial investigations of the multi-layer construction of the transport packages and the large volumes involved showed that the ideal choice for analysis is using the particle blast keywords; ***DEFINE_PARTICLE_BLAST** and ***DEFINE_PBLAST_GEOMETRY**. These provide a sensible runtime, compared to ALE, and a more reliable result compared to ***LOAD_BLAST**. As a starting point, strain rate enhancement of the materials was not used and only simple effective plastic stain based failure criteria were applied.

4 Analysis results

One of the key items being tested is the 4085 Safkeg. This consists of a containment vessel (CV) surrounded by an aluminium finned component within a stainless steel outer shell. This is shown diagrammatically in Figure 1.

The initial tests were modelled in parallel with the testing. These included an explosive charge at the base of a Safkeg and one on top of the Safkeg. The results from these analyses are shown in Figure 2.

5 Testing results

The results from the testing of an explosive charge placed at the side or on top of the Safkeg are shown in Figure 3. The general agreement, with focus on the CV deformation, is very good. It is clear that the CV is deforming in a similar way with failure predicted in a similar position. The analyses assumed that there was no contents, which will add stiffness to the CV and reduce deformation.

It was clear from these analysis results that there was sufficient confidence in the approach to explore it further and utilise it to guide further testing.

6 Future development

It is now necessary to more accurately model material failure and create finite element representations of the contents. There are also a number of variables to explore, such as the number of particles

required, how to remove “air” particles from within solids, which can lead to undesirable deformation, and how to transfer to rigid bodies for final projectile trajectories.

7 Summary

In using the particle blast modelling approach within LSDYNA, we have gained sufficient confidence in the technique that we can now use it to design experiments and test various placements that inform the next tests. This will save money and make our tests more effective.

8 Figures and Tables

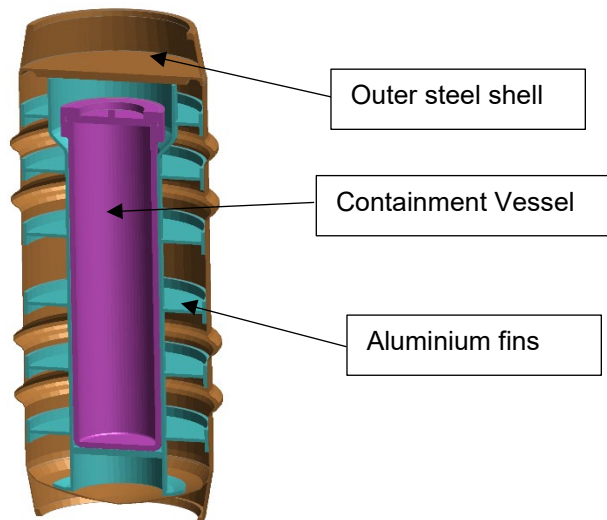


Figure 1: Diagram of 4085 Safkeg.

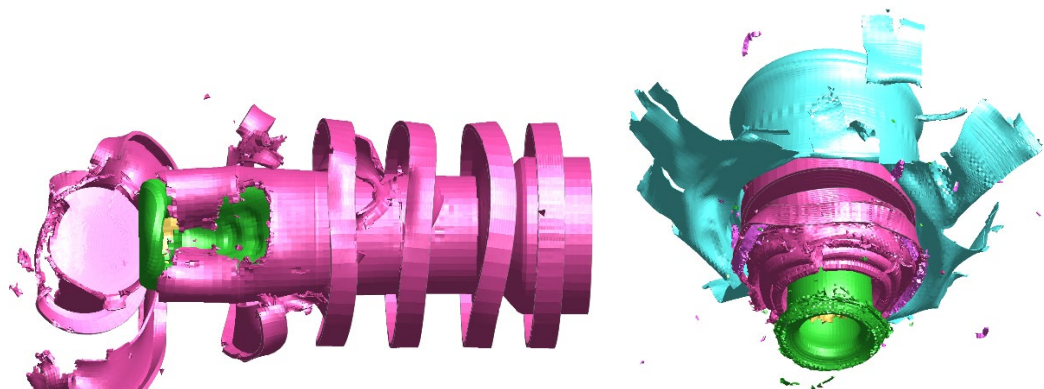


Figure 2: Analysis results



Figure 3: Results from two of the 4085 tests

Large-scale ALE and SALE LS-DYNA simulation methods exemplified by blast scenarios in a partially collapsed rock embedded facility

Raphael Heiniger¹, Bernd Hochholdingner¹, David Schröder¹, François Ubertini²

¹DYNAmore Swiss GmbH
²Dynamic Phenomena GmbH

1 Abstract

In the night from 19th to 20th of December 1947 a fire outbreak in a rock embedded Swiss army ammunition storage facility caused one of the largest artificial non-nuclear explosions. At this time, probably about 7000 tons of ammunition were stored in the facility and for two days there were repeatedly small and large detonations. The railroad tunnel, which was used for logistics, collapsed almost completely. A rockfall of about 240'000 m³ occurred and the blast event killed nine people as well as livestock. Some houses were severely damaged or destroyed. To this day it is unclear how much ammunition remnants are still buried in the partially collapsed facility and in the debris cone. The probability for a smaller explosion with about one ton of trinitrotoluene (TNT) is estimated at 300 years [1]. The Swiss government plans to completely clear the ammunition remnants starting in 2030, at an estimated cost of about 1.5 billion Swiss francs [2].

Simulation models and scale tests are used to assess the effects of explosion scenarios on the surrounding rock, infrastructure, and pressures inside the facility. Two-dimensional (2D) simulations with associated scaled real tests provide good matching results. However, in the 2D simulations, the complex geology and topology must be greatly simplified. To check the admissibility of the simplifications, a three-dimensional (3D) simulation is set up (see Fig. 1), which provides a better representation of the real geometric and geological conditions.

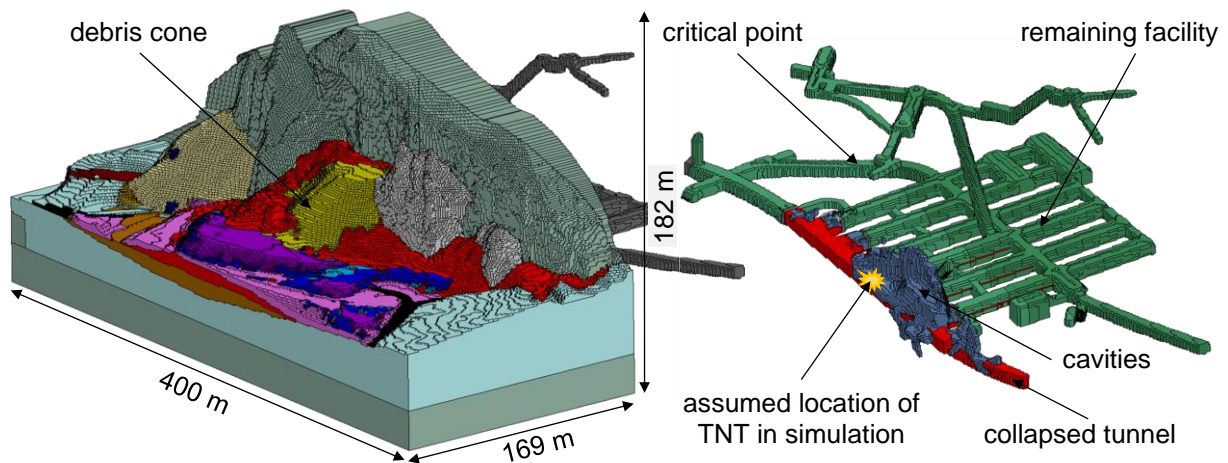


Fig. 1: 3D finite element mesh of the geology (left) and the facility (green) with the cavities resulting from the collapse (blue) and collapsed railroad tunnel (red) (right).

A voxel model on a one-meter grid with 19 different rock fractions serves as the basis for the geometry and the distribution of the geological fractions. Furthermore, point clouds from laser scans are used to refine the geometry in the collapsed areas. The intact areas of the facility are provided in Wavefront formatted files, which in turn are based on survey data and as-built drawings. LS-PrePost, ANSA and Python are used to process the geometry data into solid elements.

The different rock types are merged into three material types using a `*MAT_SOIL_AND_FOAM` material card for each type. Two material cards represent cohesive rock of low and medium strength and a third one non-cohesive boulder debris type material. The equation of state (EOS) `*EOS_JWL` in combination with `*MAT_HIGH_EXPLOSIVE_BURN` is used for the TNT. The air is modelled with `*MAT_NULL` and

*EOS_IDEAL_GAS [3]. A slip boundary condition is applied to each free segment. To obtain a realistic initial lithostatic stress state, the transient phase in which the explosive charge is ignited is preceded by a dynamic relaxation phase where the gravity is gradually applied.

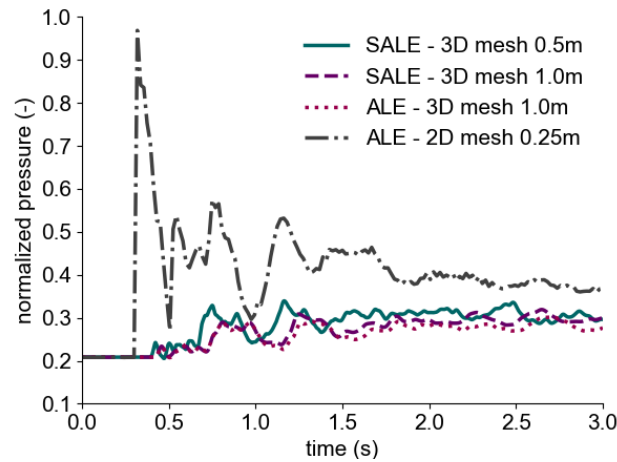


Fig.2: Representative normalized pressure at a critical point (see Fig. 1) in the facility.

The simulations are carried out with the Arbitrary-Lagrangian-Eulerian (ALE) solver within LS-DYNA and pressures on critical points are compared with the 2D simulations provided by Dynamic Phenomena GmbH. Additionally, a structured ALE (SALE) model is created and used to compare both methodologies in terms of results and performance. To identify mesh dependencies the SALE refining capabilities are used to bisect element edge length to 0.5 meter.

Solver type	Element length (m)	Number of solid elements (-)	Number of cycles (-)	Elapsed computation time			
				Initialization (h)	Dynamic relaxation phase (h)	Transient phase (h)	Total (h)
3D ALE	1.0	8390945	67262	0.05	5.14	5.93	11.13
3D SALE	1.0	8262885	57782	0.48	2.90	2.90	6.27
3D SALE	0.5	66374282	115999	2.91	41.60	40.81	85.32

Table 1: Computation times on three cluster nodes with totally 144 processors (2.8 GHz AMD EPYC 7402 24-Core) and 792GB memory using LS-DYNA R14.0 double precision version.

All 3D models show a significantly lower pressure at a critical point in the facility than the 2D model (see Fig. 2). This is caused by considering the rock embedding of the facility, an intermediate floor and concrete walls inside the facility as well as the additional large air-filled cavities which can only be represented in the 3D calculation. Comparing the same pressure between the ALE and SALE model with same mesh size show a good agreement. The SALE model requires only about 56% of the total calculation time (see Table 1) compared to the ALE model with similar element number, which highlights the advantage of the SALE solver. With the SALE capabilities the model can be refined easily which results in a larger model with 66.3 million solid elements. Pressures and velocities studied show very similar characteristics within all 3D models. Hence the coarser mesh can be considered sufficiently fine for the evaluations in this study. The large model requires twice as many cycles due to the halved critical time step size. Taking that into account it is approximately 12% more efficient than the small model.

2 Literature

- [1] Expertengruppe Risikoanalyse, "Risikoanalyse Schlussbericht", https://www.vbs.admin.ch/content/vbs-internet/de/umwelt/umweltschutz/mitholz/_jcr_content/infotabs/items/dokumente/tabPar/accordion/accordionItems/expertenberichte/accordionPar/downloadlist/downloadItems/56_1540460826779.download/180927-Risk-Safety-Expert.pdf, [Online] 2018.
- [2] Generalsekretariat VBS, "Sachstandbericht 03/2022", <https://www.vbs.admin.ch/content/vbs-internet/de/umwelt/umweltschutz/mitholz.download/vbs-internet/de/documents/raumundumwelt/mitholz/Sachstandbericht-03-2022-Mitholz-d.pdf>, [Online] 2022.
- [3] Livermore Software Technology (LST), an ANSYS Company: "LS-DYNA User's Manual, Vol. II – Material Models", 2022.

Simulation of Shock Transient Analysis on Wabtec Diesel Engines for Naval Vessels

Prabhakaran Selvaraj, Dennis Shea - Wabtec Corporation.

1 Overview

Naval vessels in military applications are under constant threat from underwater mines. Underwater mines may cause “near-miss” explosions which may be characterized as a high-pressure wave that hits a naval vessel, potentially causing severe damage to critical components on the vessels. Though these near-miss explosions may not cause any serious damage to the vessel’s structure, damage to critical equipment may debilitate the vessel’s ability to move from the danger zone. This led to the implementation of rigorous shock test procedures for all vessels in the US subject to **MIL-DTL-901 E**.

Wabtec Marine Engines have been evaluated for use in Naval vessels in collaboration with other industry leaders. A principal requirement for the engines is to prove that they can continue to operate after a near-to-ship explosion (underwater mine). The engine should be in functional state to operate the vessel to move away from the critical zone after the impact.

A Transient Shock analysis in LS-DYNA has been done to assess the engine’s ability to sustain a barge shock test. Barge testing is a scaled down version of a Full Ship Shock Test (FSST), which is expensive and a long lead time effort. The engine system and engine components were evaluated through LS-DYNA simulation before the test to identify and reduce the risks during the physical test.

2 Keywords

Marine Diesel Engines, NVR, Barge Test, Transient Shock, MIL-DTL-901D/E.

3 Process Flow Chart”

The main objective of this analysis is to get the engines ready for the barge test / shock qualification physical test. Overall system configuration and the mount locations are given in Fig.1: A simple process flow chart of entire project, used for a Wabtec Engine is given below in Fig.2: This paper explains in detail parts 3 and 4 of the flow chart, which is executed using LS-DYNA simulation software. A similar exercise can be followed for all Wabtec engine variants.

4 LS-DYNA version and Hardware

Pre and Postprocessing: LS Prepost V4.8
Solver: LS Solver R11.2.0

Intel Xeon Platinum processors of 2.1GHz with 1TB RAM
dp_mpp - double precision / multiprocessor executable
96 cores for each run.
5 to 7 days were solver time to complete each run

5 Explanation of Inputs

- A simplified analysis considering engine and alternator as INERTIA elements was done initially before running the complete 3D engine model simulation. This is only to develop the full model stagewise as the capability is being developed.
- Reused the existing engine model from Ansys and converted to LS-DYNA formulation and coupled with the baseframe and alternator.
- Combination of shell, solid, and inertia elements were used to develop the complete system.
- Fully integrated shell & 10-noded tetra solid elements were used.

- MAT024- Piecewise Linear Plasticity material model and MAT001 – Elastic material model were applied for the different components of the model except High Deformation Mounts (HDM).
- 25+ pieces of equipment mounted on the engine were considered in the simulation with 3D solid elements at appropriate mounting locations: either using merged nodes approach or “TIED Surface to Surface” contacts
- Entire system mass rollup matched with DYNA model - Missing masses like wire harnessing, bolt, nuts etc., were added at the CG of the respective part connected using CNRB
- Modal Analysis of the entire system is done in LS-DYNA itself, to extract the fundamental rigid body modes of the system. With the entire system being placed on high deformation isolator mounts, it is critical to understand the modes and to verify the model inputs.
- Dynamic Relaxation is activated in implicit analysis, to preload the model with 1g self-weight, before applying the actual shock impulse transient loads.
- DISCRETE BEAM Elements were used to simulate the HDM along with MAT067 – NONLINEAR ELASTIC DISCRETE BEAM
- A preliminary 1D calculation helps to choose the appropriate mount - providing stiffness characteristics, position and # of mounts, which is fully validated using the transient shock simulation.
- A total of 16 mounts - 8 on each side of the baseframe is considered based on the preliminary 1D tool calculations, shown in Fig.1:
- Normalized stiffness curves of the isolator mounts in all three directions are shown in Fig.3:
- Mount section definition and material definition in Dyna is shown in Fig.4:
- Input velocity impulse in vertical and athwartship directions were given together at the bottom of the isolator mounts as BOUNDARY PRESCRIBED MOTION SET. A normalized view of the shock pulse used in the analysis is shown in Fig.5:
- Impact of the secondary and tertiary motion of the underwater explosion is not considered in this simulation.

6 Results

- Compression due to preload was calculated from the implicit analysis with 1g self-weight as the preload.
- Transient shock analysis was done with compressed state as initial position of the isolators – Final relative deformation of the isolators due to shock impulse in both compression and extension is calculated from transient results.
- Relative deformation value was used to evaluate the HDM's capability.
- A comprehensive and representative table of deformation results is given in Table 1:
- Considering the vertical shock being the dominant load, the peak deformation and acceleration response was expected in the vertical (z) direction.
- Vertical deformation plots from the transient shock analysis are shown in Fig.6:, with the actual deformation scale removed due to IP issues.
- Fig.7: provides the vertical deformation values against time, at the top and bottom of the HDMs along with the relative deformation - calculated directly in LS prePost.
- Fig.8: shows the acceleration response at all four engine mounting feet that gets transferred into the engine due to the shock impulse applied at the mount bottom nodes.
- Fig.9:and Fig.10:show the vertical acceleration response at Engine CG and the corresponding Shock Response Spectrum (SRS) in frequency domain, calculated from LS-dyna output results.
- Such a response spectrum was developed for each critical component mounted on the engine, at their respective mounting locations. The SRS developed from Dyna output helps in understanding at what frequency range these sub-systems will see what level of “g” loads and displacements.
- Fig.11: shows the plastic strain over time at some of the critical points on the engine.
- With these outputs, a risk matrix was developed for all the equipment that are mounted on the engine to identify as low, medium and high risk equipment. Medium and high risk equipment were considered for further detailed study.
- With the current study completed for one of the Wabtec engine variant shows that the HDMs chosen for this application is capable to handle the shock input chosen and reduce the shock transferred to engine significantly.

7 Figures and Tables

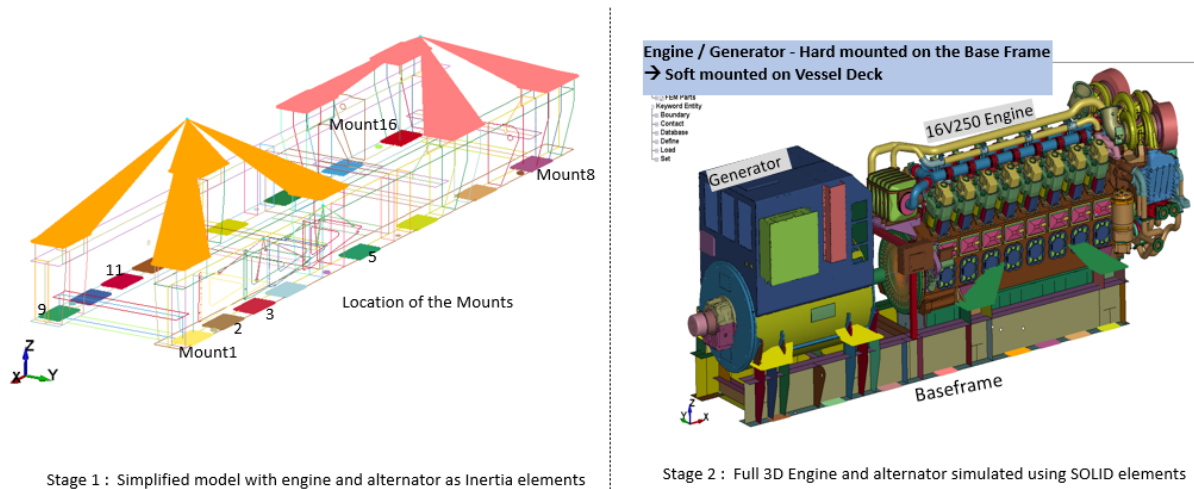


Fig.1: Wabtec Marine Engine Configuration along with Supplier's Baseframe and HDM

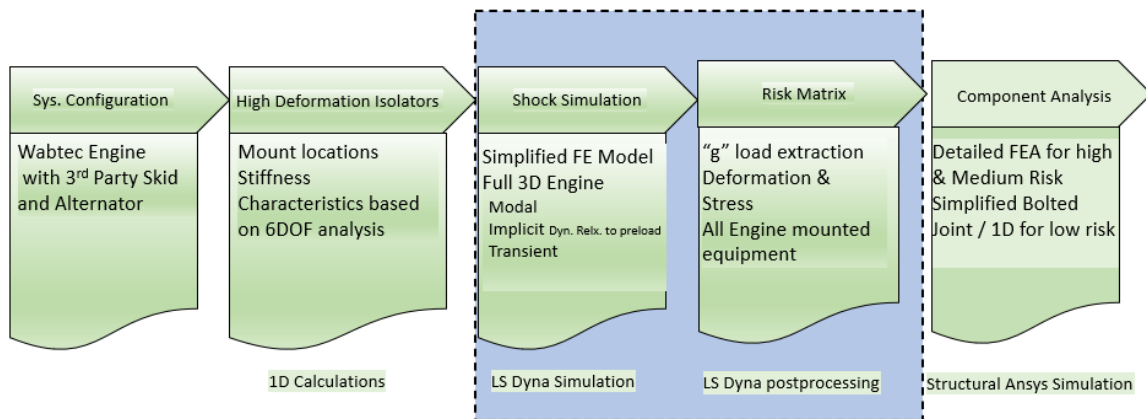


Fig.2: Process flow chart: Part 3 and 4 includes the simulations using LS-DYNA

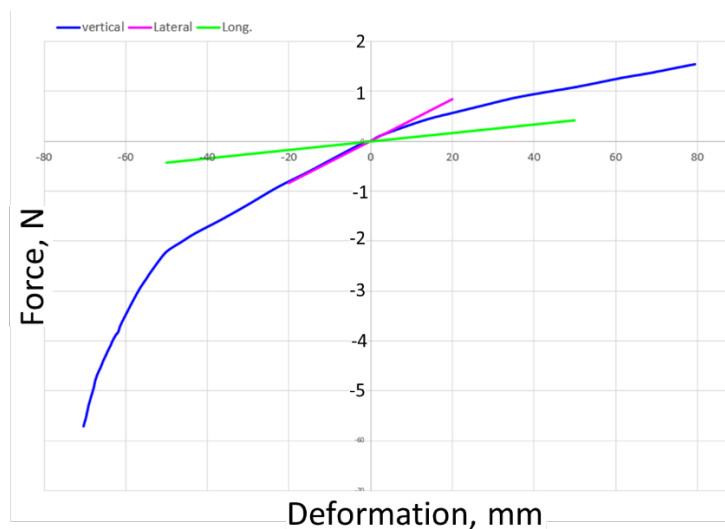


Fig.3: Normalized stiffness curves of the high deformation mounts used in simulation

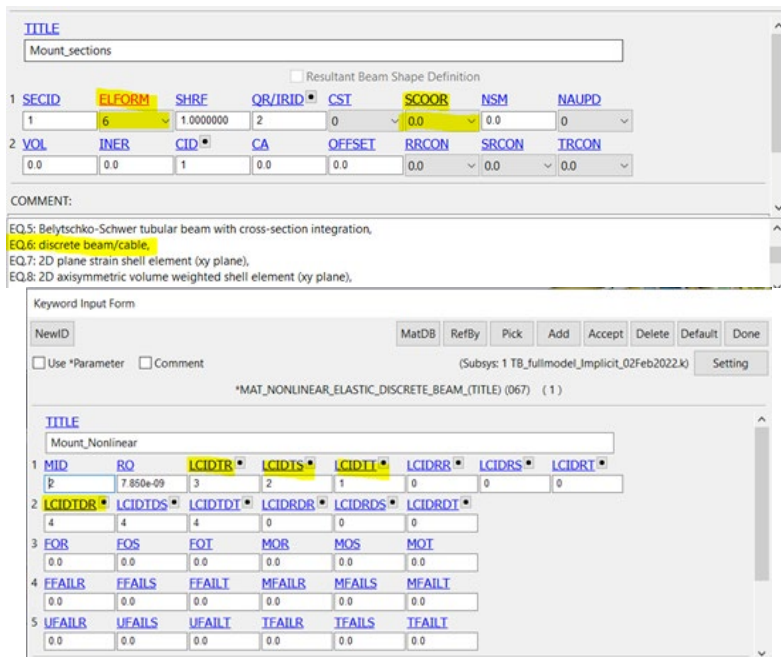


Fig.4: HDM: section definition and material model in LS-DYNA

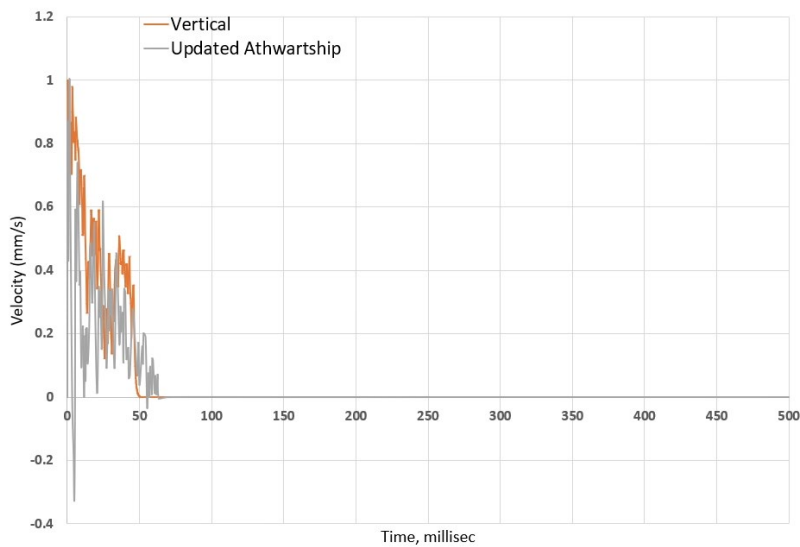
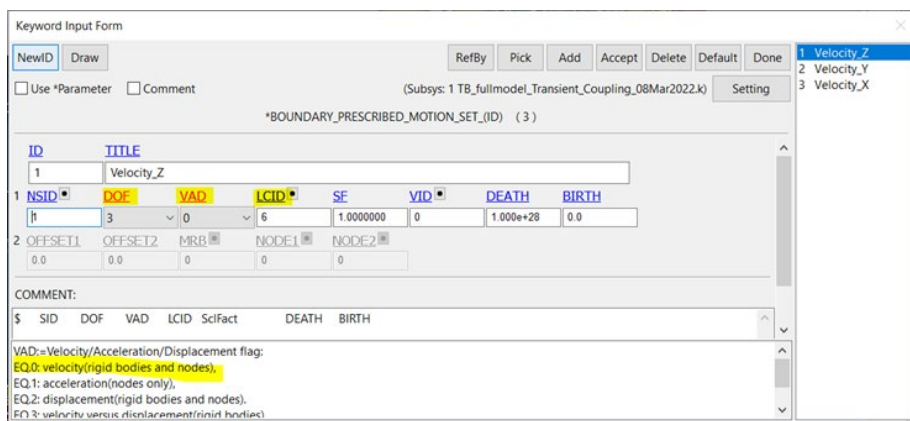
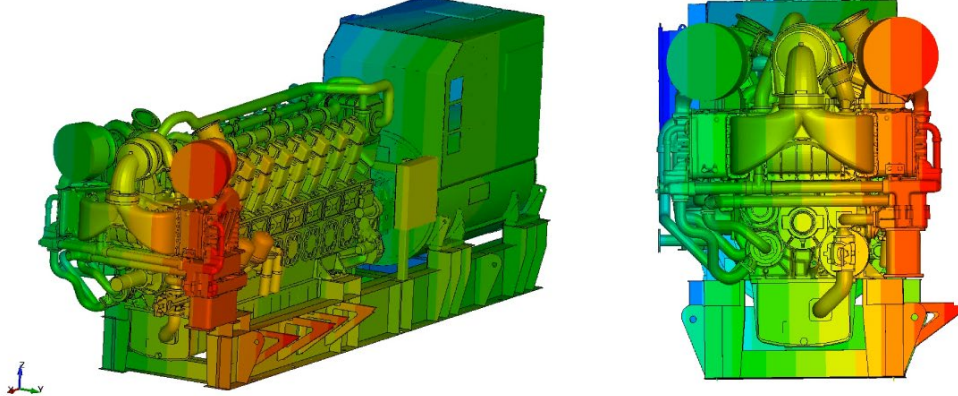


Fig.5: Normalized view of the shock impulse used in LS-DYNA

Fullmodel 16V250 LCSYS DynStf 10.5Dmp Trelleborg - Transient

Z - Displacement, mm- Animation contour



Deformation response of the system for 750ms for the shock impulse given for 50ms

Fig. 6: Z-deformation contours snapshots of the system at 100ms

Z Deformation @ one of the mount

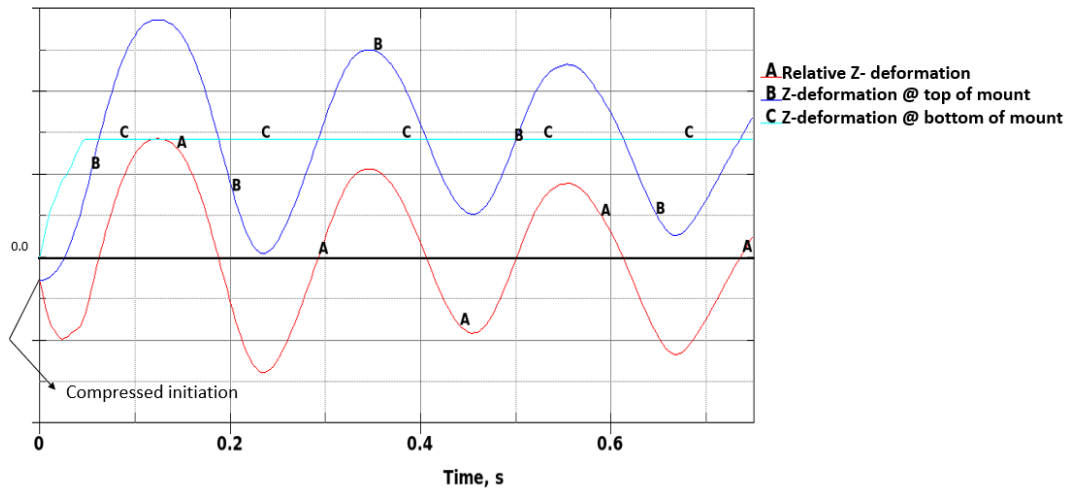


Fig. 7: Deformation at top and bottom node of HDM / Relative Deformation Vs Time

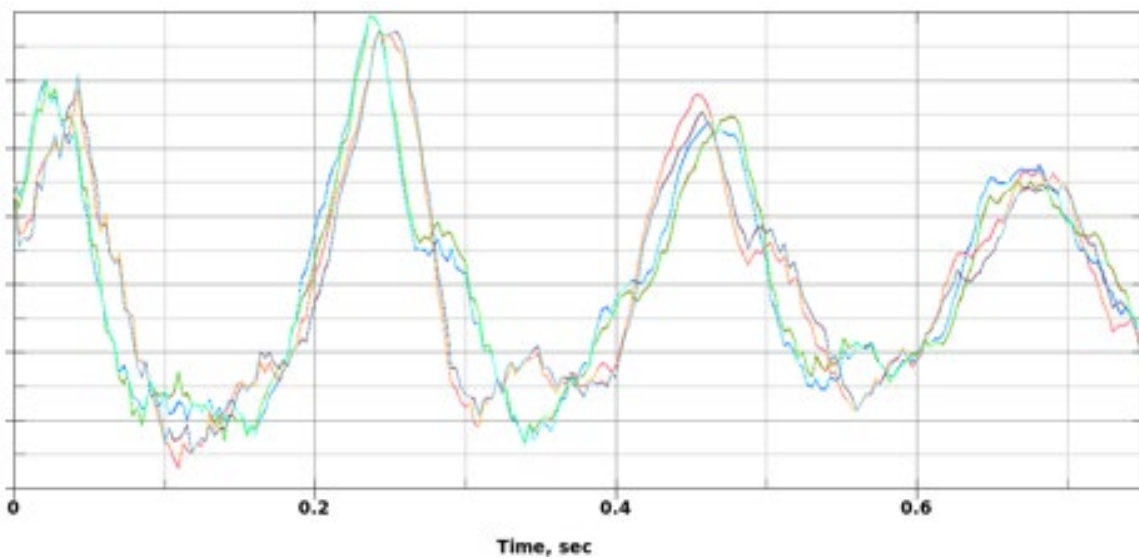


Fig. 8: Z-Acceleration (g, mm/s²) response at 4 Engine feet Vs Time

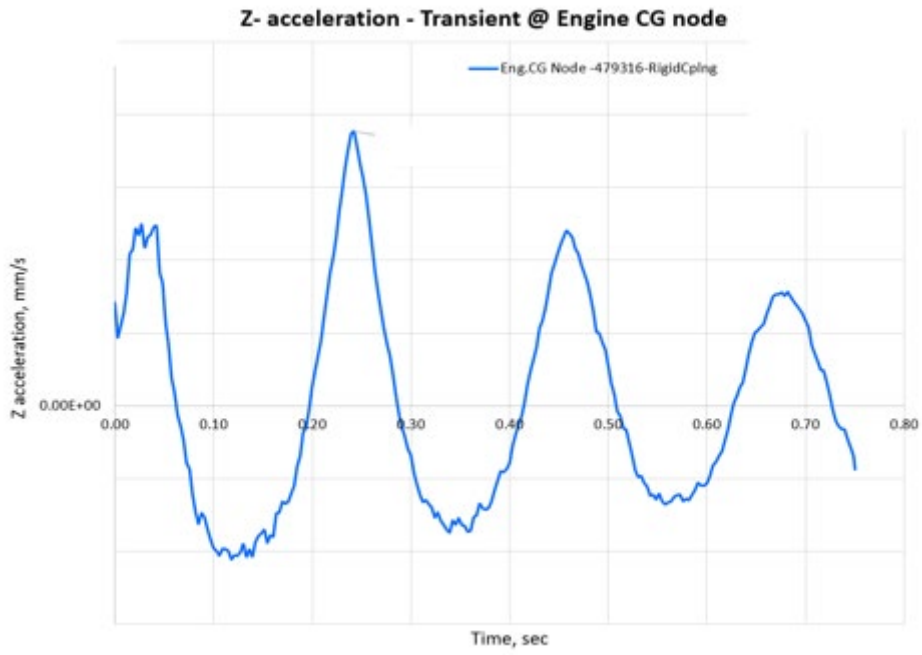


Fig.9: Vertical acceleration response at the Engine CG Vs time

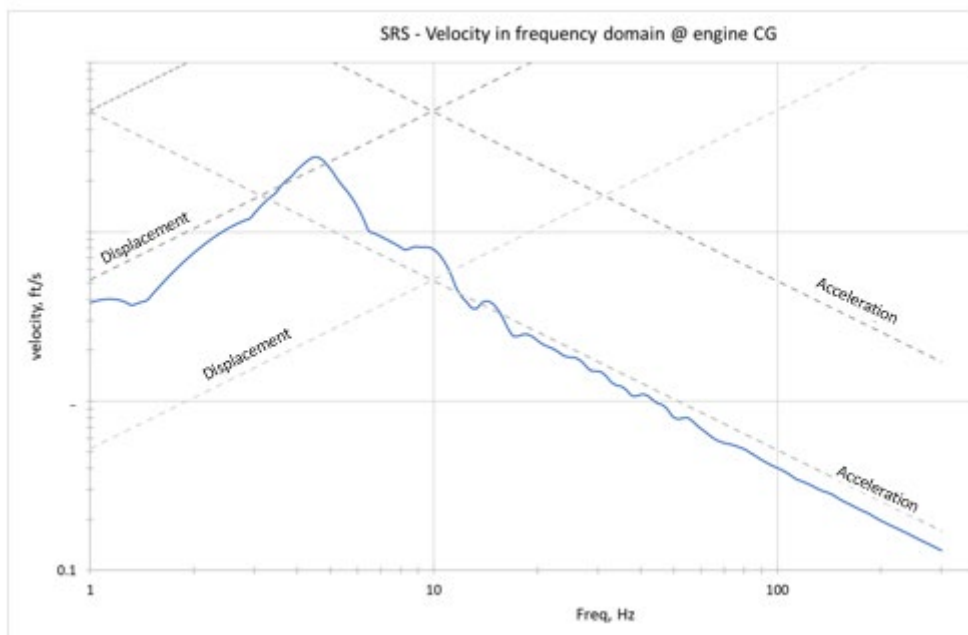


Fig.10: SRS response at Engine CG over frequency (Displacement, Velocity & Acceleration)

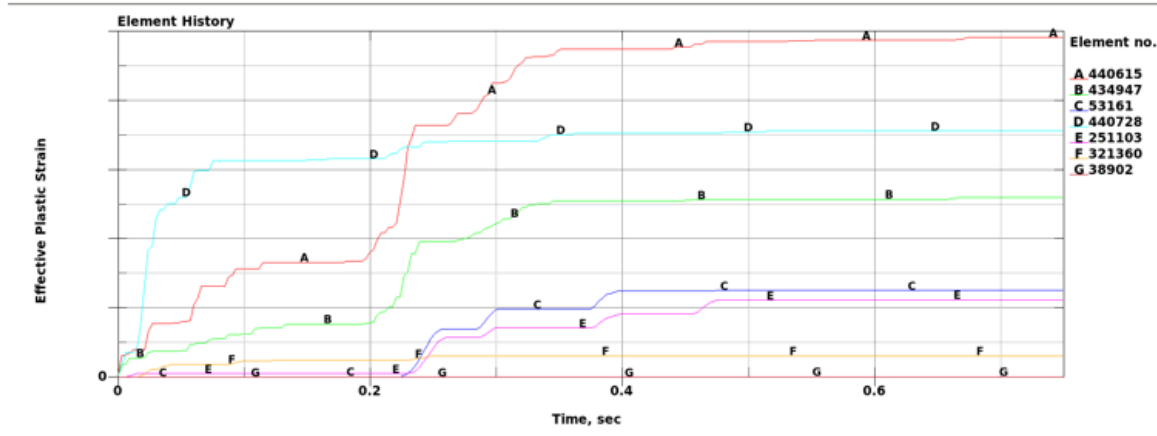


Fig.11: Effective Plastic strain over time at critical locations.

Compression due to preload*, mm			Relative deformation Transient Shock*, mm					
Mount 1	Mount 16	Mount 8	Mount 1		Mount 16		Mount 8	
			Comp.	Tens.	Comp.	Tens.	Comp.	Tens.
-14	-14	-14.3	-70	75	-55	70	-70	72

Table 1: Representative Max. relative deformation results from the simulation

8 Summary

- The transient shock analysis in LS-DYNA helped in achieving the objective of making the Wabtec engines ready for expensive barge test. High-risk components were identified in advance through the simulation, thus providing an opportunity to modify and improve the engine design before the actual test.
- Relative deformation of the high deflection mounts simulated using DISCRETE BEAM elements helped in evaluating the margins against the HDM capability.
- The simulation also helped to reduce the number of barge tests needed to be conducted to the Naval Vessel Register (NVR) certification for different variant of engines under same family.

9 Literature

- [1] LS-Dyna Manual R11.0, Vol I, Vol II and Vol III - <https://www.dynasupport.com/manuals>
- [2] DETAIL SPECIFICATION SHOCK TESTS, H.I. (HIGH-IMPACT) SHIPBOARD MACHINERY, EQUIPMENT, AND SYSTEMS, REQUIREMENTS FOR Department of Defense, US, MIL-DTL-901E, JUNE 2017
- [3] Shipboard Shock and Navy Devices for its simulation, NRL Report 7396, E.W. Clements, 1972
- [4] Technical case study from Kaizenat Technologies, Bangalore

Recent updates in linear solvers towards NVH and fatigue analysis in Ansys LS-DYNA®

Yun Huang, Tom Littlewood, Zhe Cui, Ushnish Basu, Francois-Henry Rouet, David Benson

Ansys, Inc.

1 Introduction

LS-DYNA is primarily known for its nonlinear analysis capabilities and has been used in many applications where nonlinear behavior is significant, including car crash analyses, drop-test analyses of electronic devices, penetration simulation of bullets and missiles, etc. On the other hand, LS-DYNA also has a comprehensive collection of linear solvers, including solvers for vibration, acoustics, and fatigue problems. These linear solvers were implemented to answer the requests of various users. These linear solvers can find applications in automotive, shipbuilding, and many other industries, especially in NVH and fatigue analysis in those fields. Embedded in a nonlinear software environment, these linear solvers are able to take into account pre-stress conditions, interact with some nonlinear Multiphysics solvers, and provide solutions for some comprehensive problems which would otherwise be difficult to solve with a standalone linear analysis package.

Since the last (the 15th) LS-DYNA Forum, Germany, 2020, many new features / options were implemented to these linear solvers in LS-DYNA. This paper aims at introducing the new features and options to the users of LS-DYNA.

2 Acoustic directivity plots by BEM

With the new keyword `*FREQUENCY_DOMAIN_ACOUSTIC_DIRECTIVITY`, an acoustic directivity plot can be provided by BEM acoustic computation (as the one in Figure 1). Multiple circles for the directivity plot can be defined. This feature can be useful to the users who need to identify the principal direction of acoustic wave propagation, and also the acoustic energy distribution in the space.

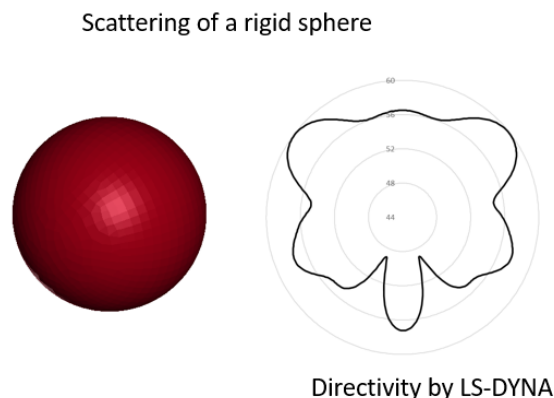


Fig.1: acoustic directivity of a sphere

3 Accelerated BEM computation by skeletonized interpolation and improved SMP for parallelism.

Starting from R13, parallelized matrix assembly with OpenMP has been implemented to LS-DYNA. For R14, improved parallelization of matrix assembly and parallelized the linear solver (GMRES) become available. Meanwhile, a SI (skeletonized interpolation) technique is implemented to speed up the matrix assembly by reducing the matrix's entries evaluation. With both improvements, the CPU time for solving a cabin model with 240k dof can be reduced from several days to a few hours.



Fig.2: Cabin model, 240 k dof

4 New options for acoustic material models

Some new options to *MAT_ACOUSTIC have been implemented to provide more flexibilities and add more capabilities to the acoustic computation. They include

***MAT_ACOUSTIC_COMPLEX**

***MAT_ACOUSTIC_DAMP**

***MAT_ACOUSTIC_POROUS_DB**

Where *MAT_ACOUSTIC_COMPLEX can be used in frequency domain acoustic computation, particularly in coupling with structural direct steady state vibration analysis (keyword *CONTROL_IMPLICIT_SSD_DIRECT), and *MAT_ACOUSTIC_DAMP define damping coefficients needed for both direct steady state dynamics and explicit transient analysis. *MAT_ACOUSTIC_POROUS_DB can be used to model porous acoustic materials (Delany-Bazley, Miki and Allard-Champoux models) for sound absorption.

5 Other updates

Updates in acoustic spectral element method

Coupled analysis of fluid-structure system

New options in fatigue analysis (restart, MPP, etc.)

6 Summary

A series of new features and options for the linear solvers have been implemented in LS-DYNA, to provide more capabilities for NVH and fatigue analysis, and to answer the need and requirements from the users. This paper provides an overall introduction of these new features and options. The areas of their application are discussed. Some examples are included to demonstrate the usage and effectiveness of these new features and options.

Acoustic simulation of RJ-45 connector assembly

Satish Kumar Meenakshisundaram¹, Sunil Acharya²,

¹ANSYS Inc,
Atrium One, 900 Victors Way Suite 350, Ann Arbor, MI

²ANSYS Inc,
2600 ANSYS Drive, Canonsburg, PA

1 Abstract

The present work discusses the structural and acoustic responses of a snap-fit assembly. Snap-fit assembly is a common feature in manufacturing of various industrial products. Especially thermoplastic components requiring mating are well-served by incorporating snap-fit features into the design. Snap fits may be engaged relatively quickly and can facilitate repeated disengagement for maintenance or repair purposes. Thermoplastic assemblies can be mass produced with injection molding relatively inexpensively and have become ubiquitous in most industries. Assembly of electrical and electronic connectors relies on the speed and ease of snap fits. A poor snap-fit insertion in these applications can mean loss of electrical connectivity as the contact area between two mating parts is crucial to the conduction path to the electrical signal. Designers typically rely on a target reaction force generated by the engagement (or disengagement) to design the snap-fit features for a specific application. This reaction force gives critical haptic feedback to the user during the assembly process or to the end-user during the product usage. Existing structural analysis tools well analyze such mechanical reaction force during the assembly. However, a user on the shop floor may often rely on a specific acoustic signature (clicking sound) to judge the quality of engagement of a snap-fit during assembly. Especially when the snap-fit features are not in a direct line of sight, such auditory feedback is helpful for the person doing the assembly. For the end-user, auditory feedback from snap-fits also feeds into the perception of the quality of a product. LS-DYNA can be deployed in the design phase to address such complex multi-physics problems in a relatively straightforward manner.

2 Introduction

RJ45 is a connector usually employed for Ethernet networking. Considering that Ethernet wires have an RJ45 connector on each end, Ethernet cables are usually also named RJ45 cables. RJ45 is the most recognized and popular connector type in the IT industry. It helps form an electrical connection between the mating parts. The mating process is a snap-fit action where the assembly latch secures the connection.

This work looks at the structural and acoustic response of an RJ45 connector assembly. First, the haptic feedback from the assembly process is simulated using a transient structural analysis with the explicit solver. The structural analysis is followed by a vibro-acoustics analysis using a boundary-element method (BEM). Finally, we demonstrate how the analysis may be deployed as a design tool to study the effect of design features and material selection on the haptic and acoustic feedback to the end-user.

3 Methodology

Numerical methods, especially Finite Element Method (FEM) and Boundary Element Method (BEM) are being used to simulate acoustic problems. The finite element method (FEM) has its own disadvantages as it requires the acoustic domain to be discretized, the farther the observation/field point the bigger the domain. This causes the computational time to dramatically surge. Alternatively, the implementation of boundary element method (BEM) solving the Helmholtz equation to compute the Sound Pressure Level (SPL (dB) proves to be more efficient as the discretization of acoustic domain is not required.

Structural response of the RJ45 connector when assembled with the housing is simulated using a transient structural analysis (explicit solver) approach. The structural response is stored in a binary file and is transformed from time domain into frequency domain using FFT. This transformed data, typically velocities in frequency domain, is then applied as boundary condition to perform the acoustics analysis. The LSDYNA keyword *FREQUENCY_DOMAIN_ACOUSTIC_BEM is used to couple the structural analysis with the acoustics counterpart. Finally, the computed sound pressure level can be transformed to time domain to obtain the acoustic feedback.

4 Results

The FEM solver coupled with BEM solver in LS-DYNA has been used to capture the haptic and acoustic feedback of the RJ45 connector's assembly process. The simulation time was decoupled in such a way that the assembly process would first take place and then, the simulation would be run for a few more seconds for the excitations to reach a steady state. For example, if the total simulation time was set to 0.25 seconds, the assembly time would be 0.15 seconds while for the remaining time (0.1 seconds) the model's excitations would be let to reach steady state in the assembled configuration. It was found that the assembly time affects the sound pressure level (SPL dB) as follows,

$$SPL\ dB \propto \frac{1}{assembly\ time}$$

On the other hand, two different material models, namely, *MAT_ELASTIC and *MAT_PIECEWISE_LINEAR_PLASTICITY were used to investigate the effect of material properties on the sound pressure level (SPL dB). The effect of material model on acoustics was observed to be negligible.

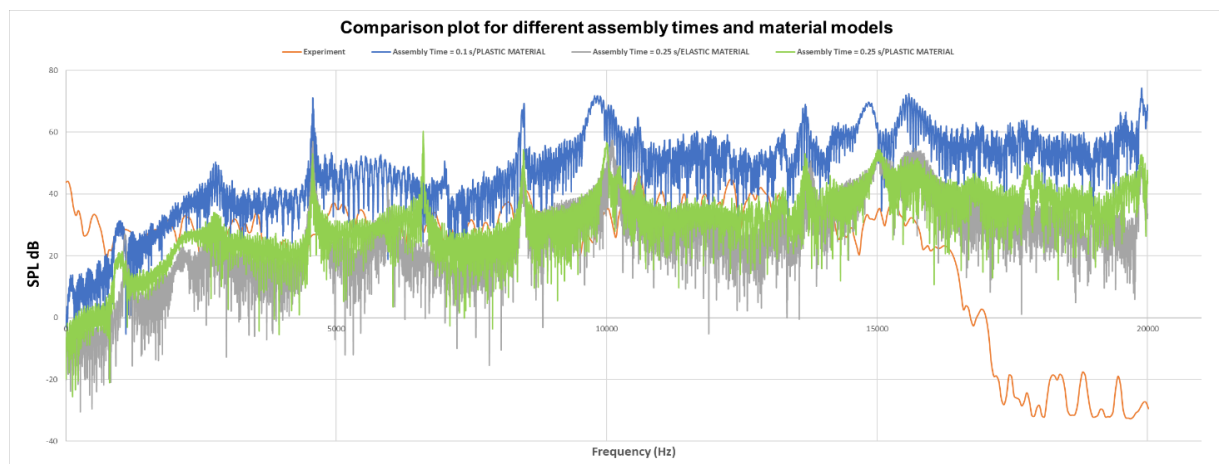


Fig 1. Comparison plot for different assembly times and material models

5 Conclusions

In this work an already existing multi-physics capability of LS-DYNA to simulate vibro-acoustics problems has been utilized. The haptic and acoustic feedback of RJ45 connector is simulated by coupling the structural solver with the acoustic solver. The methods to post-process the data into haptic and auditory feedback will be discussed during the presentation. The follow-up work will include more detailed analysis of the acoustics and impact of design and variations in material properties on the acoustic signature.

Numerical simulation of soil cutting using SPH and SPG approach

Hamid Rokhy¹, Farhad Farzaneh²

¹ Department of Aerospace Engineering, Amir Kabir University of Technology, Tehran, Iran

² Department of Civil and Environmental Engineering, Florida State University, FL, U.S

1 Introduction

Standard finite element methods have difficulty in modelling the soil cutting process due to large displacements and deformation of the mesh. The use of meshless methods overcomes this problem. In this paper, soil cutting is modelled using SPH and SPG approach and numerical results (predicted blade draft force and material flow behaviour) are compared to experimental results [1]. Two-dimensional experiments were performed by moving a vertical flat blade (350 mm height) between two glass panels (200 mm apart). More detail can be found in references [1-2].

2 Numerical model

The Finite element model of soil cutting problem using SPH approach is shown in Figure 1. In order to save the computational time, the left part of the soil sample was modeled by SPH particles while the right part of the soil sample was modeled with lagrangian elements. Instead of using "tied contact" between particle and bricks elements, Hybrid element was used to define coupling between SPH particles and Lagrangian elements of soil. Constant velocity of blade cutter was applied using *BOUNDARY_PRESCRIBED_MOTION_RIGID. Contact between the blade cutter and SPH particle was modeled with CONTACT_NODES_TO_SURFACE. The soil sample was modeled with the MAT_005 (Soil and Foam) material model.

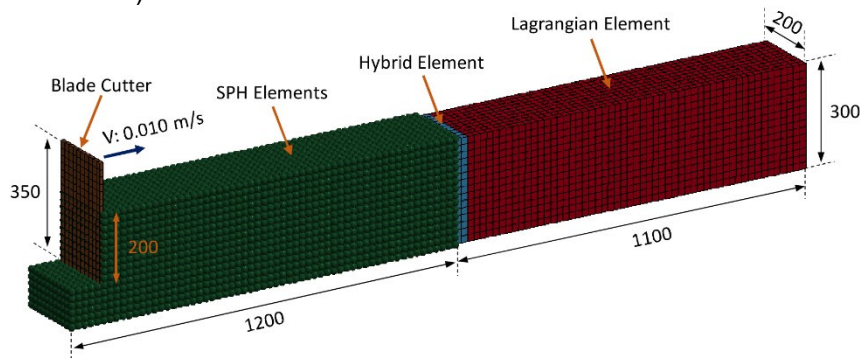


Fig.1: The FE Model of soil cutting problem (SPH approach)

Figure 2 shows the finite element model of soil cutting problem using SPG approach. In order to save the computational time, the left part of the soil sample was modeled by SPG elements while the right part of the soil sample was modeled with lagrangian elements. Same as the previous model, contact between the blade cutter and SPG elements was modeled with CONTACT_NODES_TO_SURFACE.

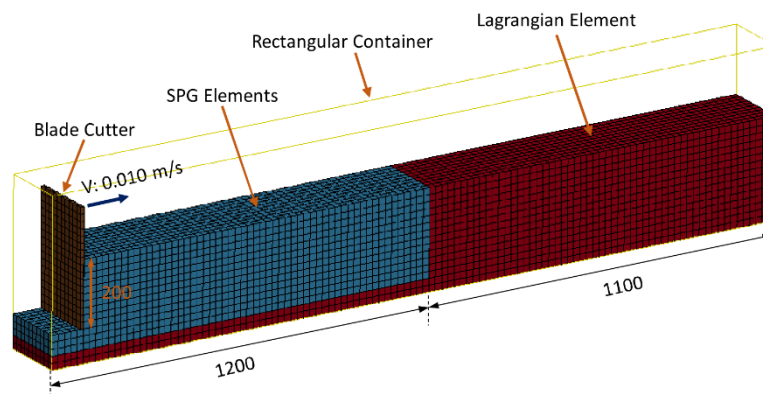


Fig.2: The FE Model of soil cutting problem (SPG approach)

3 Results and discussion

Figure 3 shows the observed in front flow of material of the blade (the experimental and SPH and SPG results). The initial blade depth was $h = 200$ mm. Snapshots were taken at displacement increments of 100 mm. The predicted shape of the heap that forms in front of the blade corresponds well to the experiment results. But the results of SPG approach is more accurate than the SPH approach. Figures 4 and 5 show the measured and simulated draft and vertical force on the blade with the initial depth $h = 200$ mm. As illustrated in these figures, SPG approach predicted with more accuracy the amount of forces applied on the blade with respect to the SPH approach.

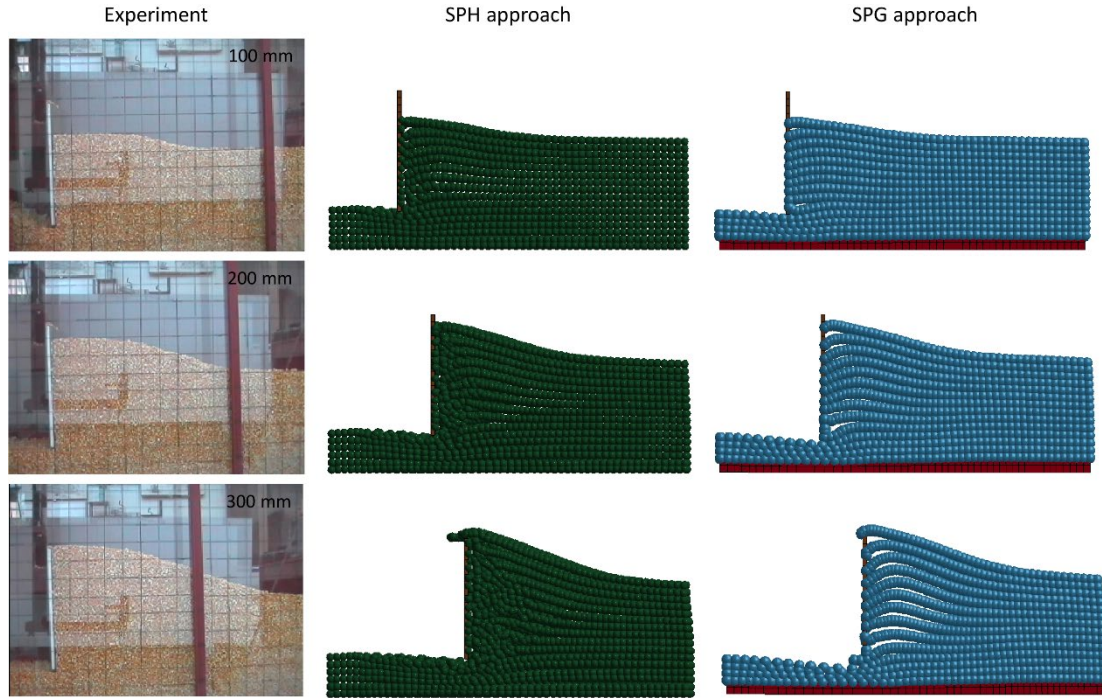


Fig.3: Comparison between experimental [1], results of corn flowing in front of the blade

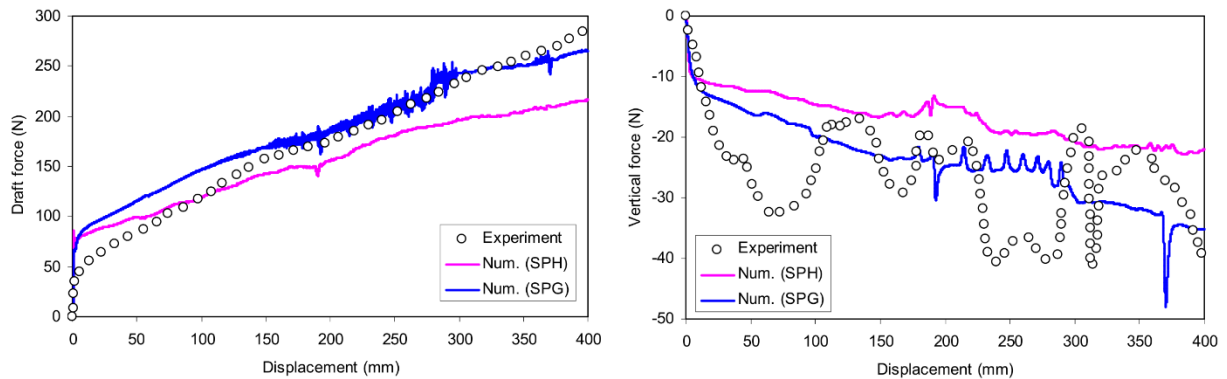


Fig.4: Left: Blade draft force, Right: Blade vertical force

4 Summary

The present numerical study investigates the performance evaluation of two meshless methods (SPH and SPG) for the simulation of soil cutting. The results showed that both methods can predict the shape of the heap that forms in front of the blade, but only SPG approach was able to predict the amount of forces applied on the blade with acceptable accuracy.

5 Literature

- [1] C. J. Coetzee, D. N. J. Els, Calibration of granular material parameters for DEM modelling and numerical verification by bladegranular material interaction. J Terramech 46 (2009)15–26
- [2] C. J. Coetzee, Forced granular flow. Msc Thesis Mechanical Engineering, University of Stellenbosch, Stellenbosch, South Africa (2000)

Investigation of various concrete material models to simulate seismic response of reinforced concrete columns subjected to cyclic loading

Hamid Rokhy¹, Farhad Farzaneh²

¹ Department of Aerospace Engineering, Amir Kabir University of Technology, Tehran, Iran

² Department of Civil and Environmental Engineering, Florida State University, FL, U.S

1 Introduction

Concrete Damage Rel3 (K&C), Winfrith Concrete Model, Continues Surface Cap Model (CSCM), and Concrete Damage Plastic Model (CDPM) are several constitutive material models in the LS-DYNA material library that can predict the behavior of concrete just by describing the compressive strength. In this paper, Low and Moehle experimental test [1] is simulated to evaluate the accuracy of these material models in simulating the seismic response of the RC columns under cyclic loading. The experimental test setup is shown in Figure 1 (all dimensions are in mm). The specimen was subjected to uniaxial lateral loading about the weak axis, with a constant axial load of 44.5 kN. This specimen had a concrete uniaxial compressive strength of 36.5 MPa. More detail can be found in reference [1].

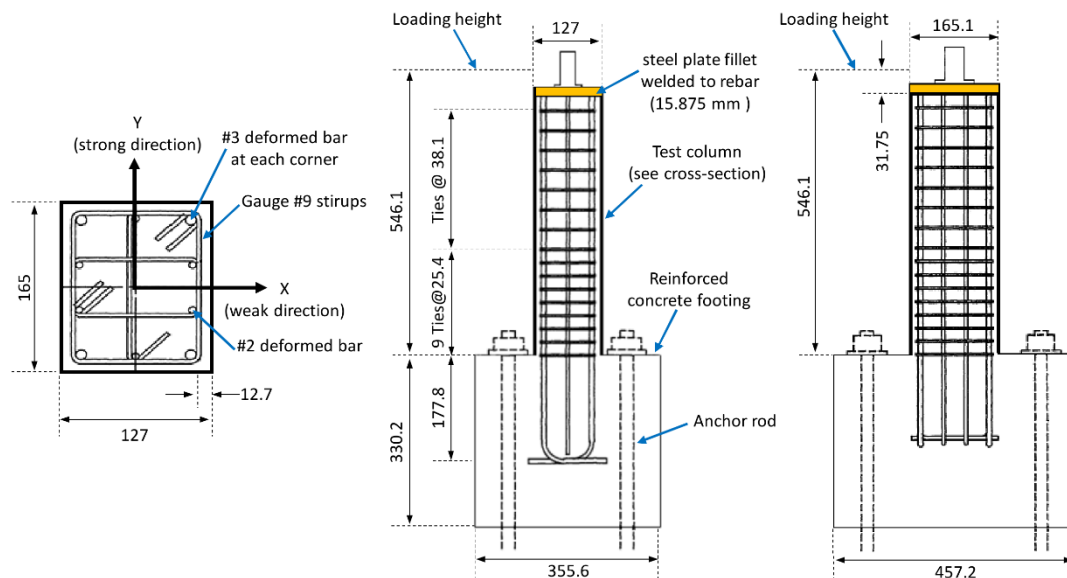


Fig.1: Test specimen configuration [1] (left: cross section, middle: X direction, right: Y direction)

2 Results and discussion

The predictions using different concrete material models and comparison with the experimental results are shown in Figure 2. The K&C model does not provide a reasonable prediction of the seismic response of the RC column because this model predicted degradation of strength and was notably lower than the test results. The CSCM prediction exhibited minor pinching than the experimental data and higher degradation of strength. The Winfrith and CPDM predicted pinching better than the previous two models but similar to CSCM; they indicate higher strength degradation. To improve the accuracy of the numerical results, the bond-slip model must be used to simulate the response of the reinforcement embedded in concrete [2]. Crack propagation (failure mode) due to cyclic loading is shown in Figure 3. It is clear that CSCM and CPDM better predict failure mode.

3 Literature

- [1] S. S. Low SS, J. P. Moehle, Experimental study of reinforced concrete columns subjected to multi-axial cyclic loading, EERC Report 87/14. Earthquake Engineering Research Center: University of California, Berkeley, USA (1987)
- [2] M. Zhao, D. E. Lehman, Ch. W. Roeder, Modeling recommendations for RC and CFST sections in LS-DYNA including bond slip, Engineering Structure, 229 (2021), 111612

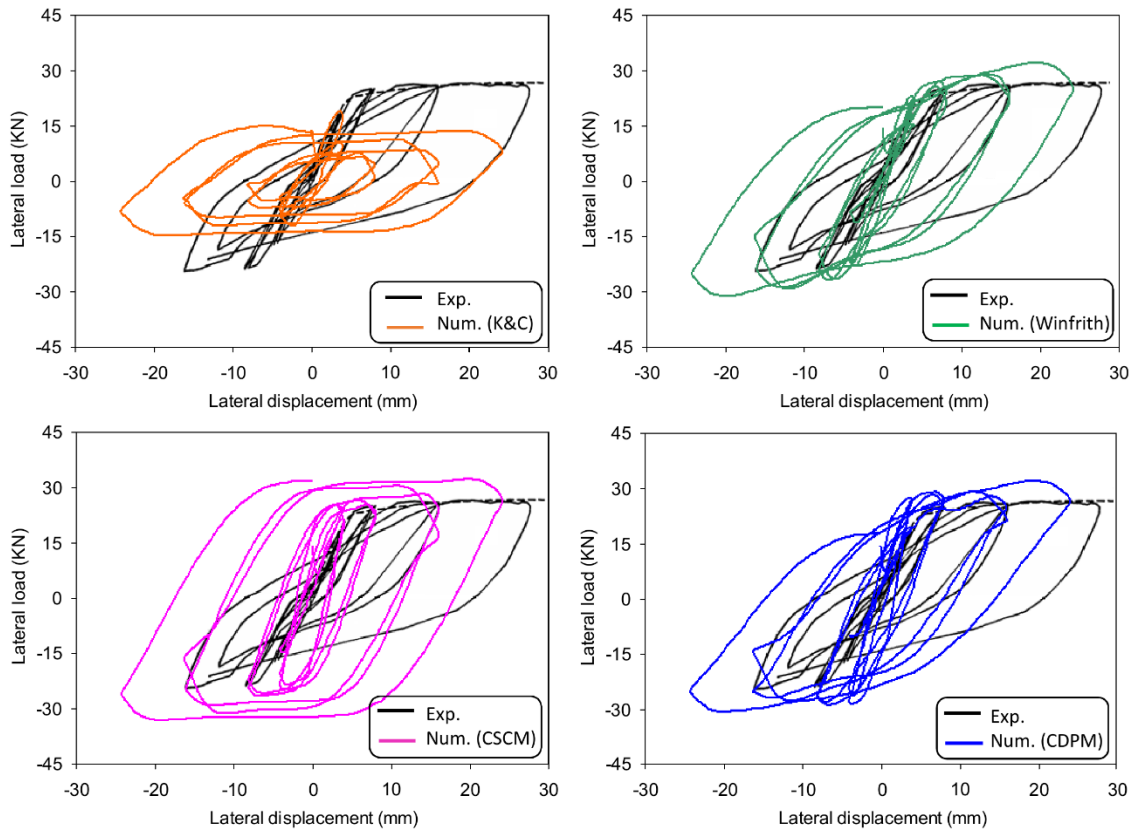


Fig.2: Predicted load–displacement curve for RC column with different material models

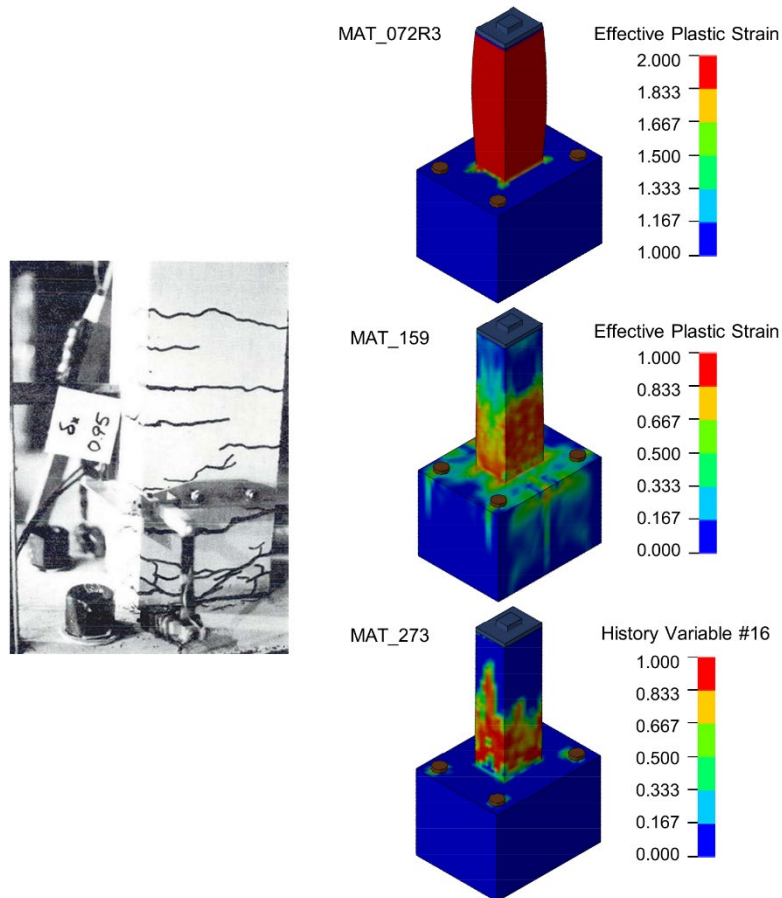


Fig.3: Crack propagation (failure mode) due to cyclic loading; left: experiment [1], right: numerical

Hydrogen Risk Analysis During Severe Accidents In A Nuclear Power Plant

J. Amponsah (MESA)



DYNAmore Gesellschaft für FEM Ingenieurdienstleistungen mbH

DYNAmore GmbH
Headquarters
Industriestr. 2
70565 Stuttgart, Germany
Tel.: +49 (0)711 - 45 96 00 - 0
Fax: +49 (0)711 - 45 96 00 - 29
E-Mail: info@dynamore.de
www.dynamore.de

DYNAmore GmbH
Office North
Im Balken 1
29364 Langlingen, Germany
Tel.: +49 (0)50 82 - 9 14 00 - 50
Fax: +49 (0)50 82 - 9 14 00 - 49

DYNAmore GmbH
Office Ingolstadt
Friedrichshofener Str. 20
85049 Ingolstadt, Germany
Tel.: +49 (0)841 - 1 29 43 24
Fax: +49 (0)841 - 12 60 48 - 38

DYNAmore GmbH
Office Berlin
Stralauer Platz 34
10243 Berlin, Germany
Tel.: +49 (0)30 - 20 68 79 10
Fax: +49 (0)30 - 20 07 83 82

DYNAmore GmbH
Office Dresden
Pohlandstr. 19
01309 Dresden, Germany
Tel.: +49 (0)351 - 31 20 02 - 0
Fax: +49 (0)351 - 31 20 02 - 29

DYNAmore GmbH
Office Braunschweig
Altewiekring 20A
38102 Braunschweig, Germany
Tel.: +49 (0)531 - 20 97 94 20
Mobile: +49 (0)170 - 761 08 48

DYNAmore GmbH
Office Munich
Oskar-Schlemmer-Straße 11
80807 München, Germany
Tel.: +49 711 4596000
Fax: +49 711 45960029

DYNAmore Material Competence Center MCC
Kolumbusstraße 47
70771 Leinfelden-Echterdingen, Germany
Tel.: +49 (0)711 - 45 96 00 - 17
E-Mail: mcc@dynamore.de

Subsidiaries

Sweden

DYNAmore Nordic AB
Headquarters
Brigadgatan 5
587 58 Linköping, Sweden
Tel.: +46 (0)13 - 23 66 80
Fax: +46 (0)13 - 21 41 04
E-Mail: info@dynamore.se
www.dynamore.se

DYNAmore Nordic AB
Office Göteborg
Bror Nilssons gata 16
417 55 Göteborg, Sweden
Tel.: +46 (0)31 - 3 01 28 60

Switzerland

DYNAmore Swiss GmbH
Technoparkstr. 1
8005 Zürich, Switzerland
Tel.: +41 (0)44 - 5 15 78 90
Fax: +41 (0)44 - 5 15 78 99
E-Mail: info@dynamore.ch
www.dynamore.ch

Italy

DYNAmore Italia S.r.l.
Piazza Castello, 139
10122 Turin, Italy
Tel.: +39 335 157 05 24
E-Mail: info@dynamore.it
www.dynamore.it

France

DYNAmore France SAS
21 av. de Paris
78000 Versailles, France
Tel.: +33 (0)1 - 39 55 81 01
E-Mail: info@dynamore.eu
www.dynamore.eu

USA

DYNAmore Corporation
565 Metro Place South, Suite 300
43017 Dublin, OH, USA
Tel.: +1 (614) 696 3303
E-Mail: info@dynamore.com
www.dynamore.com